Annual progress report of the Department of Solid State Physics 1 January - 31 December 1991

Als-Nielsen, Jens Aage; Pedersen, Jan Skov; Lebech, Bente

Publication date:
1992

Document Version
Publisher's PDF, also known as Version of record

RISØ

Risø-R-610(EN)

Annual Progress Report of the Department of Solid State Physics

1 January - 31 December 1991

Edited by J. Als-Nielsen, J. Skov Pedersen and B. Lebech

Risø National Laboratory, Roskilde, Denmark
January 1992

Annual Progress Report of the Department of Solid State Physics

Risø-R-610(EN)

1 January - 31 December 1991

Edited by J. Als-Nielsen, J. Skov Pedersen and B. Lebech

Risø National Laboratory, Roskilde, Denmark
January 1992

Abstract

Research in the department covers the field of condensed matter physics. The principal activities of the department are presented in this Progress Report covering the period from 1 January to 31 December 1991.

The condensed matter physics research is predominantly experimental utilising diffraction of neutrons and X-rays. The research topics range from studies of two- and three-dimensional structures, magnetic ordering, heavy fermions, high T_c superconductivity, phase transitions in model systems to studies of precipitation phenomena and nano-scale structures in various materials. The major interest of the department is in basic research, but projects of more applied nature are often taken up, prompted by the applicability of the developed technique and expertise.

ISBN 87-550-1788-6
ISSN 0106-2840
ISSN 0907-0249

Grafisk Service Risø, 1992

Contents

1 INTRODUCTION

The condensed matters physics research is predominantly experimental utilising diffraction of neutrons and X-rays. The neutron scattering experiments are carried out at the DR3 reactor, where the department of solid state physics operates seven spectrometers, including a small-angle neutron scattering facility, a multidetoctor powder diffractometer, a reflectometer. a four-circle diffractometer and triple axis spectrometers. The experiments using synchrotron X-ray radiation take place at HASYLAB, at DESY in Hamburg, Germany.

Neutron and X-ray diffraction are complementary techniques. The neutron has several unique properties. It can penetrate matter, the energies of neutrons are comparable to that of typical excitations in condensed matter, and so the neutron can probe such excitations. In scattering experiments, the neutron is sensitive to the magnetic moments of atoms and to nuclear isotopes and at ultralow temperatures the neutron can even be used to determine the orientation of nuclear spins. The main advantage of X-ray diffraction in our research program stems from the astounding X-ray intensity one can obtain from synchrotron sources. This allows an improvement of resolution in diffraction experiments by several orders of magnitude over possibilities with neutron scattering, and/or a minute volume of the diffracting sample such as a single atomic or molecular layer on a surface.

The research topics described in this report cover studies of two- and three-dimensional structures, magnetic ordering, heavy fermions, phase transitions in model systems, studies of high T_c superconductivity and studies of inorganic and biological materials by small-angle scattering.

Some milestones of the year have been:

- By the beginning of 1992 the neutron scattering instruments at DR3 are an *European User Facility*, partly supported by the EC as part of the *Large Installation Program*. Through 1991 this program has been prepared by appointing two new people, a scientist and a chief engineer and by upgrading of the instruments.

- Fundamental neutron scattering results in the field of superconductivity have been obtained both within studies of flux lattices and within studies of oxygen ordering in high T_c materials.

- An X-ray monochromator system has been constructed and tested. It is designed to overcome the severe heat load problem at synchrotron sources, and it will be of great significance for the beam lines of the European synchrotron, ESRF in Grenoble, where already in 1992 the first photon beams will be produced in test runs.

- In 1991 two new X-ray scattering instruments have been installed at the new *By-Pass* facility in HASYLAB in Hamburg. Hereby, the potential for high intensity X-ray measurements are greatly improved.

1.1 Quasicrystals and Twins: Two- and Five-dimensional Models

(J. Wolny and L. Pytl. , *Institute of Physics and Nuclear Techniques, Academy of Mining and Metallurgy, Cracow, Poland* and B. Lebech, *Department of Solid State Physics, Risø National Laboratory, Denmark*)

Different ways of tiling the plane without defects by using two decorating elements, *i.e.* two Robinson triangles, have previously been discussed[1,2,3]. Four classes of structures with different tiling rules and different relative concentrations of the two elements were compared: Penrose tiling, various twins, random structures and a precipitated structure. As an extension, the Robinson triangles have now been decorated using two different atoms: large ones in the corners of the triangles and small ones in positions inside the big triangles (one per triangle). The stability of the obtained structures has been investigated for a Lennard-Jones interacting potential. Structure factors have been calculated for a form factor equal to 1 for the large atoms and 0 for the small atoms. The four decorated structure classes have similar diffraction patterns exhibiting tenfold symmetry. An universal behaviour of the diffraction patterns of different structures allows definition of a similarity parameter which distinguishes quasi-crystals from the other type of structures. It is shown that the similarity parameter depends only on the concentration of small Robinson triangles. The concentration dependence of the similarity parameter exhibits singular behaviour at the Penrose concentration, indicating that a continuous transition takes place from twinned structures to quasi-crystals.

Using a five-dimensional analysis[4] it was shown that the diffraction peak intensities for all the investigated structures can be well approximated by a Debye-Waller factor calculated in perpendicular (phason) space. Mean-square values of the perpendicular-space fluctuations scale linearly with the number of atoms for all concentrations of small Robinson triangles except for the Penrose concentration. At the Penrose concentration the linear term in the mean-square perpendicular-space fluctuation dependence on the number of atoms vanishes. For random Penrose tiling a logarithmic term becomes dominating, and this changes significantly the dependence of peak intensities on the number of atoms. Analytical expressions for peak intensities have been tested for all the structures discussed above.

[1] B. Lebech, J. Wolny and L. Pytlik, (1987). *Quasicrystalline Materials*, eds. C. Janot and J.M. Dubois, World Scientific, Singapore , p. 234.
[2] J. Wolny, L. Pytlik and B. Lebech, (1983). J. Phys. C: Solid State Phys. **21**, 2267.
[3] J. Wolny, L. Pytlik and B. Lebech, (1990). J. Phys.: Condens. Matter **2**, 785.
[4] L. Pytlik, (1991). J. Phys.: Condens. Matter **3**, 2457.

1.2 Characterization and Structure Determination of Inorganic Compounds by X-Ray and Neutron Powder Diffractometry

(A. Nørlund Christensen, *Institute of Chemistry, University of Aarhus, Aarhus, Denmark*, P. Norby and S. Habekost, *Department of Chemistry, University of Odense, Odense, Denmark*. H. Fjellvåg, *Department of Chemistry, University of Oslo, Blindern, Norway*, M. Nielsen, N.H. Andersen and B. Lebech, *Department of Solid State Physics, Risø National Laboratory, Denmark*)

When combining scattering data from synchrotron X-ray and neutron powder diffractometry it is possible to solve crystal structures of inorganic compounds with unit cell volumes up to 1000 Å^3. In this way, the crystal structure of Cr_8O_{21} was determined[1].

By a similar combination of diffractometer data, a study of the temperature dependence of the unit cell parameters of the superconducting cuprate $HoBa_2Cu_3O_{7-\delta}$ was made in the temperature range from 30 to 300 K[2]. The resulting unit cell parameters are shown in Fig. 1.

A study concerning improvement of the structure models from the previous X-ray analysis using single crystal films is in progress. The analysis will be made by least squares refinement of the model structures expected from the X-ray data to neutron powder diffraction data. So far, neutron powder diffraction data have been collected for barium oxalate and silicates of La, Ce, Nd and Er.

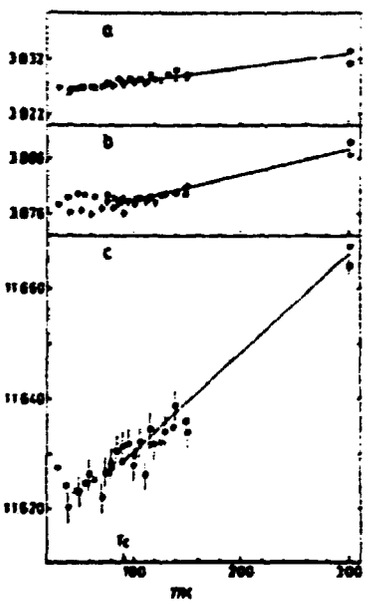

Fig. 1. Unit cell parameters (in Å) vs. temperature for $HoBa_2Cu_3O_{7-\delta}$. The open circles show neutron diffraction data, filled circles with error bars show X-ray diffraction data from HASYLAB, filled circles without error bars show X-ray diffraction data from Daresbury and filled squares with error bars are from Ref. 3. The solid curves are guides to the eye.

[1] P. Norby, A.N. Christensen, H. Fjellvåg and M. Nielsen, (1991). J. Solid State Chem. 94, 281.
[2] S. Habekost, A.N. Christensen B. Lebech, T. Wroblewski and K.P.J. O'Reilly, (1991). Acta Chem Scand. 45, 965.
[3] L.E. Conroy, A.N. Christensen and J. Bøttiger, (1987). Acta Chem. Scand. Ser. A41, 501.

1.3 Neutron Diffraction Study of the Ordering of Ni_4Mo

(A. Andreev, *Institute of Nuclear Physics, Moscow State University, Russia*, B. Lebech, *Department of Solid State Physics, Risø National Laboratory, Denmark*, L. Sarholt-Kristensen, A. Johansen and S. Steenstrup, *Physics Laboratory, University of Copenhagen, Denmark* and M.H. Nielsen, *Institute of Chemistry, University of Aarhus, Denmark*)

The extend of ordering in Ni_4Mo single crystals is known to influence the physical properties of the alloy, and probably this will change the emission patterns of components sputtered in their neutral or charged states from the single crystal Ni_4Mo under ion bombardement. Indeed, Antonov *et al.*[1] showed by computer calculations and sputter experiments with low energy argon ions ($E < 20$ keV), that the spatial distributions of Ni and Mo atoms were different in ordered and disordered Ni_4Mo crystals. The calculated and experimental Ni to Mo yield ratios exhibit maxima in the ⟨011⟩ and ⟨013⟩ directions. In these directions, the deviation from stoichiometry of the sputtered material is particularly large. In the subsequent investigation of Sarholt-Kristensen *et al.*[2] the measurements were extended to bombardment with argon ions of higher energy (80 keV). The surface layers of the bombarded crystals were analysed using Rutherford backscattering of 500 keV He^{++} ions. The analysis show no distinct difference between the ordered and disordered crystals, but in both cases ion induced segregation of Ni to the surface was observed. Quite unexpectedly, RBS analysis of the spatial distribution of the sputtered material did not show Wehner spots in the ⟨001⟩ direction in contrast to comparative measurements made on a pure (001) Ni crystal. It should be noted, that Ni–Mo alloys have been studied rather extensively and some complete phase diagrams have been published[3,4]. Grube and Schlecht[3] report an ordering reaction in the Ni rich solid solution and Harker[5] shows that a Ni–Mo alloy containing about twenty atomic percent of Mo exists above 900°C as a cubic close-packed structure. If this alloy is quenched and then maintained at temperatures below 840°C, an ordering reaction occurs which results in a slight tetragonal distortion of the cubic structure. The ordered structure can be described in terms of the tetragonal space group C_{4h}^5–I4/m (a_o=5.720 Å, c_o=3.564 Å and c/a=0.6231). The Mo atoms are situated at 2(a) sites and Ni at 8(b) sites (see Fig. 1).

The fundamental problem of the ordered Ni_4Mo structure is that it can have thirty different atom arrangements with respect to the face-centered cubic solid solution from which it forms (six orientations and five origins). Doubtless, the ordering reaction starts at many different sites in the primary disordered face-centered cubic single crystal solid solution and choose any of the thirty different ways to grow at each site. Therefore, as a result of ordering, we may have a very complicated array of Ni_4Mo crystallites in the annealed crystals. Ruedel *et al.*[6], Fu-Weng-Ling and Starke[7] and Kozlov *et al.*[8] have shown the possibility to achieve ordering by thermal refinement and finite size fully ordered Ni_4Mo crystallites appear in the primary crystals.

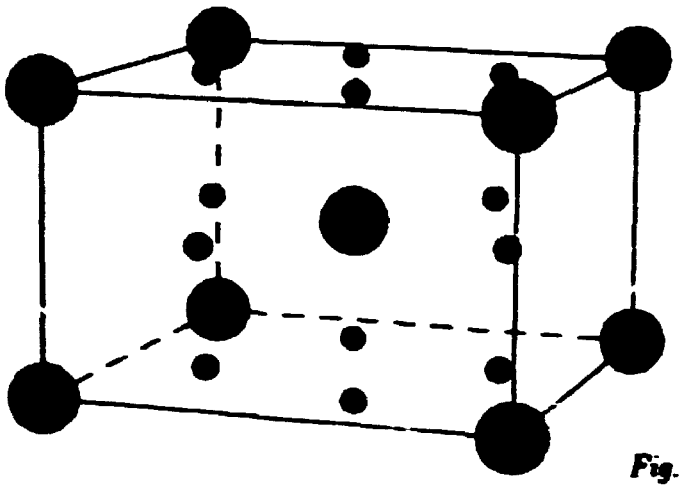

Fig. 1. Crystal structure of Ni_4Mo in the ordered state. The large spheres are Mo-atoms, the smaller ones Ni-atoms.

The aim of the present neutron diffraction investigation is to examine the state of ordering of the Ni_4Mo single crystals used in the sputter experiments[2] and to find the best annealing procedure for obtaining Ni_4Mo crystals with a high degree of order and large domain sizes. Single crystal Ni_4Mo (discs 9 mm in diameter and 3 mm thick with the (001) normal to the disc) were cut by spark-machining from a larger crystal and prepared for sputtering by mechanical polishing. In order to get a disordered crystal one of them was annealed for 15 minutes in air at about 1100°C and then quenched in water at room temperature. A second one was annealed in a vacuum chamber for 200 hours at about 700°C. The last one was also annealed in a vacuum chamber for 200 hours, but at about 840°C. Both of the latter Ni_4Mo crystals were after annealing slowly cooled to room temperature. All crystals were then mechanicaly re-polished. Four-circle neutron diffraction data on these differently prepared single crystals of Ni_4Mo have been collected and a preliminary analysis of the data indicates that the diffraction data depend strongly on the different annealing procedures. Additional reflections corresponding to superstructures of the ordered Ni_4Mo are observed. The intensities of these reflections differ for crystals annealed at 700°C and 840°C, respectively.

[1] S.L. Antonov, I.N. Ivanov, A.A. Orlikovskiy, V. Yu Vasil'chenko and V.E. Yurasova, (1990). Nucl. Instr. and Methods B48, 553.

[2] L. Sarholt-Kristensen, A. Andreev, A. Johansen, H.H. Andersen and E. Johnson, (1992). Sputtering and RBS Investigations of Ordered and Disordered Ni_4Mo. *To be published* Nucl. Instr. and Methods B.

[3] G. Grube and H. Schlecht (1938). Zeits. f. Electrochemie 44, 413.

[4] M. Hansen and N. Anderko, (1958). *Constitution of Binary Alloys*, (Mc Graw-Hill, New York).

[5] D. Harker, (1944). Jour. Chem. Phys. 12, 315.

[6] E. Ruedel, P. Delavignette and S. Amelinckx, (1968). Phys. Stat. Sol. 28, 305.

[7] Fu-Weng-Ling and E.A. Starke, (1971). Acta Met. 19, 759.

[8] E.V. Kozlov, G.V. Pushkareva, V.M. Kushnarenko, V.A. Koneva and I. Vuz'ov, (1977). Phisica v1(176), 84 (*in Russian*).

1.4 Neutron Powder Diffraction Studies of Modifications of Ni_7S_6

(H. Seim and H. Fjellvåg, *Department of Chemistry, University of Oslo, Oslo, Norway* and B. Lebech, *Department of Solid State Physics, Risø National Laboratory, Denmark*)

At low-temperatures, binary M – S (M = 3*d* element) phase diagrams are complicated by the appearrance of both stable and metastable non-stoichiometric phases with ordering between vacancies and M atoms. The present study concerns the Ni – S phase diagram (52 – 55 mol% Ni). Ni-sulfides have been studied in the form of mineral species (e.g. heazlewoodite, godlevskite, (Fe,Ni) pentlandite, millerite) by single crystal X-ray and electron diffraction. Recent, comprehensive studies indicate two stable phases at the approximate composition Ni_7S_6 (see Fig. 1). The present study reveals a more complex situation. At high temperatures, orthorhombic α–Ni_7S_6 (a_α = 3.275(1) Å, b_α = 16.470(4) Å and c_α = 11.448(3) Å at 743 K) exists between 673 and 846 K with a temperature dependent homogeneity range ($Ni_{1.17}S$ – $Ni_{1.20}S$ at 773 K). At lower temperatures, T < 723 K, orthorhombic β-Ni_7S_6 (actually $Ni_{1.170}S$; a_β = 9.316(2) Å, b_β = 11.218(2) Å and c_β = 9.399(2) Å at 295 K) is stable.

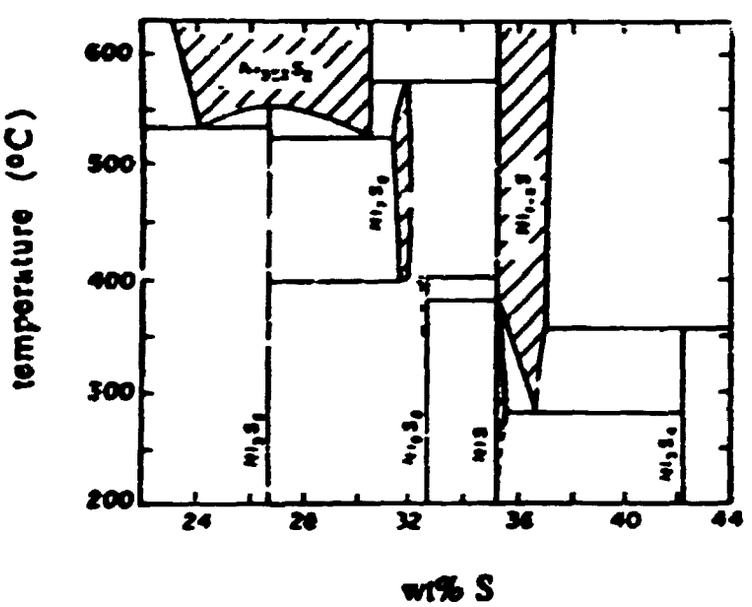

Fig. 1. Schematic phase diagram for Ni–S between 22 and 44 wt% S, which corresponds to 65.9 and 41.0 mol% Ni, respectively.

Slowly cooled, low-temperature annealed (100–250°C), as well as quenched samples were studied with powder X-ray diffraction and differential scanning calorimetry between 295 and 900 K. Quenched α–Ni_7S_6 converted over time to a phase (termed β'), which is different from β–Ni_7S_6. Low-temperature annealed samples showed complex X-ray powder patterns. Dependent on the composition, phase transitions were registered at 420, 673, 723 or 846 K upon heating. The structural relationship between the various phases, could, to some extent, be analyzed from X-ray Guinier Simon photographs, for which the film movement and temperature increase was synchronized. An example is shown in Fig. 2

Powder neutron diffraction data were collected using the multi-detector powder diffractometer (λ = 1.071 and 2.339 Å) for various low-temperature annealed and quenched

samples. The structure of β–Ni_7S_6 was confirmed and the resulting, refined occupation numbers concur with its nominal composition. Electron microscopy was used together with X-ray powder data to establish the unit cell of β'–Ni_7S_6; $a_{\beta'}$ = 6.238(1) Å, $b_{\beta'}$ = 32.830(4) Å and $c_{\beta'}$ = 11.596(1) Å, β = 101.83(1)° at 295 K. The structure of β'–Ni_7S_6 may be described on the basis of the assumed relationship $a_{\beta'} = 2a_\alpha$, $b_{\beta'} = 2b_\alpha$, $c_{\beta'} = -a_\alpha + c_\alpha$. The doubling of the b-axis was evident from electron microscopy which revealed weak additional reflections, and a probably centric lattice. So far, the Rietveld refinements of the neutron powder diffraction data are restricted to the smaller unit cell (*viz.* setting $b_{\beta'}$ = 16.41 Å). The results indicate that disordered α–Ni_7S_6 undergoes ordering of Ni and vacancies upon low-temperature annealing, forming β'–Ni_7S_6. The difficulties involved in the quenching of α–Ni_7S_6 is analogous to the situation between β–Ni_3S_2 (ordered, rhombohedral) and α– Ni_3S_2 (disordered, cubic; probably high ionic conductivity).

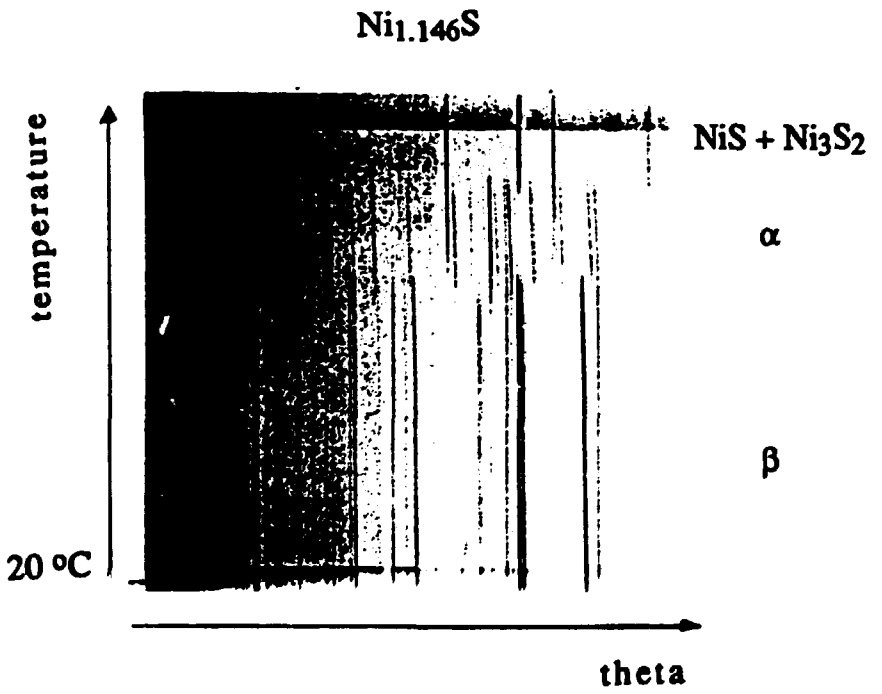

Fig. 2. Direct film-recording of high-temperature PXD photograph for $Ni_{1.146}S$, showing the phase transition sequence $\beta \longrightarrow \alpha \longrightarrow NiS + Ni_3S_2$.

1.5 Neutron Scattering Measurements on $Rb_2Cu_{1-x}Co_xF_4$, a Two-Dimensional Mixed Ferromagnet–Antiferromagnet

(A.G. Schins, A.F.M. Arts, H.W. de Wijn, *Faculty of Physics and Astronomy, and Debye Research Institute, University of Utrecht, The Netherlands*, and M. Nielsen, *Department of Solid State Physics, Risø National Laboratory, Denmark*)

The alloy $Rb_2Cu_{1-x}Co_xF_4$ represents a random mixture of the two-dimensional ferromagnet Rb_2CuF_4 and the 2-D Ising antiferromagnet Rb_2CoF_4. The system combines competing spin anisotropies and competing exchange interactions. The phase diagram shows a ferromagnetic regime for $x < 0.18$, a spin glass behaviour for $0.18 < x < 0.40$, and antiferromagnetism for $x > 0.40$ [1]. Neutron scattering measurements have been done on three crystals with $x = 0.037$, 0.083, and 0.88, having an oblique and an axial ferromagnetic phase, and an antiferromagnetic phase. Magnetic scattering was observed along ridges perpendicular to the ordering planes.

For $x = 0.037$ (oblique ferromagnetic phase) two successive transitions were observed at 5.4 and 3.3 K via, for instance, discontinuities in the temperature dependence of the magnetic ridge scattering intensity. In Fig. 1 the data for the scattering vector $q = (0, 0, 1.7)$ are shown as given by the generalized susceptibility $\chi_\perp$ and the inverse correlation length $\kappa_\perp$ of the in-plane spin component. The transition at 5.4 K is associated with the diverging susceptibility of the axial spin components. The transition at 3.3 K was found to be accompanied by the onset of planar ordering. At T=5.4 K. $\kappa_\perp$ freezes in at a value of 0.03 r.l.u., which is ten times the instrumental resolution.

In the $x = 0.083$ crystal strictly axial ordering was found for $T < 5.16$ K, and the ridge scattering at q=(1,0,1.3) was found to diverge at the same temperature. The moments in the $x = 0.88$ crystal approaches an antiferromagnetic ordering at the "transition temperature" T_N=88 K, but a truely long range order is not achieved.

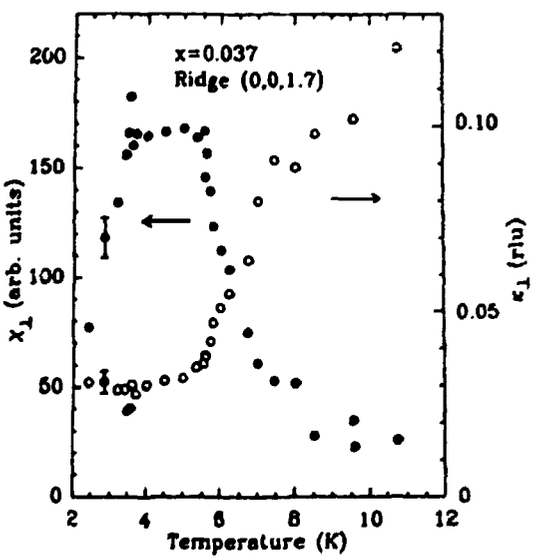

Fig. 1. Planar susceptibility $\chi_\perp$ and inverse correlation length $\kappa_\perp$ as function of temperature, obtained after deconvolution of scans across the magnetic ridge at $q = (0, 0, 1.7)$ for $Rb_2Cu_{1-x}Co_xF_4$ with $x = 0.037$.

[1] C. Dekker, A.F.M. Arts, and H.W. de Wijn, (1988). Phys. Rev. B 38, 11512.

1.6 Magnetic Ordering of Layered Perovskites

(P. Harris and B. Lebech, *Department of Solid State Physics, Risø National Laboratory, Denmark* and N. Achiwa, *Kyusho University, Fukuoka, Japan*)

The layered perovskite $(CH_3CH_2CH_2NH_2)_2MnCl_4$ (PAMC) has been investigated by neutron diffraction. PAMC is known to undergo several phase transitions on cooling from 441 K to 5 K. Our attention has been focussed on two phase transitions. One is at 111.5 K, where PAMC transforms from an orthorhombic phase with an incommensurate modulation of wave vector $(\delta + \frac{1}{3})\mathbf{b}^*$ to a monoclinic phase with a commensurate modulation of wavevector $\frac{1}{3}(\mathbf{b}^* \pm \mathbf{c}^*)$. The other transition is at 39 K where it orders into an antiferromagnetic phase with a small ferromagnetic contribution in the a-direction.

The chemical structure of the monoclinic phase is not known, but NMR results show[1], that the transformation from the orthorhombic to the monoclinic structure is caused by increasing order of the hydrogen bondings between the NH_3-groups and the chloride ions, and that the change in modulation vector is caused by a change of the tilting of the system of rigid carbon chains and $MnCl_6$ octahedra. The antiferromagnetic phase is a quasi 2D Heisenberg antiferromagnet, with a small ferromagnetic contribution. The magnetic structure gives rise to magnetic satellites, that turns out to be superimposed on the nuclear satellites[2]. This indicates that the space groups of the tilted chemical system and the space group of the antiferromagnetic system are the same.

In order to understand the interaction between the magnetic and chemical structure, we have measured the monoclinic angle as a function of temperature. This has been done by measuring the splitting of the single strong (040) orthorhombic reflection into the two monoclinic reflections along the c*-axis. An example of such a measurement at 111.5 K is shown in Fig. 1a, where a coexistence of the orthorhombic and monoclinic phases is seen. The deviation γ of the angle from 90° is shown in Fig. 1b. After a small increase γ decreases on cooling until it locks in to an almost constant value below 40 K. This lock-in transition might be caused by the magnetic order.

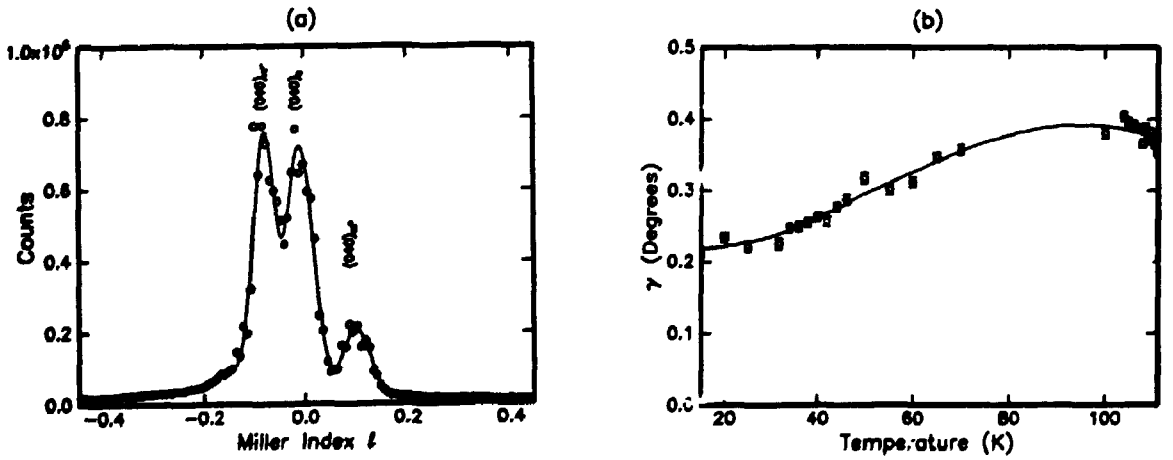

Fig. 1. (a): Scan through the (040) reflection along the c-axis (ω-scan) at 111.5 K. The coexistence of the unsplit $(040)_o$ and the split reflections $((040)_{m+}$ and $(040)_{m-})$ is seen. (b): The deviation from 90° of the monoclinic angle γ as a function of temperature.*

Also the intensities of selected magnetic Bragg reflections and satellites have been measured as a function of temperature. The result for the (0 10/3 10/3) satellite is shown in Fig. 2. Because the satellite has contributions from both the magnetic and the nuclear scattering, the intensity of this satellite is not expected to go to zero at the magnetic phase transition, but the observed increase and following decrease in intensity above T_c is surprising. This seems to indicate that there may be two and not just one phase transition around 39 K. However, the magnetic intensity of the satellites is very weak and the results will have to be confirmed by more measurements. In order to get the best result we intend to localize the satellites by employing a Maximum Entropy formalism.

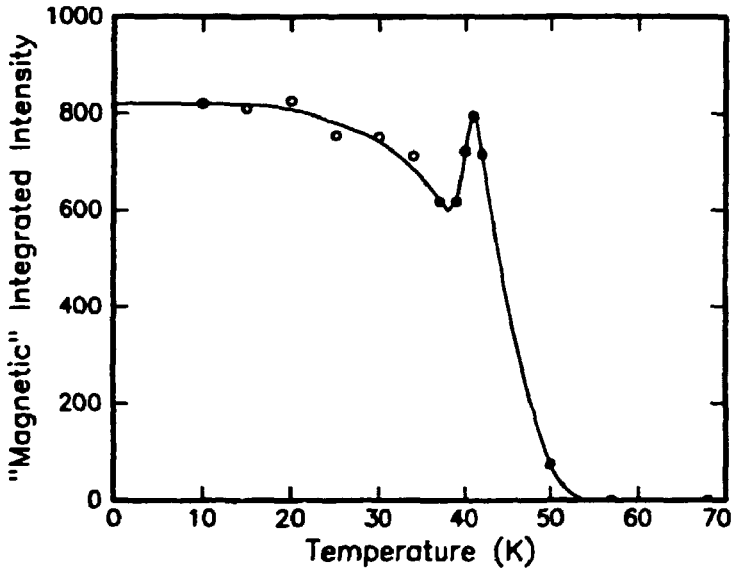

Fig. 2. Temperature dependence of the (0 10/3 10/3) satellite.

[1] P. Muralt, R. Kind and W. Bührer, (1988). Phys. Rev. B **38**, 666.
[2] N. Achiwa, T. Matsuyama and T. Yoshinari, (1990). Phase Transitions **28**, 79.

1.7 The Magnetic Phase Diagram of Rare Earth–Intermetallic Compounds

(B. Lebech, *Department of Solid State Physics, Risø National Laboratory, Denmark*, Z. Smetana, *Department of Metal Physics, Charles University, Prague, Czechoslovakia* and M. Heidelmann, *Institut für Festkörperforschung, KFA Jülich, Germany*)

The RCu_2 compounds (R = rare earths, except of La) crystallize in the orthorhombic $CeCu_2$ structure, which can be described as a stacking of alternate layers of R and Cu atoms along the c– or b–axis. The magnetic R^{3+} ions are responsible for the magnetic properties of these compounds and the long range oscillatory indirect exchange interactions between the R^{3+} ions, combined with the crystalline anisotropy, leads to long range antiferromagnetic order at low temperatures. The influence of the magnetic crystalline anisotropy can be estimated by a study of a series of isostructural RCu_2 compounds, *i.e.* compounds with different orbital moments. The impact of the exchange interactions can be considered by varying the electron concentration. In particular, substitution of Ni (with fully occupied *3d*–states) for Cu leads to a lowering of the conduction electron concentration and an increasing tendency toward ferromagnetic alignment.

The lighter of the heavy-RCu_2 have relatively simple magnetic phase diagrams[1)] with antiferromagnetically modulated structures with propagation vector $\frac{1}{3}a^*$. Because of the orthorhombic crystal structure it is reasonably easy to map the magnetic phase diagram of the light end of the heavy–RCu_2 series by powder neutron diffraction, but in the heavier end of the series the magnetic phase diagrams get increasingly more complicated and single crystal neutron diffraction data are needed. In the following two contributions we describe combined powder and single crystal neutron diffraction studies of two such compounds $TmCu_2$ and $ErCu_2$.

[1)] B. Lebech, Z. Smetana and V. Šima, (1987). J. Magn. Magn. Mater. **70**, 97.

1.8 The Magnetic Phase Diagram of $TmCu_2$

(M. Heidelmann, *Institut für Festkörperforschung, KFA Jülich, Germany*, B. Lebech, *Department of Solid State Physics, Risø National Laboratory, Denmark* and Z. Smetana, *Department of Metal Physics, Charles University, Prague, Czechoslovakia*)

The previous neutron powder diffraction studies of $TmCu_2$[1)] have confirmed the complex magnetic phase diagram suggested from the measurements of specific heat[2)] and thermal expansion[3)], but certain details of the magnetic strucutres are still unsolved. We have recently extended the neutron diffraction studies to analysis of a limited set of single crystal data and a more detailed set powder data at selected temperatures and magnetic fields with the aim of establishing the magnetic structures in the different regions of the magnetic phase diagram of $TmCu_2$.

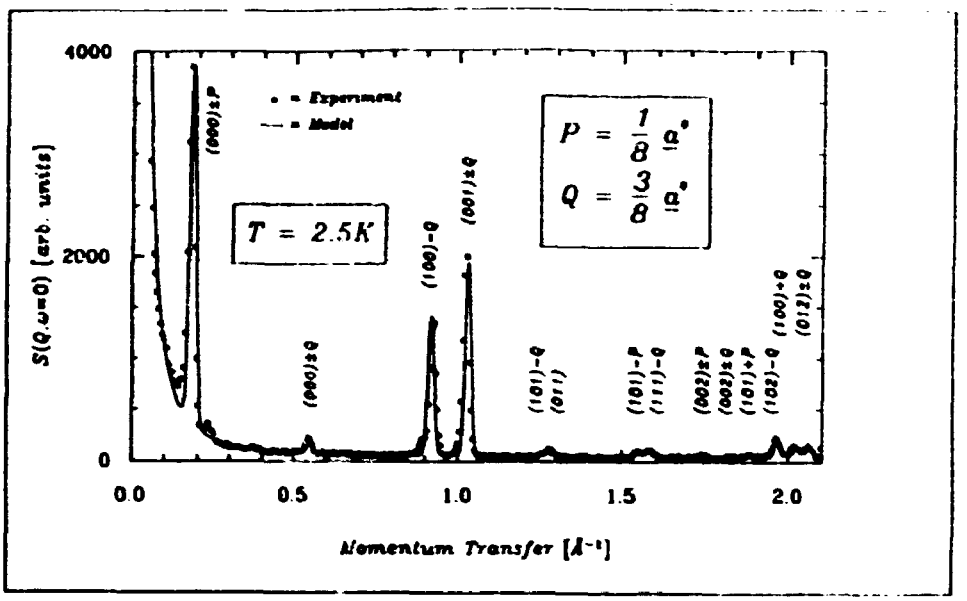

Fig. 1. Powder neutron diffraction diagram of the antiferromagnetic phase AFI in $TmCu_2$ using incident neutron of wavelength 4 Å. The solid curve shows the model fit to the magnetic structure shown in Fig. 2.

Based on the powder neutron diffraction data we find that within the experimental error the lattice parameters (a = (4.28 ± 0.02) Å, b = (6.64 ± 0.02) Å, c =(7.20 ± 0.02) Å) remain unchanged down to 1.5 K. In the low temperature phase (T < 3 K) we find that the magnetic structure may be described by a modulated structure with two Fourier components having propagation vectors $\mathbf{P} = (0.125 \pm 0.002)\mathbf{a}^*$ and $\mathbf{Q} = (0.375 \pm 0.002)\mathbf{a}^*$, i.e. they correspond to the first and third order harmonic in a commensurate magnetic structure with modulation vector $\frac{1}{8}\mathbf{a}^*$. In other words the magnetic unit cell is eight times larger in the a-direction than the chemical unit cell. Fig. 1 shows the result of a least squares fit of the diffraction pattern obtained by a superposition of the chemical structure and sinusoidally modulated Tm-site magnetic moments aligned in the b-direction. The moments on the four Tm-sites in the chemical unit cell are described by

$$\mathbf{M}_i = \mathbf{M}_\mathbf{Q} \sin(\mathbf{Q}\mathbf{R}_{iN} + \Phi_i) + \mathbf{M}_\mathbf{P} \sin(\mathbf{P}\mathbf{R}_{iN} + \Phi_i) \quad (i = 1..4) \tag{1}$$

where

$$\Phi_1 = \Phi_2 = \frac{3\pi}{8}, \quad \Phi_3 = \Phi_4 = \frac{\pi}{8},$$

$$\mathbf{Q} = 3\mathbf{P}$$

$$\mathbf{M}_\mathbf{Q} \parallel \mathbf{b} \text{ and } \mathbf{M}_\mathbf{P} \approx \frac{1}{3}\mathbf{M}_\mathbf{Q}$$

$\mathbf{R}_{iN}$ determines the positions of the Tm-sites in the unit cells, where the index i numerates the Tm-position within a unit cell and N the translation of the cell in the a-direction. The amplitude of the first harmonic $\mathbf{M}_\mathbf{Q}$ was found to be (6.8 ± 0.2)μ_B. The proposed magnetic structure is shown in Fig. 2.

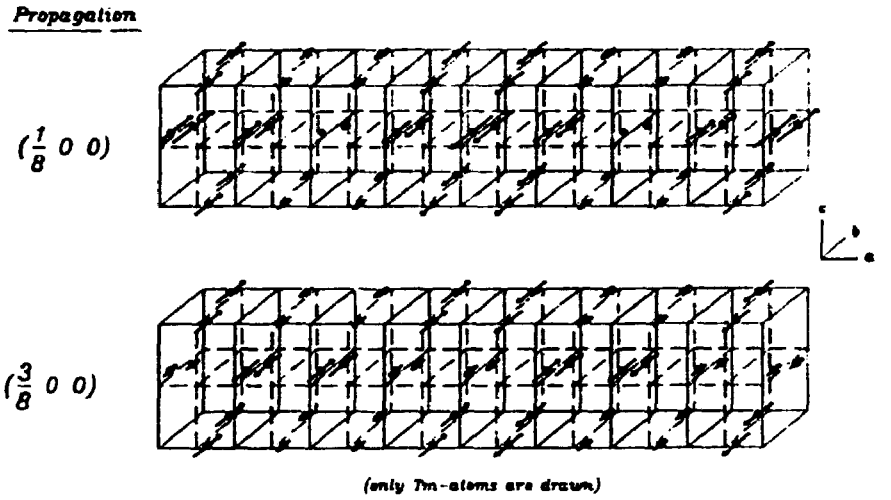

Fig. 2. Proposed magnetic structure of the AFI phase in $TmCu_2$. The unit length of the magnetic moments is arbitrary. The moment $\mathbf{M}_i$ in Eq. 1 is obtained by appropriate addition of the two components shown in the figure.

In addition to the profile refinement shown in Fig. 1 we measured the temperature dependence of the peak positions and the intensities of reflections having scattering vector close to 1 $Å^{-1}$ (see Fig. 3).

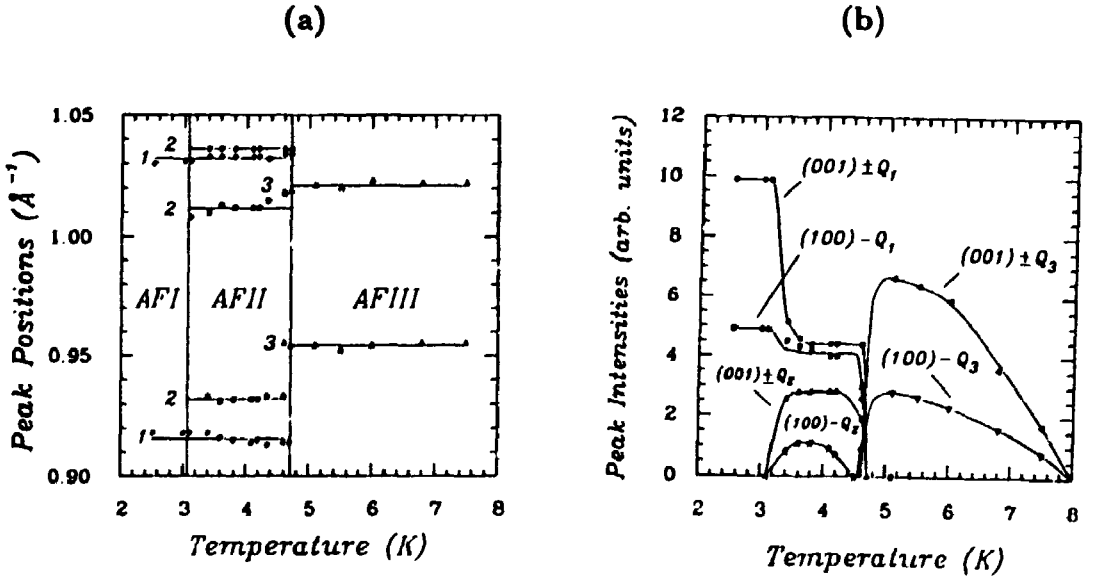

Fig. 3. Positions (a) and intensities (b) of the (100)- and (001)-satellites in $TmCu_2$.

From this data it is possible to distinguish three different magnetic phases which we designate AFI, AFII and AFIII. Until now only the propagation vector $\mathbf{Q_1} = \mathbf{Q}$ (see Fig. 3b) in AFI and AFII has been confirmed by the single crystal data. The two other propagation vectors ($\mathbf{Q_2}$ and $\mathbf{Q_3}$, see Fig. 3b) have to be at least two-dimensional, because it is impossible to find one-dimensional vectors which can describe the positions

of the magnetic Bragg peaks correctly. The vectors closest to the experimentally observed peak positions are:

$$\mathbf{Q_2} = 0.365\mathbf{a}^* + 0.018\mathbf{c}^* \quad \textit{and} \quad \mathbf{Q_3} = 0.354\mathbf{a}^* + 0.127\mathbf{b}^*$$

These vectors seem to represent incommensurably magnetic structures. Similarly to the magnetic structure in the AFI phase, the magnetic moments of the sinusoidally modulated structure are aligned along the b-direction, but any model of the incommensurably modulated phases is complex and needs to be confirmed by single crystal data.

[1] B. Lebech, Z. Smetana and V. Šima, (1987). J. Magn. Magn. Mater. 70, 97.
[2] Z. Smetana, V. Šima, J. Bischof, P. Svoboda, Š. Zajac, L. Havela and A.V. Andreev, (1986). J. Phys. F.: Met. Phys. 16, L201.
[3] V. Šima, Z. Smetana, M. Diviš, P. Svoboda, Š. Zajac, J. Bischof, B. Lebech and F. Kayzel, (1988). J. Phys. (Paris) C 8, 415.

1.9 Study of the Magnetic Order in $ErCu_2$

(Z. Smetana, *Department of Metal Physics, Charles University, Prague, Czechoslovakia* and B. Lebech, *Department of Solid State Physics, Risø National Laboratory, Denmark*)

$ErCu_2$ is another orthorhombic rare earth-intermetallic compound with a complex magnetic phase diagram with several modulated magnetic structures. It orders below $T_N = 11.8$ K and exhibits quasi-Ising like behavior with the b-axis as the easy axis of magnetization. The crystal field ground state is the well isolated Kramers doublet ($\Delta \sim 55$ K) which has a large projection of the total orbital moment along the b-axis, $\mu_b = g_J \mu_B \langle J_z \rangle \sim 9\ \mu_B$, while the projections along the a- and c-axes are very small (μ_a and μ_c are both less than $\sim 1\ \mu_B$). Further magnetic phase transitions have been observed at $T_1 = 4.3$ K and $T_2 = 6.1$ K.

Neutron diffraction studies have been done on single crystals of $ErCu_2$ in the $(\mathbf{a}^*, \mathbf{c}^*)$-plane of reciprocal space in the temperature range of 1.5 K to 20 K. As temperature decreases, $(h,0,l)^{\pm q}$ satellites with $h + l = 2n$ appear at T_N. Their intensities increase rapidly to towards $T_2 = 6.1$ K. Below T_2, the intensities of the $(h,0,l)^{\pm q}$ satellites decrease abruptly. No satellites were observed for $l = 0$. The modulation vector describing the magnetic ordering between 6.1 and 11.8 K is incommensurate with a propagation vector $\mathbf{Q} = 0.385\ \mathbf{a}^*$ and ordered non-Ising like moment μ_a. The corresponding magnetic moment lies along the a-axis and the value of μ_a estimated from the neutron diffraction data agrees well with the value obtained from the magnetization data. However, we have not found any evidence of long range ordering for μ_c nor for the large quasi-Ising component μ_a.

1.10 Study of the Magnetic Phase Diagram of MnSi close to the Critical Temperature

(C. Gregory and N. Bernhoeft, *Physics Department, University of Durham, UK*, B. Lebech, P. Harris, J. Skov Pedersen and K. Mortensen, *Department of Solid State Physics, Risø National Laboratory, Denmark*)

The cubic intermetallic compound MnSi belongs to a class of magnetic metals with the B20 crystal structure ($P2_13$). Such materials lack inversion symmetry and are capable of supporting a static spin density wave at low temperatures which within current theories[1,2] corresponds to a long range spiral magnetic structure. Other materials include the cubic polymorph of FeGe[3] and the randomly substituted $Fe_xCo_{1-x}Si$ alloys[4,5]. MnSi has a critical temperature of (29.5 ± 0.5) K with the helix propagating along equivalent ⟨111⟩ directions with a period of ~ 180 Å. In contrast, FeGe has a critical temperature of 278.7 K with the helix propagating along equivalent ⟨100⟩ directions above 211 K and along equivalent ⟨111⟩ directions below 211 K (for decreasing temperatures). In this case the periodicity is ~ 700 Å.

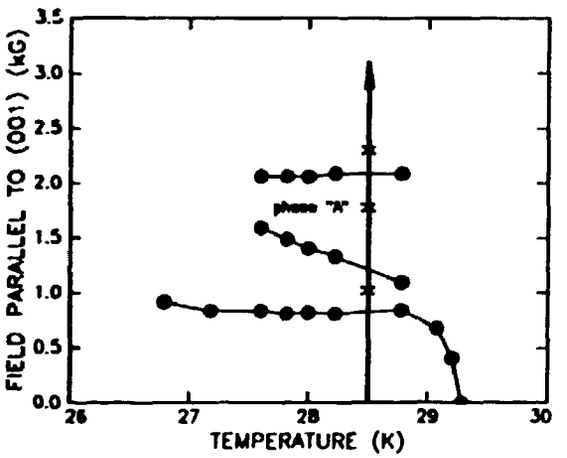

Fig. 1. Magnetic phase diagram of MnSi (H ∥ [001]) near the critical temperature[6]. The thick line marks the field sweep through 'phase A' resulting in the data shown in Fig. 2, and the crosses indicate schematically the fields at which the data shown in Fig. 2 were collected. The thin curves are guides to the eye.

Following a detailed magnetization study close to the critical temperature[6], we studied various aspects of the magnetic phase diagram including the so-called 'phase A' by small-angle neutron scattering using incident neutrons with a wavelength of 7 Å. The work was done on a cylindrical single crystal of MnSi (1.5 mm in diameter and 4 mm long) cut with the [001] axis parallel to the cylinder axis. The sample was mounted in a vertical field 5 T split coil superconducting magnet with the field was applied along the [001] direction. During the measurements the field was monitored using a calibrated Hall probe mounted close to the sample position. Figure 1 shows the magnetic phase diagram[6] of MnSi close to the critical temperature for field applied along the [001] direction. The low field region corresponds to domain reorientation and the 'phase A' lies above this field region.

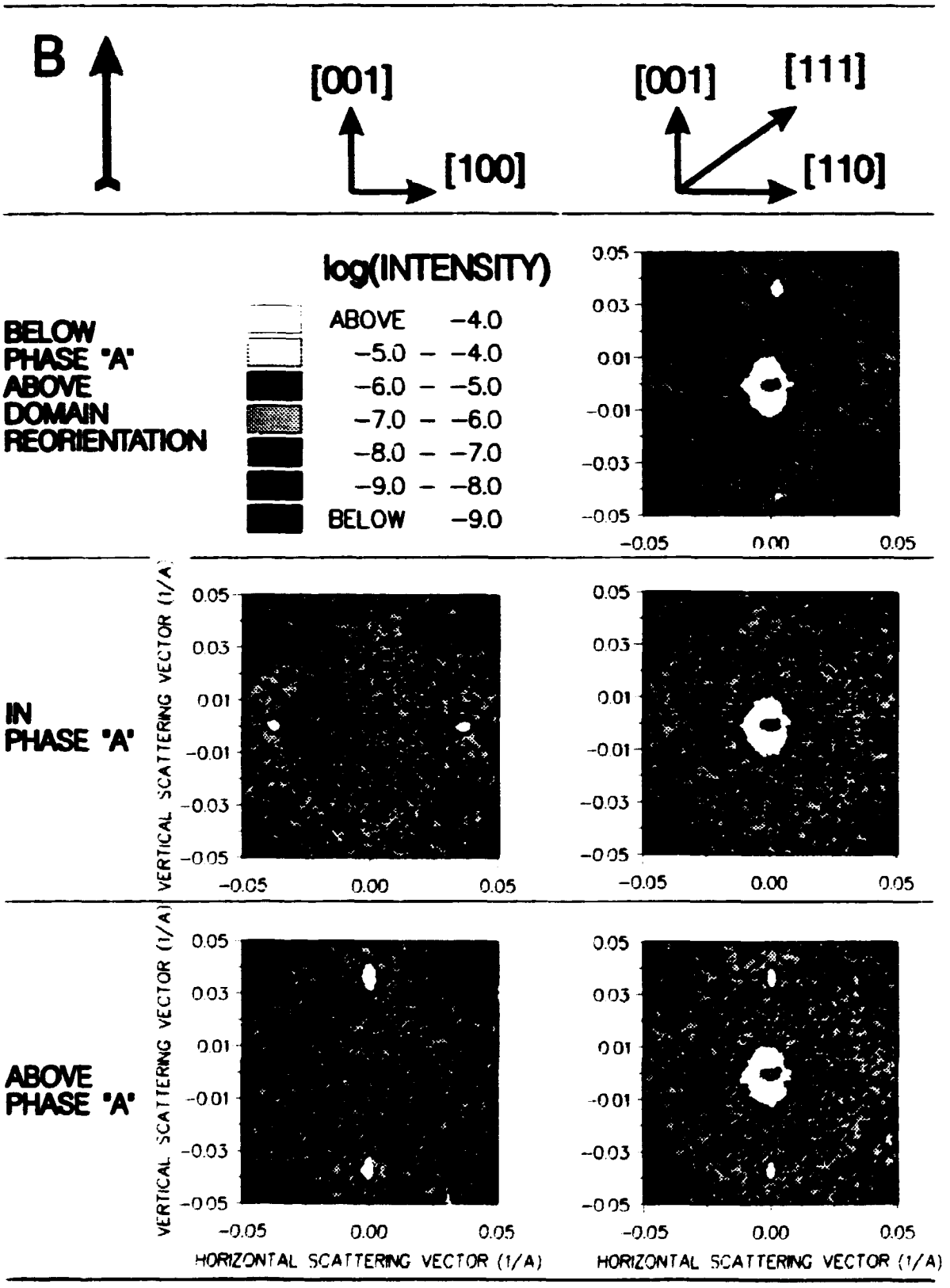

Fig. 2. Equal intensity contours SANS data (log-scale) observed in and out of 'phase A' for two different crystal orientations (see text). The background scattering from the cryomagnet (which is substantial) has been subtracted. The magnetic satellite Bragg peaks are the red-yellow spots observed at $Q \sim 0.035$ Å^{-1}. The intense scattering around (0,0) in the right hand panel is presumeably caused by insufficient subtraction of the central background.

Small-angle neutron scattering data were collected for two different crystal orientations and at different fields just below the magnetic ordering temperature. The results are summarized in Fig. 2 which shows equal intensity contours (*log-scale*) of scattering intensity in the plane defined by [100] and [001] (left) and by [110] and [001] (right).

From the data we conclude tentatively: (i) that just below 'phase A', but at fields above the domain reorientation, the helix is rotated to propagate along equivalent (100)-directions, (ii) in 'phase A' the symmetry is broken and the helix propagates only along the two (100)-directions perpendicular to the field, *i.e.* $\mathbf{q} \parallel [100]$ and [010], and (iii) above 'phase A' the helix propagate along the field direction ($\mathbf{q} \parallel [001]$). A probable explanation for this behavior may be that the constant B_2, which within current theory for Dzyaloshinskii-Moriya spirals[7,8] determines the propagation direction of the helix, is in fact field dependent and changes sign within 'phase A', going from negative to positive (in phase 'A') and then returning to negative above 'phase A'.

[1] O. Nakinishi, A. Yanase, A. Hasegawa and M. Kataoka, (1980). Solid State Commun. **35**, 995.
[2] P. Bak and M.H. Jensen, (1980). J. Phys. C.: Solid State Phys. **13**, L881.
[3] B. Lebech, J. Bernhard and T. Freltoft, (1989). J. Phys C.: Condensed Matter **1**, 6105.
[4] J. Beille, J. Voiron, F. Towfiq, M. Roth and Z.Y. Zhang, (1981). J. Phys F.: Metal Phys. **11**, 2153.
[5] J. Beille, J. Voiron and M. Roth, (1983). Solid State Commun. **47**, 399.
[6] C.I. Gregory, D.B. Lambrich and N.R. Bernhoeft, (1992). 'Magnetization Study of the Magnetic Phase Diagram of MnSi'. Proceedings of ICM91, Edinburgh, UK, September 1991. *To be published.*
[7] I. Dzyaloshinskii, (1958). J. Phys. Chem. Solids **4**, 241.
[8] T. Moriya, (1960). Phys. Rev. **120**, 91.

1.11 Nuclear Magnetic Phase Diagram of Cu

(K.N. Clausen, *Department of Solid State Physics, Risø National Laboratory, Denmark*, A.J. Annila, A.S. Oja, and J.T. Tuoriniemi, *Low Temperature Laboratory, Helsinki University of Technology, Espoo, Finland*, and H. Weinfurter, *Hahn-Meitner Institute, Berlin, Germany*)

Copper is a model system for a nearest neighbour dominated spin-3/2 ideal FCC antiferromagnet. The topology of this system is such that the magnetic interactions are inherently frustrated. Theoretical predictions for the nuclear magnetic ground state, the magnetic phase diagram, are consequently very sensitive to an accurate treatment of the magnetic interactions (see 1.12).

We have studied the nuclear magnetic phase diagram of Copper by neutron scattering measurements of the magnetic field dependence of the (100) and (0 2/3 2/3) reflections. The results are summarized in the figure and suggests the presence of a high field (100) phase for B along [100] or [110] for $0.12 < B < B_c = 0.26$ mT, intermediate field (0 2/3 2/3) structures around $B = 0.09$ mT for all field directions and a zero field (100) phase. The transition from the high field (100) phase to the intermediate field (0 2/3 2/3) phase is of first order, whereas the lower transition in the opposite direction is associated with a large region ($0.02 < B < 0.06$ mT) of coexistence between the two phases. This transition region can either be interpreted as a first order transition with large hysteresis effects or as a multi-k phase, which continuously transforms from (0 2/3 2/3) to (100).

The high field phase for B along [111] has not been observed yet. At the time of the experiments it was predicted to be (100). A search along high symmetry directions in the $(1\bar{1}0)$ plane was unsuccessful. The structure has recently been predicted to be out of the presently accessible scattering plane (see 1.12).

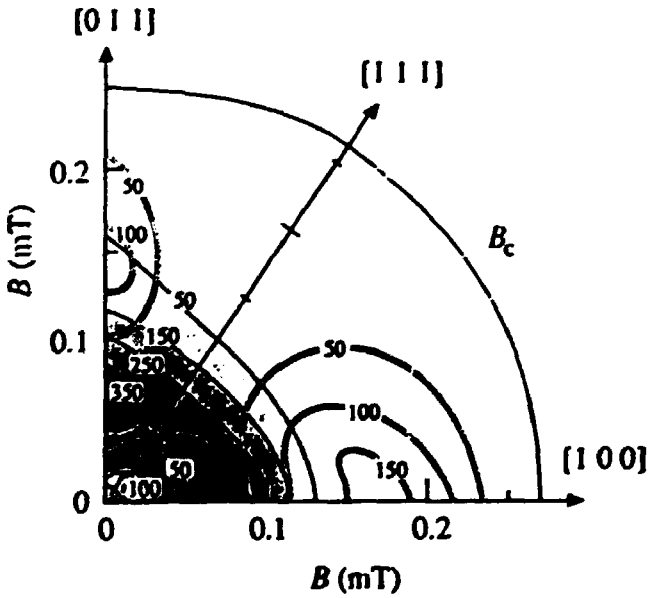

Fig. 1. Neutron intensity diagram as a function of the magnetic field in the $[u\bar{1}\,1]$ plane for temperatures below $T_c = 58$ nK. The numbers on the contour lines are in counts per seconds. (100) intensity is marked by double lines and (0 2/3 2/3) by grey shading.

1.12 Vibrationally Reduced Magnetic Interactions in Cu and the Magnetic Ordering in a Field

(P.-A. Lindgård, *Department of Solid State Physics, Risø National Laboratory, Denmark*)

The nuclear system of Cu seems to be an endless source of surprises. In spite of its basic simplicity the Cu fcc antiferromagnetic systems behaves very non-trivially. This is due to competing interactions. Based on first principles (FP) calculations[1] the nuclear antiferromagnetic structure was predicted to be a simple type I with ordering vector Q =(100) at high magnetic fields and with Q = $(\eta, \eta, 0)$ with $\eta \approx 2/3$ for intermediate fields in the [100] and the [011] directions. This was verified experimentally. However, when the field was turned in the plane containing the mentioned directions, the neutron scattering intensity disappeared for all fields close to the [111] direction.

A soft mode spin wave calculation should be accurate for discussing the onset of antiferromagnetic ordering from the polarized paramagnetic state, since the polarization is about 90% of saturation. It has not previously been exploited in this context. Within this theory the behavior cannot be understood on the basis of the FP Ruderman-Kittel (RK) interaction constants. What is lacking in our understanding for the field in this high symmetry direction? One possibility is that small neglected (anisotropic) forces play a desicive role, another such is that an explanation is possible with an even simpler set of interactions.

In both Cu and Ag the zero point motion yields a fairly substantial mean square displacement. The energy scales of the electronic-, lattice- and nuclear systems are well separated - the nuclear system sees the average of the phonon fluctuations, the electrons can adjust to these. The relative distance between two Cu nuclei fluctuates with a Gaussian distribution e^{-x^2/a^2} with $a^2 \approx 0.06$ Å^2. Assuming a free RK-function and using a folding with this distance distribution gives a reduction of the interaction constants as shown in Fig. 1. J_1 is on a linear part and is not modified, but J_2 and in particular J_3 are reduced by 20% and 40% respectively - it is difficult to estimate the reduction for the more distant neighbours.

A soft mode calculation, with for simplicity, the reduced interaction scheme $J_1 = -10J_2$ and $J_n = 0$ for $n > 2$ and the experimental strength parameter R=-0.42, was found to yield the requested behavior for the onset ordering as a function of field direction ϕ. Here ϕ is 54.74° for the [111] direction and 0 and 90° for the [100] and [011] directions. The onset order was found to be type I except for field directions in the interval $50° < \phi < 70°$ in which the order can be described as $(t + \delta, t - \delta, 0)$ with $t \approx 2/3$ and where $\delta \approx 0.05$ and slightly varying. Tests have shown that this behavior is robust for variations in R and in J_2, and also for inclusion of further reduced neighbor interactions. An observation of such a structure might indicate that the interaction scheme in Cu is even simpler and therefore more interesting than deduced from the FP-calculated RK-interaction.

[1] P.-A. Lindgård, X.-W. Wang, and B.N. Harmon, (1986). J. Magn. & Magn. Mater. 54-57, 1052.

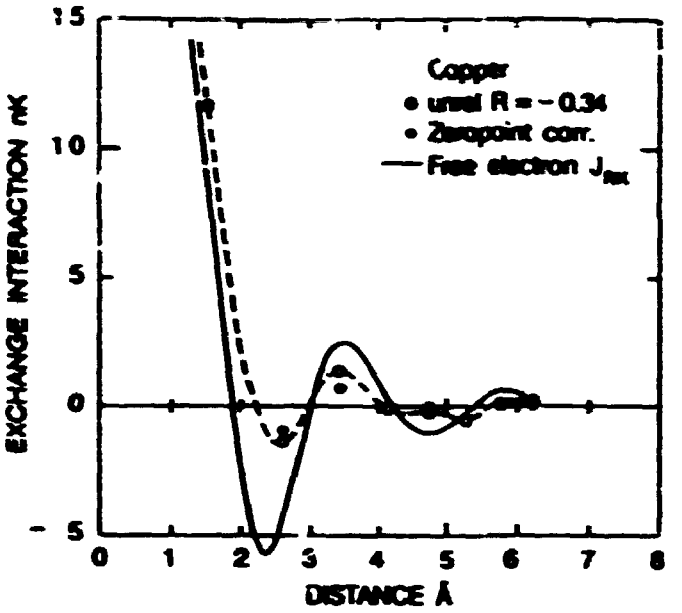

Fig. 1. Ruderman-Kittel interaction in Cu, (line) free electron approximation, ○ calculated from first principles [1] and ● same reduce by the zero-point vibrational motion.

1.13 Theory of Field Induced Magnetic Ordering in the Singlet Ground State System $CsFeBr_3$

(B. Schmid, B. Dorner, *Institut Laue-Langevin, Grenoble, France*, and P.-A. Lindgård, *Department of Solid State Physics, Risø National Laboratory, Denmark*)

Neutron diffraction experiments have been performed on the singlet ground state system $CsFeBr_3$[1] and have showed that onset of antiferromagnetic order with ordering vector at the K-point is obtained in a uniform magnetic field of 4.1 T at a temperature of 1.41 K on copper. The theory in the random phase approximation(RPA) and the correlation theory was previously developed[2] for the similar system $CsFeCl_3$, which shows onset of incommensurate ordering near the K-vector. We have calculated the renormalization of the magnetic excitation energies and the critical field H_c for $CsFeBr_3$ using the RPA theory. We find that the fully self-consistent calculation becomes very unstable and numerically difficult to control at $H > 4$ T. It is therefore difficult to determine H_c accurately. The energy gap in the dispersion curve is very small at these fields. The induced magnetization M and the renormalization parameter Q have competing effects on the energy gap. This is the sourse of the problem. The critical field is found to be around $H_c \approx 4.3$ T. As a next step, it is planned to include correlation effects using the correlation theory[3].

[1] B. Dorner, D. Visser and M. Steiner, (1990). Z. Phys. B 81, 75.
[2] P.-A. Lindgård, (1986). J. Magn. & Magn. Mater. 54-57, 1227.
[3] P.-A. Lindgård, (1983). Phys. Rev. B 27, 2980.

1.14 Calculation of the Ruderman–Kittel Interaction and the Nuclear Magnetic Ordering in Silver

(B.N. Harmon, *Ames Laboratory-USDOE, Department of Physics, Iowa State University, Ames, USA*, X.-W. Wang, *Physics Department, Florida International University, Miami, Florida, USA*, and P.-A. Lindgård, *Department of Solid State Physics, Risø National Laboratory, Denmark*)

The interactions among nuclear magnetic moments in crystal lattices are simple and understood. However, the manifestations of these interactions in terms of phase transitions, ordering structures, and correlations are rich and complex.

For Ag the conduction electron hyperfine interaction with the nuclei is much stronger than in Cu and the Ruderman-Kittel interaction is expected to dominate. However, quantum effects are expected to be larger in Ag (spin 1/2) than in Cu (spin 3/2). The smaller moment reduces in particular the dipolar interactions in Ag by two orders of magnitude relative to those of Cu. For Ag relativistic effects are important. The charge density at the nucleus is ~2.4 times larger when evaluated relativistically. However, the proper relativistic hyperfine coupling constant is not simply given by the charge density, but involves the integral of the large and small component of the relativistic wave function and it is only a factor of ~1.4 larger than the non-relativistic coupling strength. We used a self-consistent, scalar-relativistic linear augmented plane wave method to evaluate the first nine electronic energy bands and eigenfunctions. The E_k's were evaluated at 408 points in the irreducible 1/48th of the Brillouin zone. The $J(\mathbf{q})$ were then obtained at 21 different q-vectors and these values were least squares fitted to a high precision with a Fourier series, which gives the $J(R_n)$'s .

The $J(R_n)$ constants are listed in table 1 along with the corresponding values from the free electron approximation with the $J(R_n)$ scaled to give the same nearest neighbor constant. For comparison the first principles (FP) values for Cu are also included. As for Cu the primary difference relative to the free electron case is the more dominant nearest neighbor interaction for the FP-calculation. The dimensionless factor, $R = \sigma_n J(R_n)/\mu_0(\gamma\hbar)^2\rho$ determined by NMR techniques is found to have a value of -2.5±0.5, whereas the uniform susceptibility gives -1.7[1]. Using the relativistic calculation we obtain R=-2.26.

In order to determine the magnetic structure, into which the system orders by a second-order transition (in zero field) from the paramagnetic phase, we need to calculate the largest eigenvalue of the wave vector dependent suspectibility matrix $\chi^{\alpha\beta}_{\mathbf{q}}$. The transition temperature is obtained using the relation $< I^{\alpha}_{\mathbf{q}} I^{\beta}_{-\mathbf{q}} >= k_B T \chi^{\alpha\beta}_{\mathbf{q}}$. The dipole part is calculated by the Ewald method.

Assuming a continuous transition the following results are obtained. For R=-2.26 the ordering vector (star) is at the X-point with $\mathbf{Q}$=(0,0,1)$2\pi/a$. A contour plot of the maximum susceptibility component is shown of Fig. 1. One finds T_N=0.64 T_N(MF)=1.50 nK, and a Curie temperature of Θ=-4.50 nK. A calculation for R=-1.7 yields T_N=0.63 T_N(MF)=1.17 nK, and a Θ=-3.50 nK. The experimentally quoted Curie temperature is $\Theta_{exp} = -4.9 \pm 0.5$ nK and the transition temperature is T_N(exp)=0.56±0.06 nK. This is significantly lower than obtained by the correlation theory, while very good agreement

was obtained for Cu. This might indicate that the ordering in Ag, the ideal FCC, I=1/2 system is more intricate than apparent at first sight - it might well herald a discontinuous transition - or other interesting consequences of the quantum nature of the system.

[1]P.J. Makonen and S. Yin, (1991). J. Low Temp. Phys. (1991) **85**, 25.

n	R_n	$J(R_n)_{FP}$Ag	$J(R_n)_{free}$ Ag	$J(R_n)_{FP}$ Cu
1	1,1,0	-1.335	-1.335	-11.67
2	2,0,0	0.193	0.600	1.41
3	2,1,1	-0.193	-0.331	-1.31
4	2,2,0	-0.031	-0.041	0.11
5	3,1,0	0.077	0.169	0.25
6	2,2,2	0.118	0.028	0.61
7	3,2,1	-0.009	-0.095	-0.06
8	4,0,0	-0.055	-0.057	-0.18
9	4,1,1	-0.008	0.031	-

Table 1: The first-principles $(R_n)_{FP}$ RK-interaction parameters in nK for Ag, compared with the free electron approximation $(R_n)_{free}$ scaled to give the same near-neigbor constant.

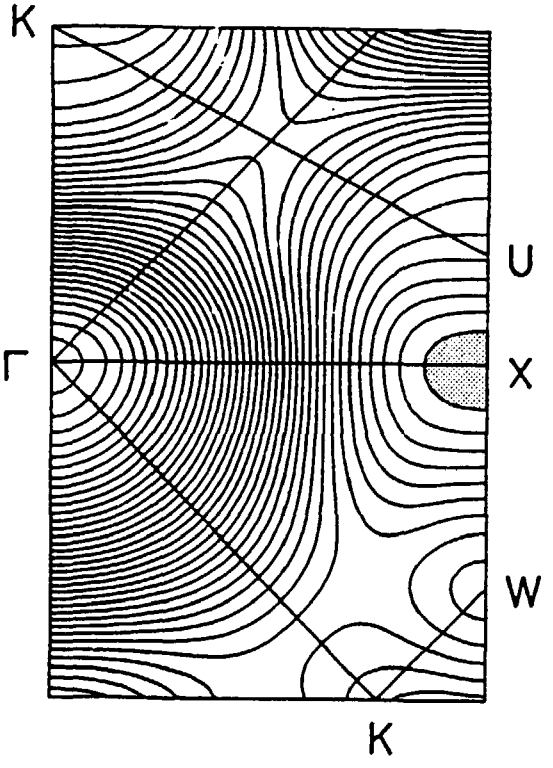

Contour plot all FCC symmetry points of the maximum susceptibility component. Upper part [1 $\bar{1}$ 0] plane, lower part [0 1 0] plane, separation 0.5 nK. Observe the clear maximum at the χ point (0 0 1)2π/a of 7.4 nK for R = -1.7. This is further enhanced for larger | R | values.

1.15 Magnetic Dynamics of $La_{2-x}Sr_xCuO_4$

(T.E. Mason, G. Aeppli, S.W. Cheong, *AT&T Bell Laboratories, Murray Hill, NJ, USA*, H. Mook, *Oak Ridge National Laboratory, Oak Ridge, TN, USA*, S.M. Hayden, *H.H. Wills Physics Laboratory, University of Bristol, Bristol, UK*, P.C. Canfield and Z. Fisk, *Los Alamos National Laboratory, Los Alamos, NM, USA*, K.N. Clausen, *Department of Solid State Physics, Risø National Laboratory, Denmark*, and J.L. Martinez, *Institute Laue-Langevin, Grenoble, France*)

Studies of the magnetic dynamics of $La_{2-x}Sr_xCuO_4$ have been carried out with particular emphasis on a sample with x=0.14 which becomes superconducting at T_c = 33 K. This material exhibits incommensurate peaks in the inelastic magnetic neutron scattering with the same geometry as found for a metallic (but not superconducting) sample with x=0.075[1]. In both cases the peak in $\chi''(\mathbf{Q},\omega)$ is shifted from the commensurate position, (π,π) (in the notation of the square lattice of the CuO_2 planes), to $(\pi,\pi) \pm \delta(\pi,0)$ and $(\pi,\pi) \pm \delta(0,\pi)$ (see inset to Fig. 1). The magnitude of the incommensuration δ increases with doping x with δ being approximately $2x$.

Figure 1 shows a collection of constant $\hbar\omega$ scans along the trajectory shown in the inset for T = 35 K ($> T_c$ = 33 K) obtained on TAS6. At the lowest energy probed, $\hbar\omega$ = 3.5 meV, there are two sharp peaks at $(\pi,\pi) \pm \delta(\pi,0)$ and $(\pi,\pi) \pm \delta(0,\pi)$ where δ = 0.245 ± 0.004. As the frequency is increased the peaks become somewhat broader, which implies shorter correlation lengths for higher energy fluctuations. The peak intensity is roughly independent of frequency, so that the q-integrated spectral weight must rise with $\hbar\omega$. The lines in Fig. 1 correspond to a least-squares fit to a form for $\chi''(\mathbf{Q},\omega)$ that describes the paramagnetic scattering from the intinerant antiferromagnet Cr[2] (appropriately modified to reflect the two dimensional Fermi surface of $La_{1.86}Sr_{0.14}CuO_4$).

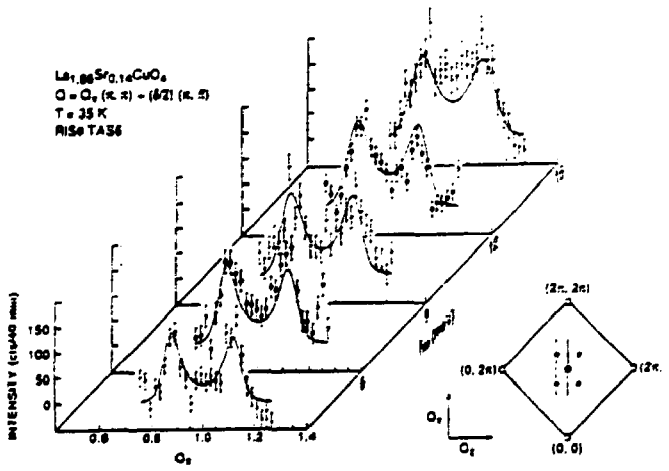

Fig. 1. Magnetic scattering at T = 35 K ($>T_c \simeq$ 33 K) obtained on TAS6. The inset shows reciprocal space with solid circles indicating locations near (π,π) with maximal magnetic response and open circles corresponding to (nuclear) Bragg points for a square lattice. The main figure consists of a series of background corrected constant energy scans, collected along the reciprocal space trajectory indicated by a dashed line in the inset.

The temperature dependence of the magnetic response is summarized in Figure 2. The top panel, a), shows the T dependence of the raw scattered intensity (closed circles) for $\hbar\omega = 4$ meV and $\mathbf{Q} = \mathbf{Q}_o = (\pi,\pi) - \delta(0,\pi)$. The gradual upward trend of the signal stops abruptly at T_c, below which there is a precipitous decline. That this decline corresponds to a substantial reduction of the magnetic response is obvious from our results for $\chi''(\mathbf{Q}_o,\omega)$ (open circles) obtained via the fluctuation dissipation theorem from the raw data, corrected for the constant background indicated by the dashed line. Figure 2b) shows the temperature dependence of κ^2, a parameter extracted from the least-squares fits mentioned above which is proportional to the zero frequency limit of the inverse correlation length squared. Figure 2c) shows the temperature dependence of the gap parameter, 2Δ, which characterizes the energy below which the decrease in scattering shown in panel a) becomes apparent. Although the actual scale for 2Δ is somewhat model dependent the evolution below T_c is well described by the temperature evolution of a BCS order parameter. This means that the development of a gap in the quasi-particle excitation spectrum, which occurs in all superconductors, is accompanied by a corresponding gap in the spin fluctuations in $La_{1.86}Sr_{0.14}CuO_4$.

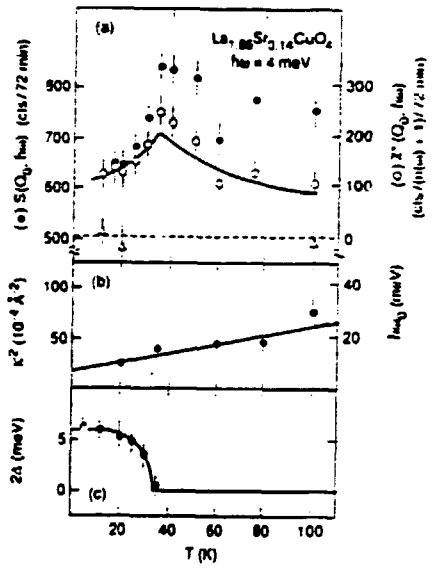

Fig. 2. a) Temperature dependence of raw intensity for $\hbar\omega = 4$ meV, with $\mathbf{Q} = \mathbf{Q}_o = (\pi,\pi) - \delta(0,\pi)$ (solid circles) and $Q = (0.55\pi, 1.15\pi)$ (open triangles). Open circles represent $\chi''(\mathbf{Q}_o,\omega)$ obtained by application of the fluctuation dissipation theorem to the data indicated by the solid circles, where the background is identified with the dashed line through the open triangles.
b) Value of κ^2 and the corresponding characteristic energy $\hbar\omega_o$ obtained from the fit described in the text.
c) Value of 2Δ obtained from fits to the data.

[1] S.W. Cheong, G. Aeppli, T.E. Mason, H. Mook, S.M. Hayden, P.C. Canfield, Z. Fisk, K.N. Clausen and, J.L. Martinez, (1991). Phys. Rev. Lett. **67**, 1791.
[2] D.R. Noakes, T.M. Holden, E. Fawcett, and P.C. de Camargo, (1990). Phys. Rev. Lett. **65**, 369.

1.16 New Studies of the Magnetic and Structural Properties of $MgCu_2O_3$ and $Mg_{1-x/2}Li_xCu_{2-x/2}O_3$

(M. Winkelmann and H.A. Graf, *Hahn-Meitner Institute, Berlin, Germany*, N.H. Andersen, *Department of Solid State Physics, Risø National Laboratory, Denmark*)

The discovery of high T_c superconductivity in Cu-O systems has stimulated renewed interest in the magnetic and electrical properties of simple oxygen containing Cu compounds. One particular example for a simple ternary Cu-O system is $MgCu_2O_3$. The Cu^{+2} ions are surrounded by a distorted oxygen octahedron similar to the La_2CuO_4-type. The equatorial Cu-O planes of the distorted (elongated) octahedra are connected via common edges to form corrugated quasi-two-dimensional layers. The system orders antiferromagnetically at $T_N \approx 90$ K. From the magnetic reflections found in the neutron powder spectra, a simple collinear model of the spin arrangement, which is compatible with the gross features of the magnetic intensity pattern[1], could be derived. We are now extending our studies to Li doped $MgCu_2O_3$ powder samples and have started to investigate differently doped powder samples. Neutron experiments on single crystals are under way.

The doping with Li leads to a drastic decrease of the Néel temperature. Magnetic susceptibility measurements show, that the 3D magnetic order is suppressed down to $T_N < 2$ K for 0.15 % Li contribution. At the same time the conductivity increases by a factor of 100. All samples, however, stay semiconductors.

Figure 1 shows the temperature dependence of the magnetic $(\frac{1}{2}\frac{1}{2}0)$ reflection, measured on the neutron spectrometer TAS1. While T_N decreases, the ordered magnetic moment, which was determined by Rietveld refinement, becomes smaller (0.35 μ_B for the undoped sample, 0.11 μ_B for the 4 % Li sample). The solid lines represent fits of the Brillouin function to the data. It can be seen, that this function fails to describe the magnetization. The Li (hole doping) leads to a depression of the magnetic order, similar to the high T_c materials in the low doping regime.

When preparing the samples it was observed, that an excess of CuO was necessary to get single phase samples. We performed measurements on the powder diffractometer at TAS3, for detailed structural analyses of these powder samples (Fig. 2). The Rietveld refinement to the data leads to the conclusion, that 10 to 15 % of the Mg sites are occupied by Cu ions. This surprising result was confirmed by additional measurements performed at smaller wavelengths and up to higher 2Θ values on the powder diffractometer D2B at the Institute Laue-Langevin, Grenoble. The Li dopant was found to be about equally distributed over the Mg and Cu sites (the total Li content was determined by a chemical analysis).

To study the unexpected Mg/Cu disorder in more detail, a small single crystal of $MgCu_2O_3$, grown from a KF flux, was investigated on a four circle X-ray diffractometer. The refinement of 362 symmetry inequivalent reflections clearly showed, that a considerable part of Mg ions are substituted by Cu (≈ 20 %). These results indicate that the $MgCu_2O_3$ structure may be stabilized by Cu ions on Mg sites. This is unusual, since the Mg sites represent centers of almost symmetric oxygen octahedra, whereas normally, the Cu^{2+}-ions prefer Jahn-Teller distorted coordination polyhedra.

It is not yet clear, how the magnetic ground state of $MgCu_2O_3$ is influenced by the Cu ions on Mg sites. As a next step in the analysis of the magnetic properties, the spin structure of $MgCu_2O_3$ will be determined in detail by a neutron diffraction study on single crystals.

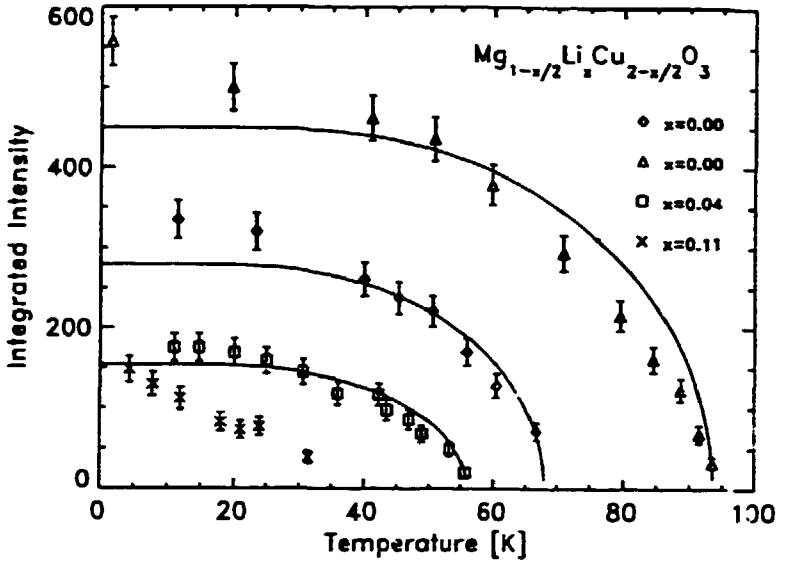

Fig. 1. Temperature dependence of the magnetic $(\frac{1}{2}\frac{1}{2}0)$ reflection (scaled to the (001) nuclear peak) for several doped and undoped samples. The solid lines represent fits with the Brillouin function.

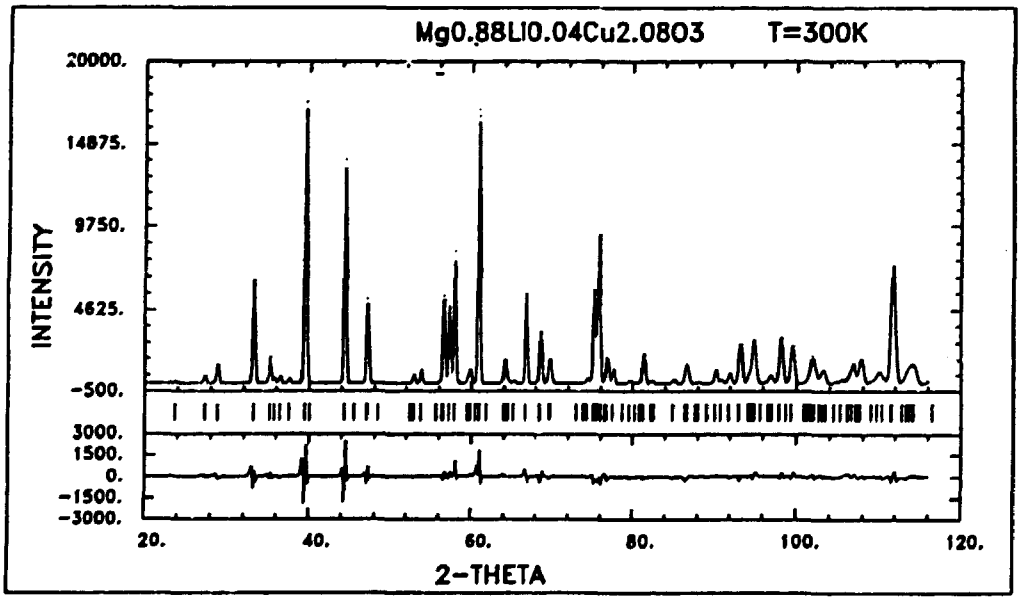

Fig. 2. The neutron powder pattern of the 4 % Li doped $MgCu_2O_3$ sample measured on TAS3. The lower part shows the difference between measured and refined patterns.

[1] T. Zeiske, H.A. Graf, H. Dachs, and K.N. Clausen, (1989). Solid State Comm. **71**, 501.

1.17 Local Oxygen Ordering in Superconducting $YBa_2Cu_3O_{6.41}$ Observed by Neutron Diffraction

(N.H. Andersen, *Department of Solid State Physics, Risø National Laboratory, Denmark*, T. Zeiske, *Hahn-Meitner Institute, Berlin, Germany*, R. Sonntag, *Universität Tübingen, Germany*, D. Hohlwein, *Hahn-Meitner Institute, Berlin, Germany and Universität Tübingen, Germany*, and T. Wolf, *Kernforschungszentrum Karlsruhe, Germany*)

The superconducting transition temperature T_c of $YBa_2Cu_3O_{6+x}$ (YBCO) is known to depend not only on the oxygen stoichiometry[1], but also on the degree of oxygen order[2]. In well equilibrated samples characteristic plateaus exist at $T_c = 93$ K for $0.8 < x < 1.0$ and $T_c = 58$ K for $0.45 < x < 0.65$. For $x < 0.3$ superconductivity disappears. Further, it is believed that superconductivity is dependent on the small orthorhombic distortion of the tetragonal structure, which is driven by the oxygen ordering due to alignment of CuO-chains in the basal plane of the structure. Orthorhombic phases are observed below a phase line in (x, T)-phase space for low T and $x > 0.3$[3]. From experimental and theoretical studies it has been established that two orthorhombic phases, Ortho-I and Ortho-II, exist. Ideal Ortho-I phase corresponds to oxygen stoichiometry $x = 1.0$, and consists of full Cu-O chains along the b-axis in the basal plane and all chains being present. Ideal Ortho-II corresponds to $x = 0.5$ with every second CuO-chain missing the oxygen. For stoichiometries deviating from the ideal ones Ortho-II phase diluted with tetragonal or Ortho-I domains, or Ortho-I phase diluted with Ortho-II-domains are expected. From Monte Carlo simulations of these oxygen ordering properties the CuO-chain structure phases have been brought in close relation to the T_c versus x variation by a phenomenological model[4].

The presence of Ortho-II phase structures have been established mainly from electron diffraction studies, but also a single crystal X-ray diffraction observation of diffuse Ortho-II superstructure reflections from an $x = 0.7$ bulk sample has been reported. In the low oxygen stoichiometry range, close to the phase line separating orthorhombic and tetragonal structures, the presence of Ortho-II phase has not been verified by bulk structural probes, and no experimental details about the size of the ordered domains have been obtained.

In the present study[5] we have carried out a neutron diffraction study of a single crystal YBCO sample with oxygen stoichiometry $x = 0.4$ and $T_c = 38$ K, as determined from the lattice parameters and AC-susceptibility, respectively. The single crystal was grown from a flux of CuO-BaO in an alumina crucible by slow cooling. The size of the sample is $6\times3\times2$ mm^3. After annealing in oxygen the cystal showed a T_c of 87 K. To develop the Ortho-II phase, the crystal was reduced by stepwise cooling under controlled oxygen equilibrium pressures. The experiments were carried out at the TAS1 triple axis spectrometer at the DR3 reactor at Risø. Special care was taken to suppress the higher harmonics of the wavelength used, $\lambda = 4$ Å, by use of two Be-filters. To improve the signal-to-noise ratio and to separate inelastic scattering events, the spectrometer was operated in the elastic mode. Superstructure reflections (hkl) were observed with $h = (2n + 1)/2$ and $k, l, n =$ integers. The profiles of the $(\frac{1}{2}\ 0\ 0)$ superstructure reflection along different directions of reciprocal space are shown in Fig. 1. In all directions, the width of the diffuse superstructure reflection is much broader than the instrumental resolution, which was determined

from scans through the (1 0 0) and the (0 0 l) (l = 1, 2 and 3) reflections. The average size of the domains with Ortho-II structure may be derived from the diffuse peak width of gaussian shape, $\xi = 1/\Delta_{FWHM}$. The results show a strong anisotropy in the correlation length of the Ortho-II phase in $YBa_2Cu_3O_{6.4}$ (see the figure). The tendency of the system to build Cu-O chains is reflected by a correlation length $\xi_b = 24b$ (90 Å) in the chain direction which is more than twice as large as the in-plane correlations perpendicular to the chains, $\xi_a = 10a$ (40 Å). In the c-direction there is only correlations to nearest and next-nearest basal planes, $\xi_c = 2c$ (22 Å), indicating that the ordering is predominatly two-dimensional. However, the presence of orthorhombic splitting was verified by high resolution neutron diffraction measurements. By scaling the integrated intensity of the superstructure reflection with that from a Bragg reflection, about 60 % of the sample may be estimated having the Ortho-II-structure. This is interesting in relation to the phenomenological model, presented in ref. 4, relating T_c to the percentage of oxygen sites in Ortho-II domains of a certain minimal size. According to this model the sample should have a $T_c \approx 35$ K (60 % of 58 K) in close agreement with the experimental observation of 38 K.

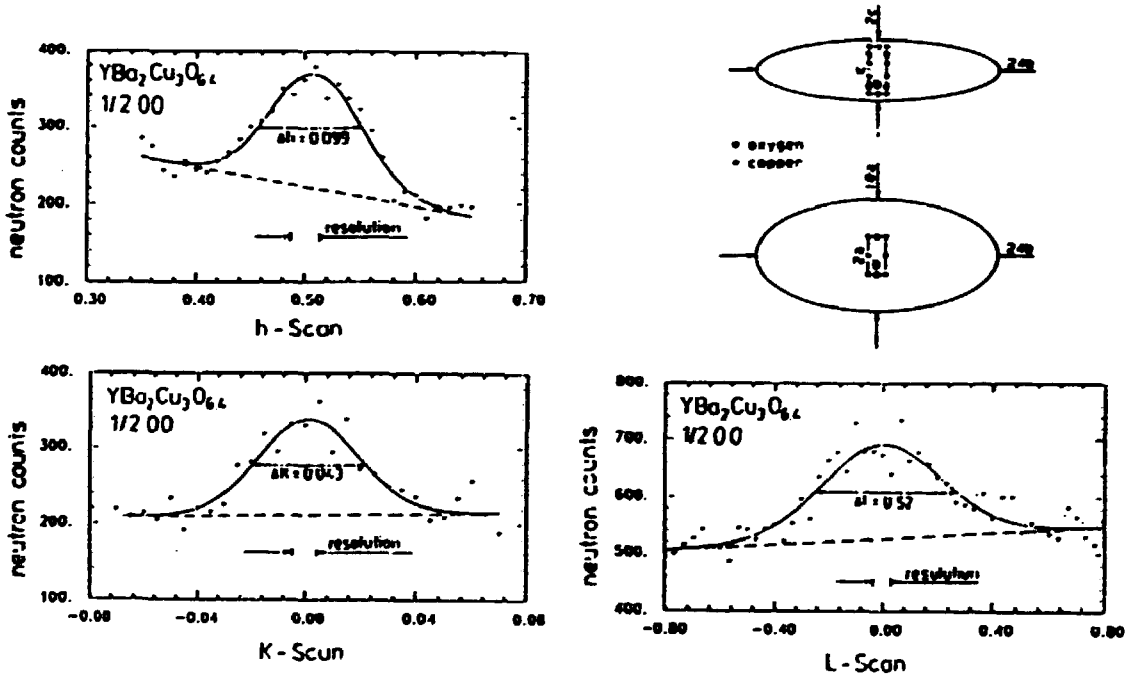

Fig. 1. Profiles of the ($\frac{1}{2}$00) superstructure reflection along the main axes in reciprocal space and corresponding average dimensions of the Ortho-II domains in real space (from ref. 5)

[1] R.J. Cava, A.W. Hewat, E.A. Hewat, B. Batlogg, M. Marezio, K.M. Kabe, J.J. Krajewski, W.F. Peck Jr., and L.W. Rupp Jr., (1990). Physica C **165**, 419.

[2] J.D Jorgensen, S. Pei, P. Leightfoot, H. Shi, A.P. Paulikas, and B.W. Veal, (1990). Physica C **167**, 571.

[3] N.H. Andersen, B. Lebech, and H.F. Poulsen, (1990). Physica C **172**, 31.

[4] H.F. Poulsen, N.H. Andersen, J.V. Andersen, H. Bohr, and O.G. Mouritsen, (1991). Letter to Nature **349**, 594.

[5] T. Zeiske, R. Sonntag, D. Hohlwein, N.H. Andersen, and T. Wolf, (1991). Letter to Nature **353**, 542.

1.18 Monte Carlo Simulations of Oxygen Ordering in the High T_c Superconductor $YBa_2Cu_3O_{6+x}$

(H.F. Poulsen, T. Fiig, N.H. Andersen, and P.-A. Lindgård, *Department of Solid State Physics, Risø National Laboratory, Denmark*, J.V. Andersen, H. Bohr, and O.G. Mouritsen *The Technical University of Denmark, Lyngby, Denmark*)

As discussed in 1.17, it has become evident, that the superconducting transition temperature, T_c, of $YBa_2Cu_3O_{6+x}$ (YBCO) depends strongly on the oxygen stoichiometry x ($0 < x < 1$, see Fig. 1), and that the specific ordering of the oxygen in the basal CuO-planes has significant influence on T_c. These CuO-planes are widely separated (11.7 Å), and the ordering properties may to a good approximation be treated within a 2D-ordering model, the *ASY*mmetric *N*ext *N*earest *N*eighbour *I*nteraction (*ASYNNNI*) model, given by the Hamiltonian:

$$\mathcal{H} = -V_1 \sum_{i,j}^{NN} n_i n_j - V_2 \sum_{i,j}^{NNN(Cu)} n_i n_j - V_3 \sum_{i,j}^{NNN} n_i n_j \qquad (1)$$

where $V_1 < 0$ is the nearest neighbour (NN) interaction, and $V_2 > 0$ and $V_3 < 0$ are anisotropic next-nearest neighbour ($NNN(Cu)$ and NNN) interactions as indicated in the inset of Fig. 2, and $n_i = 0,1$ is an occupational variable. The ASYNNNI model has been quite successful in describing the oxygen ordering and the thermodynamic properties of YBCO. It predicts two orthorhombic ordered structures, Ortho-I and Ortho-II, ideally corresponding to oxygen concentrations $x = 1.0$ and $x = 0.5$, respectively. These structures, shown in Fig. 2, consist of full Cu-O chains along the b-axis. For $x = 1.0$ all chains are full, for $x = 0.5$ every second chain is missing the oxygen. For finite temperature and for oxygen stoichiometries deviating from $x = 1.0$ and 0.5, disordering occurs with broken or missing chains and occupation on the available sites on the a-axis. The resulting structural phase diagram is shown schematically in the inset of Fig. 1.

The significance of the oxygen ordering for the superconducting transition temperature T_c has spurred significant interest in studying these properties. However, the predominant 2D-character of the basal plane oxygen ordering makes it difficult to obtain detailed quantitative information from neutron and X-ray structural studies. With reference to the success of the ASYNNNI model in describing many of the the structural and thermodynamic properties of YBCO in a quantitatively correct way, the system should be ideal for 2D Monte Carlo simulation studies. From a Monte Carlo simulation study on the ASYNNNI model (Eq. 1) the details of the equilibrium oxygen ordering for different oxygen stoichiometries have been determined, and the defect ordering configurations have been related to the superconducting transition temperature, T_c, by a minimal model[1]. Within this model it is assumed that the transfer of electrons to the CuO-basal planes, creating the necessary holes in the superconducting CuO_2-planes, is only effective if the oxygen atoms in the basal plane are included in clusters of either Ortho-I or Ortho-II symmetry having a minimal size. In direct terms T_c is expressed as:

$$T_c = \frac{1}{N_{tot}} \left(93\,K \sum_{i}^{Ortho-I} N_i + 58\,K \sum_{i}^{Ortho-II} N_i \right) \qquad (2)$$

where N_{tot} is the total number of oxygen sites, and the summations over N_i sites are restricted to those sites being members of a Minimal Size Clusters of Ortho-I or Ortho-II, respectively. The weight factors 93 K and 58 K correspond to the experimental T_c values found for the ideal Ortho-I and Ortho-II structures. The Minimal Size Clusters giving agreement with the data are the 4×4 Ortho-I and the 8×8 Ortho-II unit cells shown in Fig. 2.

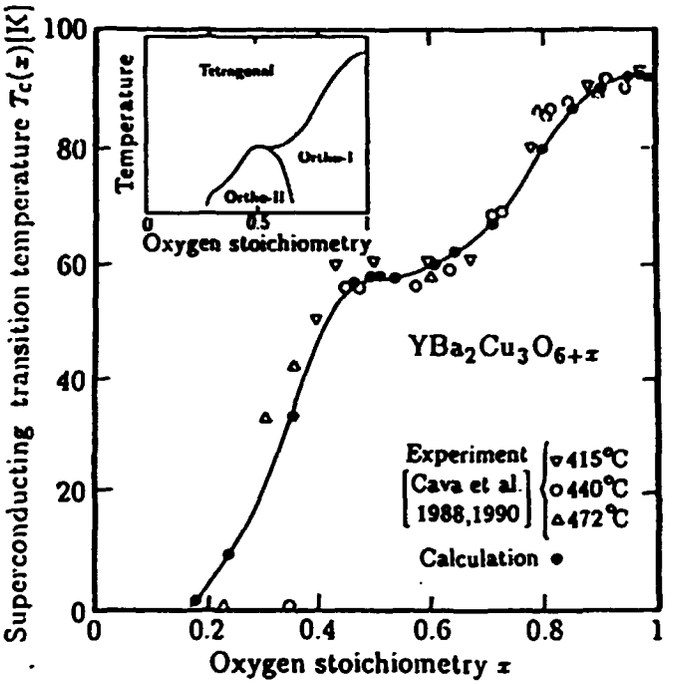

Fig. 1. The variation of the superconducting transition temperature, T_c, with oxygen stoichiometry, x, in $YBa_2Cu_3O_{6+x}$. Open symbols are experimental data from the literature obtained by annealing samples at different temperatures (Cava et al., see ref. 1). Solid circles and the solid line (guide to the eye) are results from the minimal model calculation. The inset shows schematically the structural phase diagram encompassing a tetragonal phase with oxygen order and two orthorhombic oxygen-ordered phases (Ortho-I and Ortho-II) (from ref. 1)

Further, Monte Carlo simulations have been used to study the dynamics in the oxygen ordering process of samples quenched from disordered states at high temperatures[2]. The formation of ordered domains is found to obey dynamical scaling. For a sample with $x = 0.41$ the areas of ordered domains of Ortho-II as function of time are found to scale with the time dependent increase of experimental T_c values. That is $\Delta T_c \propto A(t)^{-1}$, where ΔT_c is the deviation from the equilibrium T_c value, and $A(t)$ is the average area of the Ortho-II domains at time t. The significance of specific ordered oxygen domains for superconductivity is therefore evident both in the equilibrium and the dynamic properties.

The significance of oxygen ordering for superconductivity has been studied further in YBCO based systems where part of the Cu-atoms in the basal plane have been substituted. Such systems $YBa_2Cu_{3-y}M_yO_{6+x}$ have been realized and studied experimentally with M = Co, Fe, and Al. These cations have a higher oxidation level than Cu in the basal plane and would therefore prefer a higher oxygen coordination. As a consequence the occupation of the oxygen sites on the *a*-axis next to the M-atoms (*cf.* Fig. 2) should increase and the orthorhombic order decrease. There has been several experimental studies of the superconducting and structural properties as function of M-substitutions. For all substitutions T_c is observed to decrease with y. The structural results are more unclear and ambigous, but they show as a general trend that the orthorhombic distortions disappear for $y > 0.1$, and that the M-atoms have higher oxygen coordination than Cu.

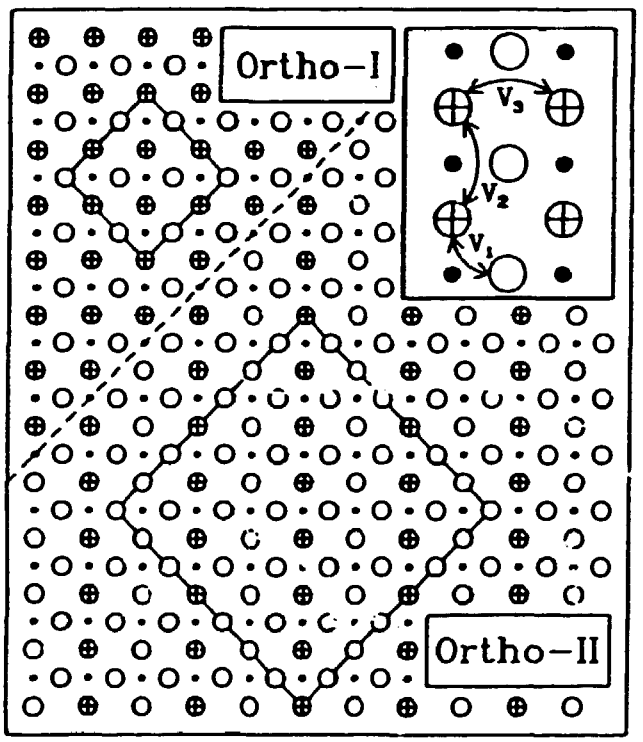

Fig. 2. Schematic illustration of the two types of orthorhombic oxygen order (Ortho-I and Ortho-II) in the basal CuO-plane of $YBa_2Cu_3O_{6+x}$. The dashed line separates the Ortho-I and Ortho-II domains. ○ denotes sites available for oxygen atoms and ⊕ denotes occupied oxygen sites. The Cu-atoms are indicated by •. The 4×4 and 8×8 squares define the Minimal Size Clusters of Ortho-I and Ortho-II types of oxygen order, respectively. The inset defines the pair interaction constants, V_1, V_2, and V_3, of the ASYNNNI model which describes the oxygen ordering process (from ref. 2).

We have also carried out Monte Carlo simulations on a modified ASYNNNI model, which considers the structural observations on M-substituted YBCO in a simple way. In order to increase the oxygen coordination around the M-atoms the repulsive nearest-neighbor-interaction constant V_1 in Eq. 1 is reduced on these sites. In the Monte Carlo studies

we have assumed that the M-atoms are randomly substituted, and a constant external chemical potential, as found for undoped YBCO with $x \simeq 1.0$, was used in order to adjust to an experimental condition of samples being prepared under identical oxygen pressures. This model accounts in a semi-quantitative way for experimental structural data such as total oxygen stoichiometry, M-atom oxygen coordination numbers, and the limit of M-substitution, $y < 0.1$, for which orthorhombic phase is observed. Differences between the data of different M-atom substitutions may be accounted for by small changes of V_1. Further, using the above mentioned minimal model, relating T_c versus x in pure YBCO (Eq. 2 and Fig. 1) to the specific Minimal Size Clusters, shown in Fig. 2, we obtain a T_c versus M-substitution y behavior, which is in surprisingly good agreement with the experimental observations. Also, the experimental results of T_c for different M-substitutions may be accounted for by changing the V_1 parameter in a similar way as for the structural results.

Despite this success of the 2D ASYNNNI model in describing many of the experimental observations in YBCO, there are structural features which are not fully understood: The 3D structural phase transformation between the tetragonal disordered phase and the orthorhombic ordered phases, and its association with the formation of twin domains. The stress energy connected with the creation of these domains will undoubtly have both intra- and interplanar components. Because the finite size phenomena associated with the twin domain formation may have important influence on the structural ordering process it has become urgent to include these additional forces in the description of the oxygen ordering process. One way of achieving this is by adding a single attractive inter-plane term to the 2D ASYNNNI model Hamiltonian (Eq. 1). Such a model has been termed "the three dimensional ASYNNNI model".

A Monte Carlo simulation study of the equilibrium behaviour and the dynamics of the 3D ASYNNNI model for a finite system has been initiated. Most notably we wish to estimate at what temperatures and x-values the stress energy is sufficiently powerfull to drive the existing 2D structural phases to have 3D registry. The study is carried out on a Connection Machine using a parallel updating algorithm taking advantage of the underlying architecture of this machine. The simulations performed constitute the first work done on the 3D ASYNNNI model. The preliminary results indicate that a pseudo phase transition separating the disordered tetragonal phase from 2D-ordered orthorhombic phases exists at higher temperatures than predicted by the 2D ASYNNNI model. In this pseudo phase the correlation length along the c-axis is negligible. At a lower temperature we obtain a second phase transition, which can be associated with the divergence of the correlation length along the c-axis. We have attributed the word pseudo to the upper phase transition and the 2D-ordered phase because the split between the two transition temperatures would disappear in the thermodynamic limit. However, the effect, which is due to the large difference between the interaction strength in the plane and perpendicular to the plane, is genuine in a finite system of the size corresponding to the twin domains of the experimental sample. Below the lower transition temperature we obtain a truely 3D ordered system.

[1] H.F. Poulsen, N.H. Andersen, J.V. Andersen, H. Bohr, and O.G. Mouritsen, (1991). Letter to Nature **349**, 594.
[2] H.F. Poulsen, N.H. Andersen, J.V. Andersen, H. Bohr, and O.G. Mouritsen, (1991). Phys. Rev. Lett. **66**, 465.

1.19 Antiferromagnetism and Metallic Conductivity in $Nb_{12}O_{29}$.

(R.J. Cava, B. Batlogg, J.J. Krajewski, P. Gammel, W.F. Peck Jr., and L.W. Rupp Jr. *AT&T Bell Laboratories, Murray Hill, USA*, H.F. Poulsen *Department of Solid State Physics, Risø National Laboratory, Denmark*)

At the heart of the controversy about the microscopic origin of superconductivity in copper oxide superconductors is the question of whether or not the antiferromagnetism associated with the single-hole $Cu^{2+}3d^9$ state is of fundamental importance. To test whether this unconventional spin-mediated superconductivity might be electron/hole symmetric, oxides of the elements with single *d*-orbital electrons, such as $Ti^{3+}(3d^1)$, $Nb^{4+}(4d^1)$, and $W^{5+}(5d^1)$ are of particular interest. Localized magnetic spin states and magnetic ordering have never been observed previously in transition-metal oxides with one or two electrons in the 4*d* or 5*d* states, because of the preference for conventional *d*-band metallic conductivity or for metal-metal bonding. In exploring the possibility of a $d^1 - d^9$ and ferroelectricity-superconductivity relationship in oxides we have found that $Nb_{12}O_{29}$, a material with a 'crystallographic shear' structure, displays simultaneously both metallic conductivity, a signature of delocalized electrons, and local-moment magnetism with an antiferromagnetic ordering temperature of 12 K[1,2]. This suggests that the bonding to oxygen of the 4*d* levels of the early-transition metals may not be sufficiently covalent to yield the kind of exotic conductivity and superconductivity observed for copper oxides.

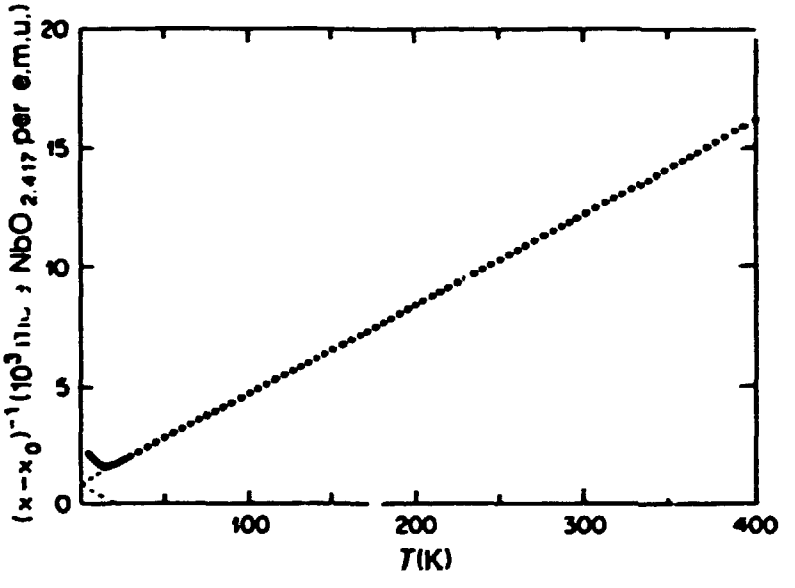

Fig. 1. The inverse magnetic susceptibility of $Nb_{12}O_{29}$ measured in a field of 1 T, plotted per mole $NbO_{2.417}$. A small constant term, $\chi_o = 9.3 \cdot 10^{-6}$ e.m.u. per mole, has been subtracted.

In Fig. 1 we present the inverse magnetic susceptibility of $Nb_{12}O_{29}$ between 5 and 400 K, plotted per mole in order to normalize to 1 Nb per formula unit. Fitting to a Curie-Weiss formula in the interval from 30 K to 400 K yields: $\chi = 9.3 \cdot 10^{-6} + 2.67 \cdot 10^{-2}/(T + 24\text{K})$. The antiferromagnetic ordering is shown by the departure of $1/\chi$ from linearity at low temperatures. Antiferromagnetic fluctuations are observed to begin near the Curie-Weiss temperature of 24 K, but χ peaks first at 12 K, suggesting that either frustration of spins or two-dimensional interactions are involved in determining the ordering temperature. The temperature dependent resistivity of polycrystalline $Nb_{12}O_{29}$ is shown in Fig. 2. The resistivity shows a rather sharp drop near the antiferromagnetic ordering temperature. Thus spin-induced scattering of the conductivity electrons make a significant contribution to the resistivity above the ordering temperature.

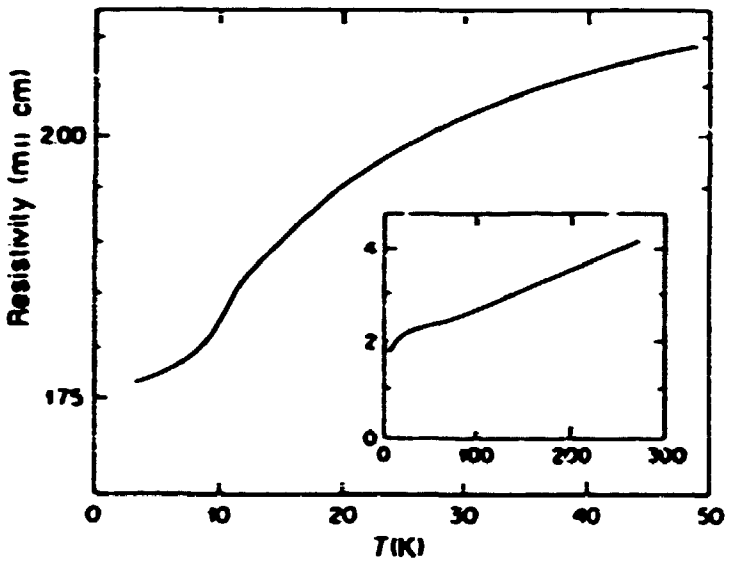

Fig. 2. Detail of the temperature-dependent resistivity of polycrystalline $Nb_{12}O_{29}$ in the vicinity of the antiferromagnetic ordering temperature. Insert: the resistivity in the temperature range: 3-300 K.

[1] R.J. Cava, B. Batlogg, J.J. Krajewski, P. Gammel, H.F. Poulsen, W.F. Peck, and L.W. Rupp Jr., (1991). Letter to Nature 350, 598-600.

[2] R.J. Cava, B. Batlogg, J.J. Krajewski, P. Gammel, H.F. Poulsen, W.F. Peck, and L.W. Rupp Jr., (1991). Phys. Rev. B 44, 13, 6973-6981.

1.20 Development of a Spin Gap in the Kondo Insulator CeNiSn

(T.E. Mason, G. Aeppli, A.P. Ramirez, N. Stücheli, E. Bucher, and T.T.M. Palstra, *AT&T Bell Laboratories, Murray Hill, NJ, USA*, K.N. Clausen, *Department of Solid State Physics, Risø National Laboratory, Denmark*, and C. Broholm, *Department of Physics and Astronomy, The Johns Hopkins University, Baltimore, MD, USA*)

Neutron scattering measurements of the spin fluctuation response of the Kondo insulator CeNiSn carried out at TAS6 and TAS7 show the development of low frequency, antiferromagnetic spin fluctuations over the same temperature range that the system crosses over from metallic heavy fermion behaviour to a semiconducting regime. At low temperatures, near the antiferromagnetic wavevector (001), there is a clear gap in the spectrum with and asymmetric lineshape characteristic of a gapped joint density of states. This is shown in the top panel of Fig. 1 (open circles) for **Q** = (0,0,1.2). As the temperature is raised above 10 K an increase in the damping of the excitation results in a filling in of the gap (closed circles). For values of **Q** further away from (001) the measured intensity of the inelastic feature at low temperatures decreases while its width increases although the energy scale is relatively unchanged (middle panel of Fig. 1). Heating to above 10 K has a similar effect to that seen at **Q** = (0,0,1.2). Measurements at **Q** = (1.2,0,0) (bottom panel) show no significant inelastic intensity indicating that the scattering near (001) arises from fluctuations polarized along a*, the easy magnetic direction. There is, however, a small quasi-elastic component which appears to be isotropic and only weakly temperature dependent. This is consistent with the eventual downturn of the resistivity below 1 K, indicating that some carriers remain at low temperatures.

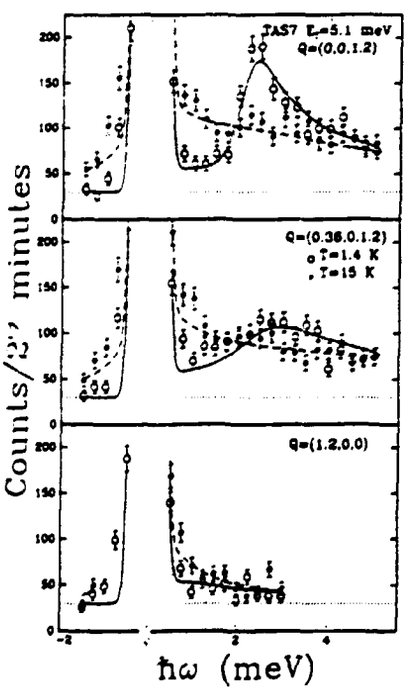

Fig. 1. Constant **Q** *scans at* **Q** *= (0,0,1.2),* **Q** *= (0.36,0,1.2), and* **Q** *= (0,0,1.2) at T = 1.4 K (o) and T = 15 K (•) measured at the TAS7 spectrometer. Note that the gap present at low temperatures, most evident at* **Q** *= (0,0,1.2), fills in on heating.*

1.21 Tetracritical Dynamics of $CsMnBr_3$

(T.E. Mason, *AT&T Bell Laboratories, Murray Hill, NJ, USA*, Y.S. Yang, M.F. Collins, and B.D. Gaulin, *Department of Physics, McMaster University, Hamilton, ON, Canada*, K.N. Clausen, *Department of Solid State Physics, Risø National Laboratory, Denmark*, and A. Harrison, *Inorganic Chemistry Laboratory, Oxford University, Oxford, UK*)

The triangular antiferromagnet $CsMnBr_3$ exhibits unusual static critical exponents due to the chiral degeneracy in the ground state brought on by lattice frustration[1]. In order to determine if the chiral nature of the ordering or the tetracriticality of the $H = 0$, $T = T_N$ phase transition has an effect of the dynamics of the phase transtion we have measured the spin dynamics at T_N using the TAS6 spectrometer. Close to the magnetic zone centre, $(\frac{1}{3},\frac{1}{3},1)$, dynamical scaling is observed to hold with a critical exponent $z = 1.47 \pm 0.06$. Further away from the ordering wave vector well defined excitations are observed whose energies show surprisingly little renormalization relative to the low temperature spin wave energies. Figure 1 shows representative scans for these two regimes. The lineshape of the scattering near $(\frac{1}{3},\frac{1}{3},1)$ is well described by a Lorentzian lineshape, indicating exponential relaxtion, while the behaviour at larger **Q** is better represented by a forced damped harmonic oscillator.

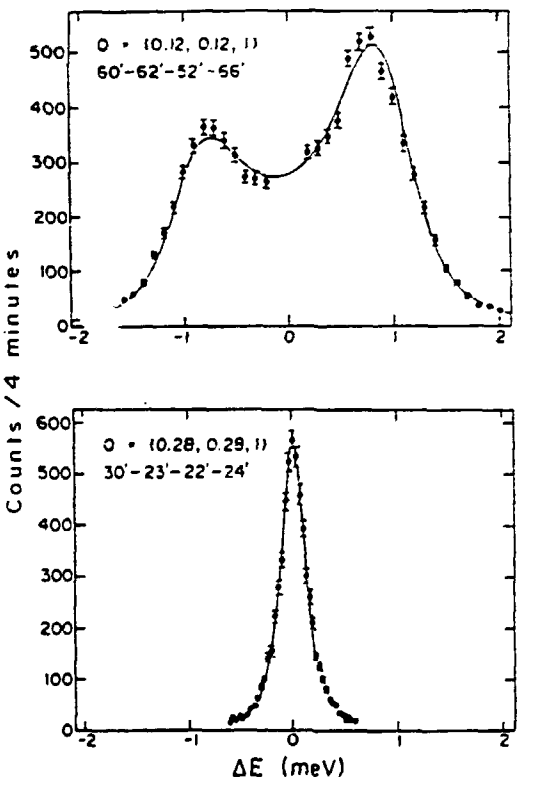

Fig. 1. Inelastic neutron scattering from $CsMnBr_3$ at $T = T_N$ for two wave vectors. The lines are the results of fits to the two forms mentioned in the text.

[1] T.E. Mason, B.D. Gaulin, and M.F. Collins, (1989). Phys. Rev. B **39**, 586.

1.22 Magnetic Field Profile of Flux Lines in Nb at 10 mK

(R.N. Kleiman, T.E. Mason, and D.J. Bishop, *AT&T Bell Laboratories, Murray Hill, NJ, USA*)

When a magnetic field exceeding H_{c1} but less than H_{c2} is applied to a type-II superconductor it penetrates the material in vortices containing one quantum of magnetic flux. In most cases the interactions between these vortices result in the formation of a flux lattice which is visible by small-angle neutron scattering due to the spatial variation of the magnetic field profile. Because the superconducting order parameter varies in real space in a similar way to the magnetic field measurements of the magnetic field profile (by measuring the form factor of the Bragg peaks associated with the flux lattice) provide information of the details of the superconducting state and Fermi surface of the superconductor. Measurements on Nb using TAS8 with 5′ and 10′ collimation have shown not only the expected sharpening of the fluxoids at low temperatures (manifested as an increase in the relative intensity of the higher order Bragg peaks) but also a substantial suppression of the even indexed Bragg reflections. Figure 1 shows that, in real space, a removal of the second order Fourier component, (2 0), reduces the curvature of the magnetic field profile between the flux vortices. The accuracy of the present measurements was limited by the rather broad 45′ mosaic of the Nb crystal used. To improve the quality of further measurements a much higher quality crystal is in preparation.

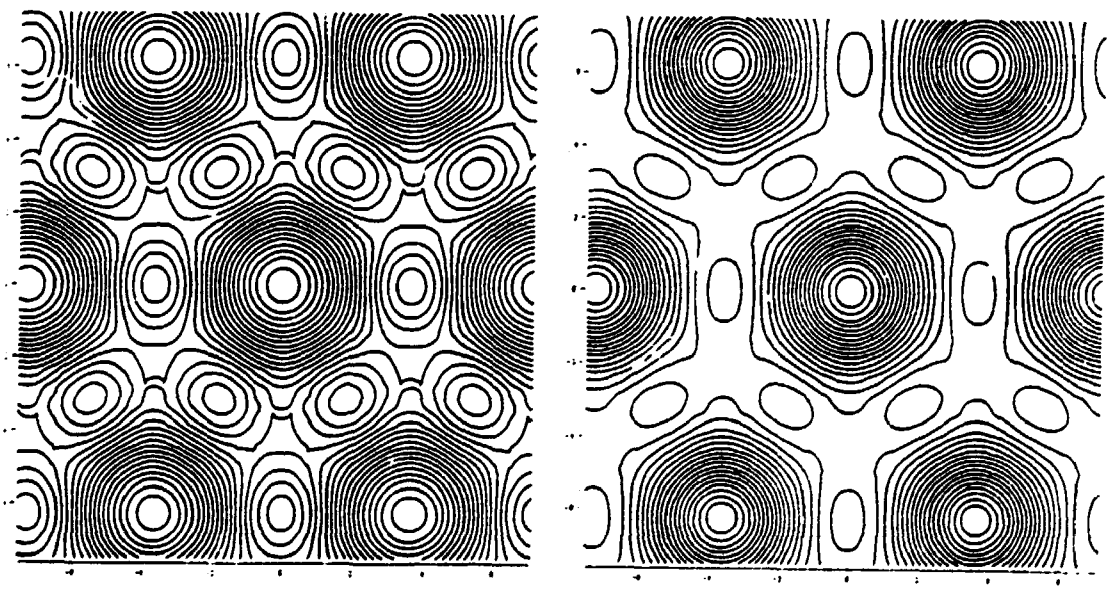

Fig. 1. Magnetic field profiles obtained using the first three Fourier coefficients [(1 0), (1 1), and (2 0)] (left) and omitting the even indexed (2 0) coefficient (right). The absence of even indexed [(2 0), (2 2), etc.] Bragg reflections corresponds to a minimizing of the curvature of the magnetic field profile in the region between flux vortices.

1.23 Spin Dynamics of the Spin $\frac{1}{2}$ Heisenberg Square Lattice Antiferromagnet $Cu(DCO_2)_2 \cdot 4D_2O$

(A. Harrison and S.J. Clarke, *Inorganic Chemistry Laboratory, Oxford University, Oxford, UK*, T.E. Mason, *AT&T Bell Laboratories, Murray Hill, NJ, USA*, and D. Visser, *Department of Physics, Loughborough University of Technology, Loughborough, UK*)

$Cu(DCO_2)_2 \cdot 4D_2O$ is an insulating antiferromagnet with the same magnetic Hamiltonian as La_2CuO_4 except that the superexchange coupling nearest neighbour Cu spin $\frac{1}{2}$ magnetic moments, J_{nn}, is about two orders of magnitude smaller. This compound therefore provides an excellent opportunity to test theories over a much wider range of energies and temperatures (relative to J_{nn}) than is possible for La_2CuO_4 and without the experimental difficulties inherent in the large energy scale of that compound. Measurements of the low energy spin waves near (0 $\bar{1}$ 0) have been carried out on the TAS1 spectrometer and some of the results are shown below. On the left are two constant-**Q** scans at (0 $\bar{1}$ 0) and (0 $\bar{1}$ 0 5) showing the zone centre response with a gap of 0.60 ± 0.05 meV due to anisotropic symmetric exchange or asymmetric exchange. There is no dependence on c^* reflecting the two-dimensional nature of the Hamiltonian. On the left of Fig. 1 two constant $\hbar\omega$ scans are shown for $\hbar\omega$ = 1.3 meV and 2.0 meV. The dispersion of the excitations away from (0 $\bar{1}$ 0) is evident in the data (right hand of Fig. 1) and the inset shows the dispersion relation derived from this work near (0 $\bar{1}$ 0) corresponding to an exchange constant of 11.0 ± 0.1 meV, in reasonable agreement with that extracted from the temperature dependence of the inverse correlation length[1]. Further work is planned to extend the meaurements to larger **Q** and $\hbar\omega$.

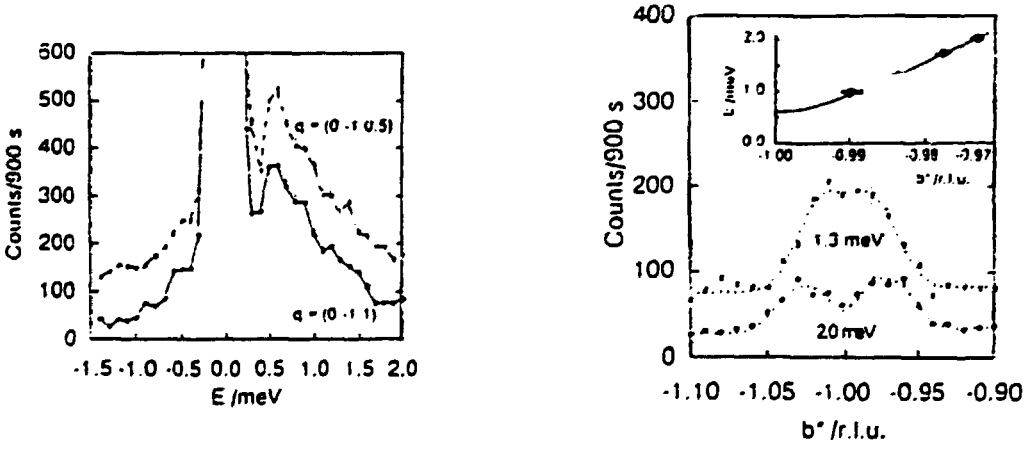

*Fig. 1. On the left are constant-**Q** scans at 4.7 K demonstrating the flat dispersion along c^* (between the magnetic layers). The zero of the upper data set has been raised by 100 counts for the sake of clarity. On the right are constant-$\hbar\omega$ scans through the antiferromagnetic zone centre. The inset shows the dispersion observed along b^* with the best fit of a classical spin wave expression shown as a solid line.*

[1] S.J. Clarke, A. Harrison, T.E. Mason, G.J. McIntyre, and D. Visser, (1991). J. Phys.: Condens. Matt. *To be published.*

1.24 Finite–Size Effects in the Magnetic Properties of Ferromagnetic Clusters

(P.V. Hendriksen and S. Linderoth, *Laboratory of Applied Physics, Technical University of Denmark, Lyngby*, and P.-A. Lindgård, *Department of Solid State Physics, Risø National Laboratory, Denmark*)

In a recent study of small Fe clusters with 50 - 230 atoms[1] it was found that the average moment per atom is below the bulk value. Some of these effects were addressed in a Monte Carlo simulation study of Ising clusters[2]. We anticipate that the Heisenberg model is more appropriate in particular for the low temperature behavior. Model calculations for the spontanous magnetization of ferromagnetic clusters of various perfect structures have been performed. The exchange interaction is modelled by a nearest neighbor Heisenberg Hamiltonian and the dipole forces are neglected. A self-consistent spin wave spectrum is found by direct diagonalization of the equation of motion for S^+ . Mean field calculations are performed for comparison and in order to infer the high temperature behavior. The finite size is found to cause large deviations from the normal Bloch $T^{3/2}$ law for the spontanous magnetization at low temperatures and to lower the Curie temperature.

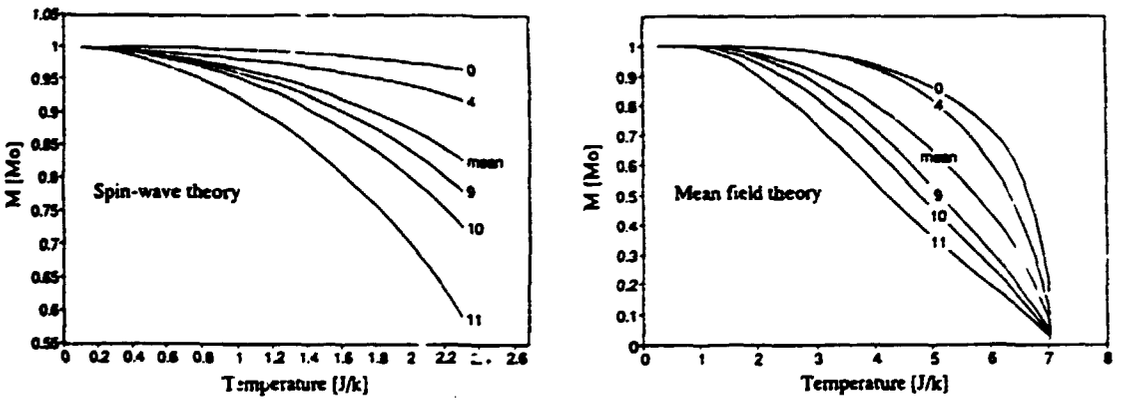

Fig. 1. Left: The temperature dependence of the spontanous magnetization calculated for an FCC cluster having 11 shells (225 spins) by self-consistent spin wave theory. Right: The same calculated by mean field theory. Curves for different layers (shells) as well as the mean-value, are shown.

[1] W.A. de Heer, P. Milani, and A. Chatelain, (1990). Phys. Rev. **65**, 488.
[2] J. Merikoski, J. Timonen, M. Mannien and P. Jena, (1991). Phys. Rev. Lett. **66**, 938.

1.25 High T_c SQUIDs Fabricated by a Bi–Epitaxial Process

(R. Kromann, *Department of Solid State Physics, Risø National Laboratory, Denmark*, J.J. Kingston, A.H. Miklich and J. Clarke, *Department of Physics, UC Berkeley, USA*, L.T. Sagdahl, *Norwegian Institute of Technology, Trondheim, Norway*, and Y. Saito *Yamanashi University, Japan*)

It is known that the critical current of grain boundaries in c-axis oriented $YBa_2Cu_3O_{6+x}$ (YBCO) depends strongly on the angle between the *a*-axes in the two grains which form the boundary. The critical current decreases about two orders of magnitude as the angle increases from 0° to 45°. This fact has been widely utilized to fabricate superconducting quantum interference devices (SQUIDs) by patterning a polycrystalline film into narrow bridges, relying on naturally occurring grain boundaries to act as weak links. From a fabrication point of view this method is far from ideal, because it is impossible to control the location on the substrate where the grain boundary will be formed.

The bi-epitaxial process offers the possibility to create a high angle grain boundary at will anywhere in an otherwise epitaxial thin film. The process can in principle be realized with any set of three different materials which grow epitaxially on each other, as long as one of them has different in-plane orientation depending on which one of the other materials it is grown on. In our case the materials involved are MgO, CeO_2 and $SrTiO_3$. The in-plane rotation (45°) arises because the lattice parameter of CeO_2 is close to $\sqrt{2}$ times that of $SrTiO_3$.

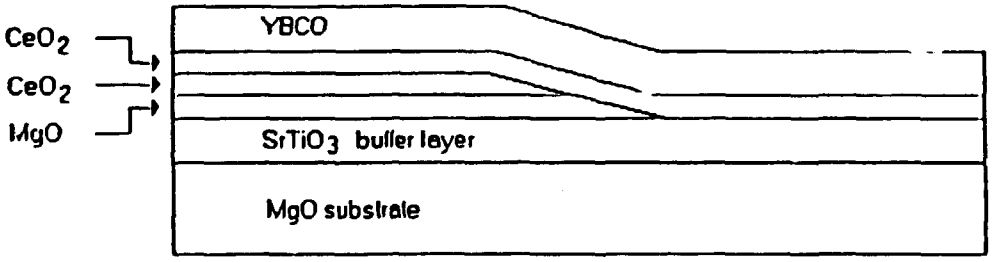

Fig. 1. The bi-epitaxial process involves a total of five thin film layers. On the left side of the grain boundary the a- and b-axes of the YBCO layer is rotated 45° with respect to the axes of the MgO substrate. On the right side the axes of the YBCO and the substrate are aligned.

The SQUIDs are fabricated by pulsed laser ablation on MgO substrates. First a buffer layer of $SrTiO_3$ is deposited followed by two very thin layers of MgO and CeO_2 (see the figure). The sample is then removed from the vacuum chamber and covered with photoresist which is patterned into the desired grain boundary. After the resist has been developed, the sample is ion milled through the CeO_2 and MgO layers on one side of the

grain boundary leaving the $SrTiO_3$ layer exposed. The resist is then removed and the sample is remounted in the deposition chamber. A thin buffer layer of CeO_2 is deposited followed by the final YBCO layer. The sample is taken through another step of photolithography and the SQUID pattern is etched into the YBCO using nitric acid. The last step in the process involves evaporation of silver through a shadow mask followed by a low temperature anneal in oxygen to form contacts to the sample.

The best devices made to date exhibit I–V characteristics consistent with the resistively shunted junction model and with a measureable critical current for temperatures up to 70 K. At 4.2 K the critical current is 100 μA and the normal state resistance is 1 Ω, giving an I_cR_n product of 100 μV. When the SQUID is biased slightly above the critical current and a magnetic field is applied, the voltage across the SQUID varies periodically in the flux quantum with an amplitude of 7.5 μV peak-to-peak. Currently, measurements of the noise level is under way, since this property will ultimately determine if these devices have practical applications in the future.

1.26 Relation Between Critical Current and In-Plane Ordering of $YBa_2Cu_3O_{6+x}$ on MgO(001) and $SrTiO_3$(001)

(R. Kromann, R. de Reus, N.H. Andersen, *Department of Solid State Physics, Risø National Laboratory, Denmark*, J.B. Bilde Sørensen, *Materials Department, Risø National Laboratory, Denmark*, P. Vase, and T. Freltoft, *NKT Research Center, Brøndby, Denmark*)

For many applications of thin-film high-T_c superconducting $YBa_2Cu_3O_{6+x}$ excellent transport critical currents are required. This may only be obtained by reliable processes for deposition of epitaxial layers without structural defects. Not only the deposition process, but also the substrate material plays a key role in obtaining superconducting films with the desired properties. In this work the crystalline quality of thin-film $YBa_2Cu_3O_{6+x}$ deposited onto MgO(001) and $SrTiO_3$(001) under almost identical conditions by a laser ablation process is investigated. The observed differences in critical current are therefore attributed to the difference in substrate type and quality. The structural analysis of the samples was carried out by X-ray diffraction and planar view high resolution transmission electron microscopy. This is the first time that a quantitative relationship between critical current and structural quality of $YBa_2Cu_3O_{6+x}$ has been established.

The $YBa_2Cu_3O_{6+x}$ films investigated all have the ideal 1:2:3 composition. No impurity phases were observed. Furthermore, the films were epitaxial with the *c*-axis perpendicular to the substrate, but minor traces of *a*-axis oriented material were observed. Films on MgO exhibited critical currents (measured at 77 K) ranging from 3.5×10^5 to 1.5×10^6 A/cm^2, whereas for films on $SrTiO_3$ a range from 2.9×10^6 to about 1.0×10^7 A/cm^2 was measured. The lower critical currents of films on MgO in comparison to films on $SrTiO_3$ are attributed to the larger in-plane mosaicity of the films on MgO. This difference in mocaicity is caused by the difference in lattice match between $YBa_2Cu_3O_{6+x}$ and the two substrate types MgO and $SrTiO_3$. The lattice match of the superconductor with the $SrTiO_3$ substrate material is close, resulting in higher quality $YBa_2Cu_3O_{6+x}$ films than in the case of MgO substrates. The differences in critical currents of the films deposited on the individual type of substrates can be explained as follows. For the films deposited onto MgO the lowering of the critical current by 75% can directly be related to the presence of smaller grains, microtwins, and an increased density of small- and high-angle grain boundaries, because approximately 5% of the $YBa_2Cu_3O_{6+x}$ film consisted of domains rotated 45° with respect to the substrate axes. For films deposited onto $SrTiO_3$ the lowering of the critical current by 70% is attributed to an increase of $YBa_2Cu_3O_{6+x}$ having the *a*-axis oriented perpendicular to the substrate from 0.6 to 8.3%.

1.27 Epitaxial Growth of High-T_c Superconducting $Bi_2Sr_2CaCu_2O_{8+x}$ Thin Films on MgO(001) and $LaAlO_3$(001)

(R. de Reus, M. Nielsen, N.H. Andersen, *Department of Solid State Physics, Risø National Laboratory, Denmark*, R. Seemann, and R.L. Johnson, *Hasylab, DESY, Hamburg, Germany*)

Superconducting $Ba_2Sr_2Ca_1Cu_2O_{8+x}$ (BSCCO) thin-films have been prepared and their structural properties have been investigated. The films are deposited by a laser ablation process in Hamburg. The electrical characterization is performed at both Hasylab and Risø National Laboratory. The structural characterization by means of X-ray diffraction is performed at Risø. Deposition of BSCCO takes place at 500°C in 1 mbar O_2 onto MgO(001) and $LaAlO_3$(001) substrates. Thereafter the samples are annealed in air for 5 min at 875°C. All films show a preferential *c*-axis orientation. However, a remarkable difference between the two types of subtrates is noticed. Whereas the BSCCO films deposited onto $LaAlO_3$ appear to be fully epitaxial (*i.e.*, also a full alignment of film and substrate in the *ab*-plane), the films deposited onto MgO appear to consist of both oriented as well as randomly distributed regions in the plane of the substrate surface. The oriented parts of the films deposited onto MgO consist of fully oriented regions, regions with a misorientation of 45°, and regions with an in-plane rotation of 11.5°. Glancing incidence X-ray diffraction showed that the oriented parts of the film are not at the film surface. Moreover, the relative amount of randomly in-plane oriented material increases with increasing film thickness. The difference in epitaxy of BSCCO on MgO and $LaAlO_3$ is attributed to the poor lattice mismatch between BSCCO and MgO on the one hand, and the very good lattice mismatch between BSCCO and $LaAlO_3$ on the other. A good lattice match most likely facilitates epitaxial growth. The origin of the different individual orientations of BSCCO on MgO is not clear. Cooling of the samples to room temperature before the post annealing step at 875°C results in a different surface morphology. Scanning electron micrographs show that the surfaces of the samples cooled to room temperature before post annealing are significantly less smooth as compared to the surfaces of samples directly heated to 875°C after deposition of the film. However, no significant changes in the structure of the films could be detected by X-ray measurements.

1.28 Prediction of Phase Formation Sequence and Phase Stability in Binary Metal–Aluminum Thin-Film Systems Using the Effective Heat of Formation Rule

(R. Pretorius*, A.M. Vredenberg, F.W. Saris, *FOM Institute for Atomic and Molecular Physics, Amsterdam, The Netherlands*, and R. de Reus, *Department of Solid State Physics, Risø National Laboratory, Denmark*)

There has been much interest in formulating rules for predicting first phase formation and subsequent phase sequence in binary metal-silicon and metal-metal systems. One of the rules stated that: "*The first compound nucleated in binary reaction couples is the most stable compound adjacent to the lowest-temperature eutectic on the bulk equilibrium phase diagram.*" As a measure of stability the melting point of the compound is taken if the compound is congruently melting, otherwise the peritectic or peritectoid temperature. After one of the elements is completely consumed during the reaction, the subsequent compound to form is the next stable phase, richer in the remaining element. For silicide formation an additional requirement is that only congruently melting phases should be taken into account. The above-mentioned rules, however, do not make direct use of thermodynamic data. It was only after introduction of the effective heat of formation ($\Delta H'$) concept that thermodynamic data could be directly used to predict first phase formation and subsequent phase sequence.

During solid-state formation of ordered compounds the entropy term at a typical reaction temperature of 300 °C is negligibly small when compared to the enthalpy of phase formation. Therefore, the change in Gibbs free energy, which is the driving force for a process to take place, can be approximated the enthalpy term, the heat of formation $\Delta H°$. As a system would always want to go to its lowest possible free energy state, it should therefore be possible to use heats of formation to predict phase formation when activation or nucleation barriers do not exist. Phase formation at a growth interface is a typical dynamic non-equilibrium process in which only one phase is formed at a time, unlike equilibrium processes where simultaneous formation of a mixture of phases can lead to the lowest free energy state for the system. The effective concentration is therefore defined as the actual concentration of the elements at the interface while reacting. The effective heat of formation, $\Delta H'$, for a given compound can thus be defined as the energy released during reaction of the elements at the interface at a given effective concentration, or:

$$\Delta H' = \Delta H° \times \left(\frac{\text{effective concentration limiting element}}{\text{compound concentration limiting element}} \right)$$

in which "limiting element" means the element whose availability (or effective concentration) at the interface is less than the stoichiometric concentration of that element in the compound. For instance, if in the case of an Al-Zr diffusion couple the effective concentrations at the growth interface would be 50 at.% Al and 50 at.% Zr, then the effective heat of formation for the growth of $AlZr_2$ is given by: $\Delta H' = \Delta H° \times (0.500/0.667)$ kJ(mol at.)$^{-1}$.

*On leave from the Ion-solid Interaction Division, Van de Graaff Group, National Accelerator Centre, Fauré, South Africa

As a first approximation of the effective concentration the concentration of the lowest temperature eutectic (liquidus) of the binary system is chosen. Since the activation energy for interdiffusion scales with the liquidus temperature, the highest mobility of the atoms, and hence interfacial reaction, is expected to occur at the concentration of lowest temperature eutectic. According to the effective heat of formation concept, the rule for first phase formation thus states:

"*The first-compound phase to form during metal-metal interaction is the phase with the most negative effective heat of formation ($\Delta H'$) at the concentration of the lowest temperature eutectic (liquidus) of the binary system.*"

When all the limiting element is consumed during first-phase formation, the effective concentration will change until $\Delta H'$ of a neighboring phase (more rich in the unreacted element than the first phase formed) becomes favorable. The effective heat of formation rule for formation sequence in metal-metal systems is thus formulated as follows:

"*After first-phase formation in metal-metal binary systems, the next phase to form at the interface between the compound phase and remaining element is the next phase richer in the unreacted element, which has the most negative effective heat of formation.*"

The simple effective heat of formation concept has been tested for a number of silicides and aluminides. In almost every case the model predicts first-phase formation as well as phase sequence correctly. The model also has been useful in explaining how the presence of impurities such as oxygen or small amounts of gold influence the effective concentration at the reaction interface and hence alter phase formation sequence during nickel and cobalt silicide formation, respectively. It has also been successful in explaining why CoSi formation is dominant at low temperatures while the formation of Co_2Si becomes significant at higher temperatures during ion-beam mixing in the Co-Si system. In a recent publication[1] the effective heat of formation rules and their applications are explained in detail and most data accessible from literature on transition-metal aluminum reactions are referenced.

[1]R. Pretorius, A.M. Vredenberg, F.W. Saris, and R. de Reus, (1991). J. Appl. Phys. 70, 3636.

1.29 Sputtering Yields from Ion-Bombarded Condensed Gases

(J. Schou, *Department of Solid State Physics, Risø National Laboratory, Denmark*, B. Stenum, H. Sørensen, *Department of Optics and Fluid Dynamics, Risø National Laboratory, Denmark*, O. Ellegaard, *Odense University Library, Odense University, Denmark*, and R. Pedrys, *Jagellonian University, Cracow, Poland*)

The studies on sputtering of the solid hydrogens have been continued with particular emphasis on the most volatile isotope, solid hydrogen. Sputtering by hydrogen ions are important for the lifetime of fuel pellets of hydrogenic material injected into plasma devices. The fast hydrogen ions generated by the neutral beam heating are very efficient in eroding the hydrogenic pellets. The yield for a 10 keV H^+ is about 150 D_2/H, 450 HD/H and 800 H_2/H for the three stable isotopes. This high yield is primarily caused by the very low binding energy of the hydrogen molecules in the solid.

The yields for all three isotopes increases strongly with energy in the region from 5 to 10 keV. This behaviour is a strong argument for electronic sputtering rather than knock-on (ordinary collision) sputtering. All known models for knock-on sputtering indicate that the yield would decrease with increasing energy. Electronic sputtering, *i.e.* erosion via electronic transitions, is correlated to the electronic stopping power. The yield for D_3^+- and H_3^+-ions incident on solid hydrogen shown in Fig. 1 is approximately a linear function of energy, *i.e.* the electronic stopping power squared. One notes that the yield in Fig. 1 for ions of equal velocity is practically identical and that all the data points lie on one curve. This confirms the assumption of electronic sputtering as being responsible for the erosion.

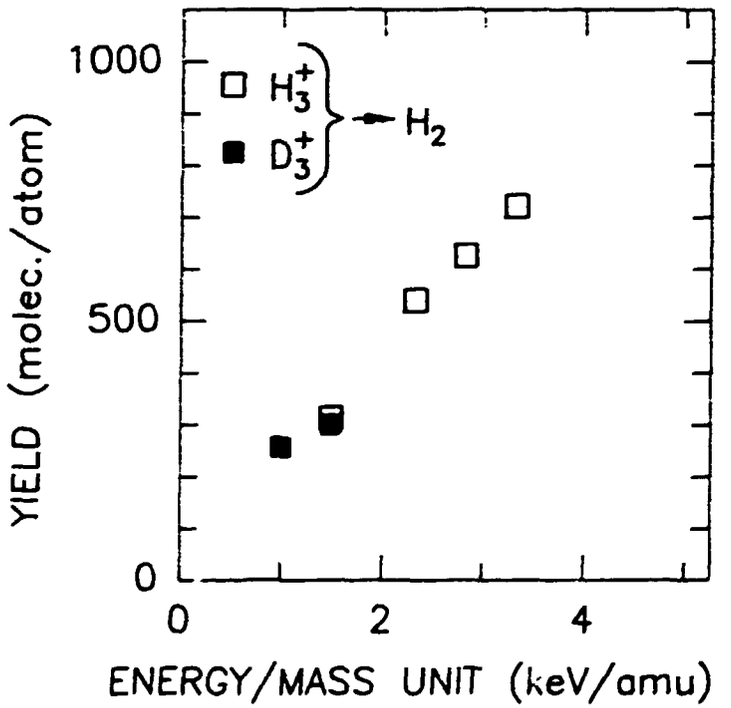

Fig. 1. The sputtering yield per atom as a function of the energy per mass unit from solid H_2. Film thickness: 3×10^{18} H_2/cm^2.

1.30 Luminescence from Pure and Impure Solid Hydrogens during Electron Bombardment

(J. Schou, *Department of Solid State Physics, Risø National Laboratory, Denmark*, B. Stenum, H. Sørensen, *Department of Optics and Fluid Dynamics, Risø National Laboratory*, P. Gürtler, *Hasylab, DESY, Germany* , and R.L. Brooks, *Physics Department, University of Guelph, Canada*)

The study of luminescence from particle-irradiated solid deuterium does not only yield information about the electronic excitations in the solid, but may also lead to data that are useful for the pellet-plasma interaction in plasma experiments. The previous work at the Risø-setup have demonstrated that solid deuterium exposed to electron irradiation emits bands which do not play any role for electron-bombarded hydrogen gas[1].

An intense new emission continuum in the red and near-infrared regime has been observed. This broad band peaking at about 815 nm has never been seen from the gas phase. It is observed already around 650 nm , and it falls off slowly with increasing wavelength. This fall-off is mainly determined by the decreasing sensivity of our detection system.

The line has been identified as radiative recombination of D-atoms in the solid. This process is possible, since the concentration of neutral atoms in the solid from dissosciative recombination may approach 1 per mille. The atoms perform a quantum diffusion in the solid by fast atom exchange in the molecules. The recombination of the atoms has to take place in the neighborhood of an ion, because the wavelength of the emitted light shows that the distance between atoms before recombination is much smaller than expected from the known atom-atom distance in the solid deuterium lattice.

[1] J. Schou, B. Stenum, H. Sørensen, K.-V. Weisberg and P. Gürtler, (1991). Nucl. Fusion 31, 589.

1.31 Secondary Electron Emission from Solids

(J. Schou, *Department of Solid State Physics, Risø National Laboratory, Denmark*, and H. Rothard, *Institut für Kernphysik der J.W. Goethe-Universität, Frankfurt, Germany*)

The studies on secondary electron emission induced by charged particle or photon bombardment on surfaces have been concentrated on the energies that are relevant for plasma-surface interaction. The data collected and the description of the physical processes comprise a review chapter in a book on the physical properties of the interaction of fusion plasma with solids.

A parallel effort has been made to extend an existing transport theory of Schou[1] for secondary electron emission from solids to heavy ions as well. This theory has been feasible for proton and electron bombardment and partly for other light ions, whereas heavy-ion impact has turned out to deviate significantly from the predictions. The analysis has demonstrated that the deviations are primarily caused by excitations of the projectile, but the instantaneous charge state of the primary ion plays also an important role.

[1] J. Schou, (1980). Phys. Rev. B 22, 2141.

1.32 Studies on Fundamental Processes of Laser Sputtering and Ablation of Simple Materials

(J. Schou, *Department of Solid State Physics, Risø National Laboratory, Denmark*, K.-V. Weisberg, *Department of Optics and Fluid Dynamics, Risø National Laboratory, Denmark*, and O. Ellegaard, *Odense University Library, Odense University, Denmark*)

An existing setup is being prepared for laser irradiation of simple materials. A simple nitrogen laser with an emission in the ultraviolet region, 337 nm, with a peak power of about 100 μW within a period of a few ns will be applied. This laser has turned out to be sufficient even for making holes in aluminium foils. The laser erosion will be studied with mass collection on microbalances and by optical spectroscopy in the region from 120 to 900 nm. Simple materials as silver, copper, oxygen, nitrogen and deuterium will be irradiated with varying power area densities. The setup will be designed in such a way that the laser may be replaced by a stronger laser.

1.33 Epitaxy of V on MgO(001)

(R. Feidenhans'l, *Department of Solid State Physics, Risø National Laboratory, Denmark)*

As an example of a metal/insulator interface we have chosen to study the V/MgO(001) system. V has a BCC crystal structure with a lattice constant of 3.024 Å and MgO has a NaCl-structure with a lattice constant of 4.2112 Å. Because 4.2112 Å/$\sqrt{2}$=2.977 Å the V lattice has only a misfit of 1.5% when it grows epitaxially on MgO(001) with the $[100]_V$ axis rotated 45° with respect to $[100]_{MgO}$ direction. To accomodate this misfit the V chooses an usual form of epitaxy: It rotates out of the surface plane by about 0.65°. The tilt angle can be calculated by purely geometrical means requiring a higher order commensurate structure at the interface. The principle is illustrated in the figure where a rotation of 5.6° is shown. This type of tilt has recently been observed in a number of HCP on BCC systems[1].

We have grown V films on MgO(001) in the Metal-MBE chamber. The MgO substrate are cleaned by heating to 750°C until a good Reflecting High Energy Electron Diffraction (RHEED) pattern is obtained. The substrate surface quality can be further improved by depositing MgO before the growth of V. The thickness of the V film range between 30 and 700 Å. Some of the V films have been capped by a MgO layer. After deposition, the films are investigated *ex-situ* by x-ray diffraction. The film thickness is measured by the thickness oscillation in the reflected X-ray signal.

The tilt of the V films is measured by the position of the $(002)_V$ Bragg reflection with respect to the MgO substrate. Although the (001) surface of MgO has four symmetry equivalent directions the V layers are tilted coherently all over the surface along one of the four < 100 > directions. The tilt direction is selected by the direction of the miscut on the surface, which is in the range of 0.1-0.3°. We plan to investigate the dependence of the tilt on the detailed preparation proccdures, *i.e.* temperature during growth, and on the substrate miscut.

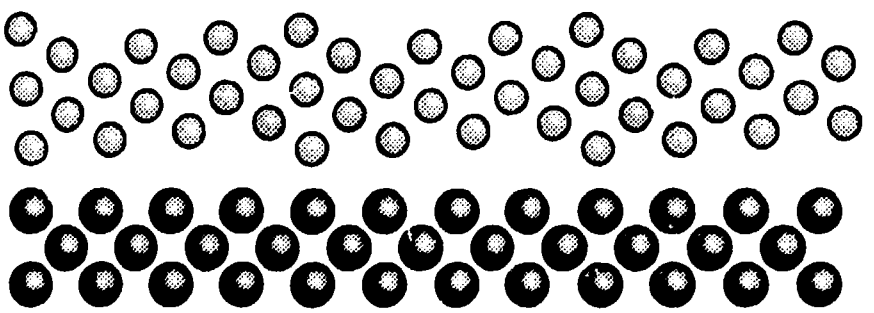

Fig. 1. Tilted BCC epilayer on FCC substrate. The tilt angle is 5.6° (side view).

[1] R. Du and C.P. Flynn, (1990). J. Phys. Condens. Matter 2, 1335.

1.34 Metal–Insulator Superlattice

(R. Feidenhans'l, *Department of Solid State Physics, Risø National Laboratory, Denmark)*

Magnesium Oxide (MgO) is an insulator with a NaCl structure. MgO can be evaporated from an electron beam evaporator[1)] and grows epitaxially on MgO(001) in the temperature range 20 to 600°C. We have investigated the growth of MgO in our metal MBE-apparatus. With Reflecting High Energy Electron Diffraction (RHEED) we can investigate the growth *in-situ*. Evaporating MgO on MgO(001) does not change the diffraction pattern, however, the background is lowered. This means that the surface quality improves. No oscillation as a function of time are observed meaning that the growth proceeds via step flow. The MgO films have been investigated by X-ray diffraction and no differences between virgin MgO(001) substrates and MgO substrates with deposited MgO could be found. This means that the films are not only epitaxial but also stoichiometric.

As described in the previous report V(001) grows epitaxial on MgO(001). However, MgO also grows epitaxial on V(001). This is already evident from the RHEED diffraction pattern. An X-ray diffraction scan of a 30 Å V(001) layer capped by 100 Å MgO is shown in Fig 1. The scan is performed along the specular rod of the surface and is measured at the BW2 beamline in HASYLAB. The broad peak at momentum transfers q=3.9 Å^{-1} arises from the (002) reflection of the V layers. The bulk position is at q=4.16 Å^{-1} and the shift must either be due to strain induced from the MgO substrate or from a chemical mixing between V and MgO. The position of the MgO(002) bulk Bragg peak is at q=2.984 Å^{-1}. The oscillation between 3.0 Å^{-1} and 3.5 Å^{-1} are finite size oscillation from the 100 Å MgO cap layer. The oscillations show that the MgO cap layer is epitaxial. Scans along the off-specular Crystal Truncation Rods show that the V film is also in-plane oriented with respect to the substrate.

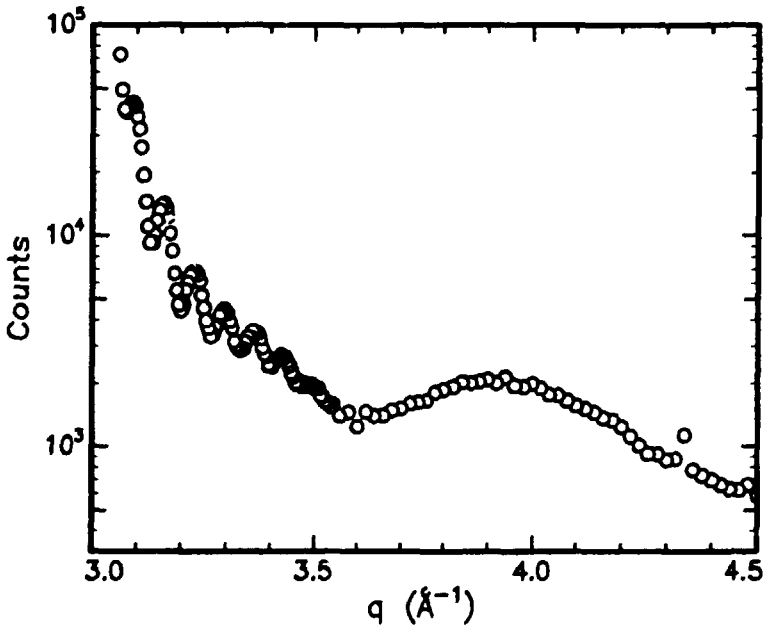

Fig. 1. X-ray diffraction scan along the specular rod of a 100 Å MgO/30 Å V/MgO(001) film. The data were measured at beamline BW2 in HASYLAB.

The observation decribed above suggest that it should be possible to make a metal-insulator superlattice. We have made a structure consisting of 7 × (30 Å V/50 Å MgO) grown on MgO(001). The growth was performed sequentially while the substrate was held at 650°C. The RHEED pattern showed that the crystallinity was maintained during growth. X-ray diffraction measurements have been made both at the rotating anode source in the department and at BW2 in HASYLAB. At the anode source a focussed graphite monochromator was used. At BW2 a double crystal Si(111) monochromator was used. The data from a scan along the specular direction are shown in Fig. 2 (not background subtracted). The better resolution at BW2 reveal more structure and shows the layering in the superlattice. A more detailed analysis is in progress. Future plans include to produce more MgO/V superlattices and to investigate the possibilities to make Fe/MgO superlattices.

[1] S. Yadavalli, M.H. Vang, and C.P. Flynn, (1990). Phys. Rev. B **41**, 7961.

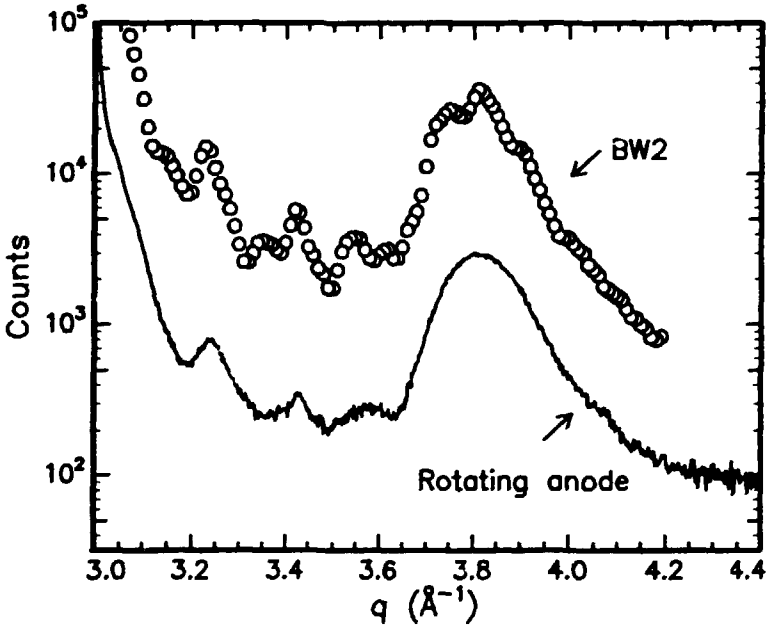

Fig. 2. X-ray diffraction scan along the specular rod of a MgO/V superlattice with nominally 7 repeats grown on MgO(001).

1.35 Metal–Insulator–Metal (MIM) structure.

(R. Feidenhans'l, *Department of Solid State Physics, Risø National Laboratory, Denmark*, F. Olsen, *IMFUFA, Roskilde University Center, Denmark)*

A Metal–Insulator–Metal (MIM) structure consists of two metals separated by an insulator. The insulator must be sufficiently thin to allow electron tunneling through the insulator when a potential is applied between the two metals. If the upper metal is thin, some of the electrons tunneling through the insulator will "shoot" through the metal out into the vacuum and the device can used as an electron emitter. We have tried to make such a device as a single crystal using the metal-MBE (MBE = Molecular Beam Epitaxy) apparatus. Because of the good epitaxy, V was chosen as one of the metals, MgO as the insulator and MgO(001) as the substrate. The substrate was cleaned by the procedure described in 1.33 and 1.34. By means of a mask system we have produced samples as shown in the figure, but unfortunately until now the two metals have been short–circuited. The samples are tested at IMFUFA, Roskilde University Center.

The V film were deposited with an electron beam evaporator and thicknesses were in the range 500–1000 Å. MgO was also evaporated with an electron beam evaporator and had thicknesses in the range 50–100 Å. The upper metal must be inert to prevent oxidation when the sample is taken out of the vacuum chamber and hence Au was chosen. Au, however, does only grow *c*-axis oriented on MgO(001) with the (111) planes parallel to the MgO(001) surface. We have tried to force the Au(001) layer to grow on MgO(001) by inserting seed layers of Ni, V or Pb a few atomic layers thick, but have not yet succeded in picking the right seed material. Ni and Pb do not grow epitaxially on MgO(001) and V makes an intermetallic compound with Au. Future plans include depositing on other substrates like $Al_2O_3(11\bar{2}0)$ to have a substrate surface with hexagonal symmetry.

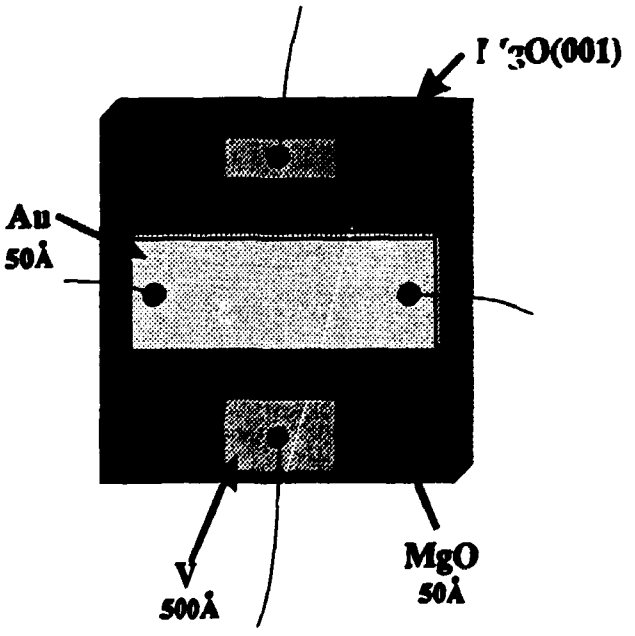

Sketch of a Metal-Insulator-Metal (MIM) structure.

1.36 Deterministic and Stochastic Lattice Gas Models

(T. Fiig, P. A. Lindgård, *Department of Solid State Physics, Risø National Laboratory, Denmark*, and H. J. Jensen, *The Niels Bohr Institute, Denmark*)

A unifying theory which explains $1/f$-noise in temporal fluctuating signals is still lacking. Recently Bak, Thang and Wiesenfeld[1] introduced a new concept, called *self-organized criticality*, and made an attempt to find such a theory. They used a cellular automaton computer, to illustrate the idea, but unfortunately, the model turned out to have a $1/f^2$ power spectrum[2]. Later a deterministic lattice gas model, very much in the spirit of the self-organized critical models studied by Bak, Tang and Wiesenfeld, were shown to have $1/f$-noise when driven by a white noise boundary condition[3].

It is generally believed[4] that a $1/f$ power spectrum is only observed in lattice gasses with deterministic dynamics, and an inclusion of a stochastic element in the updating algorithm changes the power spectrum from $1/f$ to $1/f^{3/2}$. Assuming that the diffusion equation offers an appropriate description of the lattice gas models, then renormalization group analysis show that the noise spectrum changes from $1/f$ to $1/f^{3/2}$, when there is an additional bulk noise[5].

Computer simulations, where stochasticity is included in the lattice gas models, does not follow the above predictions. What seems to be of importance is whether the bulk noise survives at a coarse grained scale. On Figs. (*a*) and (*b*) are shown the power spectrum $S(f)$ versus the frequency f for two stochastic models. In (*a*) the stochastic element is introduced by updating in a random sequential way. This produces $1/f^{3/2}$-noise, in accordance with the predictions. In (*b*) the stochastic element is introduced into the dynamics by randomly choosing which particle is allowed to move, when two or more particles wants to enter the same site. This conserves the $1/f$-noise.

(a) (b)

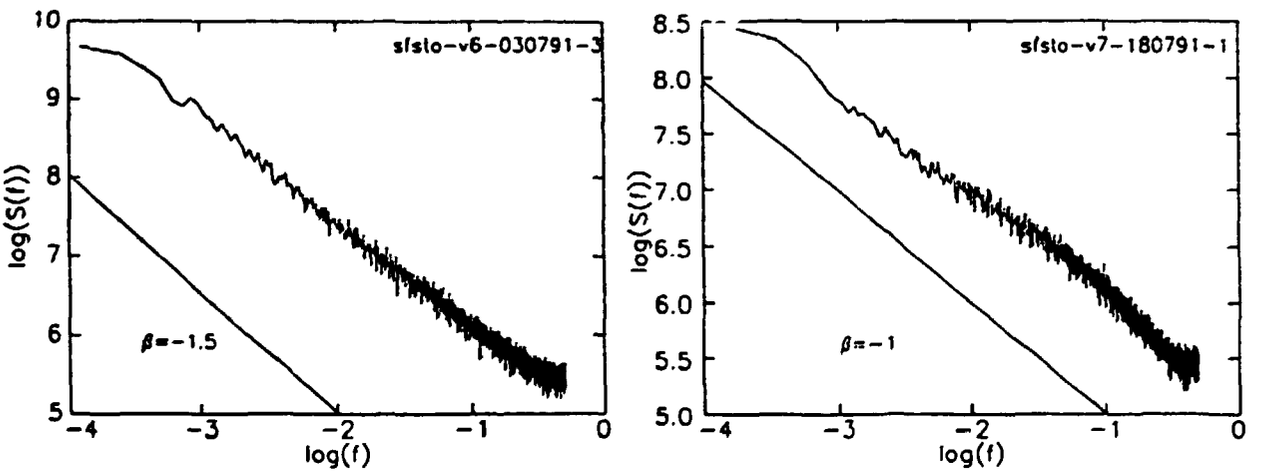

[1] P. Bak, C. Thang and K. Wiesenfeld, (1987). Phys. Rev. Lett. **59**, 381.
[2] H. Jensen, K. Christensen and H. C. Fogedby, (1989). Phys. Rev. B **40**, 7425.
[3] H. Jensen, (1990). Phys. Rev. Lett. **64**, 3103.
[4] J. V. Andersen, H. J. Jensen and O. G. Mouritsen, (1991). Phys. Rev. B **44**, 439.
[5] G. Grinstein, T. Hwa, and H.J. Jensen. Phys. Rev. B. *To be published.*

1.37 Monte Carlo Simulation of Adsorbed, Incommensurate Monolayers on Corrugated Surfaces

(E.Vives* and P.-A. Lindgård, *Department of Solid State Physics, Risø National Laboratory, Denmark*)

We have extended the previously introduced model[1] for systems of adsorbed particles on hexagonally corrugated surfaces. The model assumes a Lennard-Jones interaction between the adsorbed particles and a corrugation potential of the substrate, described by a four term Fourier expansion. This allows an investigation of the interesting case in which the optimum particle-particle distance is not commensurate with the substrate lattice vector size and to study the influence of the shape and the strength of the corrugation potential. Further, we have simulated the physics involved when varying the coverage. A highly optimized Monte Carlo algorithm has been developed. This allows us to simulate surfaces of the same size as the graphite crystallites used in most of the experiments.

For parameters close to those expected for the D_2 – D_2 and the D_2 – Graphite interactions, we have been able to reproduce the recent and most detailed experimentally determined phase diagram of D_2 on graphite. As a function of increasing coverage, at low temperatures, we have found a sequence of structures as follows: commensurate $\sqrt{3} \times \sqrt{3}$ phase (C), striped phase (α), strongly modulated phase (γ), and an incommensurate phase (IC). The 2D-structure factor has been calculated for q's up to the position of the (22) graphite substrate peak. It yields a perfect agreement with recent powder neutron diffraction measurements[2] and on single crystals, LEED experiments[3] which are restricted to low q values. In addition the simulations, of course, also give the real space picture of the structures (Fig. 1).

Studies of the α-phase suggest that the stabilization of stripes in a preferred direction, which was found in the LEED experiment[3], most probably is related to imperfections or to steps on the crystal surface. Simulations show no prefered directions. The structure of the γ-phase has been carefully analyzed. The possibility of calculating the 2D-structure factor up to high q values (larger than presently feasible experimentally) has demonstrated that the γ-phase is a 2-q, highly modulated structure with heavy but no super-heavy micro-domain walls. The micro-domains contain only $7 - 10$ particles. Figure 1 displays the calculated structure factor for the γ-phase and the drawing to the right shows the positions of the main peaks and the satellites found experimentally. Our results also show that the IC phase is a 1-q, multi (large) domain structure, which exhibits epitaxial rotation. At present, statistical uncertainities and existence of metastable domains do not allow us to ellucidate and corroborate conclusively existing theories on epitaxial rotation[4] for which D_2 on graphite represents an exceptional case.

[1] E. Vives and P.-A. Lindgård, (1990). Phys. Rev. B **44**, 1318.
[2] H. Freimuth, H. Wiechert, H.P. Schildberg, and H.J. Lauter, (1990). Phys. Rev. B **42**, 587.
[3] J. Cui and S.C. Fain Jr., (1989). Phys. Rev. B **39**, 8628.
[4] F. Grey and J. Bohr, (1991). Risø Report **R-582**, 54-55. J.P. McTague and A.D. Novaco, (1979). Phys. Rev. B **19**, 5299. H. Shiba, (1979). Journ. of the Phys. Soc. of Japan **46**, 1852.

* Supported by the Ministerio de Educación y Ciencia (Spain).

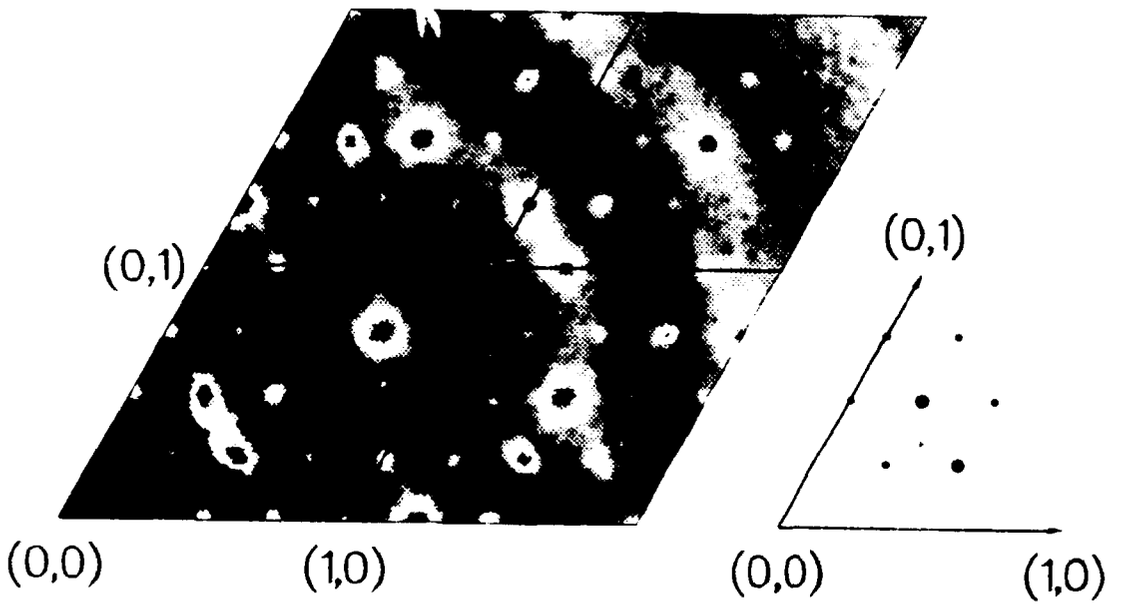

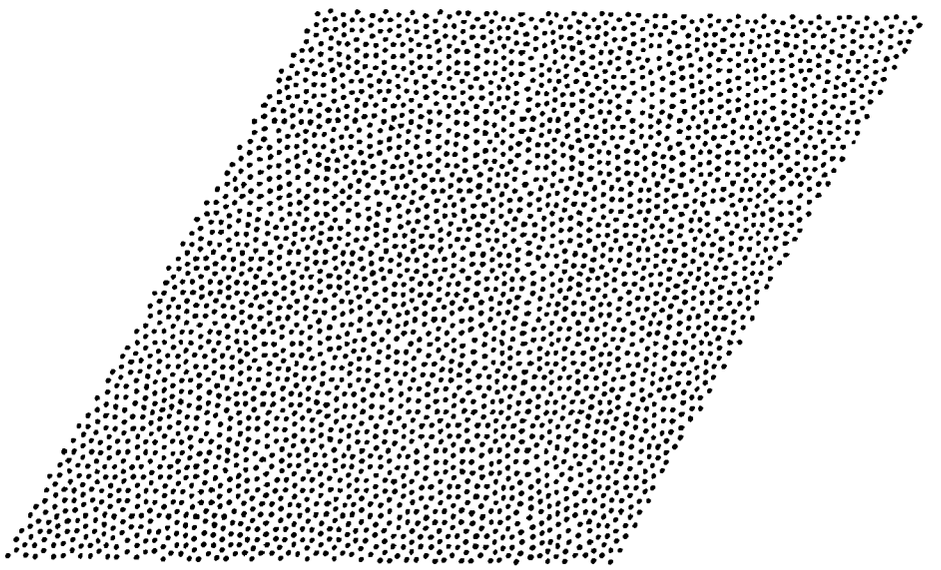

Fig. 1. Top: 2-D structure factor calculated with Monte Carlo simulation for parameters and coverage corresponding to the γ_2 phase of D_2 on graphite. The drawing to the right shows the position of the main peaks (big dots) and some of the satellites (small dots) found experimentally with respect to the (10) and (01) peaks of the graphite substrate. The position of the first peak of a $\sqrt{3} \times \sqrt{3}$ structure is indicated by a small cross. The corresponding real space picture is shown at the bottom.

1.38 Reciprocal Space Monte Carlo Simulation (RSMC)

(E. Vives, *Departament d'Estructura i Constituents de la Matèria, Universitat de Barcelona, Catalonia, Spain*, and P.-A. Lindgård, *Department of Solid State Physics, Risø National Laboratory, Denmark*)

Many real condensed matter systems can only be understood using non-simple models including competition and frustration. Among these the lattice-gas models are characterized by the fact that a set of N_p particles (atoms or molecules) is restricted to move on a lattice. In general, one represents the particles by occupancy variables $S_i = 1, 0$ ($i = 1, .., N$ being the sites of the lattice). A general pair-interaction Hamiltonian can be written, assuming translational invariance, as:

$$H = \sum_{i=1}^{N} \sum_{j=1}^{N} J_{i-j} S_i S_j, \tag{1}$$

where J_{i-j} stands for the interaction between particles separated by the vector $\mathbf{r}_i - \mathbf{r}_j$. Standard Monte Carlo (MC) simulation is a good tool for solving such models. An important problem is that if the ground state is unknown, simulations starting from disordered configurations and quenching to low T can easily be trapped in a number of metastable states. The reason is that the probability of accepting a change during the simulation is given by:

$$p = e^{-\frac{\Delta H}{k_B T}}. \tag{2}$$

At low T any changes producing big steps in energy will not be accepted. In general, changes are proposed by moving one single particle of the system. Such changes are usually not very good when the ground state is a long-period-modulated structure. A new approach is developped, which we call the RSMC method. It is a MC simulation in the reciprocal space. Every single change corresponds to the introduction of a density wave in the system. We expect that such movements will be particularly favorable when simulating modulated structures. The Hamiltonian (1) can be mapped to reciprocal space, using the expression:

$$S_{\mathbf{q}} = \frac{1}{N_p} \sum_{i=1}^{N} S_i e^{i 2\pi \mathbf{q} \mathbf{r}_i}, \tag{3}$$

where $\mathbf{q}$ are the vectors of the reciprocal lattice. The new Hamiltonian can be written as:

$$H = \sum_{\mathbf{q}} J_{\mathbf{q}} S_{\mathbf{q}} S_{-\mathbf{q}}. \tag{4}$$

The mapping is advantageous because the double summation over pairs is translated to a single summation over amplitudes. One looses information by the fact that the S_i variables are real and discret (0 or 1) while the amplitudes $S_{\mathbf{q}}$ are continuous and complex. One should take into account the following two conditions

$$S_{\mathbf{q}=0} = 1, \quad \sum_{\mathbf{q}} S_{\mathbf{q}} S_{-\mathbf{q}} = \frac{N}{N_p}. \tag{5}$$

The RSMC algorithm starts from a disordered state in which all the intensities $I_{\mathbf{q}} = | S_{\mathbf{q}} |^2$ with $\mathbf{q} \neq 0$ are equal. The conditions (5) suggest that we should propose exchanges of

the amount of intensity ΔI between different points q and q', as well as simple changes of the complex phases. Such proposed changes are accepted according to the same probability as in (2). With no other restrictions such an algorithm generates reciprocal space configurations that correspond to real configurations with non-integer particles. To solve that problem we add a penalty function to the Hamiltonian, increasing the energy when a particle is different from 0 or 1:

$$H = \sum_{\mathbf{q}} S_{\mathbf{q}} S_{-\mathbf{q}} + \lambda \sum_{i=1}^{N} f(S_i), \quad f(x) = x^2(1-x)^2. \tag{6}$$

Using this method we have simulated the 2d ANNNI (anistropic nearest and next-nearest neighbor Ising) model[1]. Indexing the sites on the square lattice by i (columns) and j (rows) one can write the Hamiltonian as:

$$H_{ANNNI} = \sum_{i,j} J_0 S_{i,j} S_{i,j-1} + J_1 S_{i,j} S_{i+1,j} + J_2 S_{i,j} S_{i+2,j},$$

with $J_0 < 0$, $J_1 < 0$, $J_2 > 0$. When $J_2/J_1 \approx -0.5$ and T is moderately low, the competition between the nearest neighbour and the next-nearest neighbours columns stabilizes modulated structures like ...**111000111000**..., called < 3 >, or < 4 >, etc.. Such phases are very difficult to obtain with standard MC methods. RSMC has proved to be succesfull in this case. Figure 1 shows an example of the < 3 > phase. In the near future the RSMC method will be used to locate the phase transitions of the ANNNI model and compare with the phase diagram obtained using low-temperature expansions.

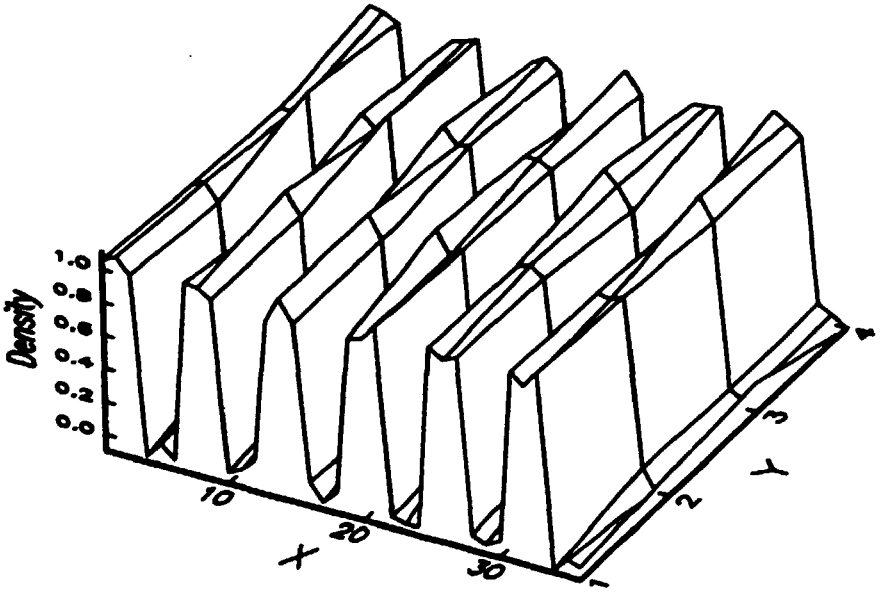

Fig. 1. Density of a 4 × 36 ANNNI model on a square lattice with $J_0 = 1$, $J_1 = 1$, $J_2 = -0.5$, $N_p = 72$ and $T = 0.3$ showing the < 3 > phase. The simulation has been done with a penalty parameter $\lambda = 4$.

[1] J. Yeomans, (1988). Solid State Physics 41, 151.

1.39 Order, Disorder and Structure of Crystals of C_{60}/C_{70}

(J. Bohr, *Department of Solid State Physics, Risø National Laboratory, Denmark*, D. Gibbs, S.K. Sinha, L.E. Berman, *Brookhaven National Laboratory, USA*, W. Krätschmer, *Max-Planck-Institut für Kernphysik, Heidelberg, Germany*, G. Van Tendeloo, *University of Antwerp, Belgium*, E. Larsen, and H. Egsgaard, *Department of Combustion Research, Risø National Laboratory, Denmark*)

Single crystals with two different morphologies, and with black and brown colours, of C_{60} with about 12% C_{70} have been studied by synchrotron X-ray diffraction. Integrated intensities from eight reflections show that the charge distribution of the C_{60} cluster is shell-like giving rise to an oscillatory behavior in the diffraction intensities. From the intensities, the distance between diametrically opposite carbon atoms has been determined to be 7.24±0.22 Å. The thickness of the charge distribution of the shell can be estimated as 3.06 Å and the cavity within a C_{60} cluster to have a diameter of about 4.18 Å. The finite longitudinal width of the diffraction peaks from black crystals indicates a lack of long-range crystalline order. The rocking curves are about 7° broad and depict an unusually smooth behavior. This may be indicative of a glassy or hexatic phase. High-resolution electron microscopy allows small crystallites with a relatively well-defined orientation relationship to be identified. In contrast, brown crystals have long-range order.

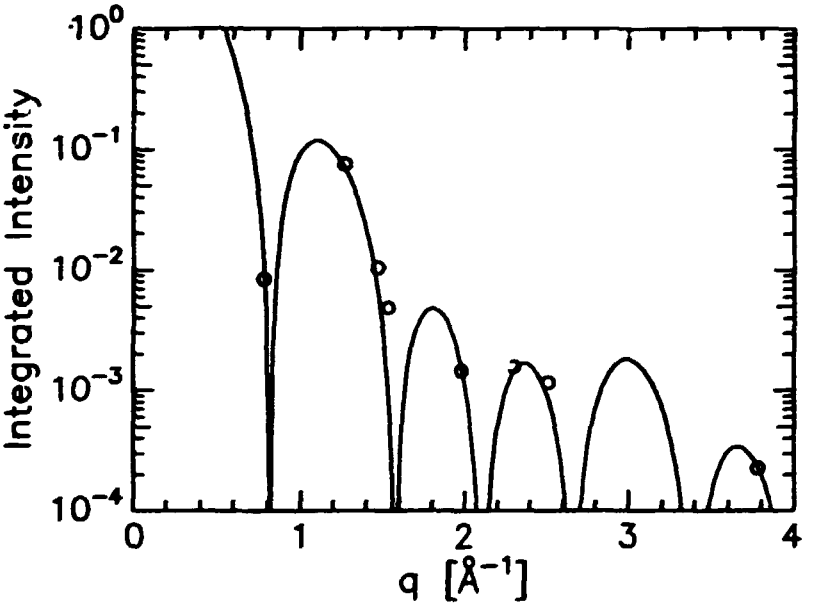

Fig. 1. Best fit by a shell with a finite thickness: Radius R_0=3.62 Å, thickness D=3.06 Å, and thermal parameter B=2.5 Å².

1.40 Phase Transformation in Solid C_{60}/C_{70}: an Electron Microscopy Study

(J. Bohr, *Department of Solid State Physics, Risø National Laboratory, Denmark*, G. Van Tendeloo, M. Op de Beeck, S. Amelinckx, *University of Antwerp, Belgium*, and W. Krätschmer, *Max-Planck-Institut für Kernphysik, Heidelberg, Germany*)

Crystals of icosahedral C_{60}/C_{70} clusters have been studied using electron diffraction and high-resolution electron microscopy. The as-grown crystals are found to be hexagonally close packed (HCP) but with a significant amount of stacking defects. Under electron irradiation the hexagonal crystal transform into a face-centered cubic (FCC) structure. Figure 1a shows an area of the sample which is partly transformed. The upper left part of the figure shows the hexagonal close packed structure. The lower right shows an area with the face centered cubic structure. Figures 1b and 1c shows high magnifications of the two structures.

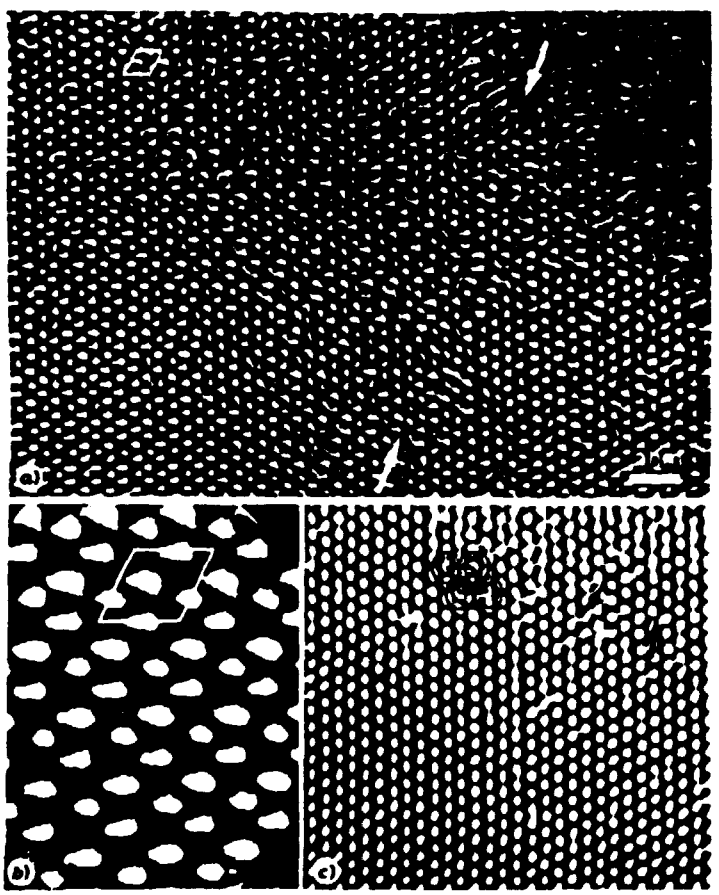

Fig. 1. High resolution image of a crystal of C_{60}/C_{70} clusters: a) image where both HCP (upper left part) and FCC (extreme lower right part) are coexisting. When viewing along the horizontal dot rows the 1/3 offset of the extra bright rows can be observed in the lower right corner. The two arrows indicate the border-line between HCP and FCP. b) high magnification processed image of the HCP phase of C_{60}; the unit cell is outlined; c) high magnification of the FCC phase of C_{60}, the arrows indicate larger clusters present in a matrix of C_{60} clusters.

1.41 Model Independent Analysis of Specular Relectivity Data

(J. Skov Pedersen, *Department of Solid State Physics, Risø National Laboratory, Denmark*)

An approach for analysing neutron and X-ray specular reflectivity data from stratified media having variation in the scattering length density near the surface has been developed. The method has its origin in small-angle scattering and it is composed of two steps: (i) Indirect Fourier Transformation[1] giving the profile correlation function $p(z)$ of the derivative $d\rho/dz$ of the scattering length density, (ii) square-root deconvolution[2] giving $d\rho/dz$ and ρ, the scattering length density profile. The only requirement for applying the method is that the scattering length density varies only in a limited range. In nearly all cases the approach does not require any knowledge of the chemical composition of the surface layer, and consequently incorporates a certain degree of objectivity. The method gives the smoothest profile which agrees with the experimental reflectivity data. It has been tested on simulated reflectivity data for a series of different surface profile, and subsequently used for analysing experimental data from fluorocarbon amphiphiles on water and salt solutions. The tests on simulated data show that the indirect Fourier transformation gives correlation functions agreeing very well with the corresponding functions of the original profiles. It is further demonstrated that the square-root deconvolution gives reliable results for the scattering length density profiles.

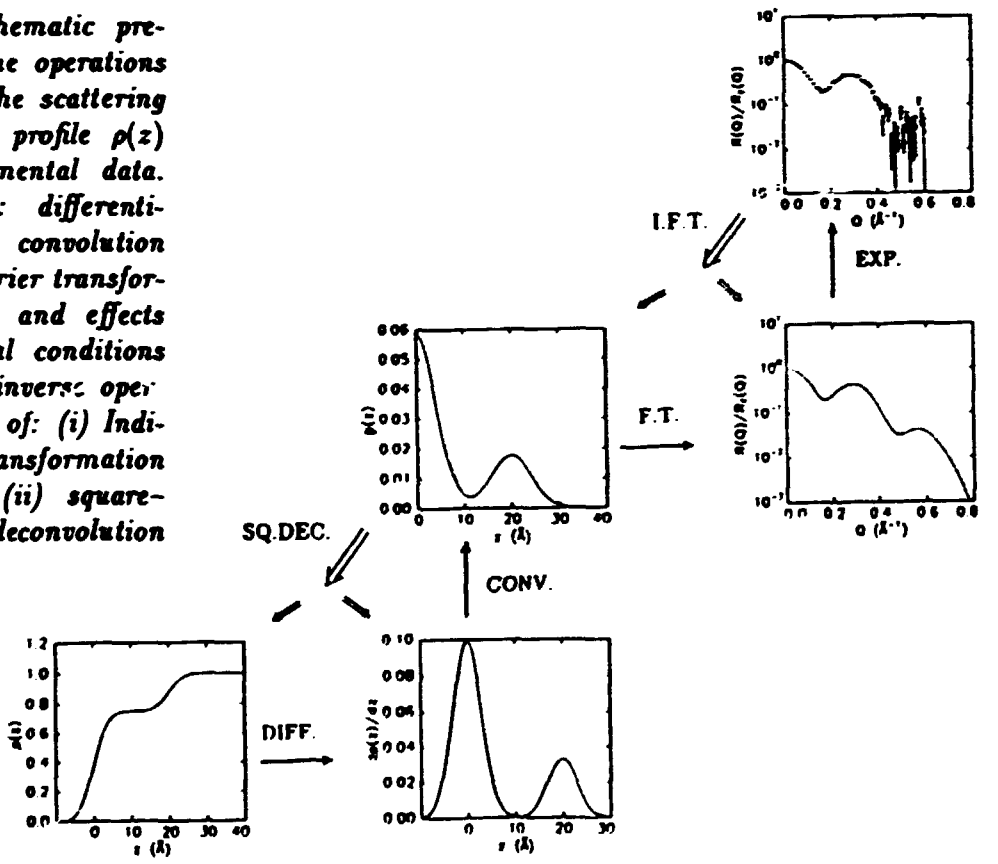

Fig. 1. Schematic presentation of the operations leading from the scattering length density profile $\rho(z)$ to the experimental data. The steps are: differentiation (DIFF.), convolution (CONV.), Fourier transformation (F.T.) and effects of experimental conditions (EXP.). The inverse operations consists of: (i) Indirect Fourier transformation (I.F.T.) and (ii) square-root deconvolution (SQ.DEC.).

[1] O. Glatter, (1977). J. Appl. Cryst. **10**, 415–421.
[2] O. Glatter, (1981). J. Appl. Cryst. **14**, 101–108.

1.42 Proteins at Interfaces: Neutron Reflectivity Measurements as a New Powerful Tool for Structural Investigations with Spatial Resolution on the Molecular Length Scale

(M. Lösche, M. Piepenstock, *Institut für physikalische Chemie, Johannes-Gutenberg Universität, Mainz, Germany*, K. Kjær, J. Als-Nielsen and D. Vaknin, *Department of Solid State Physics, Risø National Laboratory, Denmark*)

Structural investigations of molecular organic layers at aqueous surfaces have been conducted at the neutron reflectometer in the guide hall of the DR3 reactor. In a first study,[1] the structural properties of a monomolecular layer of a phospholipid, dipalmitoylphosphatidylcholine (DPPC), have been worked out. With the help of older X-ray reflectivity data from DPPC monolayers[2] the structure has been deduced with better resolution and reliability than would have been feasible using either of the techniques alone. A new method of refining data sets from both techniques simultaneously has been developed.[3] The results show that the phospholipid molecules in the monolayer at a lateral pressure, π = 42 mN/m, have structural properties very similar to DPPC in the bilayers which are the structural constituents of vesicle suspensions. The thicknesses of the hydrophobic chain region of the molecules (d_{chain} = 16 Å in the monolayer) and the chain tilt angles (t = 33°) agree to within 10% for the two systems, and the partial volumes of the lipid molecule in the films (V_{lipid}= 1124 Å^3) agree better than 2%. The extension of the hydrophilic head groups of the molecules into the water compartment is slightly larger in the monolayer case. Despite this fact, the head groups are sparingly hydrated with only about four interpenetrating water molecules per lipid molecule.

Whereas lipid monolayers, due to their low thickness, $d \simeq$ 25Å, are hard to characterize by neutron reflectivity alone, we found that molecular protein layers, prepared at functionalized lipid surface monolayers, are very well suited for neutron investigations due to their increased total layer thickness. In a model study on the streptavidin/biotin receptor/ligand system[4] (see Figure (c)) we showed that the protein forms a monomolecular layer on binding to a biotinylated lipid layer at the surface (Figures (a,b)). The streptavidin (SA) layer thickness, $d_{protein}$ = 44 Å, was correlated with the dimensions of the protein as known from X-ray crystallography[5]. Using a lipid with a short spacer moiety between the recognition group and the hydrophobic anchor[6] we found that SA binds spatially closely to the lipid monolayer as we were not able to detect water intervening between protein and lipid layers. In contrast, we quantified the water content of the two-dimensional (2D) protein aggregate: $N_w \simeq$ 260 per protein. This result means that only about 5 Å of water separate neighbouring protein molecules on average. The area per protein (plus interstitial water) in the films is $A_o \simeq$ 2900 Å^2, a lateral packing density comparable to the SA density in 3D crystals.

We found that structure formation may critically depend on the isotopic content of the sample. While the strength of any structural investigation of organic specimen based on neutron techniques relies on contrast variation, we found indications that $^2H/^1H$ exchange may affect the details of the formation of molecular aggregates. This is presumably due to changes in the strength of hydrogen bonds and to detuning the balance between the ordering Van-der-Waals interactions between lipid chain segments and the kink density in the chains creating local disorder. This result is of general importance for the inter-

pretation of neutron scattering experiments conducted to resolve the structure of organic samples. We have attempted to assess structural identity of different isotopically substituted samples by monitoring the macroscopic lateral structure of SA films by fluorescence microscopy[7]. In a number of measurements on different SA/lipid systems we have observed that the constitution of the lipid monolayer critically determines the structure of the protein monolayer underneath. Lateral protein packing densities between $1/(2700\ Å^2)$ and $1/(10000\ Å^2)$, equivalent to 93 wt% or 25 wt% of protein, respectively, have been observed. The mechanistic reasons for this sensitive dependence on the lipid monolayer is not well understood. In order to clarify these problems, X-ray reflectivity measurements on the same systems have been performed[8].

[1] D. Vaknin, K. Kjær, J. Als-Nielsen, and M. Lösche, (1991). Biophys. J. 59, 1325.
[2] C. A. Helm, H. Möhwald, K. Kjær, and J. Als-Nielsen, (1987). Europhys. Lett. 4, 697.
[3] D. Vaknin, K. Kjær, J. Als-Nielsen, M. Lösche, (1991). Makromol. Chem., Macromol. Symp. 46, 383.
[4] D. Vaknin, J. Als-Nielsen, M. Piepenstock, and M. Lösche, (1991). Biophys. J. *In press.*
[5] W. A. Hendrickson, A. Pähler, J. L. Smith, Y. Satow, E. A. Merritt, and A. P. Phizackerley, (1989). Proc. Natl. Acad. Sci. USA 86, 2190.
[6] R. Blankenburg, P. Meller, H. Ringsdorf, and C. Salesse, (1989). Biochemistry 28, 8214.
[7] M. Piepenstock, D. Vaknin, J. Als-Nielsen, and M. Lösche. *Manuscript in preparation.*
[8] M. Piepenstock, D. Vaknin, K. Kjær, J. Als-Nielsen, H. Ringsdorf, A. Diederich, and M. Lösche. *Manuscript in preparation.*

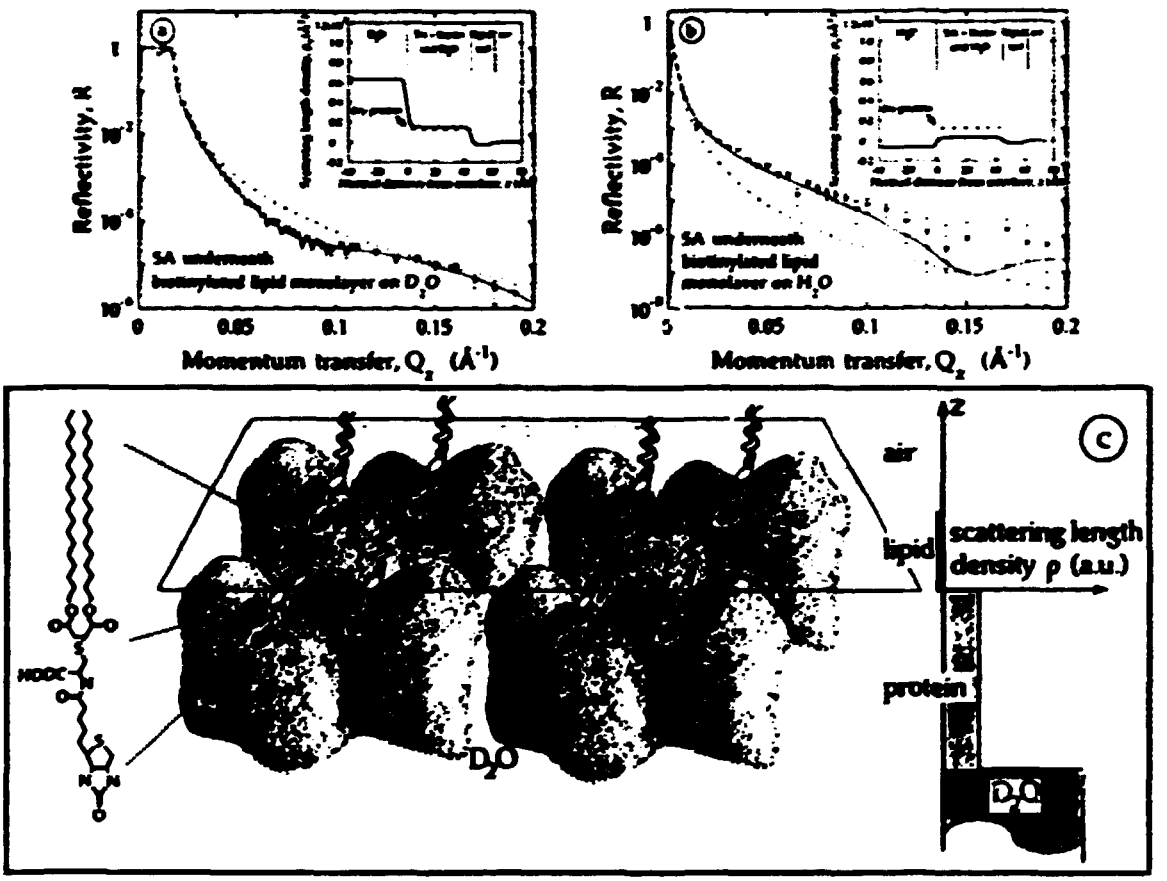

1.43 Neutron and X-ray Reflectivity Studies of Lamellar Films of Diblock and Triblock Copolymers.

(W.H. de Jeu, I.W. Hamley, P. Lambooy, *FOM-Institute for Atomic and Molecular Physics, Amsterdam, The Netherlands*, D. Vaknin, K. Kjær, J. Skov Pedersen, *Department of Solid State Physics, Risø National Laboratory, Denmark*, P. van Hutten, R. Seyger, and G. Hadziioannou, *Department of Chemistry, Groningen University, The Netherlands*).

Specular reflectivity of neutrons or X-rays can be used to determine the scattering density profile of a material perpendicular to its surface. We have applied these techniques to the study of the surface ordering of lamellar phases of A-B diblock and A-B-A triblock copolymers. In block copoplymers where the number of A and B monomers is approximately equal such phases are found below a temperature called the microphase separation temperature. The constraint of separation of A and B layers leads to significant distortions of the chain conformation away from the Gaussian state found in the disordered melt. The ends of the block copolymer molecules are thought to be confined to the interfaces between parallel lamellae and the characterisation of these interfaces is thus essential to an understanding of this organisation.

Neutron reflectivity is an ideal means to study such features using the contrast variation technique with selective deuterium isotope labelling of B monomers, so that A and B layers can be distinguished. We performed such studies on d-poly(styrene)/poly(2-vinylpyridine)(pSd/pVP) copolymers deposited on a silicon wafer using the neutron reflectometer at Risø. X-ray reflectivity is insensitive to the internal structure of the polymer film, but can consequently be used to provide an independent measure of total film thickness. It can also give information on the roughness of the polymer-substrate and polymer-air interfaces. X-ray reflectivity experiments on the same samples used for the neutron experiments were performed using the high resolution triple axis diffractometer at the FOM institute, Amsterdam.

Modelling of the neutron scattering length density profile provides layer thickness and the interfacial widths. We find that, as expected, in both di- and tri-block samples the pSd segregates preferentially to the surface whilst the layer adjacent to the substrate is pVP. We find that the top pSd layer is expanded by ~10% compared to half the thickness of internal pSd layers. There is an indication that for the triblock samples the scattering length density is higher in the top layer than in the others. Figure 1 shows a reflectivity curve for a triblock sample, together with an example of a model scattering length density profile. For the triblock copolymers there are interesting consequences resulting from the density profile. Firstly, surface segregation of one block together with the constraint of layering leads to a looping of the polymer in the top layer. Secondly, parts of the top layer can be readily lost, leaving 'islands' or 'holes' of looped polymers on the surface. Evidence for this is most graphically illustrated by X-ray reflectivity profiles, which show pronounced 'beating' (see Fig. 2), which is interpreted as arising from scattering from regions in the sample with two distinct thicknesses, which differ by one layer thickness. Atomic Force Microscopy measurements in progress in Groningen support this picture of the surface.

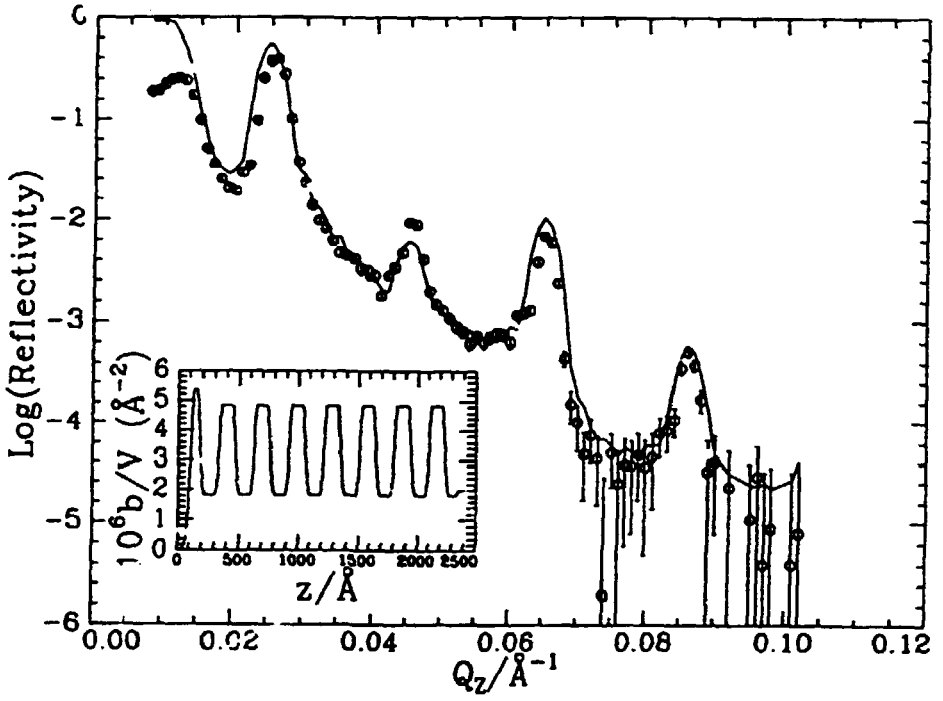

Fig. 1. Neutron reflectivity measured for a 30 K-60 K-30 K (M_W) triblock copolymer of d-(polystyrene) and poly(2-vinylpyridine) deposited on Si(111) (circles), together with a model curve (solid curve), calculated from the scattering density profile shown in the inset.

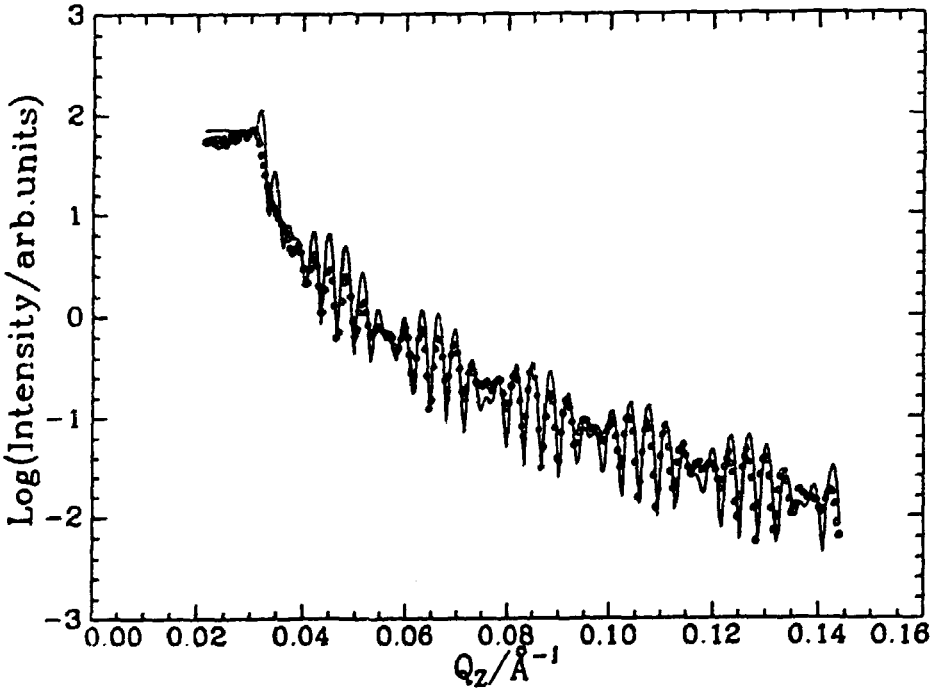

Fig. 2. Measured X-ray reflectivity as a function of Q_z for a triblock copolymer (circles). The pronounced 'beating' comes from the presence of two discrete film thicknesses, the model (solid curve) is for equal proportions of 1610 Å and 1912 Å thich sample.

1.44 Low–Symmetry Phases of Phospholipid Monolayers in the Coexistence Region of Their Phase Diagram

(R. M. Kenn, C. Böhm, H. Möhwald, *Institut für physikalische Chemie, Johannes-Gutenberg Universität, Mainz, Germany*, J. Als-Nielsen and K. Kjær, *Department of Solid State Physics, Risø National Laboratory, Denmark*)

Phospholipid monolayers at the air/water interface are interesting not only due to their biological relevance, but also because th y exhibit a large variety of structural conformations. In contrast to fatty acids, whose structural behaviour we have previously reported[1], they consist of two hydrophobic chains, which are linked together by a hydrophilic head group. Thus, one may expect influences of this linkage on their structure. In the case of fatty acids over pure water, at least four different phases with rectangular symmetry have been found, and none with a lower symmetry.

We report grazing incidence X-ray diffraction on two phospholipids, DMPE (L-α-dimyristoylphosphatidylethanolamin) and DSPE (L-α-distearoylphosphatidylethanolamin), which differ only in the length of their hydrophobic chains (*cf.* Fig. 1). Figures 2 and 3 summarise the results. At high surface pressures, a hexagonal structure is found. Decreasing the pressure, in both samples a transition into a phase with rectangular symmetry occurs, (pressures β for DMPE (Fig. 2); γ and β for DSPE (Fig. 3)). Upon decreasing the pressure further, (with increasing area per molecule), a splitting of the peaks into a triplet is observed, where the reflection maxima occur at different vertical components Q_z of the scattering vector. This splitting is more pronounced for the case of DSPE, due to the longer chains of this compound.

We suggest that this reduction of symmetry of the unit cell is due to the linkage of the two chains by the head group. This hypothesis is supported by analogy to the results of Leveiller *et al.* for arachidic acid on the surface of a $CdCl_2$ solution, where an oblique structure is observed[2]. Concurrently, in this system a commensurate head group lattice, formed by a crystalline Cd^{++} layer, could be identified. In the systems reported here, no reflections due to the head groups could be found, which is possibly due to the absence of long range positional order.

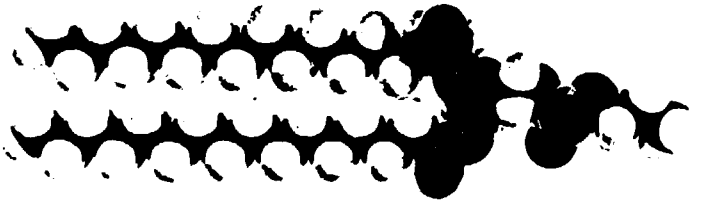

Fig. 1. $n = 10, 12, 14, 16$ *for DLPE, DMPE, DPPE, DSPE.*

[1] R. M. Kenn, C. Böhm, A. M. Bibo, I. R. Petersen, H. Möhwald, K. Kjær, and J. Als-Nielsen, (1991). J. Phys. Chem. **95**, 2092.
[2] F. Leveiller, D. Jacquemain, M. Lahav, L. Leiserowitz, M. Deutsch, K. Kjær, and J. Als-Nielsen, (1991). Science **252**, 1532–1536.

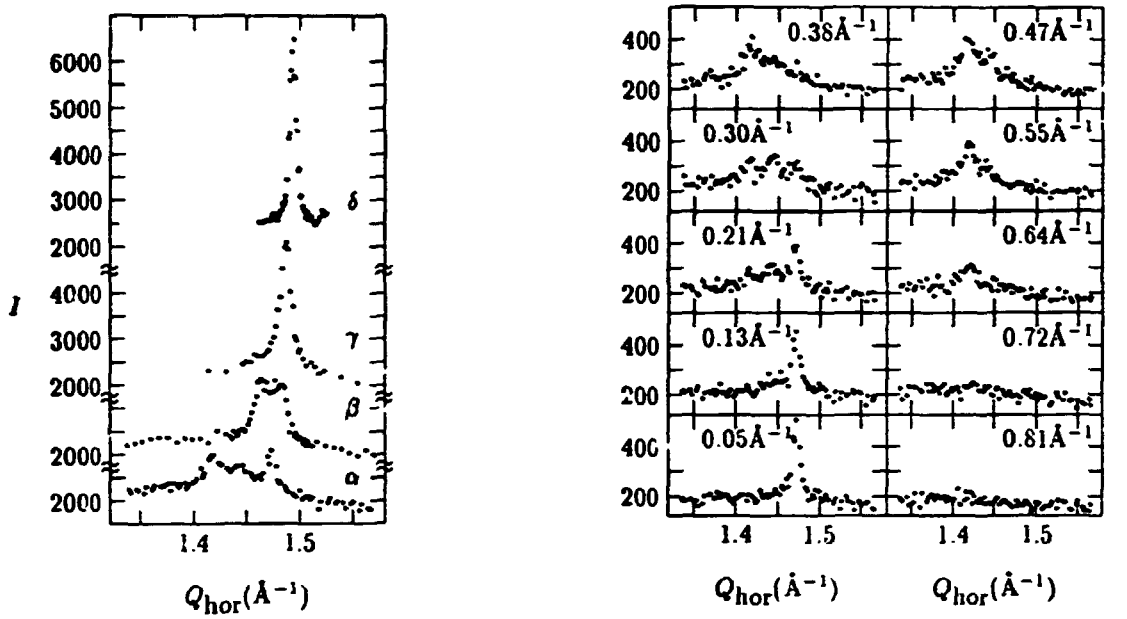

Fig. 2. Left: Q_z integrated intensity vs. horizontal scattering vector for DMPE monolayers at 20°C and different lateral pressures: α : 12 mN/m, β : 20 mN/m, γ : 27 mN/m and δ : 35 mN/m. Right: Scattered intensity vs. horizontal scattering vector for Q_z values indicated in the figure, (DMPE, 20 °C, Π = 12 mN/m, peak "α" of the left figure).

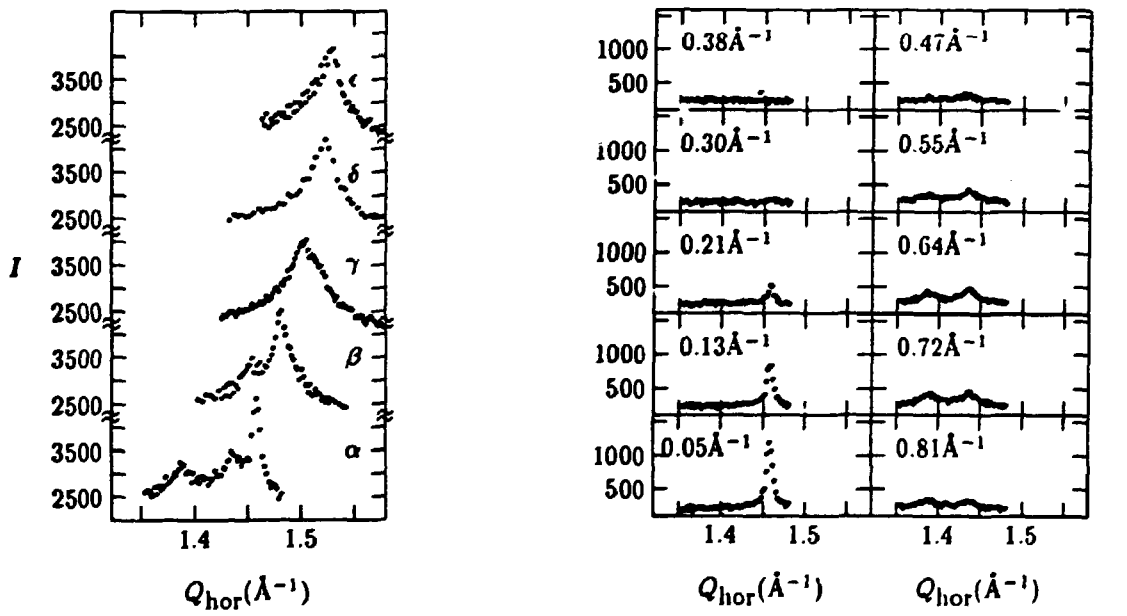

Fig. 3. Left: Q_z integrated intensity vs. horizontal scattering vector for DSPE monolayers at 13°C and different lateral pressures: α : 1 mN/m, β : 20 mN/m, γ : 30 mN/m, δ : 40 mN/m and ε : 50 mN/m. Right: Scattered intensity vs. horizontal scattering vector for Q_z values indicated in the figure, (DSPE, 13°C, Π = 1 mN/m, peak "α" of the left figure).

1.45 Influence of Chirality on Phospholipid Monolayer Structure

(C. Böhm, H. Möhwald, *Institut für physikalische Chemie, Johannes-Gutenberg Universität, Mainz, Germany*, L. Leiserowitz, M. Lahav, *Dept. of Materials and Interfaces Weizmann Institute of Science, Rehovot, Israel*, J. Als-Nielsen and K. Kjær, *Department of Solid State Physics, Risø National Laboratory, Denmark*)

Grazing-incidence X-ray diffraction studies of lipid monolayers have yielded a wealth of information on the arrangement of the aliphatic 'tails' of the monolayer molecules. No information has been obtained, as yet, on 'head' group order because no discernible contribution from the head groups to the diffraction signal has been identified. In an effort to derive information about the ordering of the phosphatidylethanolamine (PE) heads in monolayers of DPPE (dipalmitoyl-PE: a PE 'head group' linked with *two* hydrocarbon 'tails', *cf.* Fig. 1 of 1.44) we have studied the influence of chirality in the head on monolayer structure and on the crystallisation of water soluble phosphorylethanolamine (PEA) at the monolayer.

Figure 1 shows the scattered intensity *vs.* in-plane scattering vector q_{xy}, for the pure enantiomer, L-DPPE (all left-handed molecules), and for racemate DL-DPPE (*i.e.*, consisting of equal amounts of left- and right-handed molecules), at low surface pressure. Scans are shown for various out-of-plane scattering vectors q_z. For the pure enantiomer three distinct peaks are seen at $q_{xy} = 1.38$, 1.425 and 1.47 Å^{-1} (for $q_z = 0.7$, 0.5 and 0 Å^{-1}, respectively), indicative of an oblique unit cell. In other lipid monolayers, the symmetry of the lattice of the hydrocarbon tails has never been lower than centered-rectangular, except in the case of strong interactions between the head groups[1)], and thus we speculate that the break of symmetry seen here may be due to the PE head groups linking the two hydrocarbon tails, if the head groups are uniformly oriented. Hence, a (centred-)rectangular lattice may reappear in the absense of head group order. Apparently, this is the case for the racemic mixture (Fig. 1, right) which gives only two distinct peaks in the powder pattern: at $q_{xy} = 1.405$ and 1.48 Å^{-1} (for $q_z = 0.55$ and 0 Å^{-1}, respectively), in evidence of a centred-rectangular lattice with the aliphatic chains uniformly tilted towards their nearest neighbours.

The observation that an enantiomeric 'impurity' suffices to destroy the head group order is in accordence with our finding that PEA crystallisation (requiring ordered PE head groups) was possible only under L-DPPE monolayers and not under the DL-DPPE mixture.

[1)] F. Leveiller, D. Jacquemain, M. Lahav, L. Leiserowitz, M. Deutsch, K. Kjær, and J. Als-Nielsen, (1991). Science **252**, 1532-1536.

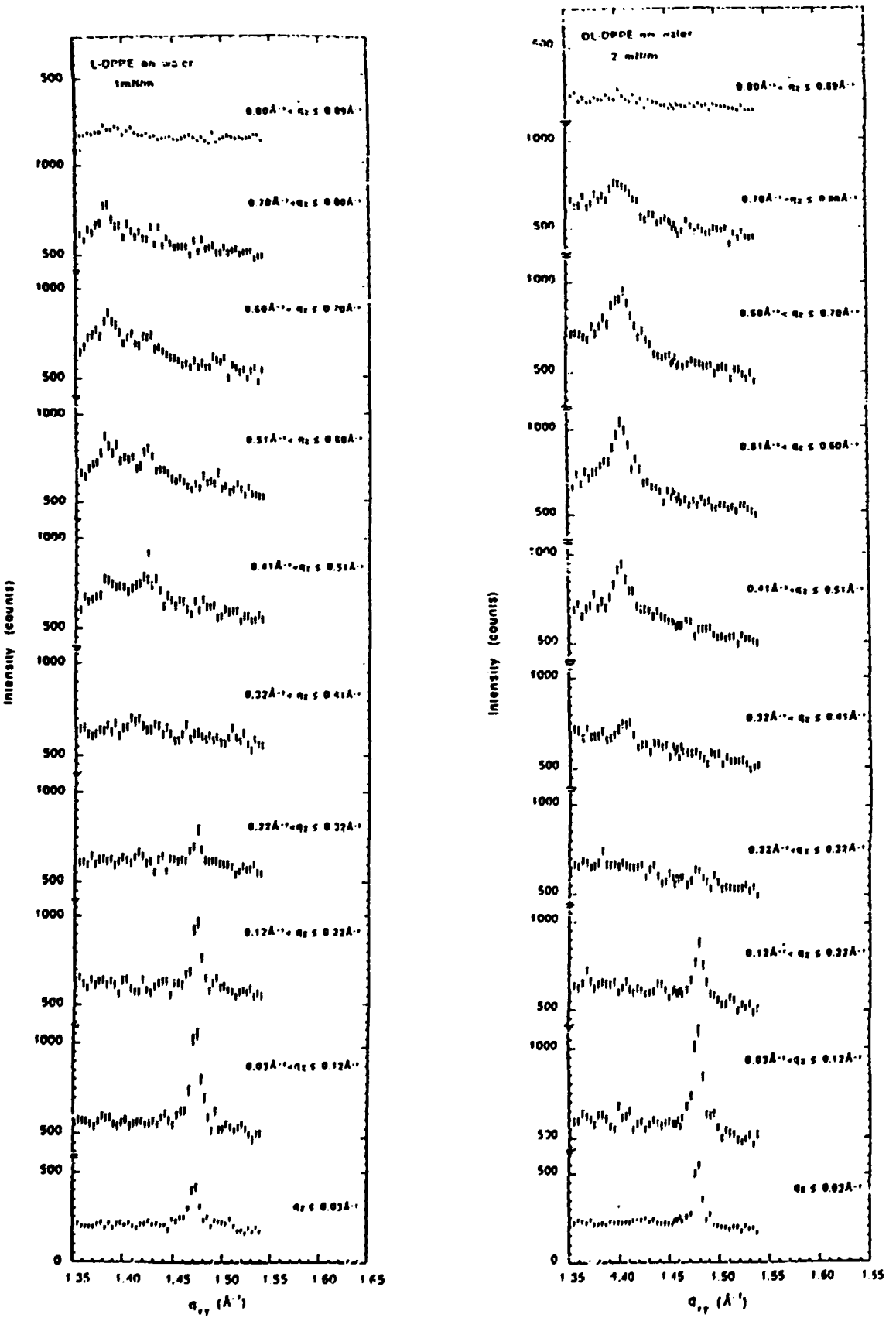

Fig. 1. Grazing-incidence diffraction data. Left: L-DPPE at 1 mN/m surface pressure. Right: DL-DPPE at 2 mN/m.

1.46 Determination of Two-Dimensional Crystal Structures of Monolayers of Amphiphilic Molecules at the Air–Water Interface

(F. Leveiller, D. Jacquemain and L. Leiserowitz, *Department of Materials and Interfaces, Weizmann Institute of Science, Rehovot, Israel*, J. Als-Nielsen and K. Kjær, *Department of Solid State Physics, Risø National Laboratory, Denmark*)

Grazing incidence X-ray diffraction (GID) measurements have been performed using the liquid surface diffractometer at the synchrotron beamline D4 in HASYLAB at DESY, Hamburg, on uncompressed monolayers of several amphiphilic molecules ($R-CO_2H$, R-OH, $R-CONH_2$, where R denotes an alkyl chain C_nH_{2n+1}) over water at a temperature of 5°C. All these monolayers formed crystalline self-aggregates with lateral order ranging in extent from 200 Å to 1000 Å [1]. It has proven possible to determine not only the unit cell dimensions and the general molecular packing characteristics of the two-dimensional crystals from the Bragg rod intensity profiles of the GID data, but also details of the crystal structure almost at atomic resolution. This was done via a two-pronged approach: by fitting molecular models to the Bragg rod intensity profiles, complemented by lattice energy calculations[2]. The latter method proved invaluable in fixing those molecular orientation parameters which were insensitive to the Bragg rod data, as illustrated for a monolayer of the acid $C_{29}H_{59}CO_2H$ in Figs. 1, 2 and 3 and for a monolayer of the alcohol $C_{31}H_{63}OH$ in 1.47. In particular, it was possible to distinguish between two structures which differ only by a 180° rotation around the molecular axis since there is a calculated energy difference of 4.3 kcal/mole between the energy minimum structure and its 180° rotational counterpart (see Fig. 3, arrows).

[1] D. Jacquemain, F. Leveiller, S. P. Weinbach, M. Lahav, L. Leiserowitz, K. Kjær, and J. Als-Nielsen, (1991). J. Am. Chem. Soc. **113**, 7684.
[2] F. Leveiller, D. Jacquemain, L. Leiserowitz, K. Kjær, and J. Als-Nielsen, (1991). *Manuscript in preparation.*

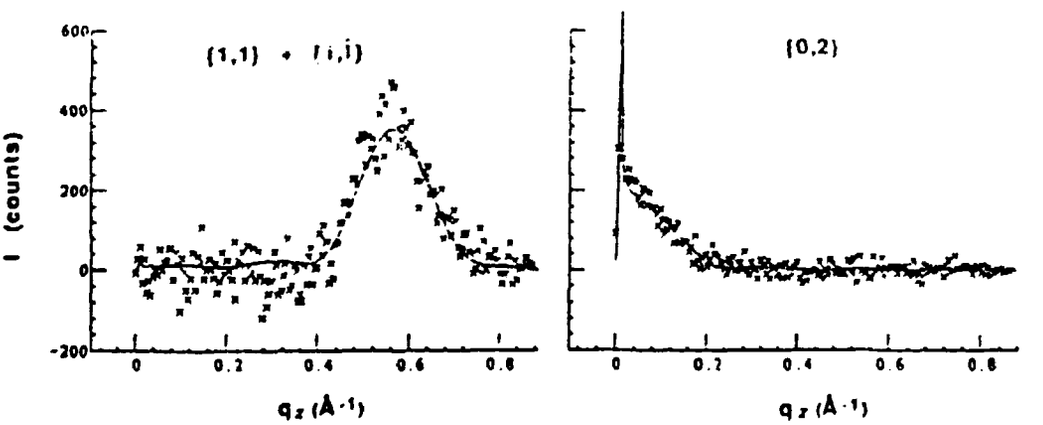

Fig. 1. Measured and calculated (full line) Bragg rod profiles for the acid amphiphile $C_{29}CO_2H$ packing with p1 plane group symmetry as shown in Fig. 2.

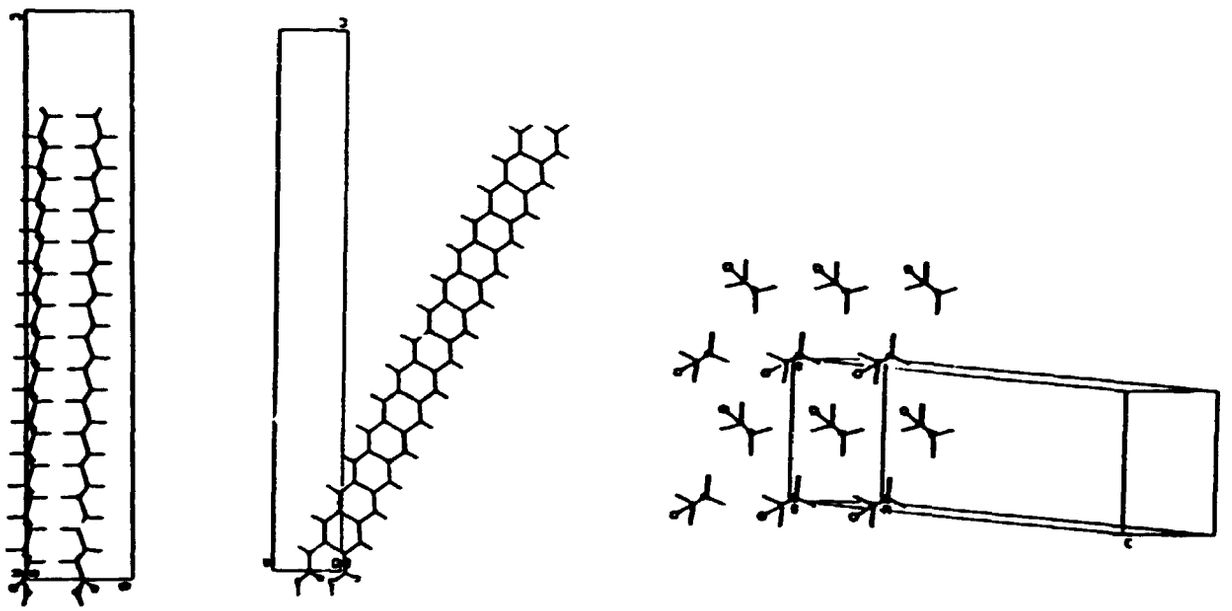

Fig. 2. Molecular packing arrangement for $C_{29}CO_2H$: the molecules are tilted by 27° from the vertical in a direction deviating from that of the **a** *axis by 4.5°; (left) as viewed along the* **a**-*axis, (center) the* **b**-*axis, (right) and along the molecular axis.*

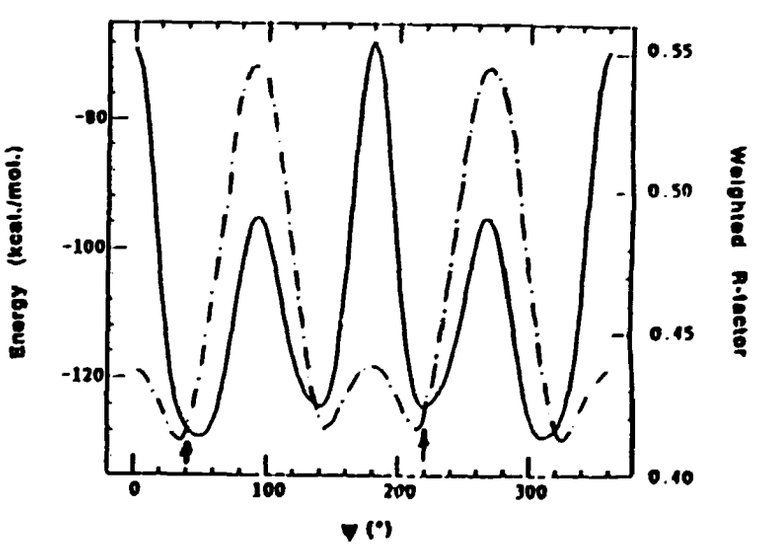

Fig. 3. Weighted R-factor for the fit shown in Fig. 1 (dashed-dot line) and lattice energy (full line) for $C_{29}CO_2H$ as a function of Ψ, the angle of molecular axial rotation, for the molecular model presented in Fig. 2.

1.47 Two-Dimensional Structure of Self-Aggregates of Amphiphilic Alcohols by Grazing Incidence X-ray Diffraction

(J.-L. Wang, F. Leveiller, D. Jacquemain, M. Lahav, and L. Leiserowitz, *Department of Materials and Interfaces, Weizmann Institute of Science, Rehovot, Israel*, and J. Als-Nielsen and K. Kjær, *Department of Solid State Physics, Risø National Laboratory, Denmark*).

Grazing incidence X-ray diffraction (GID) measurements performed on the liquid surface diffractometer at beamline D4 in HASYLAB at DESY, Hamburg showed that, in monolayers on water at 5°C, amphiphilic alcohol molecules ($C_nH_{2n+1}OH$, n=23,30,31) spontaneously form large 2D-crystalline clusters[1]. The two-dimensional structures of these clusters have been determined at almost atomic resolution using Bragg rod fittings and lattice energy calculations[2]. We could show for instance that it was possible, using the complementarity of the two methods, to determine the molecular orientation and the plane group symmetry of the alcohol crystals unambiguously[3]. Further, our refinements of the model to the data proved sensitive to minor structural changes in the model structures; fits performed with different conformations of the $-CH_2OH$ head group pinpointed a model with an all-*trans* conformation[3]. Finally, the structure refinement also shows that better fits to the Bragg rod data for both the alcohol and acid monolayers (*cf.* 1.46 reporting on $C_{29}H_{59}COOH$) were obtained by a minor relaxation of the two-dimensional plane group symmetry. As an example, we show the observed and calculated Bragg rod intensity (Fig. 1A) as well as the deduced molecular packing (Fig. 1, B-D) for the monolayer structure of $C_{31}H_{63}OH$, where the symmetry was relaxed from (rectangular) *pg* to (oblique) *p*1 by a minor adjustment of the packing arrangement.

[1] D. Jacquemain, F. Leveiller, S. P. Weinbach, M. Lahav, L. Leiserowitz, K. Kjær, and J. Als-Nielsen, (1991). J. Am. Chem. Soc. **113**, 7684.
[2] F. Leveiller, D. Jacquemain, L. Leiserowitz, K. Kjær, and J. Als-Nielsen. *Manuscript in preparation.*
[3] J.-L. Wang, F. Leveiller, D. Jacquemain, M. Lahav, L. Leiserowitz, K. Kjær, and J. Als-Nielsen. *Manuscript in preparation.*

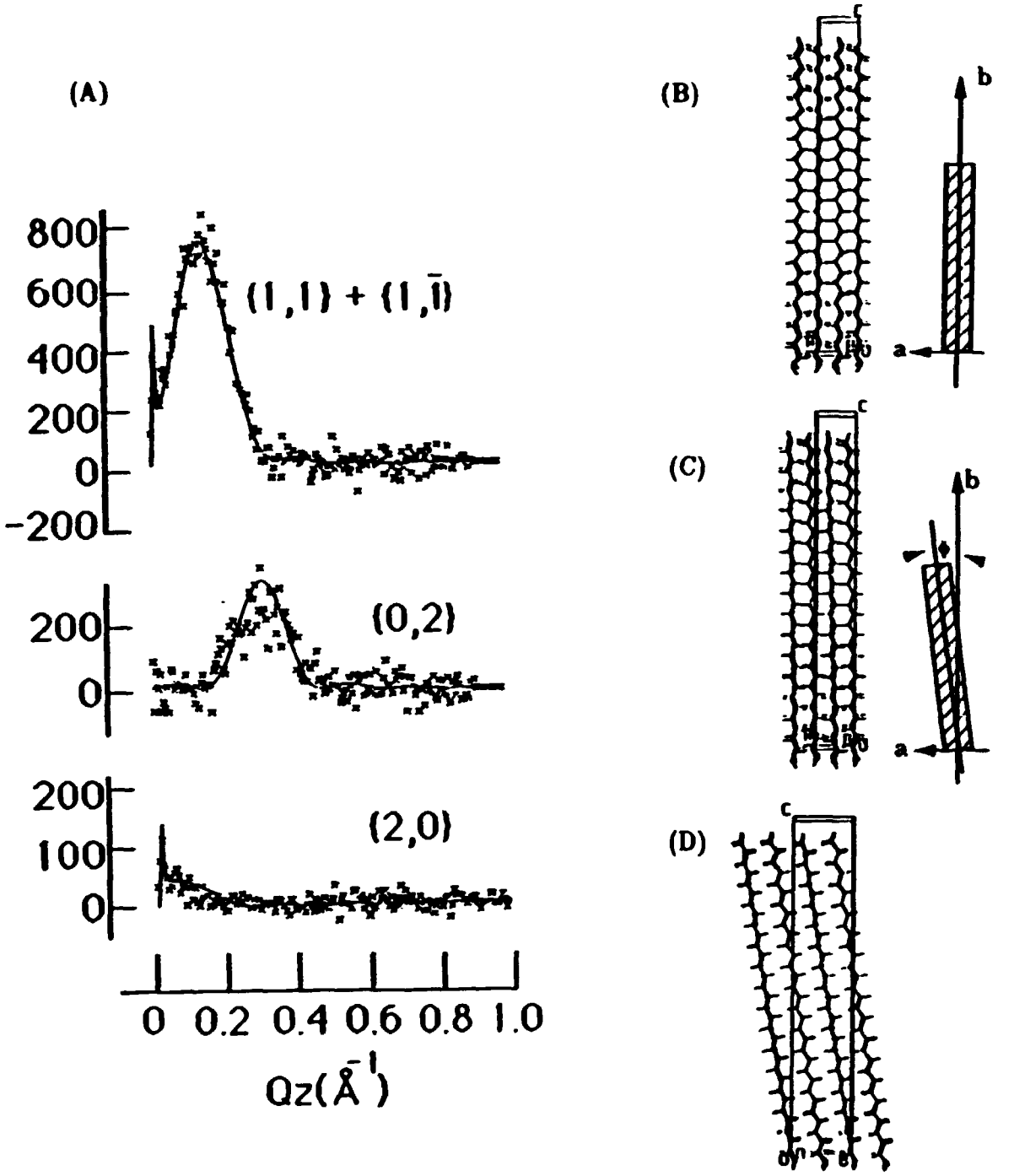

Fig. 1. (A) Calculated and observed Bragg rod profile for the $\{1,1\} + \{1,\bar{1}\}$, $\{0,2\}$, *and* $\{2,0\}$ *reflections for the* $C_{31}H_{63}OH$ *monolayer packing with* p1 *plane group symmetry as shown in (C) and (D). (B-D) Molecular packing arrangements for* $C_{31}H_{63}OH$. *(B), for big* pg *plane group viewed along the* b*-axis, the tilt direction is in the direction of the* b*-axis; (C), the relaxation of the symmetry to plane group* p1 *yields a tilt direction which deviates from the direction of the* b*-axis by an angle* $\phi=9.1°$; *(D), same packing arrangement as in (C) but viewed along the* a*-axis.*

1.48 Effect of Solvent on Two-Dimensional Crystal Growth

(S. Weinbach, D. Jacquemain, F. Leveiller, M. Lahav, and L. Leiserowitz, *Department of Materials and Interfaces, Weizmann Institute of Science, Rehovot, Israel*, J. Als-Nielsen and K. Kjær, *Department of Solid State Physics, Risø National Laboratory, Denmark*)

We have studied the effect of solvent on growth and structure of 2-D crystals of uncompressed monolayers of long chain amide systems ($C_{19}H_{39}CONH_2$, $C_{19}H_{39}CONHC_2H_4CONH_2$) using grazing incidence X-ray diffraction (GID). Last year we examined the effect of the solvents formic acid (HCO_2H) and formamide ($HCONH_2$) on the 2-D crystal growth of the monolayer $C_{19}H_{39}CONH_2$. Over pure water and over 1M formamide solution the monolayer formed crystalline aggregates with an average lateral coherence length of *ca.* 300 Å. Over a 1M formic acid solution, no GID peaks were visible, indicating little or no lateral order. The inhibiting effect of formic acid was explained in terms of repulsion between lone-pair electrons of neighboring formic acid molecules bound to the monolayer molecules. Recently we performed an analogous set of GID experiments with $C_{19}H_{39}CONHC_2H_4CONH_2$ as the monolayer. Over pure water (Fig. 1, top) we obtained three sharp and distinct GID peaks indicating a high lateral order with molecules arranged in an oblique cell. Over 1M formic acid solution (Fig. 1, center), we obtained GID peaks similar in position and intensity to those over pure water. Unlike the monolayer $C_{19}H_{32}CONH_2$, the presence of two amide groups in the molecule of $C_{19}H_{39}CONHC_2H_4CONH_2$ overcomes the repulsive effect of the formic acid, permitting pronounced crystalline growth. Over 1M formamide (Fig. 1, bottom), we obtained not only crystalline aggregation of the monolayer, but further, the intensities of the two peaks at 2θ=21.0° and 21.4° (λ=1.41 Å), as compared to those over pure water or 1M formic acid, indicate that formamide solvent is bound in an ordered manner to the monolayer head group. We plan to determine the detailed structures of the monolayer and the monolayer bound to solvent molecules from the Bragg rod data. These GID results strongly suggest ordered nonionic solvent molecules bound to a monolayer: results akin to the GID results obtained on bound monolayers of Cd^{2+}:arachidate which demonstrated ordered Cd ion binding[1].

[1] F. Leveiller, D. Jacquemain, M. Lahav, L. Leiserowitz, M. Deutsch, K. Kjær and J. Als-Nielsen, (1991). Science **252**, 1532.

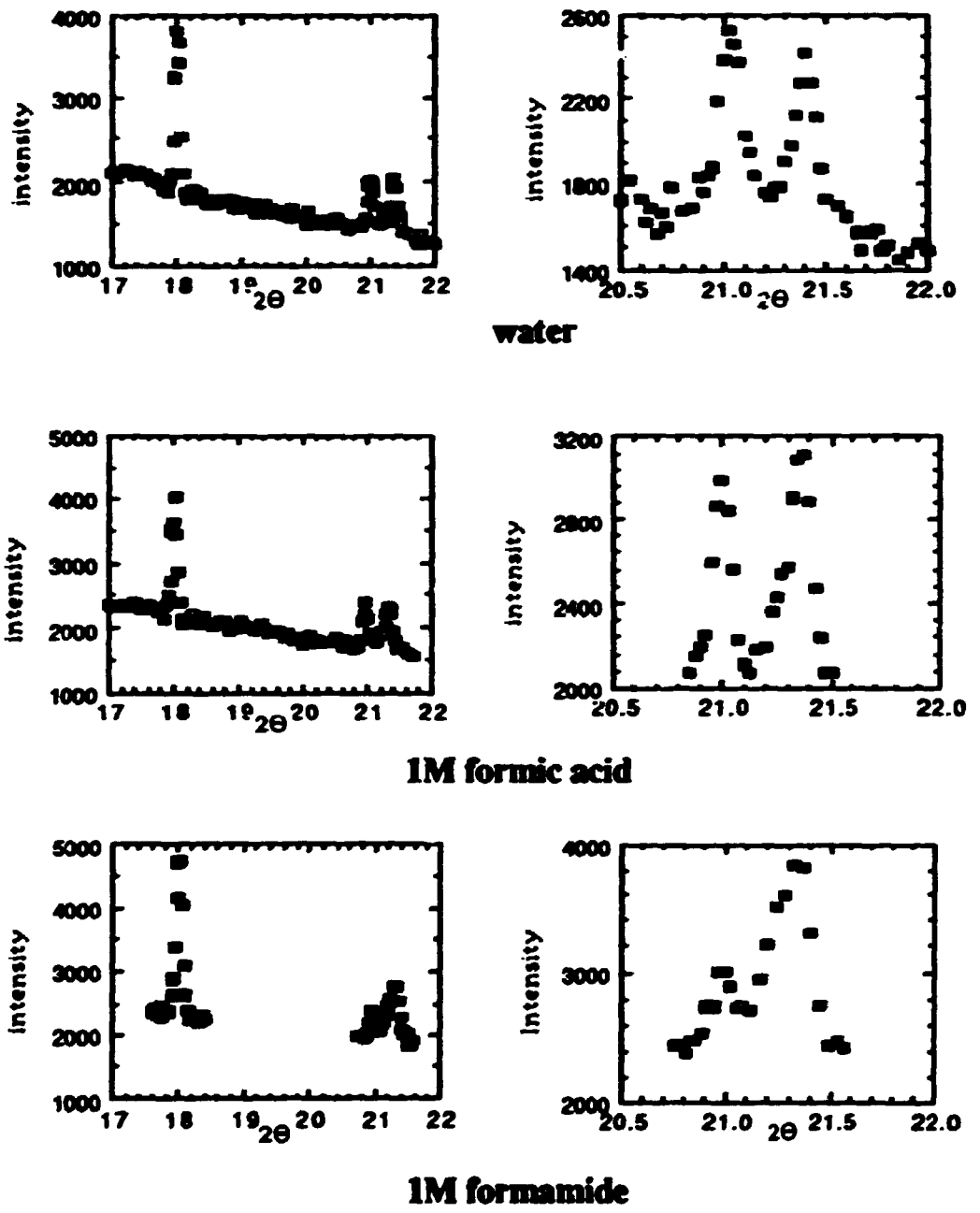

Fig. 1. GID pattern of $C_{19}H_{39}CONHC_2H_4CONH_2$ over pure water, 1M formic acid, and 1M formamide.
Left: integrated over $0.0 < q_z < 0.5$ Å^{-1};
Right: integrated over $0.16 < q_z < 0.85$ Å^{-1}.

1.49 Solution Structure and Interaction of Thiol–Ester Proteins

(R. Österberg, *The Swedish University of Agricultural Science, Uppsala, Sweden*, A. Ikai, *Tokyo Institute of Technology, Japan*, and K. Mortensen, *Solid State Physics Department, Risø National Laboratory, Denmark*)

Within the family of native thiol–ester proteins there are monomers, dimers and tetramers with monomeric molecular masses ranging from 185 to 200 kDalton. One kind of monomeric thiol–ester proteins are those involved in the cascade reaction of the complement system. For instance, activation of the *classical* or the so–called *alternative pathway* occurs via enzymatic cleavage of the proteins C3 and C4, respectively. In a series of SANS and SAXS studies we have characterized the C3, C4, and C5 proteins and analyzed their reactions of activation in some detail[1–4].

The dimeric and tetrameric thiol–ester proteins seem to function mainly by inhibiting, binding and eliminating proteases from the blood stream. The tetramer might have formed as a result of gene duplication since dimers are only found among animals on a lower level of evolution such as lobster, crayfish, and hagfish. Our SAXS–study on the hagfish dimer yielded information which could be analyzed in the form of a molecular model not only for the dimers but also for the tetramers and their reaction products[5].

More recently, we have analyzed SAXS and SANS data from a monomer which function among rats and mice both as a protease inhibitor and as an acute phase protein. The result indicates that two domains within this protein can attain different equilibrium conformations. Of recent interests are also the tetrameric protease inhibitors from eggs of hen and crocodile, ovomacroglobulins. They simulate the structure and reactions of human α_2–macroglobulin, in spite of the fact that they do not contain any labile thiol–esters. Although we have good SANS data for the scattering vector $q < 0.25$ Å^{-1} for the native protein and its methylamine analogue, protease binding also has to be investigated by both SAXS and SANS before this study is complete.

[1] R. Österberg, B. Malmensten, U. Nilsson, G. Eggertsen, and J. Kjems, (1988). Int. J. Biol. Macromol. **10**, 15–20.
[2] R. Österberg, U. Nilsson, and G. Eggertsen, (1985). J. Biol. Chem. **260**, 12970–12973.
[3] R. Österberg, U. Nilsson, T. Stigbrand, and J. Kjems, (1989). Eur. J. Biochem. **183**, 507–511.
[4] R. Österberg, B. Malmensten, T. Bovie, U. Nilsson, T. Stigbrand, and K. Mortensen, (1991). Molecular Immunology **28**, 959–963.
[5] R. Österberg, B. Malmensten, and A. Ikai, (1991). Biochemistry **30**, 7873–7875.

1.50 Studies on Humic Acid Structure and Metal Ion Binding under Various Environmental Conditions

(R. Österberg, *The Swedish University of Agricultural Science, Uppsala, Sweden*, O. Wahlberg, *Department of Inorganic Chemistry, KTH, Stockholm, Sweden*, and K. Mortensen, *Solid State Physics Department, Risø National Laboratory, Denmark*)

Recent advances in biological disciplines have created a demand for ever deeper research not only in special biological fields, but also in neighboring fields involving the whole biosphere. Thus, a logical expansion would be a correlation of biological data with environmental factors so that, in the future, processes such as optimization of ecosystems can be better understood. For instance, an improvement of life processes in the plant and animal kingdoms seems possible once operative forces and fluxes in the ecosystem are better known.

One such ecosystem of great importance for the biosphere is the humic acid system. It is present in soils and all natural water systems and it is the key system for the transport of nutrient to the plant kingdom. Due to its amphipatic character it binds both hydrophilic and hydrophobic compounds, involving not only essential metal ions and organic compounds but also toxic metal ions as well as herbicides and pesticides. In our studies on humic acids, initiated by the late prof. Lindqvist, SANS has proven to be the most appropriate and powerful method. It is combined with high-precision electromotive force methods. Our recent findings are summarized below:

i) Humic acids are highly aggregated at pH-values corresponding to those of 'acid rain fall', pH 4-6. The aggregation is H^+-catalyzed.

ii) The largest clusters show average radius of gyration in the range 250 - 300 Å, and the results appears to be independent of source and method of preparation[1]. The distance distribution function, $p(r)$, shows that the magnitude of the maximum distance within the largest clusters is of the order of magnitude 1000 Å.

iii) Detailed analysis of the SANS-data on the basis of structural models has been initiated, however, polydispersity makes it complicated.

[1] R. Österberg, I. Lindqvist, and K. Mortensen, (1991). *Submitted.*

1.51 Temperature Dependence of the Kinetics of Urea–Induced Dissociation of Human Plasma α_2–Macroglobulin

(B. Sjöberg, S. Pap, *Department of Medical Biochemistry, University of Göteborg, Sweden*, and K. Mortensen, *Department of Solid State Physics, Risø National Laboratory, Denmark*)

Human α_2–macroglobulin (α_2M) is one of the major proteinase inhibitors of blood plasma. It is unique among plasma proteinase inhibitors in its broad spectrum of reactivity for proteinases. α_2M consists of four identical polypeptide chains. Two of these chains are linked together by disulfide bonds. Two such disulfide bonded dimers are associated by so-called 'non-covalent' interactions forming the native tetramer. It is therefore possible to produce two types of half-molecules, either by breaking the non-covalent bond, or by breaking the disulfide bond. The disulphide inter-subunit contacts seem to be very well defined, because α_2M easily dissociates into half-molecules upon reaction with dithiothreitol. This dithiothreitol induced dissociation is reversible in the sense that the half-molecules can be reassociated to a particle having the characteristics of native α_2M[1]. Breaking the non-covalent bond appears to be more complicated, and the dissociation needs either a large amount of dodecyl sulphate or urea, or very low pH. In any case the reaction is irreversible, and the native structure is lost upon dissociation. In the present investigation small angle scattering (neutron and X-ray) has been used in order to get further insight into the non-covalent bond. Urea was used for the dissociation, and the kinetics in the dissociation of α_2M was measured as a function of temperature. In the figure is shown representative examples of experimental data for the dissociation at three temperatures, as represented by the relative forward scattering, *i.e.* molecular mass relative to the native α_2M It was found that the reaction has a marked minimum in dissociation rate at 15°C. By analyzing these data in terms of transition–state theory it was found that the dissociation is associated with a large and positive change in heat capacity, which is interpreted as a melting associated with hydrophobic interactions. We therefore propose, that the non-covalent bonding in α_2M is a result of hydrophobic interactions[2].

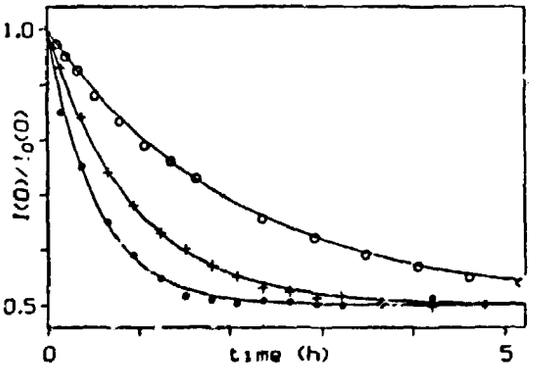

Fig.1. SANS data of urea-induced dissociation of α_2M as observed at -2.1°C (•), 21.0°C (o), and 29.7°C (+)

[1] B. Sjöberg and S. Pap, (1985) Eur. Biophys. J. 278, 325-328.
[2] B. Sjöberg, S. Pap, and K. Mortensen, (1991). *Manuscript submitted.*

1.52 Structure of RecA–DNA Complexes Studied by Small Angle Neutron Scattering Measurements on Flow-Oriented Samples

(B. Nordén, C. Elvingson, M. Kubista, *Department of Physical Chemistry, Chalmers University of Technology, Göteborg, Sweden*, E. Sjöberg, *Department of Medical Biochemistry University of Göteborg, Sweden*, H. Ryberg, M. Ryberg, *Department of Plant Physiology, University of Göteborg, Sweden*, K. Mortensen, *Department of Solid State Physics, Risø National Laboratory, Denmark* and M. Takahashi, *Institute de Biologie Moléculaire du CNRS, Straßbourg, France*)

RecA is a protein which plays a key role in the DNA repair function, including the promotion of general genetic recombination. In the presence of ATP, RecA binds cooperatively to DNA forming rigid fibrous complexes in which RecA monomers are arranged in a helical manner around DNA. The DNA is accommodated in the interior of the helix. Since RecA fibers can simultaneously accommodate at least two DNA molecules, it has been suggested that the recombination takes place inside the RecA fiber. The present study focuses on the structure of RecA–DNA complexes in solution. In the course of the recombination reaction DNA bases make complexes that represent intermediates in the recombination reaction. Knowledge of the structure of these pairs is believed to give important insight into the recombination mechanism. It is especially important to learn about the orientation of the DNA bases. The studies have been performed on samples subjected to shear flow, which leads to macroscopic orientation of the elongated molecules. In addition to neutron scattering, absorption of linearly polarized light (*linear dichroism*) has been used. In the figure is shown a contour plot of the SANS pattern of a RecA:DNA complex with double stranded DNA, as obtained at rest and when flow-oriented. The subsidiary maxima seen in both plots reflect the helical pitch of approximately 100Å. The oriented sample clearly shows an anisotropic pattern, as expected. Analysis of the anisotropic data gives indication that the RecA:DNA of both double and single stranded DNA display almost perpendicular base orientation.[1,2]

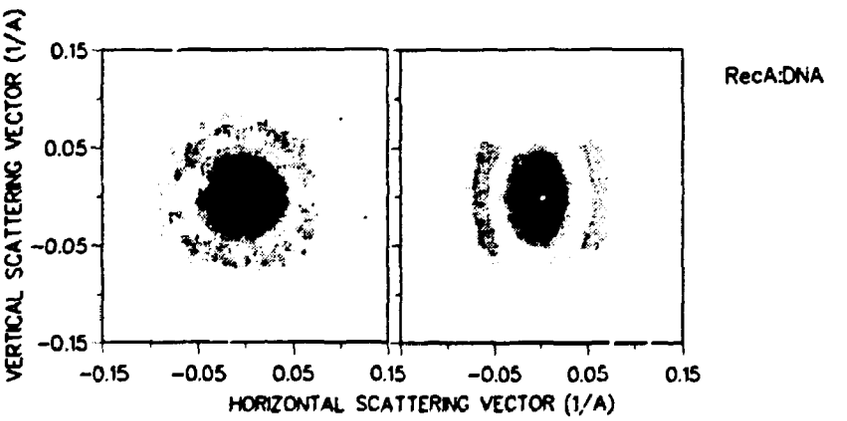

Fig. 1. 2D SANS data on RecA:DNA as obtained without (left) and with shear-orientation (right).

1) B. Nordén, C. Elvingson, T. Eriksson, M. Kubista, B. Sjöberg, M. Takahashi, and K. Mortensen, (1990). J. Mol. Biol. **216**, 223, and B. Nordén, C. Elvingson, M. Takahashi, M. Kubista, B. Sjöberg, H. Ryberg, M. Ryberg, and K. Mortensen (199?) *Manuscript submitted.*

1.53 Structural Investigations of Type A Influenza Virus by SANS

(K. Duff, A. Cudmore, J. Bradshaw, *Edingburgh University, Scotland, U.K.* and J. Skov Pedersen *Department of Solid State Physics, Risø National Laboratory, Denmark*)

Small-angle neutron scattering experiments have been initiated in order to elucidate the physical structure of influenza A virus under a variety of conditions. It was hoped that the experiments performed would, at conclusion, provide a low-resolution structural model in terms of concentric shells and give information on finer detail changes resulting from addition of antibodies and, separately, from changing the sample environment to an acidic medium. Strucural work has previously been done on the type B influenza virus[1].

The results obtained from the first SANS measurements were unfortunately inconclusive. The samples' polydispersity was too high, resulting in a general smoothing of the profile and a subsequent loss of details. The purpose of the first set of measurements was to identify problems in connection with the sample preparation and handling, and the results will therefore be very helpful in the future work.

In particular, discussions involving virologists have indicated that our disappointing results may be caused by one or more of the following:

i) Our samples may have incurred damage due to freezing/thawing during preparation resulting in damage to viral envelopes.
ii) Viral samples should not be concentrated for diffraction work until just before the experiment, as a variety of aggregations may occur.
iii) The initial sample must be as monodisperse as possible.

Since the SANS measurements, we have worked on the problems and the next experiments will be used to assertain whether we have solved the problems which have been linked with the sample production. Specifically, preparation has been reorganised as such:

i) At no time during sample preparation the influenza isolates will be frozen; they will be always kept at 4°C.
ii) The samples will be transported to Denmark in a dilute state and will only be concentrated minutes before the data collection.
iii) The final viral samples will be put in a gel exclusion column twice instead of only once to further guarantee monodispersity.

Therefore, although the results from the first measurements were dissapointing, they have led to a better understanding of the unique sample requirements for solution scattering neutron diffraction of viral samples.

[1] S. Cusack, R.W.H. Ruigrok, P.C.J. Krygsman and J.E. Mellena, (1985). J. Mol. Biol. **186**, 565-582.

1.54 Contrast Variation Studies of Clathrin Coated Vesicles by Small-Angle Neutron Scattering

(R. Bauer, S. Hansen, *Department of Mathematics and Physics, Royal Veterinary and Agricultural University, Denmark*, Moira Behan, David Clark, Gareth Jones, *Daresbury Laboratory, U.K.*, K. Mortensen and J. Skov Pedersen, *Department of Solid State Physics, Risø National Laboratory, Denmark*)

The hormonal regulation of a living cell is mediated through clathrin coated vesicles. The vesicles are fragments of a cell membrane which are coated by the protein named clathrin[1]. During 1991, scattering experiments (described in Bauer *et al.*[2]) on clathrin coated vesicles have been continued. We have demonstrated that the structural information on coated vesicles can be obtained using neutron scattering and contrast variation. The results obtained by this method are consistent with information from other methods of measurements on clathrin coated vesicles. Contrast variation neutron scattering has demonstrated in a non-intrusive manner the presence of a lipid membrane inside the clathrin coat.

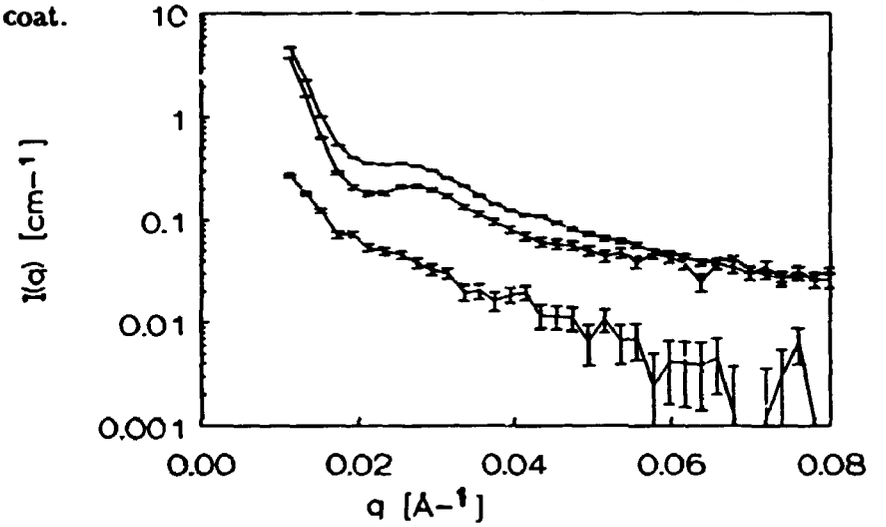

Fig. 1. SANS spectra from contrast variation on clathrin coated vesicles in 0 % (middle curve), 42 % (lower curve) and 75 % D_2O (upper curve).

A main feature of the experiment is that a characteristic peak in the neutron scattering profile (figure) which is apparent in D_2O as well as in H_2O disappears upon contrast matching of the protein component of the coated vesicles in 42 % D_2O. Neutron as well as dynamic light scattering give a coated vesicle size of about 900 Å in H_2O and D_2O, but for neutron scattering the diameter decreases when matching out the protein coat of the clathrin coated vesicles. From the contrast matching point found for the clathrin coated vesicles, it is demonstrated that the clathrin cages do contain internal membrane. The mass of 33×10^6 Dalton and composition of 75% protein and 25% lipid found from the analysis of the small-angle scattering data are both in good agreement with values reported in the literature. The stability and purity of the samples used have been checked by dynamic light scattering and cryo-electron microscopy.

[1] B.M.F. Pearse, (1975). J. Mol. Biol. **97**, 93.
[2] R. Bauer, M. Behan, G. Jones, S. Hansen, K. Mortensen, T. Særmark and L. Øgendal, (1991). J. Appl. Cryst. **24**, 815.

1.55 Structural Investigations of AOT–Microemulsions

(S.H. Chen, S.L. Chang, *MIT, Cambridge, MA, USA*, R. Strey, *Max-Planck Institute of Biophysical Chemistry, Göttingen, Germany*, J. Samseth, *Institute of Energy Technology, Kjeller, Norge*, and K. Mortensen, *Department of Solid State Physics, Risø National Laboratory, Denmark*)

In three–component micro–emulsions composed of oil, water and surfactant, the microstructure can continuously vary from a collection of water droplets suspended in oil (W/O) to a collection of oil droplets suspended in water (O/W), each coated with a monolayer of surfactant. In a recent study[1] we have demonstrated a continuous inversion from a W/O micro–emulsion at low temperature to an O/W micro–emulsion at high temperatures within the *one–phase channel* of AOT/water/decane (AOT is an ionic surfactant sodium–bis–ethylhexylsulpho–succinate). These studies were obtained with an oil/water weight fraction α=0.40 and a an AOT/(oil+water) weight fraction of γ=0.12. At lower content of AOT, on the other hand, the structural transformation has been shown to go through an intermediate state of a bi–continuous micro–emulsion within the on–phase channel which occurs at hydrophile–lipophile balance. New experiments have shown[2,3] that this channel is an L_3–phase, *i.e.* a one–phase system where the surfactant bilayers, swollen by for example oil, wrap around water domains forming a bi–continuous structure.

[1] S.H. Chen, S.L. Chang, J. Samseth, and K. Mortensen, (1991). J. Phys. Chem. **95**, 7427.
[2] S.H. Chen, S.L. Chang, R. Strey, and P. Thiyagarajan, (1991) J. Phys.: Condensed Matter **3**, F91.
[3] R. Strey *et al.*, (1991). J. Phys. Chem. **95**, 7510.

1.56 Micellar Shape and Size in Deoxycholate Micelles

(J. Samseth, *Institute of Energy Technology, Kjeller, Norway*, E. Rosenquist, *Statens Institut for Folkehelse, Norway*, K. Mortensen, *Department of Solid State Physics, Risø National Laboratory, Denmark*, and S. Chang, *MIT, Cambridge, MA, USA*)

In the attempt to make a vaccine against meningitis B it has recently been proposed to use the surfactant deoxycholate to bind the active ingredient, which is a lipo-polysaccharide. Deoxycholate is a molecule found in the bile of the human body and in the presence of lipo-polysaccharides it known to form aggregates. Deoxycholate is therefore expected to be an ideal carrier of the vaccine with minimal secondary effects. The goal of the present study is to determine the possibly structures of deoxycholate-lipopolysaccharides aggregates. In the initial phase the pure deoxycholate surfactant system has been studied. The structure appear to be dependent on the pH value. At low pH deoxycholate forms a gel, whereas micelles are formed at higher pH. In the present experiments we have studied the system at pH-values of 8.6 and 10.2. *Tris* buffer was used to control the pH, and NaCl was added in order to control the interaction between deoxycholate micelles. EDTA was added to eliminate possible Ca^{++} ions present in the system. The results shows that rod-like micelles with diameter of approximately 20 Å are formed in both cases.

1.57 Micelle Formation in Acqueous Solutions of the Tri-block Copolymer, PEO–PPO–PEO

(K. Mortensen and J. Skov Pedersen, *Department of Solid State Physics, Risø National Laboratory, Denmark*)

With the increase of specific polypeptide drugs arising from recombinant DNA techniques, there has become a great need for new tools to optimally deliver these drugs. A possible route to control the drug release is to incorporate the polypeptides into a water-soluble polymer matrix, such as poloxamers. Poloxamers are triblock copolymers of polyethyleneoxide and polypropyleneoxide (PEO–PPO–PEO). Because of a dramatic change in hydrophobicity of the PPO–block, poloxamers behave quite uniquely as a function of temperature: at low temperature the triblock units are dissolved as individual molecules, whereas aggregates appear at high temperatures. The structure of the aggregates has been the subject of some controversy, perhaps because different molecular compositions result in different structures. A large class of poloxamers aggregates into micelles, as originally shown by light scattering experiments. Details of these micelles have, however, until now not been known. It has been speculated that they are rod–like, and thereby can explain the thermo–reversible gel–transition, observed at high concentrations, as resulting from a percolation threshold of these rods. In the attempt to gain more insight into the micelle formation, small angle neutron scattering experiments has been made on the poloxamer P85, which is a 4500 Dalton molecule with 49% PEO. The scattering function, which has been analyzed using indirect Fourier transformation, reveals a variety of phases as the temperature is changed. At low temperatures, $T \leq 10°C$, and low concentration, the unimers are dissolved as individual Gaussian chains. At temperatures of the order of 20°C, the polymers aggregate into spherical micelles, with a relative dense core, presumably of the hydrophobic PPO, surrounded by the water soluble PEO–blocks. At higher temperatures the micelles form a liquid dominated by strong correlations, as can be described by a hard–sphere interaction model. At even higher temperatures these correlations disappears while the overall size of the objects apparently remains almost unchanged. In the figure is shown an example of the scattering function of a 1% P85 aqueous solution as obtained at 27°C, and the corresponding distance distribution function $p(r)$.

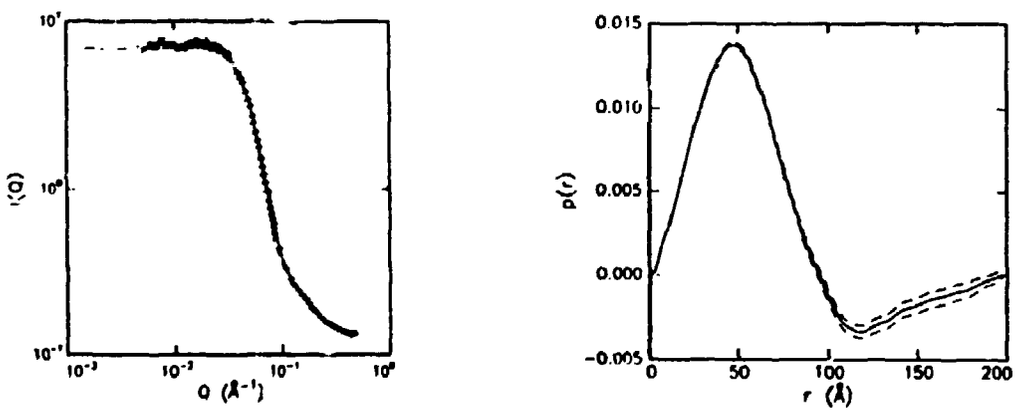

Fig. 1. The scattering function of a 1% P85 aqueous solution as obtained at 27°C, and the corresponding distance distribution function p(r). The function is typical for a spherical object at relative high concentration (~10% volume fraction).

1.58 Inverse Melting Transition in Acqueous Solution of Triblock Copolymer Micelles

(K. Mortensen, *Department of Solid State Physics, Risø National Laboratory, Denmark*, W. Brown, *Department of Physical Chemistry, University of Uppsala, Sweden*, and B. Nordén, *Department of Physical Chemistry, Chalmers University of Technology, Göteborg, Sweden*)

The structural properties of an aqueous solution of a 10.8 kDalton triblock copolymer of polyethyleneoxide (PEO) and polypropyleneoxide (PPO): PEO_{97}–PPO_{39}–PEO_{97} have been studied by small-angle neutron scattering. Three different phases appear. At low temperature (T <15°C) the block-copolymers are dissolved as individual Gaussian chains (unimers). At intermediate temperatures the hydrophobic nature of PPO cause aggregation into a liquid of micelles. At even higher temperatures (T >35.6°C) the micellar liquid 'freezes' into a crystalline powder. The structure factor of the micellar liquid follows that of interacting hard spheres, with a volume fraction which increases linearly with temperature until it reaches a critical value, ϕ_c, at which the micellar liquid crystallizes. The crystalline phase is body-centered cubic (BCC). Application of shear to the crystalline powder abruptly transforms the powder into a single crystal. The bond-correlation length of the BCC phase is, however, only of quasi long-range order, namely of the order of 5–10 lattice constants. The orientational order, on the other hand, covers the whole sample, *i.e.* length scales of the order of cm. These findings strongly indicate a 3D-cubatic lattice, somewhat analogous to the 2D-hexatic phase proposed as an intermediate between a liquid and a classic crystalline phase in two dimensions.

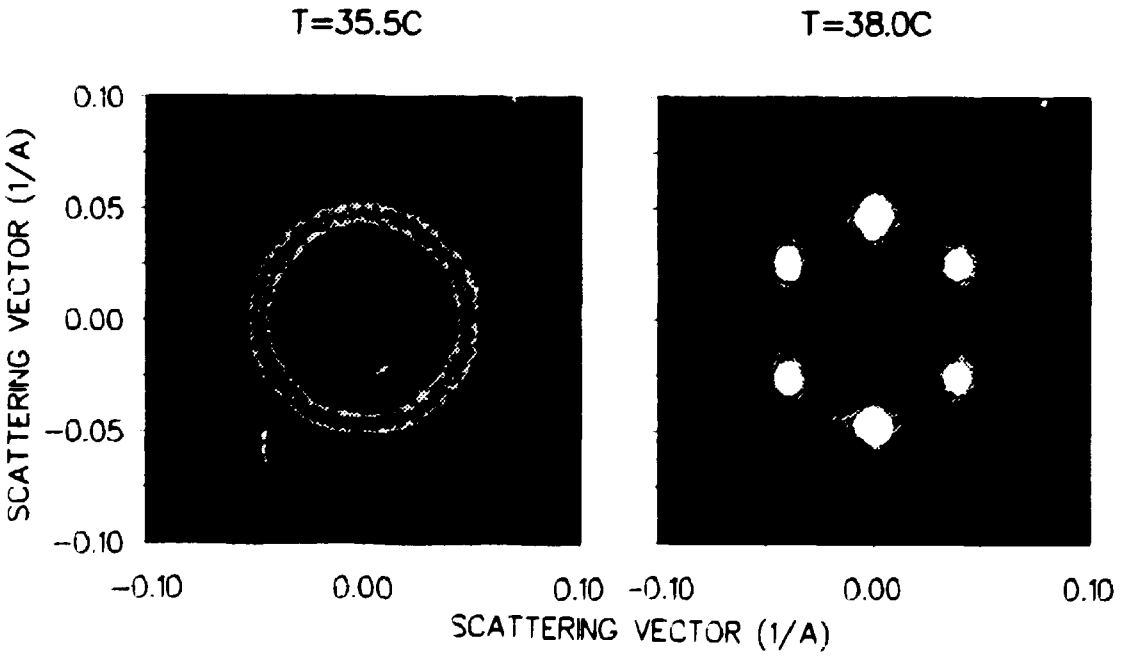

Fig. 1. Scattering pattern as obtained at low temperature (left) and at high temperature (right), showing the liquid-to- crystal transition.

1.59 Small-Angle Neutron Scattering on Microphase-Separated Multiblock Copolymers

(J. Samseth, *Department of Physics, Institute of Energy Technology, Kjeller, Norway*, R.J. Spontak, S.D. Smith, *Corporate Research Division, Proctor & Gamble Company, Cincinnati, Ohio, USA*, and K. Mortensen, *Department of Solid State Physics, Risø National Laboratory, Denmark*)

When block copolymers undergo microphase separation, a microstructural network results, imparting the materials with desirable homopolymer properties while retaining intimate phase contact. Microstructural elements in such systems can appear as dispersed microdomains (spherical or cylindrical) or *bi/co-continuous* microdomains (lamellar, double diamond or possibly other structures), depending principally on the molecular composition. Over the past two years, we have employed small-angle neutron scattering (SANS) to study a set of poly(siloxaneimide) (PSI) multi-block copolymers[1,2]. These materials possessed identical chain lengths and similar compositions, but varied significantly in their molecular architecture. Two of the copolymers consisted of constant length blocks, while the other was a randomly-coupled multiblock copolymer. SANS analysis of these microphase-separated copolymers revealed differences in both microstructural order and size. The studies also permitted us to correlate microstructure with different processing routes, thereby elucidating subtle structure-property relationships and permitting determination of the glass-transition temperature (T_g) and expansion-coefficients of the copolymers.

In the present study, we have studied the effect of adding a *random-monomer block* between the pure end blocks of a poly(styrene-*b*-isoprene) block copolymer, thereby changing the AB architecture to an A(A/B)B one. In this case, the system behaves as a diblock copolymer with an extended interphase in one limit and as a two-component triblock copolymer in the other limit[3]. Copolymers of approximately equal molecular weight, but different degrees of middle-block addition (10, 20, 30, and 40%) have been synthesized and subjected to SANS studies. Phase contrast for the neutron scattering has been enhanced by selective deuterating the styrene component of the middle random block. Resulting SANS spectra obtained with the beam parallel to the plane of the polymer film (*edge-on geometry*) indicate that the copolymers are all anisotropic, exhibiting well oriented lamellae. Detailed description of these spectra, in terms of microstructural dimensions such as the periodicity and inter-phase thickness, are forthcoming.

[1] J. Samseth, K. Mortensen, J.L. Burns, and R.J. Spontak, (1992). J. Appl. Polym. Sci. *In the press*

[2] J. Samseth, R.J. Spontak, and K. Mortensen, (1992). J. Polym. Sci., Polym. Phys. Ed. *Submitted.*

[3] J.M. Zielinski, and R.J. Spontak, (1992). Macromolecules. *Submitted.*

1.60 Order, Disorder and Fluctuations in Diblock Copolymers

(K. Almdal, *Polymer Group, Risø National Laboratory, Denmark*, F. Bates, J. Rosedale, and K. Koppi, *University of Minnesota, Minneapolis, USA*, and K. Mortensen, *Department of Solid State Physics, Risø National Laboratory, Denmark*)

Incompatibility effects in block copolymers give rise to a variety of possibly phases, due to the particular chemical structure. These phases includes at least four 'crystalline' ordered mesophases. The phase behavior of diblock copolymer melts are governed mainly by the three molecular parameters: the overall degree of polymerization (N), the relative volume fraction of each component (f), and the interaction parameter (χ) as mainly given by the specific types of monomers, and the temperature ($\chi \sim 1/T$). To a good approximation it is the product χN that dictates whether a particular block copolymer will be ordered ($\chi N \geq 10$) or disordered, whereas the consequence of varying the molecular symmetry (f) is found in the resulting crystal structure. According to mean-field theory, one should expect the following sequence of phases as χ is raised (lowering T): disordered liquid like, spherical domains arranged as a BCC lattice, hexagonally packed cylinders, and lamellae. Including fluctuations will to some degree suppress the cubic state. In a series of studies, including small angle neutron scattering as well as rheological measurements on the diblock copolymer polyethylenepropylene-polyethylethylene (PEP-PEE), we have found evidence that fluctuations play an important role in the phase behavior, as verified by a transition directly from hexagonally packed rods to disordered phase in a sample far from symmetric ($f = 0.77$). Other compositions of PEP-PEE reveal, however, experimental findings which are not in agreement with any present theory. For a ($f = 0.65$) composition, for example, we find for a shear oriented sample scattering pattern as shown in the figure, when the incoming neutron beam is perpendicular to the shear plane. At the lowest temperature a lamellae phase is identified, and at the highest temperature the scattering function reveal that of disordered composition fluctuation in agreement with the function given by Leibler (Macromolecules (1980) **13**, 1602). At intermediate temperatures, on the other hand, the ordered phases are different from those theoretically predicted. The structure of these phases have still not been conclusively determined although the data give indications of a catenoid lamellae phase and some kind of bi-continuous ordered phase just below the order disorder transition.

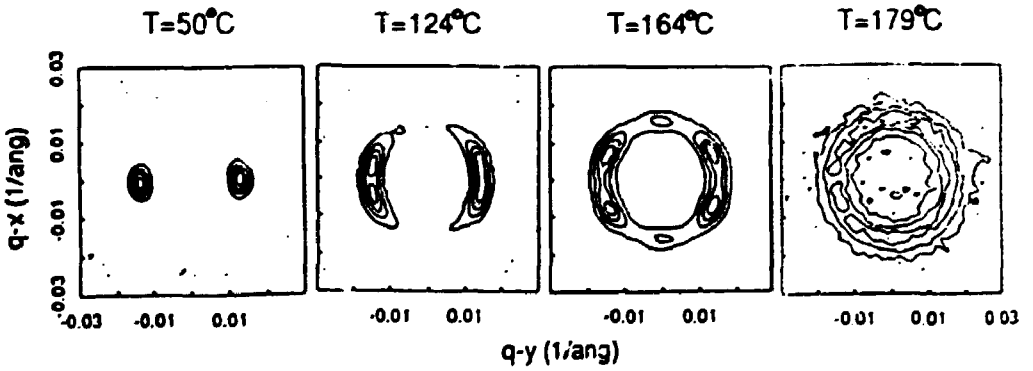

Fig. 1. Two dimensional scattering pattern of shear-oriented PEP-PEE ($f = 0.65$), showing characteristics of the four different phases.

1.61 Meanfield to Ising Crossover for Binary Polymer Mixtures

(D. Schwahn, S. Janssen, T. Springer, *IFF, Forschungszentrum Jülich, Germany*, G. Meier, *Max-Planck-Instute for Polymer Research, Mainz, Germany*, and K. Mortensen, *Department of Solid State Physics, Risø National Laboratory, Denmark*)

For a great variety of alloys, the composition fluctuations has been studied, and described in terms of mean-field description and Ising-behavior. Because of the very large molecular mass of polymers, it was expected that mean-field characteristics should dominate the phase behavior in polymer blends, and the cross-over from mean-field to non-meanfield (Ising) behavior should occur only very close to the critical point[1]. Measurements of the composition fluctuations in a high molecular weight blend, PVME-PS (polyvinylmethylethylene-polystyrene), actually showed a cross-over to Ising behavior only 2° below the critical temperature T_c[2]. A similar transition was found by Bates *et al.*[3]. According to the theory of de Gennes and others the transition to Ising behavior should, for binary polymer blends, occur at a temperature T_* given by the Ginzburg-Landau criterium:

$$\epsilon \equiv (T_* - T_c)/T_* \sim 1/N ,$$

assuming that the the polymer-polymer (Flory-Huggins) interaction parameter is proportional to $1/T$, as usually observed. ϵ is the reduced temperature and $N = \sqrt{(N_1 \times N_2)}$. N_1 and N_2 being the number of monomers in the two polymer types. Thus, one should expect to find a very simple relationship between the regime of Ising behavior and the degree of polymerization (N). In the attempt to study this Ginzburg-Landau relationship, we have measured the composition fluctuations, and thus the mean-field and Ising behavior of a series of PMPS-PS (Polypmethylphenylsiloxane- polystyrene). In the figure is shown an example of the resulting susceptibility as represented by the inverse forward scattering of SANS studies. The mean-field and non-mean-field regimes are clearly seen. Also within the two-phase regime ($T - T_c < 0$), reproducible characteristics are observed, which still have to be analyzed. The series of experiments on samples of different N_1 and N_2 shows, however, that the simple Ginzburg-Landau relation is not sufficient to account for the molecular weight dependence of the cross-over regime.

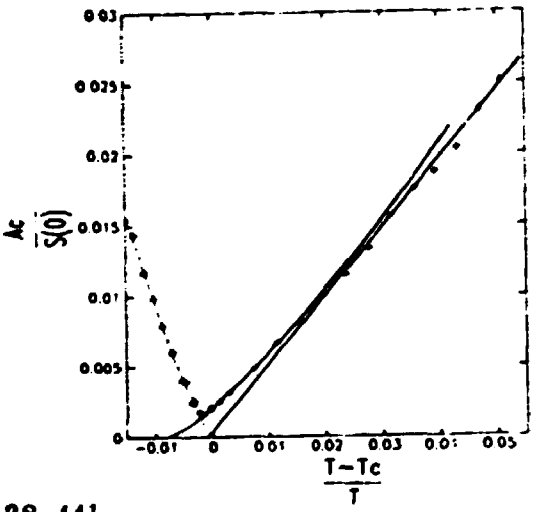

Fig. 1. The inverse forward scattering of PMPS-PS versus reduced temperature.

[1] P. de Gennes, (1977). J. Phys. Lett. **38**, 441.
[2] D. Schwahn, K. Mortensen, and H. Yee-Madeira, (1987). Phys. Rev. Lett. **58**, 1544.
[3] F.S. Bates, (1990). Phys. Rev. Lett. **65**, 1893.

1.62 Small-angle Neutron Scattering of Plasticized Poly(Vinyl Chloride)

(R. L. Scherrenberg, H.R. Reynaers, *Catholic University Leuven, Heverlee, Belgium*, K. Mortensen, *Department of Solid State Physics, Risø National Laboratory, Denmark*, and C. Gondard, *LVM Tessenderlo Chemie, Tessenderlo, Belgium*)

Plasticized PVC samples exhibit a prominent interference peak in the small angle scattering region. This peak has generally been attributed to the specific penetration of the plasticizer in the non-crystalline regions resulting in a scattering contrast between the unplasticized crystalline regions and the plasticized amorphous regions (model 1)[1-3]. However, the possibility that an interference peak arises from a phase separation between the plasticizer and the PVC (model 2) has never been investigated. SANS patterns of the plasticized PVC samples with a varying volume fraction deuterated tetrahydronaphatalene ($C_{10}D_{12}$), as shown in Fig. 1, clearly reveal a correlation peak. The intensity of this peak (q=0.04 Å^{-1}) increases as a function of the volume fraction of the plasticizer due to the enhanced scattering contrast. Good agreement is found between the experimental data and theoretical calculations based on model 1, assuming a crystalline volume fraction of 5-10%. This latter value is in line with the reported degree of crystallinity of commercial PVC. The appearance of a second peak at the highest volume fraction plasticizer (left figure), on the other hand, proves to be related to phase separation between PVC and the plasticizer. Preliminary orientation experiments (right figure) demonstrate that plasticized PVC can be oriented easily. An oriented sample which has been kept under stress for two days exhibits still a considerable degree of orientation in spite of the fact that the system is well above the glass-transition temperature. However, the oriented structure disappears completely after release of the stress, thus suggesting that the observed structural features originates from a physical network.

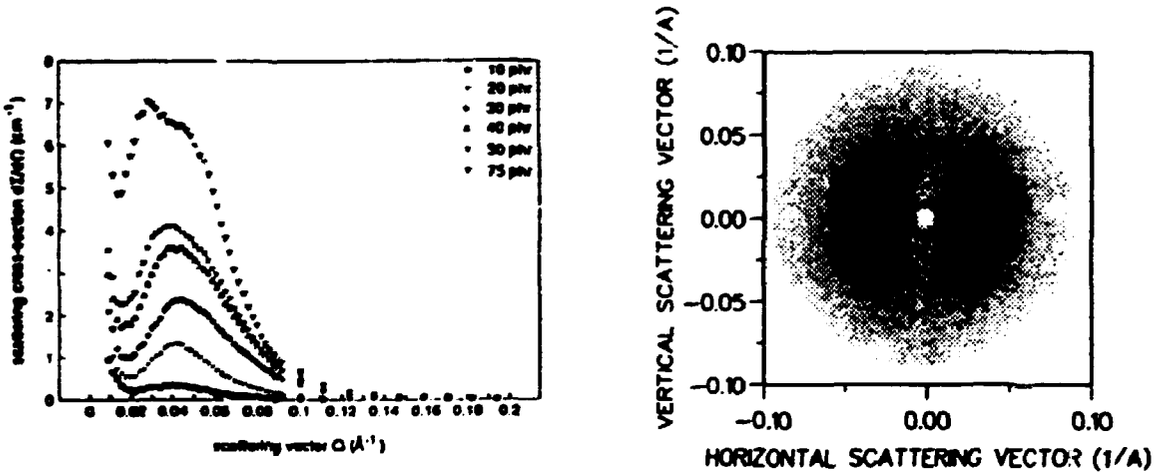

Fig. 1. SANS data of plasticized PVC as obtained with various volume fractions plasticizer (left), and 2D scattering pattern of stress oriented plasticized sample (right).

[1] C.J. Singleton, *et al.* (1977). J. Macromol. Sci.-Phys. **B14** 29.
[2] H.R. Brown, M. Kasakevich and G.D. Wignall, (1986). Polymer **27**, 1345.
[3] D.G.H. Ballard, A.N. Burgess, J.M. Dekoninck, and E.A. Roberts, (1987). Polymer **28**, 3.

1.63 Chain Conformation in Glassy Syndiotactic Polystyrene

(S. Stölken, B. Ewen, *Max-Planck Institute for Polymer Research, Mainz, Germany* and K. Mortensen, *Department of Solid State Physics, Risø National Laboratory, Denmark*)

The molecular chain conformations of macromolecules are expected to depend strongly on the tacticity of the chain molecules, *i.e.* the ordering of side-groups within the planar zig-zag structure of typical polymers. On the basis of the rotational-isomeric-state model[1], Flory has calculated the conformation and thereby the scattering function for polymers with different tacticities. The Gaussian random coil conformation is expected only for atactic polymers, *i.e.* polymers with randomly oriented side-groups. Experimentally, however, not only atactic but also isotactic (side-groups all at same side) shows Gaussian characteristics[2,3]. Using the Risø-SANS instrument, the structure of syndiotactic polystyrene have been studied, *i.e.* polystyrene with the side-groups alternating on either sides of the back-bone polymer chain. As seen from the Fig. 1, this polymer shows a small, but distinct increase in Iq^2 with q, in opposition to the Gaussian behavior, which results in a plateau in this so-called Kratky plot. For comparison, the scattering function for a Gaussian chain is included in the plot. We therefore conclude that the short sequences of syndiotactic polystyrene are non-Gaussian.

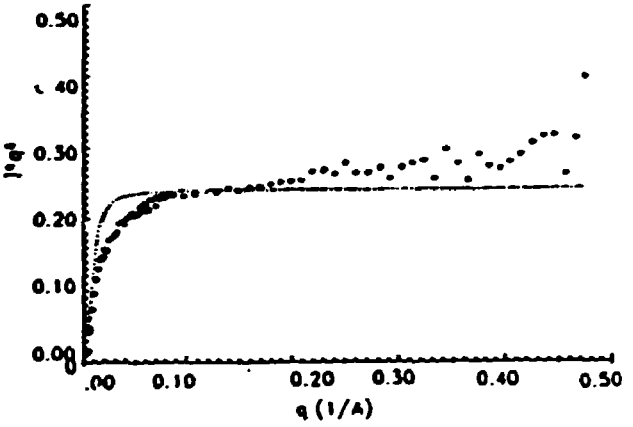

Fig. 1. Kratky plot ($I(q)q^2$ vs. q) of syndiotactic polystyrene (o) and for the Debye model for a Gaussian chain (broken line).

[1] P.J. Flory, (1989). *Statistical mechanics of chain molecules* (Hanser Publ., New York.)
[2] J.P. Cotton, D. Decker, H. Benoit, B. Farnoux, J. Higgins, G. Jannink, R. Ober, C. Picot, and J. des Cloizeaux, (1974). Macromolecules 7, 863.
[3] J.M. Guenet, C. Picot, and H. Benoit, (1979). Macromolecules 12. 86.

1.64 Critical Scattering of Polystyrene Blended with the Statistical Copolymer Polycyclohexylacrylate–Butylmetrhacrylate

(T. Hack, M. Stamm, V. Abetz, *Max-Planck-Institute for Polymer Research, Mainz, Germany*, and K. Mortensen, *Department of Solid State Physics, Risø National Laboratory, Denmark*)

The phase behavior of polystyrene, PS, mixed with the copolymer P(CHA-BMA) composed of statistically distributed cyclohexylacrylate (CHA) and butylmethacrylate (BMA) is expected to show interesting results, since P-CHA is compatible with PS, whereas P-BMA is incompatible with PS. Small angle neutron scattering has been used to study the phase behavior by measuring the critical scattering of a polymer blend of deuterated polystyrene (PSd) and protonated P(CHA-BMA). At low temperatures PS and P(CHA-BMA) form a one-phase system, whereas phase-separation is observed at high temperature, i.e. PS-P(CHA-BMA) has a *lower critical temperature*. By changing the molecular composition, it appears to be possible to shift the critical temperature, T_c. If, for example, the BMA content of the copolymer is increased, T_c will decrease. Since the glass transition T_g, on the other hand, is not affected by varying the composition it may be possibly to change the difference between T_c and T_g, and thereby the kinetics involved in the decomposition. It is the goal to study the initial states of spinodal decomposition after temperature jumps into the two-phase region. The first investigations were, however, made to get information about details on the phase diagram, and the interaction parameter χ. In the figure is shown typical scattering curves, as presented in the Zimm-plot I^{-1} *vs* q^2 where I is the intensity and q is the scattering vector. From the forward scattering obtained from fits to these scattering curves, we obtain a spinodal of T_s=169.0°C for the shown sample: $PS_{0.35}$-$P(CHA\text{-}BMA)_{0.65}$.

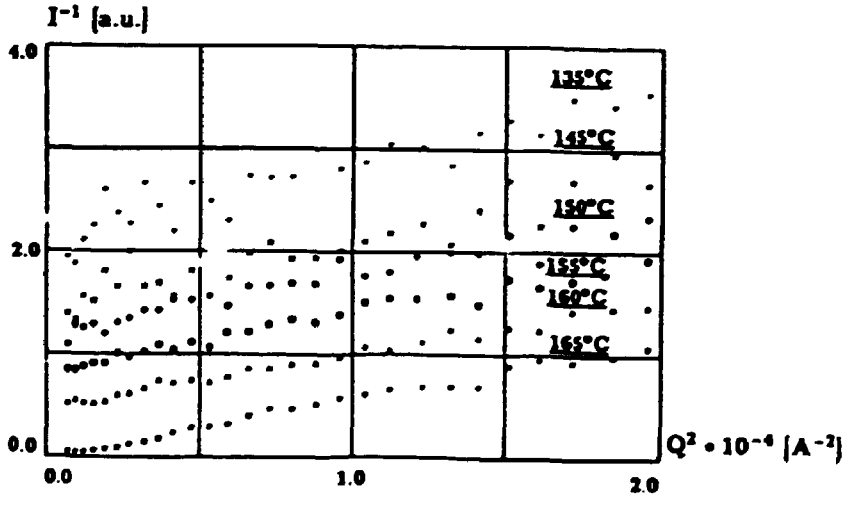

Fig. 1. Zimm-plot of a mixture of a statistical copolymer (65%) and polystyrene (35%), as obtained at different temperatures.

1.65 SANS Studies of Polydiethylsiloxane in the Melt and in a Solution

(H. Schlottke, B. Ewen, *Max-Planck-Institute for Polymer Research, Mainz, Germany,* and K. Mortensen, *Department of Solid State Physics, Risø National Laboratory, Denmark*)

Because of incompatibility effects the specific chemical structure of block copolymers leads in some cases to formation of ordered microstructures (mesophases). Partial crystallinity within a polymer can also give rise to mesophases, when regions of crystalline and amorphous phases alternate regularly. In recent years a new class of polymers, which do not contain any 'classic mesogenic groups' in their molecular structure, has been shown also to form mesophases. Polydiethylsiloxane (PDES) and polydipropylsiloxane (PDPS) are examples of this class. The molecular origin of the mesophase formation is yet not understood, but it has been speculated that it may be related to some kind of self-ordering of long segments of the macromolecules. Support for this explanation have come from viscosity measurement indicating that the molecules are stiffer in the melt than in the solution. In the attempt to gain more insight into the mesophase of PDES, small angle neutron scattering studies has been initiated on a series of PDES-samples dissolved in toluene. The concentration range will cover the range from dilute polymer solutions to the pure PDES-melt. The polymer used is anionic polymerized PDES with molecular weight, M_w=240,000, and a narrow molecular weight distribution. The first studies were done on rather dilute samples dissolved in deuterated toluene. In Fig. 1 is shown Zimm-plots (I^{-1} vs. q^2, I being the intensity and q the scattering vector), as obtained with 15 Å neutrons and a sample-to-detector distance of 6 meter. From the slope and intercept of these curves, one gets information on the characteristic correlations lengths of the polymer matrix. Analysis of the data is still in progress.

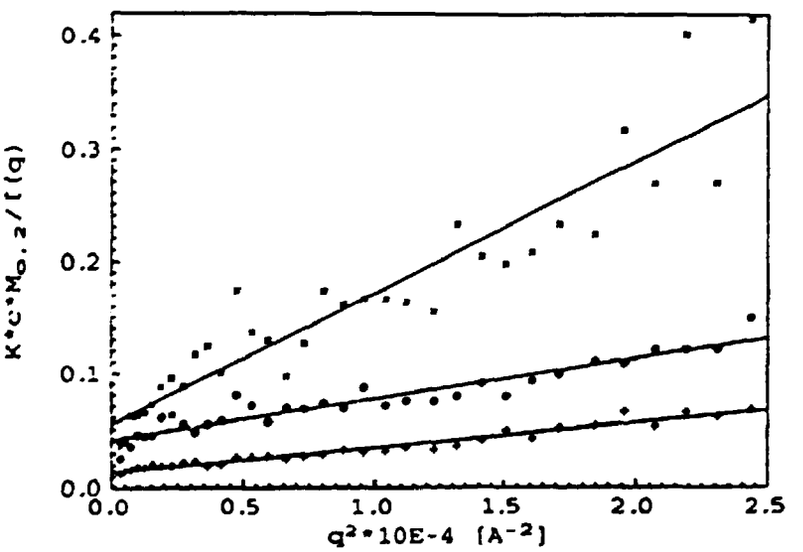

Fig. 1. Scattering function of PDES dissolved in toluene.

1.66 Saturation Swelling of Randomly Cross-Linked PDMS Gels Produced by Electron Irradiation

(A.N. Falcão, J. Skov Pedersen, and K. Mortensen, *Department of Solid State Physics, Risø National Laboratory, Denmark*)

Random cross-linking of a polymer melt, will produce a gel above a certain cross-link density and a network of connected polymers will span the system. In the presence of a good solvent for the polymer the network swells reaching an equilibrium configuration ultimately determined by the microscopic conformation of the network strands. Previous scattering experiments[1,2] have shown that the classical *phantom network* picture of a regular network whose elementary strands expand upon swelling is not able to give an universal explanation of the deformation process. New mechanisms like topological rearrangements at a scale larger than the network mesh size were suggested to account for large scale deformations with no apparent deformation of the elementary strand itself. These processes should be particularly relevant for low cross-linked samples.

We report work on the structure characterization of polydimethylsiloxane (PDMS) networks. A commercially available PDMS was used. Its molecular weight distribution was characterized by gel permeation chromatography (GPC) revealing a very broad distribution with a long low molecular weight tail (M_w=77500 and $M_w/M_n = 4.5$). The networks used in the study were produced by irradiation of the polymer melt with 10 MeV electrons, under a N_2 atmosphere. The gel weight fraction dependence on the received dose was determined and the *gelling dose* estimated to be $\simeq$ 45 kGy. The cross-link G_{cross}, and main-chain scission G_{sci} probability were calculated from the molecular weight distribution obtained by GPC, by fitting expressions derived in the framework of the Flory-Stockmeier theory to the gel fraction data. The agreement between the measurements and the fit of the theoretical expression was good, and the G values for cross-link and scission are respectively 0.0002 and 0.00001 units/100 eV. Samples were swollen to saturation in good solvents for PDMS. From each network sample (each cross-link density) three separate pieces were used. They were swollen in different solvents (cyclohexane, toluene and xylene). For the first two the interaction parameters with PDMS are well reported in the literature. They were used together with the equilibrium swelling ratios Q to estimate within the classical phantom network model the molecular weight of the strands in between elastically effective links. For the samples with higher cross-link densities we found reasonable agreement between the values obtained from different solvents, but for the lower cross-link densities systematic deviations were found. Molecular weights in between elastically effective links were also estimated from the molecular weight distribution and the gel fractions using Scanlan's method of counting effective strand. A reasonable agreement with the predictions of the phantom model was found only for the highly cross-linked samples. These results confirm that, at least for the low cross-linked samples, the explanation of the network swelling needs to consider mechanisms other than phantom deformation.

Small-angle neutron scattering measurements were performed on twelve different samples cross-linked at doses ranging from 80 kGy to 1 MGy (with corresponding gel fractions ranging from $\sim$ 40% to 95%). The networks were measured after being swollen to saturation in fully deuterated *p-xylene*. The samples used were not exctracted. The shape

of the scatted intensity curves obtained is very much dependent on the radiation dose received. They all share the common feature of having the high q part very similar to the one produced by semi-dilute solutions with the same polymer concentration (these were also measured for the sake of comparison). However, at intermediate and low q values, the signal from the gel departures clearly from solution-like behavior. There is evidence of the presence of large scale heterogeneities in the gel, their spatial extent being reduced with increasing cross-link density.

The system was modeled as a solution-like matrix with heterogeneities resulting from regions where differences in cross-link density produce an excess or depletion in polymer density. The large scale fluctuations were assumed to be fractal up to a certain cut-off lenght ξ. The solution-like fluctuations were modeled by a function that has the limiting Lorentzian behavior at low scattering vector q, and exhibits the characteristic power law dependence $q^{5/3}$ for values of q higher than the solution correlation length. With a fractal dimension $d_f = 5/3$ for the large scale fluctuations, we obtained good fits to the scattered intensities for all but the very high cross-linked samples. The values of the correlation lenght characteristic of the large scale fluctuations are shown in the figure together with the saturation swelling ratios. ξ has a clear divergence at a dose significantly higher than the gel point. Similar behavior is not seen in the swelling data at the same irradiation dose.

The results show qualitative agreement with a prediction of a model that has been proposed to explain the structure of swollen gels[3]. It was suggested that strands trapped by cross-links produced in first neighbor contact points (the so-called *frozen blobs*) form clusters that will percolate through the system at a cross-link density considerably higher than the one associated with the gel point for the polymer chains. The model describes the clusters as percolation clusters that are partially diluted upon swelling. Although in the present experiment, the fractal dimension is not very far from the prediction $d_f = 1.6$, the concentration depence found ($\xi \simeq c^{-4/5}$) disagrees with the power law $\xi \simeq c^{-5/3}$ predicted from the model.

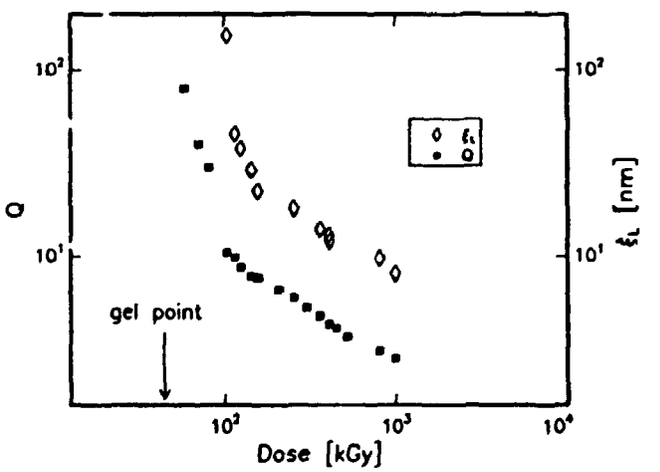

Fig. 1. Swelling ratios Q and correlation length characteristic of the large scale density fluctuations ξ given, in a log-log plot as a function of irradiation dose. The gel point value is indicated by the arrow.

[1] J. Bastide and L. Leibler, (1988). Macromolecules **21**, 2647.

[2] J. Bastide, L. Leibler and J. Prost, (1990). Macromolecules **23**, 1821.

[3] J. Bastide, E. Mendes, F. Boué, M. Buzier, and P. Lindner, (1990). Makromoleculare Chemie **40**, 81.

1.67 SANS Study of the Local Conformation Changes Produced by Swelling in Randomly Cross-Linked PDMS Gels

(A.N. Falcão, J. Skov Pedersen, K. Mortensen, *Department of Solid State Physics, Risø National Laboratory, Denmark*, and F. Boué, *Laboratorie Léon-Brillouin, C.E.N. Saclay, France*)

Irradiating a polymer melt with high energy electrons randomly creates radicals that, following diffusion processes, will react forming chemical links. These links are expected to be produced close to contact points between the chains in the melt. At sufficiently high irradiation doses large ramified clusters of polymers will be formed and above a certain threshold a macroscopic network will be created. It has been suggested that this random linking process is equivalent to a site percolation on a lattice, the resulting polymer clusters having the shape of percolation clusters: highly polydisperse and interpenetrated, the large ones being self-similar[1]. In the melt, the clusters should not be detected by scattering techniques, since no contrast between the locally higher and lower cross-linked regions is expected. In contact with a good solvent for the polymer, the network will swell. It is reasonable to expect that the solvent adsorbed in the network will preferably occupy regions where the local cross-link density is lower, because local rearrangements of the chains will be more difficult in locally high cross-linked regions. The swelling process is thus a very heterogeneous one. Increasing the swelling degree will progressively reveal the inner structure of the highly cross-linked regions. Important density fluctuations will be present, spanning progressively larger distances. An adequate choice of solvent, will allow for high contrast between high and low local cross-link densities, enabling scattering techniques to probe the structure of the polymer network. Measuring the same network at different swelling ratios, Q, will also give information on the local conformation changes that take place upon swelling.

We report preliminary results of a small-angle neutron scattering study performed on polydimethylsiloxane (PDMS) networks with different cross-link densities prepared by electron irradiation. Prior to the scattering measurements the remaining soluble part was extracted. Five samples were used. Their saturation swelling ratios were $Q_{i,max}$=15.0, 10.3, 7.4, 4.8 and 3.4. Each sample was measured at all possible Q values belonging to the above set (*i.e.* all those lower than its saturation Q_{max}). This procedure allows also to compare the structure of samples with considerably different cross-link densities at the same swelling degree. Figure 1 shows, normalized to concentration, the spectra obtained for the sample with Q_{max} = 10.3.

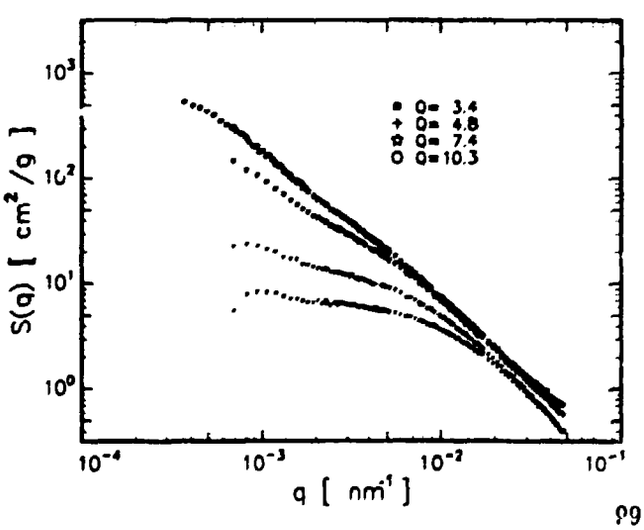

Fig. 1. Absolute intensities, measured at swelling ratios, Q=3.4, 4.8, 7.4 and 10.3 for the sample whose saturation swelling ratio is Q_{max}=10.3. The intensities are normalized by concentration.

The expected increase in the intensity scattered at low q vector is observed. The density fluctuations in the system were modeled as a superposition of fractal large scale fluctuations with an upper cutoff ξ_L, and a solution-like contribution (characterized by a small scale correlation length ξ_s. Figure 2 shows results for the characteristic length of the large scale fluctuations obtained from samples whose Q_{max} is 15.0, 10.3 and 7.4. The inset shows the ratio ξ_L/ξ_s.

The rate at which ξ_L increases with Q is dependent on cross-link density, increasing with decreasing cross-link density. This is consistent with the fact that in low cross-linked networks the chains are free to rearrange over larger distances. Moving toward the maximum swelling limit, the rate of increase of ξ_L is lower, the effect being more clear with increasing cross-link density. Large scale rearrangements (like unfolding) will be relatively less important in explaining the process of solvent adsorption in the network. This is confirmed by the behavior of the ratios ξ_L/ξ_s.

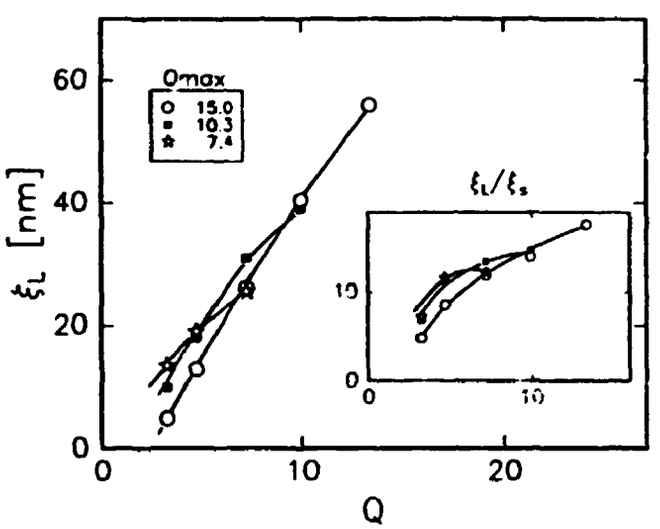

Fig. 2. Correlation length characteristic of the large scale density fluctuations, ξ_L versus swelling degree for the samples whose saturation swelling ratio, Q_{max} is 7.4,10.3 and 15.0. The inset shows for the same samples and the same swelling, the ratios beteen ξ_L and the characteristic lenght of the small scale density fluctuations ξ_s. The lines are guides to the eye

[1]J. Bastide, E.Mendes, F. Boué, M. Buzier and P. Lindner, (1990). Makromoleculare Chemie 40, 81.

1.68 SANS from Isothermally Sintered Base–Catalysed Silica Aerogels

(K.D. Joensen, *Danish Space Research Institute, Lyngby, Denmark*, and J. Skov Pedersen, *Department of Solid State Physics, Risø National Laboratory, Denmark*)

Base–catalysed silica aerogels have, through the use of systematic investigations with SAXS and SANS[1,2], been demonstrated to consist of basic silica particles with a characteristic dimension of 40 Å. These particles are assembled into networks of a fractal nature. On larger length scales these fractal "islands" make up the bulk of the silica aerogel. The size of the fractal island is correlated with the aerogel density[1].

Isothermal sintering is a densification process commonly used in altering the characteristics of ceramics, glasses and aerogels. The process involves heating the material to a high temperature, at which sintering occurs, remaining at that temperature for some time and then lowering the temperature. Sintering constitutes a densification lacking any weight reduction. At the Danish Space Research Institute considerable experience has been gained in sintering base–catalysed aerogels for use in Cerenkov detectors[3].

At the Risø SANS facility, SANS spectra for one non–sintered sample and six sintered samples were obtained. The sintered samples had all been isothermally sintered at DSRI from aerogels of density 248 kg/m^3, resulting in densities from 393 kg/m^3 to 573 kg/m^3. The sintering had been performed at 1000°C, for periods up to an hour. The non–sintered sample had a density of 286 kg/m^3.

Figure 1 shows the obtained spectra in log–log plot, after azimuthal averaging, background subtraction and normalisation with water. *S* indicates a sintered sample, and *NS* a non–sintered sample. The number preceding the letter, is the density of the sample measured in kg/m^3. In order to avoid crowding the figure, each spectrum has been multiplied by 3 compared to the one immediately below. The absolute cross section shown is correct for the non–sintered sample.

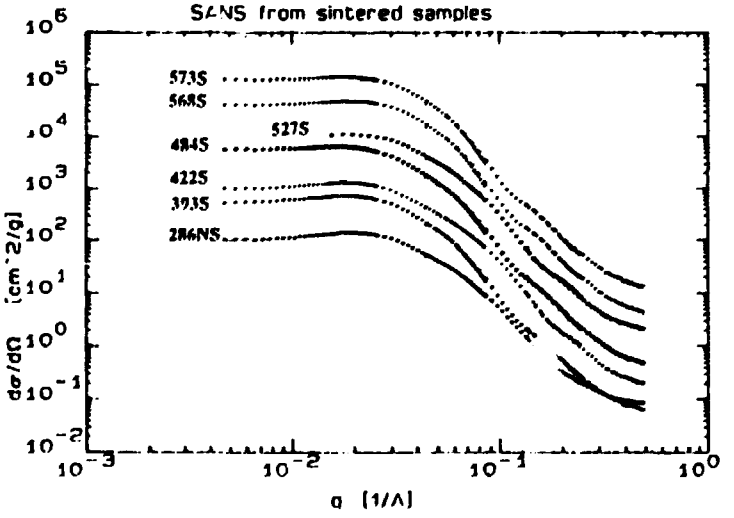

The spectra for the non–sintered sample can be be characterised as follows: i) at small q, correlations between the fractal islands cause a small peak[2], ii) at 0.03–0.07 Å^{-1} the

curve is nearly linear with a slope around -2 corresponding to fractal behaviour, iii) above 0.1 $Å^{-1}$ the slope of the curve changes to around -4.5 (in slightly different from Porod Law predicting a slope of -4), iii) above 0.25 $Å^{-1}$ the curve is dominated by incoherent background probably arising from hydrogen absorbed on the surface of the basic particles.

Two of the sintered samples (422S and 527S) are very similar to the non-sintered sample, except in the region above 0.1 $Å^{-1}$. Here a slope of about -5.6 and a small bump at 0.23 $Å^{-1}$ is observed before incoherent background becomes dominant at a comparatively diminished level. The lower incoherent background is probably caused by elimination of the hydrogen through condensation reactions early in the heating process. The observed slope and the bump bears close resemblance to the scattering seen from a system of spheres with a limited size distribution (where the bump is the remnant of the second maxima in the formfactor). For the other sintered samples (393S, 484S, 568S, and 573S) a similar deviation from the Porod Law and a small bump is observed. For these samples the bump is situated at 0.17 $Å^{-1}$. In the model of a polydisperse system of spheres this would indicate a size distribution with a somewhat larger average size, than for the two previous samples. In addition these spectra are very different in the fractal region in that the extension of this region is greatly reduced. Finally it can be seen that the absolute intensity at very small angles is significantly larger for these samples, than for any of the other samples.

The microstructural effects of the isothermal sintering, indicated by our spectra, is thus that the original aerogel, consisting of basic particles with a broad size distribution (resulting in scattering in agreement with the Porod Law), is densified primarily through reshaping of the basic particles level and restructuring of the fractal network. This is what could be expected. However, the observed narrowing of the size distribution after sintering is quite unexpected. Such a narrowing has very recently been reported in experiments examining the hypercritical drying of alcogels in production of aerogels[4], but to our knowledge such a narrowing has never been reported in connection with sintering from aerogels. In disagreement with Emmerling *et al.*[5] we find that the correlation between density of the sintered and microstructural parameters is ambiguous. Thus the main conclusion of our study is that the sintering does give rise to microstructural changes. Further spectra obtained from carefully prepared and documented samples are necessary to further illuminate the importance of the sintering history.

The samples investigated by SANS at Risø were later investigated in a newly developed SAXS set-up at DSRI. When taking the respective setup resolution into effect the SANS and SAXS spectra were in excellent agreement.

[1] D. Posselt, (1990). *Structural and Thermal Studies of Silica Aerogel*, Ph.D. Thesis, Risø-M-2915. Risø Report
[2] P.W. Schmidt, (1991). J. Appl. Cryst. 24, 414.
[3] I.L. Rasmussen, (1989). Coll. Phys. Suppl. Jour. Physique 4, 221.
[4] P. Wang, A. Emmerling, W. Tappert, O. Spormann, J. Fricke, and H.-G. Haubold, (1991). J. Appl. Cryst. 24, 777.
[5] A. Emmerling, R. Gerlach, R. Goswin, J. Gross, G. Reichenauer, and J. Fricke, (1991). J. Appl. Cryst. 24, 781.

1.69 Small Angle Scattering on Carbon Fibers

(J. Wolny and A. ' polnicka, *Institute of Physics and Nuclear Techniques, Academy of Mining and Metallurgy, Cracow, Poland* and T. Freltoft, *Department of Solid State Physics, Risø National Laboratory, Denmark*)

Carbon fibers of various origins and treatments exhibit a remarkable resemblance in their basic structural features. The structural unit appears to be a ribbon-shaped graphite layer in which no correlation exists between the general direction of the borders of the ribbon and the direction of the a-axis of the internal two-dimensional hexagonal structures of the ribbons. The ribbons have widths of about six Ångstrøms and lengths of several thousand Ångstrøms. A certain number of these ribbons are aligned parallelly to form a micro-fibril. These fibrils are wrinkled and their packing is imperfect so that a number of long, thin voids occur at the boundaries between the micro-fibrils.

The carbon fibers were obtained by heat treatment of polyacrylonitrile (PAN) at 1000 and 2600°C after previous oxidation. The initial parallel orientation of the fibers was conserved by the formation of macroscopically oriented bundles. Small angle neutron scattering from the fibers in vacuum and by using the contrast variation method (benzene or D_2O) was observed using incident neutrons of wavelengths between 3 and 60 Å. The resulting diffraction patterns are extremely anisotropic (see Fig. 1) and the anisotropy increases with decreasing values of the scattering vector. The anisotropy is less pronounced for samples immersed in heavy water, in agreement with previous results[1]. This means that the anisotropy comes from scattering on the fiber's skin. The observed diffraction spectra have been corrected for background scattering and normalized to a water spectrum. When analyzed using the Guinier approximation we obtained values for the radius of gyration between several and thousand Ångstrøms.

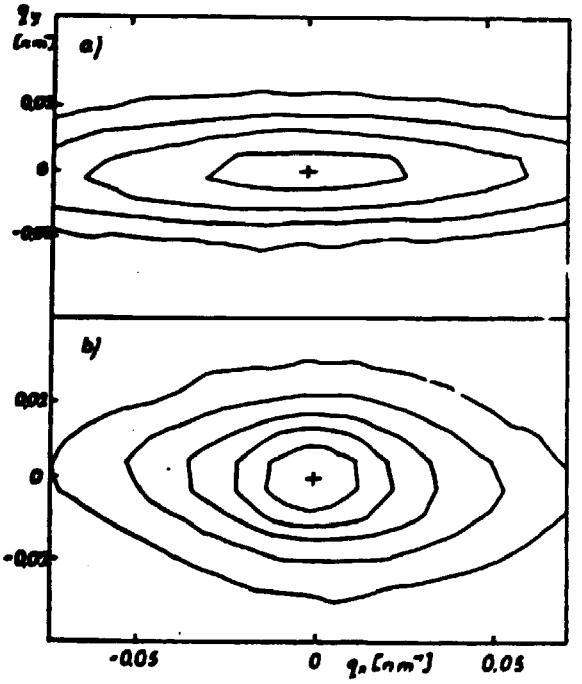

Fig. 1. Contours of constant intensity (10^n, n = 2, 2.5, 3, 3.5 and 4) for carbon fibers in vacuum (a) and in D_2O (b).

[1] L. Cser, M. Kocsis, L. Kõszegi, A. Oleś, A. Topolnicka, and J. Wolny, (1987). Phys. Stat. Sol. (a) **103**, 39.

1.70 A SANS Study of the Aluminium–Lithium–Hydrogen System

(C.G. McCracken, D.E.J. Talbot, *Brunel University, Uxbridge, U.K.* and J. Skov Pedersen, *Department of Solid State Physics, Risø National Laboratory, Denmark*)

The Al–Li–H system has been investigated by the use of a modified Sievert's apparatus[1]. Three aluminium lithium binary alloys with 1, 2, and 3 wt% lithium were investigated. Samples from each alloy were degassed under high vacuum and at high temperature. The samples were then equilibrated with research grade hydrogen at predetermined temperatures and pressures by means of radio frequency heating and a barometric arrangement. The samples were then quenched by an external blast of compressed cold air. After the system was evacuated, the samples were reheated under high vacuum and all the dissolved gas was collected and measured. From these measurements, the hydrogen solubility in these alloys was determined for the given temperature and pressure ranges.

Analysis shows that there is a composition dependent critical temperature, at which the hydrogen solubility increases with decreasing temperature. These critical temperatures occur in the single phase region of each alloy. The decreased slope of the Van't Hoff isobars, below the critical temperatures for each alloy indicates that the binding enthalpy of each system has increased. Further analysis show that the hydrogen solubility of pure FCC metals is higher than that for the Al-Li binary alloys. This leads us to believe that the single phase region of the Al-Li-H system was composed of aluminium lithium rich clusters strongly bonded to the hydrogen atoms.

A series of high purity Al-2wt% Li alloy samples have been deuterated above and below its critical temperature within the single phase region, quenched and prepared for examination by Small Angle Neutron Scattering (SANS). These samples were aged and measured over an extended period at 95°C. The figure show some of the SANS results. From the data it is seen that hydrogen concentration has an until present unknown but important effect on the ageing of these alloys. The rate of the development of the δ–phase precipitates is decreasing with increasing hydrogen content. Our preliminary analysis shows that the radius of the precipitates follows: $R = K \cdot t^{1/\alpha}$, where t is the time. α is close to 6 independent of the hydrogen content, whereas the rate constant K decreases with increasing hydrogen content.

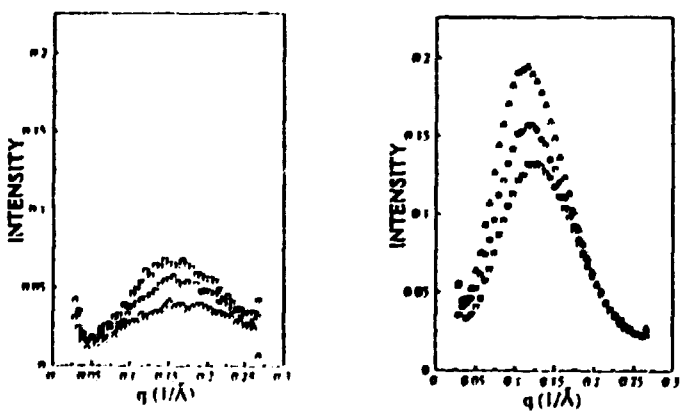

Left-hand side: at time t=0. Right-hand side: t≈70 hrs. (o): low deuterium, (□): high deuterium, (△): no deuterium content.

[1] P.N. Anyalebechi, D.E.J. Talbot and D.A. Granger, (1989). Met. Trans. B **20B**, 523.

1.71 SANS and TEM Studies of Krypton Bubbles in Bulk Samples of Copper an Nickel

(J. Skov Pedersen, *Department of Solid State Physics, Risø National Laboratory, Denmark*, M. Eldrup and A. Horsewell, *Materials Department, Risø National Laboratory, Denmark*)

The samples investigated in the present work were bulk samples of Cu containing 3 at. % Kr and Ni containing 4 at. % Kr. The samples were obtained from Harwell, U.K., where they have been produced by a combined sputtering and deposition technique [1].

We have previously described the results of an isochronal annealing study of the Cu(Kr) system for the as-prepared samples as well as those annealed to 275, 425 and 575°C [2]. The small-angle scattering measurements at large scattering vectors were measured with a neutron wavelength of 3.2 Å, which we recently recognized gave rise to double-Bragg scattering contamination of the spectra. The sample annealed to 575°C were therefore remeasured with 6 and 3 Å neutrons and the contribution from double-Bragg scattering was determined and subtracted from the previous measurements. The size distributions of the Kr bubbles have been determined from the corrected data using the method described by Glatter[3]. The size distributions were also determined by electron microscopy for the samples annealed to 275, 425 and 575°C. Excellent agreement between the two techniques is obtained on absolute scale for 275 and 425°C. Figure 1 shows the results for 425° from SANS and TEM (histogram). A broad size distribution is determined by both techniques. However, for 575°C the two distibutions have the same shape, but the one determined by TEM is shifted to smaller radii. The loss of large bubbles from the TEM analysis is not unexpected since large bubbles etch out during the electropolishing applied when preparing the samples for TEM. A significant number of large bubbles are then not counted by the TEM analysis.

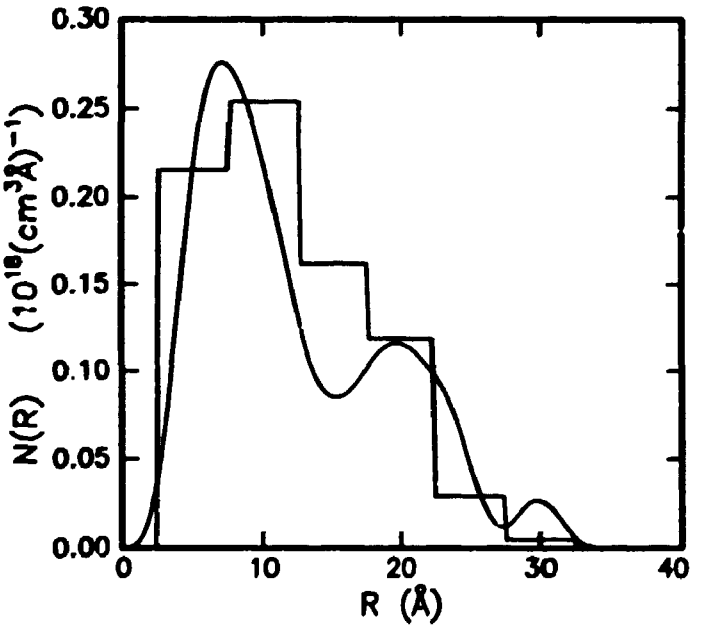

Fig. 1. The size distribution at 425°C from SANS (smooth curve) and TEM (histogram).

We have also preformed an isochronal annealing study of the Ni(Kr) system by the SANS technique. The samples were measured as prepared and annealed at ten temperatures from 200 to 1270°C. At the lowest annealings the small-angle scattering spectra have two contributions: one from bubbles with a radius of about 12 Å and another from much larger bubbles with a radius of abc · 300 Å. Below 350°C the radius of the small bubbles increases only slightly whereas it increases more steeply above this temperature, reaching a value of about 25 Å at 710°C. In the same temperature range, the radius of the large bubbles changes only slightly. At around 700°C the sample starts to loose mass due to outgassing suggesting a percolation of the bubbles. Above 700°C the two components in the SANS spectra merge, indicating a single characteristic size of the bubbles/pores as the sample starts to sinter and collapse. The results from SANS are in good agreement with previous studies by the positron annihilation technique[4].

We have recently initiated time-resolved *in situ* isothermal annealing studies of Cu(Kr) by the SANS technique. Measurements at 310 and 410°C have been performed. The temperature 310°C is just above the onset of bubble growth (0.4× the melting point) and 410°C is at 0.5× the melting point where thermal vacancies start to influence the bubble growth. In the preliminary data analysis we have used a monodisperse hard-spheres model with four parameters: the radius of the bubbles R, the hard-spheres interaction radius R_{HS}, the volume fraction η of the hard-spheres and an overall scale factor. The time dependence of the radius follows the relation:

$$R(t)^{\alpha} - R(0)^{\alpha} = K \cdot t$$

where K is a growth constant and t is the time. For 310°C the exponent α is about 29 which is much larger than any theory predicts. At 410° the exponent is about 8. A power of 2 is predicted by Ostwald ripening theories whereas powers of 3, 4 or 5 are predicted by bubbles migration and coalescence theories for different diffusion mechanisms. The theories assume low gas pressure and ideal gas behaviour. For higher pressures the powers increase [5] both for the ripening model and for the migration and coalescence models.

[1] D.S. Whitmell, R.S. Nelson, K.J.S. Smith and G.J. Bauer, (1983). Eur. Appl. Res. Reports- Nucl. Sci. Techn, 4, 513.

[2] M. Eldrup, J. Skov Pedersen, A. Horsewell, K.O. Jensen and J.H. Evans, (1991). In: *Fundamental Aspects of Inert Gas Behaviour in Solids.* S.E. Donnelly and J.H. Evans (eds.) (Plenum) p. 221.

[3] O. Glatter, (1980). J. Appl. Cryst. 13, 7.

[4] K.O. Jensen, M. Eldrup, N.J. Pedersen and J.H. Evans, (1988). J. Phys. F: Met. Phys. 18, 1703.

[5] D. Kaletta, (1983). Radiation Effects 78, 245 and P.F.P. Fichter, H. Schroeder and H. Trinkaus, (1991). In: *Fundamental Aspects of Inert Gas Behaviour in Solids.* S.E. Donnelly and J.H. Evans (eds.) (Plenum) *to be published.*

1.72 The 3-dimensional Resolution Function for Small-Angle Scattering Set-ups

(P. Harris and J. Skov Pedersen, *Department of Solid State Physics, Riso National Laboratory, Denmark*)

A general analytical calculation of the 3-dimensional resolution function for small angle scattering set-ups has been done. The main components of the set-up are a mechanical velocity selector, two circular pin-holes, defining the beam direction and an area-sensitive detector. The purpose of the calculation is to be able to do proper data analysis for single crystal measurements; for instance measurements of long range magnetic order in compounds like FeGe[1] and MnSi (see 1.10). The small angle approximation is not used specifically and the calculations can be used also for other scattering geometries of the same type. It is straight-forward to extent the calculations to set-ups using monochromator crystals.

Due to finite collimation, monochromatisation and detector resolution, neutrons with scattering vectors $\mathbf{q}$ in a range around the nominal scattering vector $\langle\mathbf{q}\rangle$ contributes to the scattering for a certain instrumental setting. The resolution function $R(\langle\mathbf{q}\rangle,\mathbf{q})$ describes the distribution of scattering vectors $\mathbf{q}$ around $\langle\mathbf{q}\rangle$, and the measured intensity for the setting $\langle\sigma\rangle$ is proportional to

$$I(\langle\mathbf{q}\rangle) = \int R(\langle\mathbf{q}\rangle,\mathbf{q})\frac{d\sigma(\mathbf{q})}{d\Omega}d\mathbf{q}$$

In order to describe the performance of the actual set-up we have employed the analytical beamline analysis presented by Skov Pedersen and Riekel[2]. The distribution of the incoming neutrons is described as a function of two position parameters x, y in the plane perpendicular to the beam direction, x', y' the corresponding angles relative to the incoming beam direction and the wavelength deviation $\Delta\lambda/\lambda$. By applying Gaussian approximations for the distribution and the transmission functions of the apertures one can calculate the distribution at the sample position:

$$I_y(y,y')I_x(x,x')I_\lambda(\Delta\lambda/\lambda) = e^{-\frac{1}{2}(ay^2+by'^2+dyy')}e^{-\frac{1}{2}(gx^2+hx'^2+jxx')}e^{-\frac{1}{2}e(\Delta\lambda/\lambda)^2}$$

When a mechanical velocity selector is used we assume that the correlation between x, x', y, y' on one hand and $\Delta\lambda/\lambda$ on the other is zero. a, b, c, d, g, h and j are given in terms of the experimental set-up. The detector resolution has been incorporated at the sample position by adding the variance of this to the variance due to the finite size of the slits.

The 3-dimensional calculation of the change in q-vector $\Delta\mathbf{q} = \mathbf{q} - \langle\mathbf{q}\rangle$ due to the finite value of the displacement x, y, the divergence x', y' and the difference in wavelength $\Delta\lambda$ of the incoming neutron, can be calculated, and can be written as:

$$\Delta\mathbf{q} = \mathbf{A}x + \mathbf{B}x' + \mathbf{C}y + \mathbf{D}y' + \mathbf{E}(\Delta\lambda/\lambda)$$

where the vectors **A**, **B**, **C**, **D** and **E** are given by the nominal q-vector, the nominal wavelength and the distance from the sample to the detector.

The resolution function is obtained as:

$$\begin{aligned} R(\langle \mathbf{q} \rangle, \mathbf{q}) &= K \int I_y(y,y') I_x(x,x') I_\lambda(\Delta\lambda/\lambda) dx dx' dy dy' d(\Delta\lambda/\lambda) \\ &\times \delta(\Delta q_x - E_x(\Delta\lambda/\lambda) - A_x x - B_x x' - C_x y - D_x y') \\ &\times \delta(\Delta q_y - E_y(\Delta\lambda/\lambda) - A_y x - B_y x' - C_y y - D_y y') \\ &\times \delta(\Delta q_z - E_z(\Delta\lambda/\lambda) - A_z x - B_z x' - C_z y - D_z y') \end{aligned}$$

where K is a normalization constant. The δ-function conditions integrates three parameters: x', y' and $\Delta\lambda/\lambda$ and the resolution function is then found by calculating the integral which is over a Gaussian that only depends on x and y.

In order to check the results from the analytical calculations, we have compared them with Monte Carlo simulations. The Monte Carlo simulations are performed as follows: First a nominal scattering vector is chosen and the corresponding position on the detector is calculated. The neutron wavelength is chosen randomly from a Gaussian distribution. The positions on the apertures where the neutron passes are chosen randomly. Finally the detector resolution is incorporated by generating a position on the detector from a Gaussian distribution around the nominal position. The wavelength and the positions are used for calculating the actual scattering vector which is finally stored in a 3-dimensional histogram.

A comparison of the results from the analytical calculation and the simulation is shown for a typical example in the figure. The figure shows a good agreement between calculations and simulations.

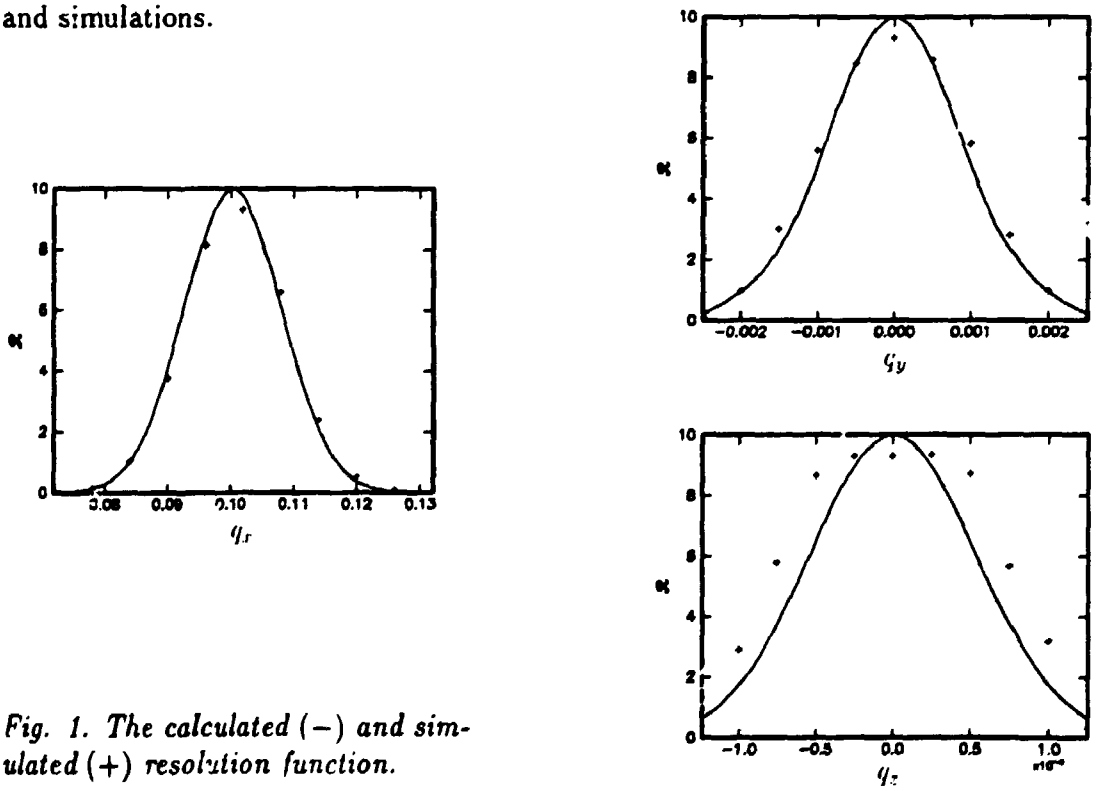

Fig. 1. The calculated (−) and simulated (+) resolution function.

[1] B. Lebech, J. Bernhard and T. Freltoft, (1989). J. Phys.: Cond. Mat. **1**, 6105.

[2] J. Skov Pedersen and C. Riekel, (1991). J. Appl. Cryst. **24**, 893.

1.73 X-Ray Diffraction at the By-Pass beamline BW2 in HASYLAB

(S. Bang, R. Feidenhans'l and M. Nielsen, *Department of Solid State Physics, Risø National Laboratory, Denmark*)

A new X-ray diffractometer has been constructed and installed at the just opened *By-Pass* facility in HASYLAB at DESY in Hamburg. During the last two weeks of running time in 1991 the beam line BW2, where the new instrument is installed, was opened for the first time. The different components in the beamline and in the instrument were aligned and tested. The main characteristics of the new instrument are:

- Vertical scattering plane
- Rod scan facilities, allowing the grazing angle of both the incomming and of the scattered beam to be varied between 0 and 20 °.
- Accomodates heavy sample equipment like UHV-chambers, furnaces or cryostats.
- Accomodates monitor and detector for magnetic X-ray scattering.

The beamline BW2 is constructed by HASYLAB and includes:
- The wiggler, 28 periods, B=1.01 T, K = 13.2, E_c=13.6 keV at the minimum gab 30 mm.
- A plane mirror, which was not available during the first test period.
- A double Si(111) monochromator.
- A double-focussing mirror.
- Motorized slits.

An ideal performance was found for all components in the beam line and the instrument with the only exception being the monochromator crystals. As experienced in the existing wiggler beam line in HASYLAB, W1, the heat load on the first crystal degrade the "rocking curve" of the double monochromator severely. A detailed characterization of this effect was carried out during the test run on BW2, and an improved design of the monochromator crystal cooling is prepared in HASYLAB.

Even with the existing crystals a significant increase in the X-ray intensity was obtained at BW2 as compared to the existing W1 line. The diffractometer and the beam line make a very powerfull facility for structural measurements, in particular on surfaces and interphases, but the instrument is flexible enough to be usefull for a wide range of diffraction studies.

1.74 Horizontal Scattering Diffractometer on Beam Line BW1 in HASYLAB at DESY, Hamburg

(J. Als-Nielsen, K. Kjær, J. Linderholm, S. Bang, *Department of Solid State Physics, Risø National Laboratory, Denmark*, P. Skaarup, E. Vogeley and E. Hansen *Electronics Department, Risø National Laboratory, Denmark*)

In HASYLAB at DESY, Hamburg, Germany, the electron storage ring DORIS has been rebuilt to by-pass the 'Crystal Ball' High-Energy Physics experiment in order to accomodate seven new wigglers and undulators which provide synchrotron radiation.

At beam line BW1 the beam from a 56-pole wiggler (later to be replaced by an undulator) is twice reflected from a flat and a focussing mirror. A double Silicon monochromator may be inserted between the two mirrors to provide – in the hutch 33 meters from the wiggler – a monochromatic beam to be used by a vertically scattering diffractometer installed by HASYLAB.

In a different mode – to be described here – the white, mirror-reflected beam is used by a diffractometer constructed and built by Risø. The diffractometer (*cf.* Figs. 1–3) consists of monochromator stage with one beryllium crystal[1)] (0.25 mm thick; 0.2 mrad mosaic spread) reflecting from the (002) planes in a Laue (transmission) geometry. The advantage of this approach is that, due to the low absorption cross-section of beryllium, most of the white beam is transmitted by the crystal, thus alleviating the otherwise very severe heat load problems. Further, any thermal distortion of the crystal – while it will of course adversely affect the optical quality of the monochromatised beam – will not cause a loss of monochromatic intensity. This is in contrast to the usual schemes with two monochomator crystals where intensity loss results from thermal distorsion of the first crystal. The beryllium crystal is water-cooled at the edges and also by helium gas. Further, variable apertures immediately in front of the crystal serve to control the beam size.

The main scattering plane of the monochromator – and of the rest of the diffractometer – is horizontal. This is to advantage when using heavy sample environments (cryostats, *etc.*) and it is essential for the study of 2D-'crystalline' domains in monolayers on the surfaces of liquids. For the latter purpose, by tilting the monochromator, the beam can be deflected downwards at an angle $\alpha_i \leq 10^\circ$ onto the horizontal liquid surface.

The instrument comprises some twenty stepper-motorized movements (*cf.* table 1): For the monochromator, horizontal and vertical translations, horizontal and vertical apertures, crystal rotation, tilt and 2θ. Down-stream from the monochromator, the sample stage has over-all horizontal and vertical translations, rotation, and a goniometer with two crossed arcs and two translations. Two independent 2θ-movements allow measurement of X-rays specularly reflected from the liquid surface and, simultaneously, of rays laterally diffracted by the two-dimensional 'crystals' in a monolayer at the liquid surface. Optical benches (PI system) before and after the sample carry slits and detectors and can be made to follow the incident and exit beams in the vertical plane (α_i, α_f; two movements for each).

The instrument is run by Risø's TASCOM program, a flexible general-purpose program for controlling experiments. TASCOM runs in the BW1 μVAX and communicates via a GPIB bus with Risø's ECB electronics which performs low-level tasks such as generating stepper motor pulses, checking for limit switches, generating a live display of motor positions in millimeters or degrees, and allowing for manual movement of motors by means of a joy-stick.

Function	TASCOM name	Unit	Description	Location†
TF_M	TFM	mm	Horizontal Translation @ Floor	M
TZ_M	TZM	mm	Vertical Translation	M
HA_M	HAM	step	Horizontal Aperture	M
VA_M	VAM	step	Vertical Aperture	M
ω_M	OMM	Deg.	Crystal Rotation	M
G_M	GM	step	Crystal tilt (Goniometer)	M
$2\theta_M$	2TM	Deg.	Horizontal arm Rotation	M-S
α_i	INAN	Deg.	Vertical Incidence Angle to Sample	M-S
	RO1	Deg.	Vertical PI arm Rotation	M-S
	TZ1	mm	Vertical PI arm Translation	M-S
TF_S	TFS	mm	Horizontal Translation @ Floor	S
ω_S	OMS	Deg.	Sample Rotation	S
TZ_S	TZS	mm	Vertical Translation	S
GU_S	GUS	Deg.	Upper Goniometer	S
GL_S	GLS	Deg.	Lower Goniometer	S
TU_S	TUS	mm	Upper Translation	S
TL_S	TLS	mm	Lower Translation	S
$2\theta_S^L$	2TL	Deg.	Horizontal Lower arm Rotation	S-D
$2\theta_S^U$	2TU	Deg.	Horizontal Upper arm Rotation	S-D
α_f	EXAN	Deg.	Vertical Exit Angle from Sample	S-D
	RO2	Deg.	Vertical PI arm Rotation	S-D
	TZ2	mm	Vertical PI arm Translation	S-D
A_{mol}	BAR	step	Langmuir trough: Barrier Translation	S

†) M = monochromator; S = sample; D = detector.

Table 1. Movements of the BW1 horizontal scattering diffractometer.

The instrument was commisioned with beam on in November 1991. The flux density into the hutch is at present lower than the design value by a factor of several hundreds. This factor is due in part to the fact that a focussing mirror with the design radii is not yet available, so that the area of the beam in the hutch is enlarged by a factor of *ca.* 20. Further causes of loss are at present being investigated at HASYLAB.

[1]) Kindly provided by A. Freund, ESRF, Grenoble, France.

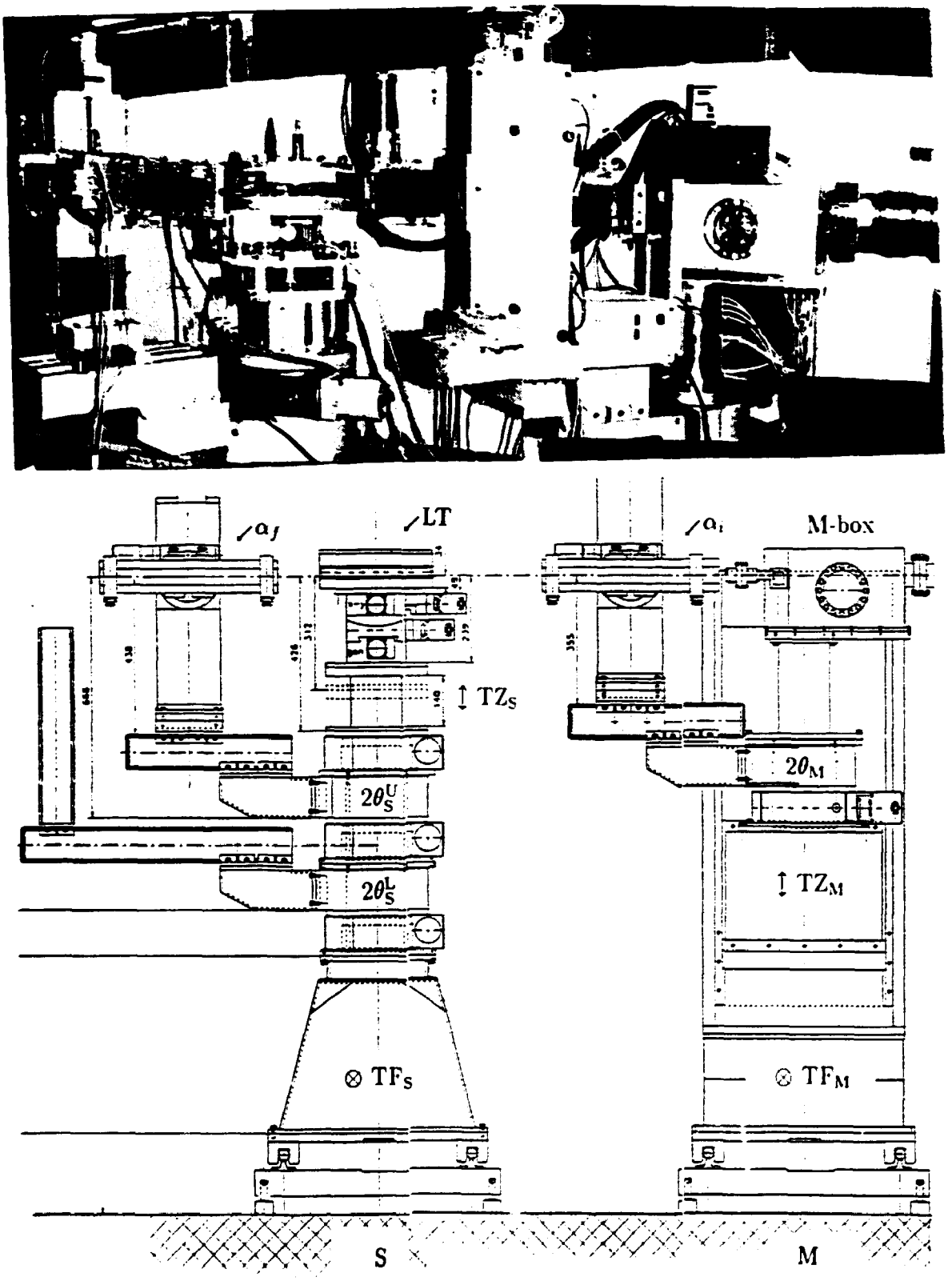

Fig. 1. Side view of the instrument, showing (right to left):
(M) the monochromator tower with (M-box) the beryllium crystal and associated mechanics in a helium-filled box, and (α_i) the mechanics for producing the incidence angle α_i;
(S) the sample tower with (LT) Langmuir Trough, ($2\theta_S^U$, $2\theta_S^L$) two independent horizontal $2\theta_S$-movements and (α_f) mechanics for producing the vertical exit angle α_f.

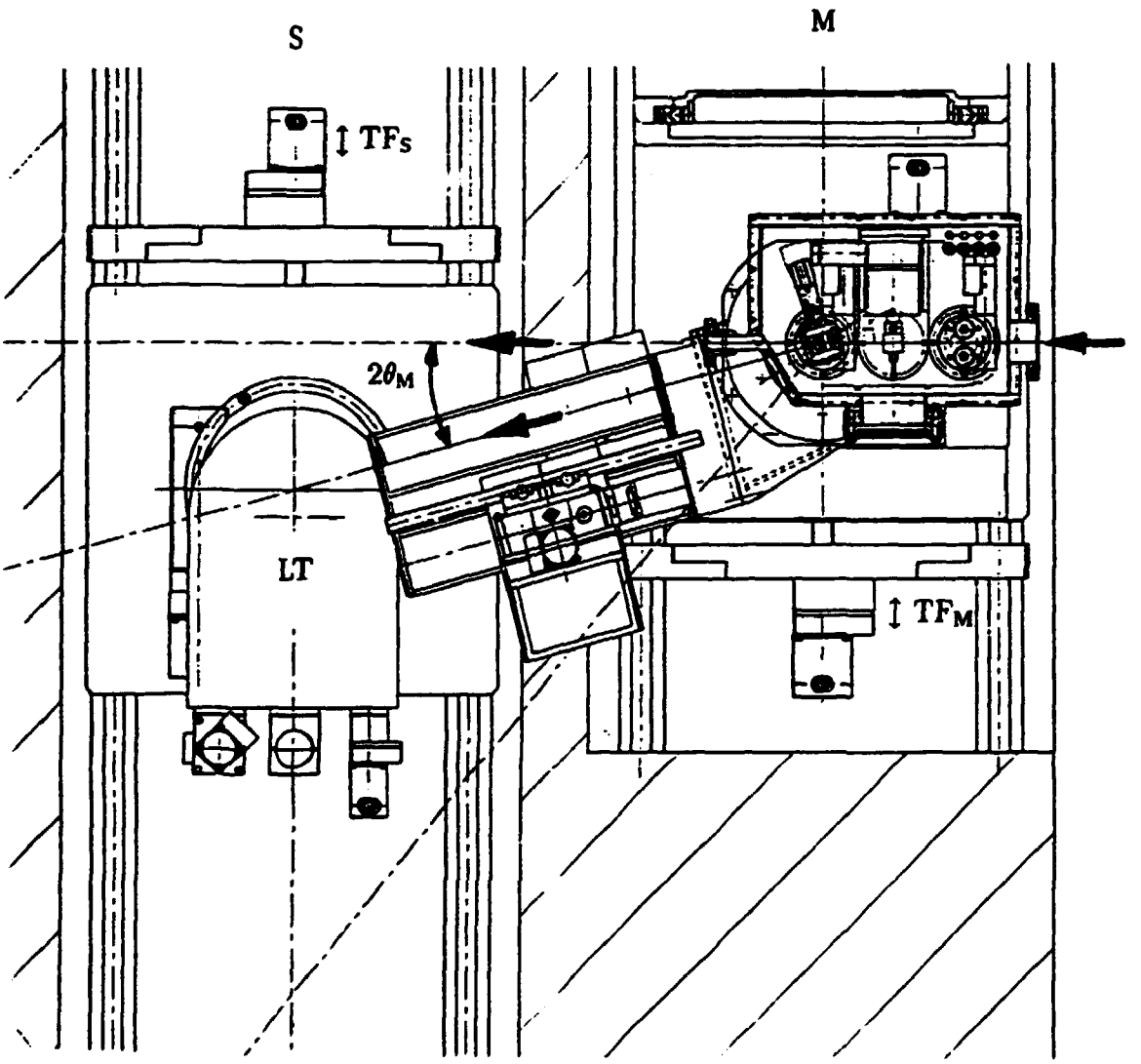

Fig. 2. Top view of the instrument .

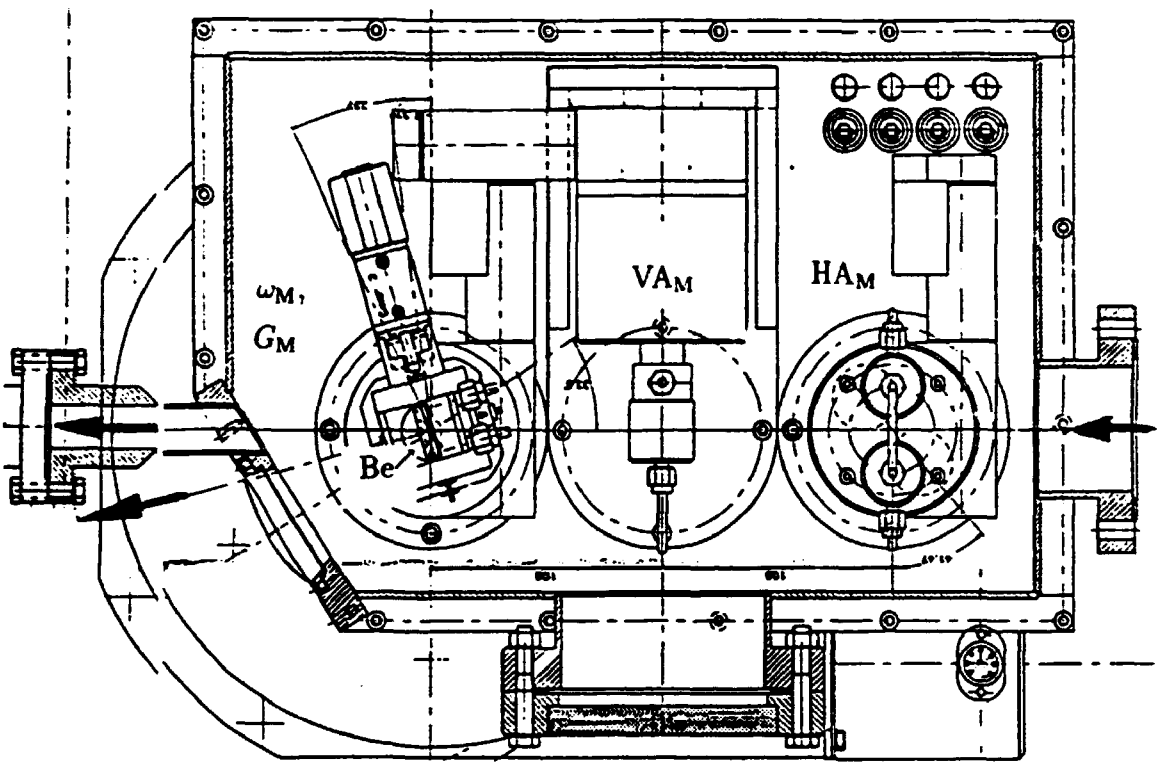

Fig. 3. Top view of the monochromator box with (right to left) (HA_M) horizontal aperture, (VA_M) vertical aperture and (Be) Beryllium crystal with (ω_M) crystal rotation and (G_M) tilt .

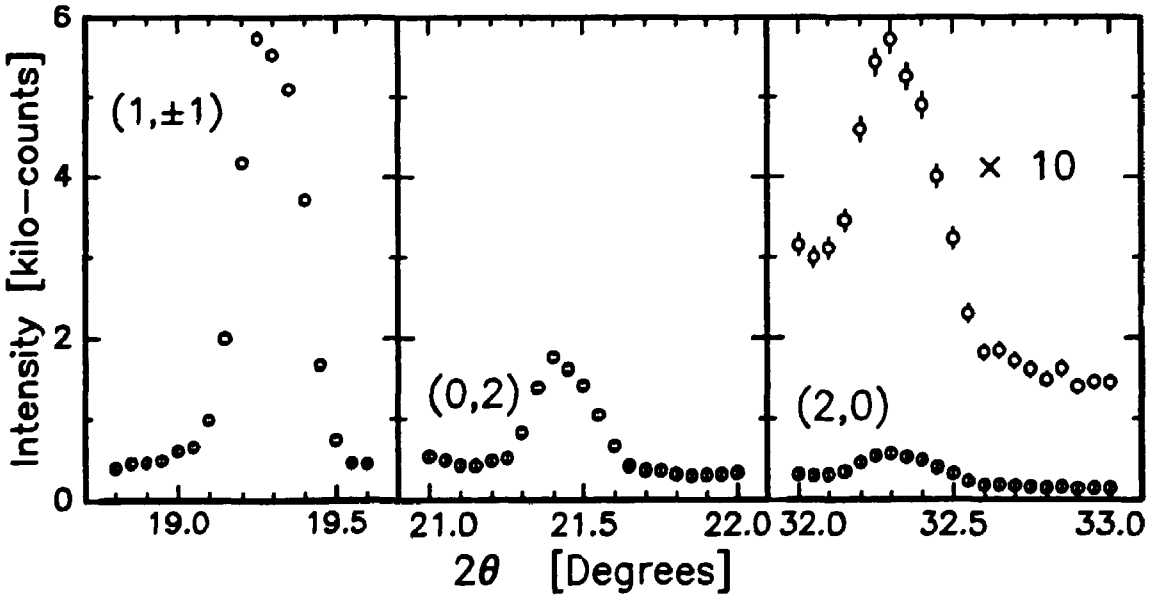

Fig. 4. First Grazing-Incidence Diffraction peaks measured at beam line BW1, from a Langmuir monolayer of $CH_3(CH_2)_{28}COOH$ on a 10^{-3} M $CdCl_2$ solution at pH = 8.85 and $T = 16°C$.

1.75 A Gasvolumetric System for Oxidation and Reduction of High T_c Superconductors under Controlled Conditions

(N.H. Andersen, S. Nielsen and A. Nordskov, *Department of Solid State Physics, Risø National Laboratory, Denmark*, and P. Jønck, *The Technical University of Denmark, Lyngby, Denmark*)

A PC–controlled gasvolumetric system for oxidation and reduction of high T_c superconductors under controlled conditions has been developed. The advantage of the method is that changes in the oxygen content may be determined with high accuracy from the ideal gas law, and oxidation/reduction kinetics may be measured from the time variations of the oxygen pressure. Equilibrium conditions of the sample may be assured by monitoring when the oxygen pressure has decayed, and the equilibrium values may be used to establish the chemical potential of the oxygen in the sample.

The system, shown in the figure, consists of an oxygen reservoir (V_1 = 398 ml) with pressure guages P1 (MKS Baratron 220B, internal volume V_3 = 18.0 ml, full range 1 Torr) and P1000 (MKS Baratron 170M, internal volume V_4 = 8.0 ml, full range 1000 Torr) connected via a canulla tube to the sample container V_5 (V_5 = 58.8 ml). The system has an external oxygen supply (99.999 % purity) and an oil-free pump system (Alcatel Drytel 30, final pressure $< 5\times10^{-6}$ mbar). It is operated via pneumatic valves AV1, AV2, AV4, AV5, AV6 and AS, and leak valves (VAT DN 16) NV1 and NV2 to reduce inlet and pumping speed to a suitable level. The pump is also connected to valve AV6 for fast evacuation of the system. A safety system with pressure monitor PS connected to the pneumatic valve PS is included to prevent over–pressure damage of the system. Inlet/outlet of oxygen may be carried out in a controlled way keeping track on the number of moles let into or out of the system and absorbed/desorbed by the sample. All valves used for this purpose may be operated by the PC or manually. Additional manual valves MV1, MV2, and MV3 may be used to disconnect part of the system under certain operations. The oxygen reservoir, pressure guages, valves and internal connections are thermostatically controlled at a temperature of 38.3±0.1°C. All materials are in stainless steel, except for the sample tube which may be either quartz or stainless steel, depending on application. It is observed that quartz may leak or degas to an extend that limits the accuracy of the oxygen content for small samples (less than one gramme) and the equilibrium pressures below about 2 mbar.

The sample container may be mounted in a tubular furnace for separate preparation of samples with specific changes in oxygen content, measurements of oxygen equilibrium pressure, and oxidation or reduction kinetics. It may also be mounted in neutron or X-ray furnaces for on–line diffraction experiments in connection with oxidation/reduction processes.

Calibration of the system volumes, including the oxygen reservoir, internal and external tubes, pressure guages, and sample container is carried out by reference to an external standard. In the calibration procedure the heated part of the sample container is considered.

The TASCOM command language. developed for operation of the Risø neutron and X-

ray spectrometers, is used to control the system. TASCOM programs for calibration, testing, measuring temperature and pressure, and running sample preparation routines have been developed. With a sample weights of about 15 g of the high T_c supercondcutor $YBa_2Cu_3O_{6+x}$ an accuracy in relative oxygen variations better than $\Delta x = 0.003$ may be obtained. The system may be used for both smaller and larger samples and with other gases. A gas mixing system with accurate flow control is available and may be used to load the system or flow the sample with the desired gas. For preparation of smaller samples, *e.g.* single crystals, the main oxygen reservoir V_1 may be excluded to increase the sensitivity of the pressure–mole relation.

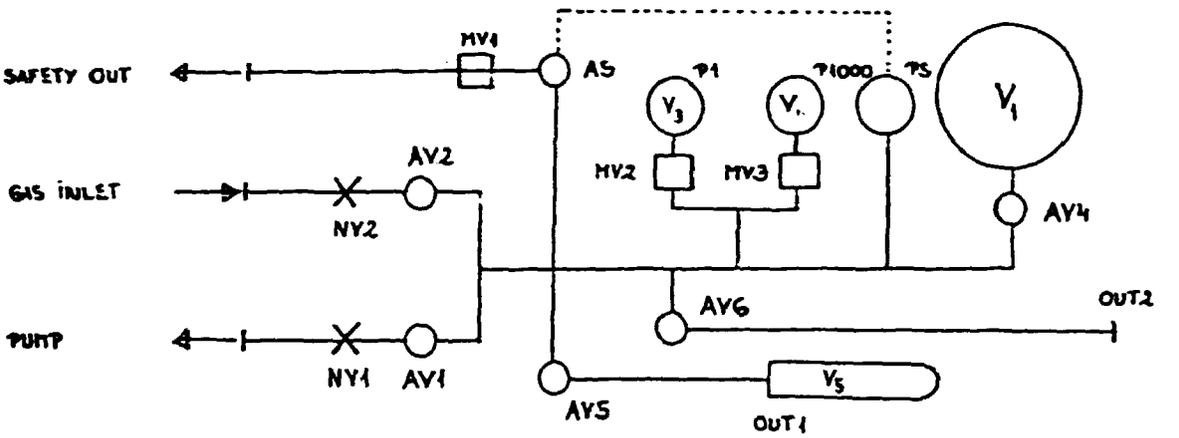

Fig. 1. Scematic presentation of the PC-controlled gasvolumetric system. Pneumatic valves AV1, AV2, AV4, AV5, AV6 and AS are used to control oxygen inlet/outlet, including safety regulations of the system. NV1 and NV2 are leak valves to reduce oxygen inlet/outlet speeds. Manual valves MV1, MV2 and MV3 are also included. Pressures are measured by pressure guages P1 (full runge 1 Torr) and P1000 (full range 1000 Torr). PS is the safety pressure monitor. Internal volumes are indicated V_1, V_3, and V_4, and the sample container volume V_5.

1.76 The liquid He plant

(K. Christensen and M. Nielsen, *Department of Solid State Physics, Risø National Laboratory, Denmark*)

For the year 1991 the following quantities of liquid He were delivered: 38250 liter. Of this 30000 liter He are used outside Risø

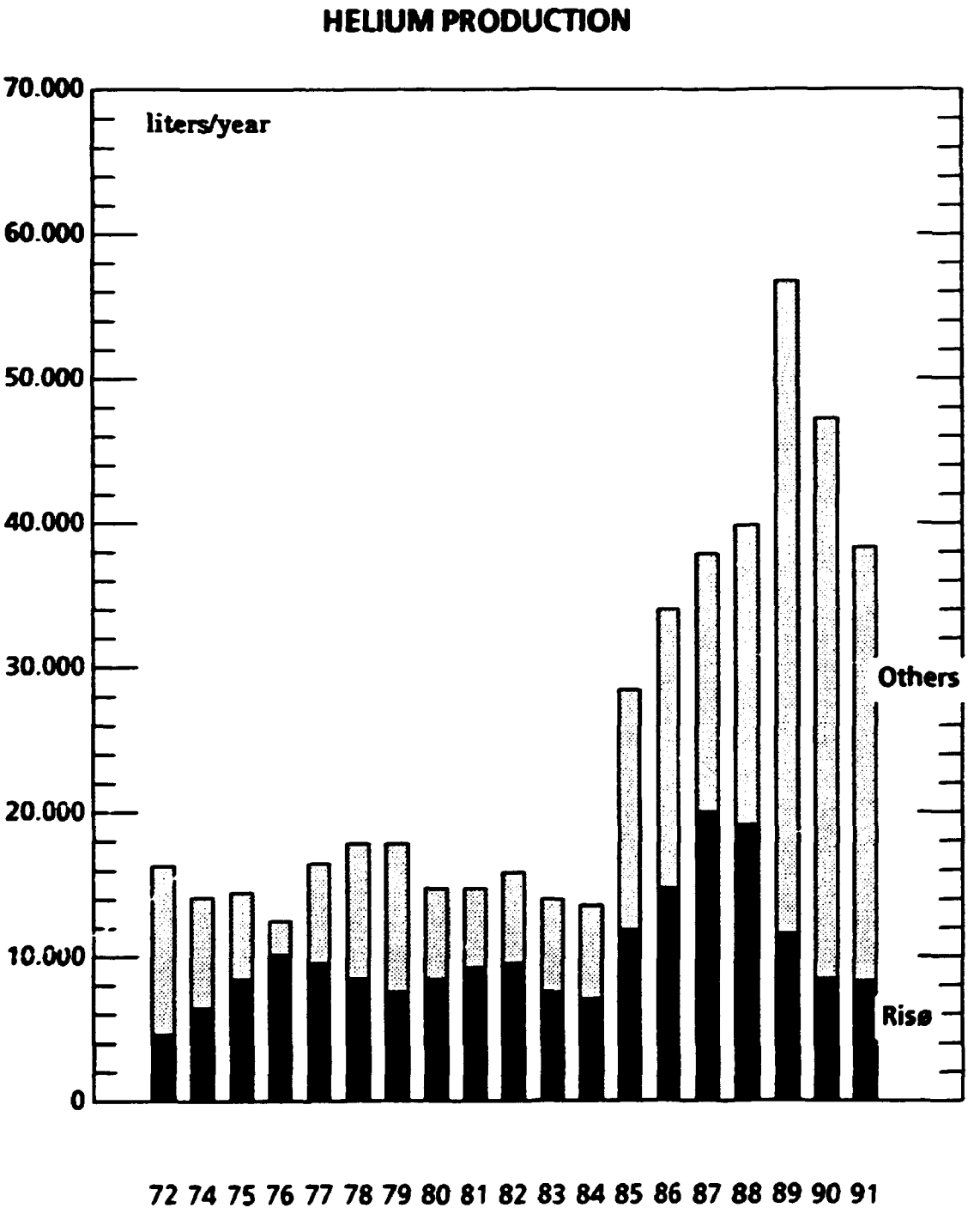

2 PARTICIPANTS IN THE WORK IN THE DEPARTMENT

Scientific Staff

Als-Nielsen, Jens (Head)
Andersen, Niels Hessel
Bohr, Jakob
Buras, Bronislaw (Part time consultant)
Clausen, Kurt Nørgaard
Feidenhans'l, Robert
Grey, François (Until 30 April)
Kjær, Kristian
Lebech, Bente
Lebech, Jens (From 1 July)
Lindgård, Per-Anker
Mackintosh, Allan (Part time consultant)
Mortensen, Kell
Nielsen, Mourits
Pedersen, Jan Skov
Schou, Jørgen

Ph.D. Students and Students

Falcão, Antonio
Fiig, Thomas (From 1 March)
Harris, Pernille
Jønck, Pia (Until 1 August)
Kromann, Rasmus
Poulsen, Henning Friis
Thoft, Nina Bjørn (From 20 October)

Technical Staff

Bang, Steen
Bredgaard, Agner (Temporary assistant)
Breiting, Bjarne (Until 30 June)
Christensen, Kaj
Hansen, Poul-Erik (Until 5 March)
Hansen, René (From 4 November)
Jensen, Louis Gordon (Temporary assistant)
Kjær, Torben
Linderholm, Jens
Lund, Morits
Nielsen, Steen
Nordskov, Arne
Petersen, Andreas (Temporary assistant)
Petersen, Henrik (Temporary assistant)
Rasmussen, Ove

Stahl, Kim (From September 12)
Theodor, Keld
Thuesen, Allan

Secretaries

Frederiksen, Lajla
Jensen, Lene (Apprentice from 1 December until 31 December)
Kloster, Margit
Hansen, Berit (Apprentice until 30 June)

Guest Scientists, Long Time Visitors and Post Docs

Howard, B.	(Until 1 April)
Kennard, C.	University of Queensland, Australia
Mason, T.	AT&T Bell Laboratory, Murray Hill, New Jersey, USA
Pengra, David	(From 1 October)
de Reus, Roger	
Vaknin, D.	(Until 15 October)
Vives, Eduard	University of Barcelona, Spain

Short Time Visitors (more than one week)

Aeppli, G.	AT& T Bell Laboratories, Murray Hill, New Jersey, U.S.A.
Andresen, A.	IFE Kjeller, Norway
Auffermann, G.	The Technical Highschool of Aachen, Germany
Bates, F.	University of Minnesota, Minnesota, U.S.A.
Bernhoeft, N.	Durham University, U.K.
Bishop, D.	AT& T Bell Laboratories, Murray Hill, New Jersey, U.S.A.
Boué, F.	Laboratorie Léon-Brillouin, Saclay, France
Broholm, C.	Johns Hopkins University, Baltimore, U.S.A.
Brown, W.	Uppsala University, Uppsala, Sweden
Bruls, G.	Johannes-Gutenberg Universität, Mainz, Germany
Böhm, C.	Johannes-Gutenberg Universität, Mainz, Germany
Börjesson, L.	Chalmers Institute of Technology, Göteborg, Sweden
Chang, S-L.	M.I.T., Massachusetts, U.S.A.
Chen, S-H.	M.I.T., Massachusetts, U.S.A.
Nørlund Christensen, A.	University of Aarhus, Denmark
Clarke, S.	Oxford University, U.K.
Conrad, H.	IFF, Forshungszentrum, Jülich, Germany
Cowley, R.	Clarendon Laboratory, Oxford, UK
Cudmore, A.	University of Edingburgh, U.K.
Duff, K.	University of Edingburgh, U.K.
Fjellvåg, H.	University of Oslo, Norway
Freund, A.	ESRF, Grenoble, France

Gibbs, D.	Brookhaven National Laboratory, U.S.A.
Gregory, C.	Durham University, U.K.
Gürtler, P.	HASYLAB, DESY, Hamburg, Germany
Habekost, S.	University of Odense, Denmark
Hack, T.	Max-Planck-Institute for Polymer Research, Mainz, Germany
Hadfield, R.	Clarendon Laboratory, Oxford, U.K.
Hamley, J.	FOM Institute, Amsterdam, The Netherlands
Harrison, A.	Oxford University, U.K.
Hass, H.	Johannes-Gutenberg Universität, Mainz, Germany
Hayden, S.	University of Bristol, U.K.
Hayes, W.	Clarendon Laboratory, Oxford, U.K.
Heidelmann, M.	IFF, Forshungszentrum, Jülich, Germany
Jansson, S.	IFF, Forshungszentrum, Jülich, Germany
Jehan, D.	Clarendon Laboratory, Oxford, U.K.
de Jeu, W.	FOM-Institute, Amsterdam, The Netherlands
Keen, D.	Clarendon Laboratory, Oxford, U.K.
Kleimann, R.	AT& T Bell Laboratories, Murray Hill, New Jersey, U.S.A.
Kubista, M.	Chalmers University of Technology, Göteborg, Sweden
Leiserowitz, L.	Weizmann Institute, Rehovot, Israel
Leveiller, F.	Weizmann Institute, Rehovot, Israel
Lösche, M.	Johannes-Gutenberg Universität, Mainz, Germany
Majewski, J.	Weizmann Institute, Rehovot, Israel
Meier, G.	Max-Planck-Institute for Polymer Research, Mainz, Germany
McGreevy, R.	Clarendon Laboratory, Oxford, U.K.
McCracken,C.G.	Brunel University, Uxbridge, U.K.
McMarrow, D.	Clarendon Laboratory, Oxford, U.K.
Mugamilah	Hahn-Meitner Institute, Berlin, Germany
Müller, P.	The Technical High School of Aachen, Germany
Nield, V.	Clarendon Laboratory, Oxford, U.K.
Norby, P.	University of Odense, Denmark
Nordén, B.	Chalmers Institute of Technology, Göteborg, Sweden
Papp, S.	University of Göteborg, Sweden
Pedrys, R.	Jagellonian University, Cracow, Poland
Piepenstock, M.	Johannes-Gutenberg Universität, Mainz, Germany
Proudfoot,G.G.	AERE Harwell, Oxfordshire, U.K.
Rosendale, J.	University of Minnesota, Minneapolis, U.S.A.
Samseth, J.	IFE Kjeller, Norway
Sandey, A.	M.I.T., Massachusetts, U.S.A.
Scherrenberg, R.	University of Leuven, Leuven, Belgium
Schlottke, H.	Max-Planck-Institute for Polymer Research, Mainz, Germany
Schwan, D.	IFF, Forshungszentrum Jülich, Germany
Schmid, B.	Institute Laue-Langevin, Grenoble, France
Seim, H.	University of Oslo, Norway
Seto, H.	Hiroshima University, Japan
Shinns, A.	University of Utrecht, The Netherlands
Sinclair, R.	AERE Harwell, U.K.
Sjöberg, B.	University of Göteborg, Sweden
Skjetne, E.	IFE Kjeller, Norway

Smetana, Z.	Charles University, Prague, Czechoslovakia
Sonntag, R.	University of Tübingen, Germany
Stolken, S.	Max-Planck-Institute for Polymer Research, Mainz, Germany
Szalóki, I.	Kossuth University, Debrecen, Hungary
Takahashi, M.	CNRS, Strassbourg, France
Visser, D.	Loughborough University, U.K.
Weber, D.	Johannes-Gutenberg Universität, Mainz, Germany
Weinfurter, H.	Hahn-Meitner Institute, Berlin, Germany
de Wijn, H.	FOM Institute, Amsterdam, The Netherlands
Wicks, J.	Clarendon Laboratory, Oxford, U.K.
Winkelmann, M.	Hahn-Meitner Institute, Berlin, Germany
Wolny, J.	Academy of Mining and Metallurgy, Cracow, Poland
Zeiske, T.	Hahn-Meitner Institut, Berlin, Germany
Österberg, R.	Swedish Agricultural University, Uppsala, Sweden

Awards and Degrees

Bohr, J., Dr. Scient., Copenhagen University, Denmark
Schou, J., Dr. Scient, University of Odense, Denmark
Posselt, D., Ph.D., The Technical University, Denmark

Jakob Bohr has been appointed Research Professor from 1 July

3 PUBLICATIONS AND EDUCATIONAL ACTIVITIES IN THE DEPARTMENT

3.1 Publications

AARNINK, W.A.M., BLANK, D.H.A., ADELERHOF, D.J., FLOKSTRA, J., ROGALLA, H., SILFHOUT, A. VAN, and REUS, R. DE (1991). Interdiffusion Studies on High-T_c Superconducting $YBa_2Cu_3O_{7-\delta}$ Thin Films on Si(111) with a $NiSi_2/ZrO_2$ Buffer Layer. Appl. Surf. Sci. **47**, 199-203.

ALS-NIELSEN, J. (1991). Diffraction, Refraction and Absorption of X-Rays and Neutrons - A Comparative Exposition. (Risø National Laboratory, Roskilde), 47 p.

ALS-NIELSEN, J. (1991). X-Ray Reflectivity Studies of Liquid Surfaces. In: Handbook on Synchrotron Radiation. **3**. Brown, G.S. and Moncton, D.E. (eds.) (North-Holland, Amsterdam), 471-503.

ANDERSEN, N.H., LEBECH, B., and POULSEN, H.F. (1991). Study of the Structural Phase Diagram, Oxygen Bulk In-Diffusion, and Equilibrium Partial Pressure of $YBa_2Cu_3O_{6+x}$. In: Advances in Superconductivity III. 3. International Symposium on Superconductivity. ISS '90, Sendai, 6-9 November 1990. Kajimura, K., Haykawa, H. (eds.) (Springer-Verlag, Tokyo), 449-452.

ANDERSEN, N.H. and POULSEN, H.F. (1991). International Interesse for Superleder-Teori. (International Interest in Theory of Superconductivity). Risø Nyt **2**, 10-11.

ANNILA, A.J., CLAUSEN, K.N. OJA, A.S., TUORINIEMI, J.T., and WEINFURTER, H. (1991). Neutron Diffraction Studies of the Nuclear Magnetic Phase Diagram of Copper. TKK-F-A-685, 49 p.

BAUER, R., BEHAN, M., HANSEN, S., JONES, G., MORTENSEN, K., SÆRMARK, T., and ØGENDAL, L. (1991). Small-Angle Scattering Studies on Clathrin-Coated Vesicles. J. Appl. Cryst. **24**, 815-821.

BOHR, H., BOHR, J., BRUNAK, S., COTTERILL, R.M.J., FREDHOLM, H., LAUTRUP, B., and PETERSEN, S.B. (1991). Neural Network Applied to Protein Structure. AIP Conf. Proc. **239** (American Institute of Physics, New York). 293-310.

BOHR, J. (1991). Observations of Low-Dimensional Effects?. Europhys. Lett. **14**, 85-86.

BOHR, J. (1991). Surface Structures, Magnetic Structures, and Small Inclusions, as Studied by X-Ray Diffraction. Risø-R-585, 69 p.

BOHR, J. (1991). Epitaxial Clusters in Single Crystal Hosts. Z. Phys. D **20**, 215-218.

BOHR, J., GRÅBÆK, L., ANDERSEN, H.H., JOHANSEN, A., JOHNSON, E., SARHOLT-KRISTENSEN, L., SURGANOV, V., ROBINSON, I.K., BRODDIN, D., and TENDELOO, G. VAN. (1991). X-ray Diffraction Studies of Kr and Pb Inclusions in

Aluminium. In: Fundamental Aspects of Inert Gases in Solids. Donelly, S.E. and Evans, J.H. (eds.) (Plenum Press, New York), 265-276.

BOHR, J., JENSEN, B. SKYTTE, EGSGAARD, H., and LARSEN, E. (1991). "Buckminsterfulleren - en ny slags kulstof! (Buckminsterfullerene - a New Form of Carbon). Risø Nyt 4, 2-3.

BROHOLM, C., LIN, H., MATHEWS, T.P., MASON, T.E., BUYERS, W.J.L., COLLINS, M.F., MENOVSKY, A.A., MYDOSH, J.A., and KJEMS, J.K. (1991). Magnetic Excitations in the Heavy Fermion Superconductor URu_2Si_2. Phys. Rev. B **43**, 12809-12822.

BØJSØE-JØRGENSEN, P., JUUL JENSEN, D., CLAUSEN, K.N., THORSEN, K.A., and HIROSAWA, S. (1991). Texture in Neodymium-Iron-Boron Permanent Magnets. In: Metal Matrix Composites - Processing, Microstructure and Properties. 12. Risø International Symposium on Materials Science, Risø, 2-6 September 1991. Hansen, N., Juul Jensen, D., Leffers, T., Lilholt, H., Lorentzen, T., Pedersen, A.S., Pedersen, O.B., and Ralph, B. (eds.) (Risø National Laboratory, Roskilde), 277-282.

CASTÁN, T. and LINDGÅRD, P.-A. (1991). Domain-Growth Kinetics and Aspects of Pinning: A Monte Carlo Simulation Study. (1991). Phys. Rev., B **43**, 956-964.

CAVA, R.J., BATLOGG, B., KRAJEWSKI, J.J., GAMMEL, P., POULSEN, H.F., PECK JR., W.F., and RUPP JR., L.W. (1991). Antiferromagnetism and Metallic Conductivity in $Nb_{12}O_{29}$. Nature **350**, 598-600.

CAVA, R.J., BATLOGG, B., KRAJEWSKI, J.J., POULSEN, H.F., GAMMEL, P., PECK JR., and RUPP JR., L.W. (1991). Electrical and Magnetic Properties of $Nb_2O_{5-\delta}$ Crystallographic Shear Structure. Phys. Rev. B **44**, 6973-6981.

CHEN, S.H., CHANG, S.L., STREY, R., SAMSETH, J., and MORTENSEN, K. (1991). Structural Evolution of Bicontinous Microemulsions. J. Phys. Chem. **95**, 7427-7432.

CHEONG, S.W., AEPPLI, G., MASON, T.E., MOOK, H., HAYDEN, S.M., CANFIELD, P.C., FISK, Z., CLAUSEN, K.N., and MARTINEZ, J.L. (1991). The Incommensurate Magnetic Fluctuations in $La_{2-x}Sr_xCuO_4$. Phys. Rev. Lett. **67**, 1791.

CHOU, H., TRANQUADA, J.M., SHIRANE, G., MASON, T.E., BUYERS, W.J.L., SHAMOTO, S., and SATO, M. (1991). Neutron-Scattering Study of Spin Fluctuations in Superconducting $YBa_2Cu_3O_{6+x}$ (x=0.40, 0.45, 0.50). Phys. Rev. B **43**, 5554-5563.

CLAUSEN, K.N., WESTERMANN, J.,and OLSEN, K.B. (1991). The Risø Cold Neutron Source. in Proceedings from International Workshop on Cold Neutron Sources. Russell, G.J. and West, C.D. Eds. report LA-12146-C (Los Alamos National Laboratory, USA), 57-63.

COWLEY, R.A., COPE, N., WANKLYN, B., MASON, T.E., and BUYERS, W.J.L. (1991). Magnetic Properties of $RbVF_4$. J. Phys.: Condens. Matt. **3**, 2953-2961.

DORNISCH, D., MORITZ, W., SCHULZ, H., FEIDENHANS'L, R., NIELSEN, M., GREY, F., and JOHNSON, R.L. (1991). Au/Si(111): Analysis of the $(\sqrt{3} \times \sqrt{3})R$ 30° and 6 × 6 Structures by In-plane X-ray Diffraction. Phys. Rev. B **44**, 11221-11230.

ELDRUP, M., PEDERSEN, J.SKOV, HORSEWELL, A., JENSEN, K.O., and EVANS, J.H. (1991). Comparison of Results from Different Experimental Techniques (SANS, TEM, PAT, SEM) Applied to Bulk Cu and Ni Containing Krypton. In: Fundamental Aspects of Inert Gases in Solids. Donelly, S.E. and Evans, J.H. (eds.) (Plenum Press, New York), 221–229.

ELSENHANS, O., FISCHER, P., FURRER, A., CLAUSEN, K.N., PURWINS, H.G., and HULLIGER, F. (1991). Incommensurate and Commensurate Magnetic Long-Range Order in Metallic $REPd_3$ Compounds of Rare Earths (RE=Nd, Tb, Dy, Er, Tm, Yb). Z. Phys. B **82**, 61-75.

FEIDENHANS'L, R. (1991). Overflader og deres Krystallografi (Surfaces and Their Crystallography). Kvant **2**, 9-12.

FEIDENHANS'L, R., GREY, F., JOHNSON, R.L., and NIELSEN, M. (1990). Determination of the Cu(110)-c(6×2)-O Structure by X-Ray Diffraction. Phys. Rev. B **44**, 1875-1879.

FEIDENHANS'L, R., GREY, F., NIELSEN, M., and JOHNSON, R.L. (1991). Structure and Ordering of Metal Overlayers on Si(111) and Ge(111) Surfaces. Kinetics of Ordering and Growth at Surfaces. Lagally M.G. (ed.) (Plenum Press, New York), 189-207.

FREDHOLM, H., BOHR, H., BOHR, J., BRUNAK, S., COTTERILL, R.M.J., LAUTRUP, B., and PETERSEN, S.B. (1991). A Novel Approach to Prediction of the 3-Dimensional Structure of the Protein Backbones by Neural Networks. In: Advances in Neural Information Processing Systems 3. Lippmann, R.P., Moody, J.E., and Touretzky, D.S. (eds). (Morgan Kaufmann Publ., San Mateo, USA). 523-529.

FRELTOFT, T., BUTTREY, D.F., AEPPLI, G., VAKNIN, D., and SHIRANE, G. (1991). Magnetic Correlations and Their Dependence on Excess Oxygen in $La_2NiO_{4-\delta}$. Phys. Rev. B **44**, 5046-5056.

GREY, F. and BOHR, J. (1991). Fra LEGO og DUBLO til Groning af Kunstige Krystaller. (From LEGO and DUBLO to the Growth of Artificial Crystals). Risø Nyt **1**, 12-13.

HABEKOST, S., CHRISTENSEN, A. NØRLUND, LEBECH, B., WROBLEWSKI,T., and O'REILLY, K.P.J. (1991). Superconducting Cuprates and Related Oxides. IV. Temperature - Unit Cell Parameter Relationships of $HoBa_2Cu_3O_{7-\delta}$. Acta Chem. Scand. **45**, 965-967.

HANSEN, S. and PEDERSEN, J. SKOV (1991). A Comparison of Three Different Methods for Analysing Small-Angle Scattering Data. J. Appl. Cryst. **24**, 541-548.

HAYDEN, S.M., AEPPLI, G., MOOK, H:; RYTZ, D., HUNDLEY, M.F., and FISK, Z. (1991). Magnetic Fluctuations in $La_{1.95}Ba_{0.05}CuO4$. Phys. Rev. Lett. **66**, 821-824.

HOWARD, B.K. and BOHR, J. (1991). Binary Magnetic Structures in HoEr. Physica Scripta **T39**, 96 (1991).

JACQUEMAIN, D., LEVEILLER, F., WEINBACH, S.P., LAHAV, M., LEISEROWITZ, L., KJÆR, K., and ALS-NIELSEN, J. (1991). Crystal Structure of Self-aggregates of Insoluble Aliphatic Amphiphilic Molecules at the Air-water Interface. An X-ray Synchrotron Study. J. Am. Chem. Soc. **113**, 7684-7691.

JØRGENSEN, J.-E. and ANDERSEN, N.H. (1991). Neutron Diffraction Study of $Pb_2Sr_2HoCu_3O_8$. Acta Chem. Scand. **45**, 19-22.

KAKURAI, K., STEINERT, M., PYNN, R., and KJEMS, J. (1991). Inelastic Polarized Neutron Scattering from $S = 1$ Antiferromagnetic $CsNiCl_3$ in an Applied Field. J. Phys.: Condens. Matter **3**, 715-726.

KENN, R.M., BÖHM, C., BIBO, A.M., PETERSON, I.R., MÖHWALD, H., ALS-NIELSEN, J., and KJÆR, K. (1991). Mesophases and Crystalline Phases in Fatty Acid Monolayers. J. Phys. Chem. **95**, 2092-2097.

KJÆR, K., ALS-NIELSEN, J., KENN, R.M., BÖHM, C., TIPPMANN-KRAYER, P., PETERSON, I.R., BIBO, A.M., HELM, C.A., MÖHWALD, H., LEVEILLER, F., JACQUEMAIN, D., WEINBACH, S., LEISEROWITZ, L. and DEUTSCH, M. (1991). X-Ray Scattering Studies of Fatty Acid Films on Water and on $CdCl_2$ Solutions. Makromol. Chem. Macromol. Symp. **46**, 89-96.

LANDER, G.H., BROOKS, M.S.S., LEBECH, B., BROWN, P.J., VOGT, O., and MATTENBERGER, K. (1991). Measurement of Anisotropy Constant in US with Polarized Neutrons. J. Appl. Phys. **69**, 4803-4806.

LEBECH, B., WULFF, M. and LANDER, G.H. (1991). Spin and Orbital Moments in Actinide Compounds. J. Appl. Phys. **69**, 5891-5896.

LEDERER, H., MORTENSEN, K., MAY, R.P., BAER, G., CRESPI, H.L., DERSCH, D., and HEUMANN, H. (1991). Spatial Arrangement of σ-Factor and Core Enzyme of *Escherichiacoli* RNA Polymerase. A Neutron Solution Scattering Study. J. Mol. Biol., **219**, 747-755.

LEVEILLER, F., JACQUEMAIN, D., LAHAV, M., LEISEROWITZ, L., DEUTSCH, M., KJÆR, K. and ALS-NIELSEN, J. (1991). Crystallinity of the Double Layer of Cadmium Arachidate Films at the Water Surface. Science **252**, 1532-1536.

LINDGÅRD, P.-A. (1990). Theory of a New Type of Antiferromagnetism in the Ideal fcc System Cu. J. Magn. Magn. Mater. **90/91**, 138-140.

LINDGÅRD, P.-A., and T. CASTÁN, T. (1991). The $t^{-1/4}$ Universality Class: Theory and Simulation of Slow Domain Growth after Quenches to Low and Finite Temperatures. In: Disorder in Condensed Matter Physics. Blackman J.A. and Tagüeña J. (eds.) (Clarendon Press, Oxford), 405-411.

MAJKRZAK, C.F., KWO, J., HONG, M., YAFET, Y., GIBBS, D., CHIEN, C.L., and BOHR, J. (1991). Magnetic Rare Earth Superlattices. Advances in Physics **40**, 99-189.

MARGAÇA, F.M.A., FALCÃO, A.N., SALGADO, J.F. and CARVALHO, F.G. (1991). Solving the Problem of SANS Instrument Optimization. J. Appl. Cryst. **24**, 994-998.

MARGAÇA, F.M.A., FALCÃO, A.N., SEQUEIRA, A.D., and SALGADO, J.F. (1991). Optical Effects on Neutron Guide Tubes Produced by Collimation. J. Appl. Cryst. **24**, 531-536.

MASON, T.E., and BUYERS, W.J.L. (1991). Spin Excitations and the Electronic Specific Heat of URu_2Si_2. Phys. Rev. B **43**, 11471-11474.

MAYER, H.M., STEINER, M., STÜßER, N., WEINFURTER, H., KAKURAI, K., DORNER, B., LINDGÅRD, P.-A., CLAUSEN, K.N., HOCK, S., and RODEWALD, W. (1991). Inelastic Neutron Scattering Measurements on $Nd_2Fe_{14}B$ Single Crystals. J. Magn. Magn. Mat. **97**, 210-218.

MOOK, H.A., AEPPLI, G., HAYDEN, S.M., FISK, Z., and RYTZ, D. (1991). Neutron Scattering Measurements of the Magnetic Excitations of High-Temperature Superconducting Materials. In: Dynamics of Magnetic Fluctuations in High-Temperature Superconductors. NATO Advanced Research Workshop on Dynamics of Magnetic Fluctuations in High-Temperature Superconductors, Aghia Pelaghia, 9-14 October 1989. Reiter, G., Horsch, P. and Psaltakis, G.C. (eds.) (Plenum Press, New York) (NATO Advanced Science Institutes Series B: Physics, 246), 21-34.

MORTENSEN, K. (1991). Microphase Separation in Bilayer Membranes. Biological Inspired Physics, Peleti, L. (ed.) (Plenum Publ.), 157-163.

MOURITSEN, O.G., SHAH, P.J., ANDERSEN, J.V., POULSEN, H.F. and BOHR, H. (1991). Computer Simulation of Phase Separation and Ordering Processes in Low-Dimensional Systems. Phys. Scr. **T38**, 55-65.

NORBY, P., NØRLUND CHRISTENSEN, A., FJELLVÅG, H., and NIELSEN, M. (1991). The Crystal Structure of Cr_8O_{21} Determined from Powder Diffraction Data: Thermal Transformation and Magnetic Properties of a Chromium-Chromate-Tetrachromate. J. Solid State Chem., **94**, 281-293.

NORDÉN, B., ELVINGSON, C., ERIKSSON, T., KUBISTA, M., SJÖBERG, B., TAKAHASHI, M. and MORTENSEN, K. (1990). Structure of a RecA-DNA Complex from Linear Dichroism and Small-Angle Neutron-Scattering in Flow-Oriented Solution. J. Mol. Biol. **216**, 215-228.

PEDERSEN, J. SKOV and RIEKEL, C. (1991). Resolution and Flux at the Sample for Small-Angle X-ray Scattering Calculated in Position-Angle Wavelength Space. J. Appl. Cryst **24**, 893-909.

POSSELT, D., KJEMS, J.K., BERNASCONI, A., SLEATOR, T., and OTT, H.R. (1991). The ThermalConductivity of Silica Aerogel in the Phonon, the Fracton and the Particle-Moide Regime. Europhys. Lett. **16**, 59-65.

POULSEN, H.F. ANDERSEN, N.H., ANDERSEN, J.V., BOHR, H., and MOURITSEN, O.G. (1991). Relation Between Superconducting Transition Temperature and Oxygen Ordering in $YBa_2Cu_3O_{6+x}$. Nature **349**, 594-596.

POULSEN, H.F., ANDERSEN, N.H., ANDERSEN, J.V., BOHR, H., and MOURITSEN, O.G. (1991). Dynamical Scaling of Oxygen Ordering in $YBa_2Cu_3O_{7-\delta}$. Phys. Rev. Lett. **66**, 465-468.

POULSEN, H.F., ANDERSEN, N.H., ANDERSEN, J.V., BOHR, H., and MOURITSEN, O.G. (1991). Lattice Gas Simulation of Oxygen Ordering in $YBa_2Cu_3O_{6+x}$ Showing Dynamical Scaling. Modern Phys. Lett. B **5**, 827-832.

POULSEN, H.F., ANDERSEN, N.H., and LEBECH, B. (1990). Twin-Domain Size and Bulk Oxygen In-Diffusion Kinetics of $YBa_2Cu_3O_{6+x}$ Studied by Neutron Powder Diffraction and Gas Volumetry. Physica C **173**, 387-397.

PRETORIUS, R., VREDENBERG, A.M., SARIS, F.W., and REUS, R. DE. (1991). Prediction of Phase Formation Sequence and Phase Stability in Binary Metal-Aluminium Thin-Film Systems Using the Effective heat of Formation Rule. J. Appl. Phys. **70**, 3636-3646.

ROSS, D.K., McKERGOW, M.W., WITCHELL, D.G., and KJEMS, J.K. (1991). Neutron Diffraction Studies of Domain Growth Associated with the 50 K Anomaly in Pd-D. J. Less-Common Metal. **172/174**, 169-182.

SCHAMPER, C., MORITZ, W., SCHULZ, H., FEIDENHANS'L, R., GREY, F., JOHNSON, R.L., and NIELSEN, M. (1991). Static Lattice Distortions and the Structure of Au/Si(111)-(5x1): An X-Ray-Diffraction Study. Phys. Rev. B **43**, 12130-12133.

SCHOU, J. (1991). Erosion of Volatile Elemental Condensed Gases by keV Electron and Light-Ion Bombardment. Risø-R-591, 1-159.

SCHOU, J., KRUIT, P., and NEWBURY, D.E. Eds., (1991). Fundamental Electron and Ion Beam Interactions with Solids for Microscopy, Microanalysis and Microlithography, Proceedings of the 8th Pfefferkorn Conference. Scanning Microscopy Supplement 4, 1-370.

SCHOU, J., STENUM, B., SØRENSEN, H., and WEISBERG, K.-V. (1991). Radiation in the Wavelength Range 120-900 nm from keV Electron Bombardment of Solid Hydrogens. Nucl. Fusion **31**, 589-591.

SJÖBERG, B., PAP, S., JÄRNBERG, S.-E., and MORTENSEN, K. (1991). Kinetics of the Urea-Induced Dissociation of Human Plasma α_2-Macroglobulin as Measured by Small-Angle Neutron Scattering. Biochem. J. **278**, 325-328.

SLEATOR, T., BERNASCONI, A., POSSELT, D., KJEMS, J.K. and OTT, H.R. (1991). Low-Temperature Specific Heat and Thermal Conductivity of Silica Aerogels. Phys. Rev. Lett. **66**, 1070-1073.

STENUM, B., ELLEGAARD, O. SCHOU, J., SØRENSEN, H., and PEDRYS, R. (1991). Sputtering of Frozen Gases by Molecular Hydrogen Ions. Nucl. Instr. Methods B **58**, 399-403.

STENUM, B., SCHOU, J., ELLEGAARD, O., SØRENSEN, H., and PEDRYS, R. (1991). Sputtering of Solid Hydrogenic Targets by keV Hydrogen Ions. Phys. Rev. Lett. **67**, 2842-2845.

TENDELOO, G. VAN, BEECK, M. OP DE, AMELINCKX, S., BOHR, J:, and KRÄTSCHMER. (1991). Phase Transformation in Solid C_{60}/C_{70}: An Electron Microscopy Study. Europhys. Lett., **15**, 295-300.

VAKNIN, D., KJÆR, K., ALS-NIELSEN, J., and LÖSCHE, M. (1991). Structural Properties of Phosphatidylcholline in a Monolayer at the Air-water Interface. A Neutron Reflection Study and Reexamination of X-ray Reflection Measurements. Biophys. J. **59**, 1325-1332.

VAKNIN, D., ALS-NIELSEN, J., PIEPENSTOCK, M., and LÖSCHE, M. (1991). Recognition Processes at Functionalized Lipid Surfaces Observed with Molecular Resolution. Biophys. J. **60**, 1545-1552.

VAKNIN, D., KJÆR, K., ALS-NIELSEN, J., and LÖSCHE, M. (1991). Structural Properties of Phosphatidylcholine in a Monolayer at the Air/Water Interface. Biophys. J. **59**, 1325-1332.

VAKNIN, D., KJÆR, K., ALS-NIELSEN, J., and LÖSCHE, M. (1991). A new Liquid Surface Neutron Reflectometer and its Application to the Study of DPPC in a Monolayer at the Air/Water Interface. Makromol. Chem. Macromol. Symp. **46**, 383-388.

VIVES, E. and LINDGÅRD, P.-A. (1991). Substrate Inluence on Two-Dimensional Solids and Liquids: A Monte Carlo Simulation Study. Phys. Rev. B **44**, 1318-1328.

VIVES, E. and LINDGÅRD, P.-A. (1991). Two Dimensional Solids and Liquids Influenced by Small and Large Substrate Potential. Phys. Scripta. **T38**, 70-74.

ZEISKE, T., SONNTAG, R., HOHLWEINB, D., ANDERSEN, N.H., and WOLF, T. (1991). Local Oxygen Ordering in Superconducting $YBa_2CU_3O_{6.4}$. Nature **353**, 542-544.

ÖSTERBERG, R., MALMSTEN, B., BOIVE, T., NILSSON, U., STIGBRAND, T., and MORTENSEN, K. (1991). Correlation Between the Human and Porcine Complement System: A Small-Angle Scattering Study of Cross Immunity and Methylamine - Induced Conformational Changes of Porcine C3 and C4 Proteins. Molecular Immunology. **28**, 959-963.

3.2 Conferences

ALS-NIELSEN, J., Complementarity of Neutron and X-ray Reflectivity. 1991 Gordon Research Conference on X-Ray Physics, New Hampshire, U.S.A. (August).

ALS-NIELSEN, J., Synchrotron X-Ray and Cold Neutron Reflection Studies of Amphiphilic Monolayers. NATO ASI Structure and Dynamics of Supramolecular Aggregates and Strongly Interacting Colloids, Aquafredda di Mareatea, Italy (June).

ALS-NIELSEN, J. and FREUND, A.K., Monochromator on a Synchrotron Undulator Source for Liquid Surface Studies, International Conference on Synchrotron Radiation Instrumentation, Chester, U.K. (July).

ANDERSEN, J.V., POULSEN, H.F, ANDERSEN, N.H., BOHR, H., and MOURITSEN, O.G. Ageing and stuctural stability of Oxygen in YBaCuO Superconductor via a diffusion model. The 1991 March Meeting of the American Physical Society, Cincinnati, Ohio, USA (March).

ANDERSEN, N.H., ANDERSEN, J.V., BOHR, H., LEBECH, B., MOURITSEN, O.G., and POULSEN, H.F., Structural and Thermodynamic Properties of Oxygen Ordering in $YBa_2Cu_3O_{6+x}$. 2nd Nordic Symposium on Superconductivity, Røros, Norway (January).

ANDERSEN, N.H., ANDERSEN, J.V., BOHR, H., LEBECH, B., MOURITSEN, O.G., and POULSEN, H.F., Oxygen Ordering and Superconductivity in $YBa_2Cu_3O_{6+x}$, Swedish High-T_c Superconductivity Meeting, Stockholm-Turku, Sweden (May).

ANDERSEN, N.H., BANDARANAYAKE, P.W.S.K., CAREEM, M.A., DISSANAYAKE, M.A.K.L., KABER, R., LUNDÉN, A., MELLANDER, B.-E., NILSSON, L., THOMAS, J.O., and WIJAYASEKERA, C.N., Paddle-Wheel versus Percolation Mechanism for Cation Transport in Some Sulphate Phases. 8th International Conference on Solid State Ionics (SSI-8), Lake Louise, Canada (October).

ANNILA, A.J., CLAUSEN, K.N., LINDGÅRD, P.-A., LOUNASMAA, O.V., OJA, A.S., SIEMENSMEYER, K., STEINER, M., TUORINIEMI, J.T., and WEINFURTER, H. (1991). Neutron Diffraction Studies of the Nuclear Magnetic Phase Diagram of Copper. International Conference on Magnetism. Edinburgh, UK (September).

BATES, F.S., ALMDAL, K., KOPPI, K., and MORTENSEN, K., Multiple Ordered Phases in a Block Copolymer Melt. American Physical Society March Meeting, Cincinnati, USA (March).

BATES, F.S., ALMDAL, K., and MORTENSEN, K., Order and Disorder in Block Copolymer Melts. American Physical Society March Meeting, Cincinnati, USA (March).

BOHR, J., X-ray and Neutron Scattering Studies of Rare Earth Spin Structures. 11th General Conference of The Condensed Matter Division, Exeter, England (April).

BOHR, J., Magnetic Structure Investigations by Synchrotron X-ray Scattering. Convegno Scientifico Annuale, Sorrento, Italy (October).

BOHR, J., Magnetic and Dichroic Effects in Resonant X-ray Scattering. Fundamentals of X-ray Absorption, Aussois, France (October).

BOHR, J., X-ray Studies of C_{60}. Dansk Fysisk Selskab og Dansk Optisk Selskabs Årsmøde (The Annual Meeting of the Danish Physical Society and the Danish Optical Society), Odense, Denmark (November).

ELLEGAARD, O., STENUM, B., SCHOU, J., SØRENSEN, H., and PEDRYS, R., Enhanced Sputtering of Condensed Gases by Molecular Ions. The 14th International Conference on Atomic Collisions in Solids, Salford, UK (July).

FEIDENHANS'L, R., X-ray Crystallography on Surfaces. Erste Gemeinsame Deutsche Kristallografen Tagung (First Joint Meeting of German Crystallografers), München, Germany (March).

FEIDENHANS'L, R., X-ray Diffraction Studies of Light Elements on Metal Surfaces. III European Conference on Surface Crystallography, San Miniato, Italy (May).

FEIDENHANS'L, R., Surface X-ray Crystallography and STM-Images, II'nd International Conference on Surface X-ray and Neutron Scattering, Bad Honnef, Germany (June).

FEIDENHANS'L, R., Surface X-ray Crystallography. 12th European Conference on Surface Science, Stockholm, Sweden (September).

HARMON, B.N., WANG, X.-W., and LINDGÅRD, P.-A., Calculation of the Ruderman-Kittel Interaction and the Nuclear Magnetic Ordering in Silver. International Conference on Magnetism. Edinburgh, UK (September).

HARRIS, P., LARSEN, S., and LEBECH, B., Crystal and Magnetic Structure of $KMnCl_3$. 24. Danske Krystallografmøde (The 24th Meeting of Danish Crystallographers), Risø, Denmark (June).

HELM, C. A., TIPPMANN-KRAYER, P., KENN, R. M., MÖHWALD, H., KJÆR, K., ALS-NIELSEN, J., The Phases of Phosphatidyl Ethanolamine Monolayers Studied by Synchrotron X-Ray Scattering. II'nd International Conference on Surface X-Ray and Neutron Scattering, Bad Honnef, Germany (June).

HENDRIKSEN, P.V., LINDEROTH, S., and LINDGÅRD, P. -A., Ferromagnetism in small Clusters. Danish Physical Society, Spring Meeting, Nyborg, Denmark (May).

HENDRIKSEN, P.V., LINDEROTH, S., and LINDGÅRD, P.-A. Ferromagnetism in Small Clusters. International Conference on Magnetism. Edinburgh, UK (September).

JUUL JENSEN, D., LORENTZEN, T., SKOV PEDERSEN, J., and CLAUSEN, K.N. The DR3 Risø Reactor as a User Facility for Applied Neutron Scattering Experiments:

Texture, Internal Strain and Applied Small Angle Scattering. 2. European Conference on Advanced Materials and Processes. EUROMAT-91, Cambridge, UK (July).

KENN, R. M., BÖHM, C., MÖHWALD, H., KJÆR, K., and ALS-NIELSEN, J., X-Ray Diffraction Studies of Amphiphilic Monolayers at the Air-Water Interface. II'nd International Conference on Surface X-Ray and Neutron Scattering. Bad Honnef, Germany (June).

KJÆR, K., Experimental Studies of Amphiphilic Monolayers. Workshop on Structure of Self-Assembled Amphiphilic Molecules. H. C. Ørsted Institute, Copenhagen, Denmark (May).

KJÆR, K., Røntgen- og Neutronreflektion fra Væskeoverflader, (X-Ray and Neutron Reflection from Liquid Surfaces). 24. Danske Krystallografmøde (The 24th Meeting of Danish Crystallographers), Risø, Denmark (June).

KJÆR, K., ALS-NIELSEN, J., KENN, R. M., BÖHM, C., TIPPMANN-KRAYER, P., HELM, C. A., MÖHWALD, H., LEVEILLER, F., JACQUEMAIN, D., LAHAV, M., LEISEROWITZ, L., and DEUTSCH, M., X-Ray Scattering Studies of Organic Monolayers on Electrolytic Solutions. II'nd International Conference on Surface X-Ray and Neutron Scattering, Bad Honnef, Germany (June).

KLEIMAN, R.N., BROHOLM, C., AEPPLI, G., BUCHER, E., STÜCHELI, N., BISHOP, D.J., CLAUSEN, K.N., HOWARD, B., MORTENSEN, K., and PEDERSEN, J.S., Neutron Scattering of the Flux Lattice on the Heavy Fermion Superconductor UPt_3. American Physical Society March Meeting, Cincinnati, USA (March).

LARSEN, E., and BOHR, J., Buckminsterfullerene's Kemi og Fysik (The Chemistry and Physics of Buckminsterfullernes). MODECS (Molecular Design of Chemical Systems) Møde, Roskilde, Denmark (April).

LEBECH, B., Modulated Magnetic Structures in Rare–Earth and Transition Metal Compounds. International Conference on Neutron Scattering, Oxford, UK (August).

LEBECH, B., and SMETANA, Z., Neutron Scattering Study of Magnetic Order in $ErCu_2$. International Conference on Neutron Scattering, Oxford, UK (August).

LEBECH, B., and WOLNY, J., Commensurate–Incommensurate Magnetic Phase Transitions in Nd and Nd–rich Nd–Pr Metal Alloys. Danish Physical Society, Spring Meeting, Nyborg, Denmark (May).

LEBECH, B., and WOLNY, J., Commensurate–Incommensurate Magnetic Phase Transitions in Nd and Nd–rich Nd–Pr Metal Alloys. International Conference on Magnetism, Edinburgh, UK (September).

LINDGÅRD, P. -A., Vibrationally Reduced Magnetic Interactions in Cu and Ag and the Magnetic Ordering in a Magnetic Field. Danish Physical Society, Spring Meeting, Nyborg, Denmark (May).

LINDGÅRD, P. -A., Structure of Solid and Liquid Adsorbate Layers, Workshop on Computer Simulation in Statistical Mechanics. Lyngby, Denmark (June).

LINDGÅRD, P. -A., Monte Carlo Simulation of Domain growth. Summer School on Modern Problems in Condensed Matter Research, Bialowieza, Poland (June).

LINDGÅRD, P. -A., Vibrationally Reduced Magnetic Interactions in Cu and Ag and the Magnetic Ordering in a Magnetic Field. International Conference on Magnetism, Edinburgh, UK (September).

LINDGÅRD, P. -A., Theory and Modeling of the Martensitic Transformation. European Symposium on Martensitic Transformations and Shape Memory Properties, Aussois, France (September).

LINDGÅRD, P. -A., Incommensurate Magnetic Structures and Magnetic Excitations. XXIst European Symposium on the Dynamical Properties of Solids, Autrans, France (September).

MASON, T.E., AEPPLI, G., HAYDEN, S.M., MOOK, H., CLAUSEN, K.N., CHEONG, S.-W., and FISK, Z., The Incommensurate Magnetic Fluctuations in $La_{2-x}Sr_xCuO_4$. Danish Physical Society, Spring Meeting, Nyborg, Denmark (May).

MASON, T.E., COLLINS, M.F., and GAULIN, B.D., Universality in a Triangular Antiferromagnet. American Physical Society March Meeting, Cincinnati, USA (March).

MASON, T.E., HARRISON, A., CLARKE, S.J., MCINTYRE, G.J., and VISSER, D., Magnetic Ordering and Fluctuations in the S=1/2 Square Heisenberg Antiferromagnet $Cu(DCO_2)_2\,4D_2O$. American Physical Society March Meeting, Cincinnati, USA (March).

MASON, T.E., YANG, Y.S., COLLINS, M.F., GAULIN, B.D., CLAUSEN, K.N., and HARRISON, A., Tetracritical Dynamics of $CsMnBr_3$. International Conference on Magnetism, Edinburgh, UK (September).

MAYER, H.M., STEINER, M., STÜSSER, WEINFURTER, H., KAKURAI, K., DORNER, B., LINDGÅRD, P. -A., CLAUSEN, K.N., HOCK, S., RODEWALD, W., and VERHOOEF, R., Inelastic Neutron Scattering Measurements on $Nd_2Fe_{14}B$ and $Y_2Fe_{14}B$. International Conference on Magnetism, Edinburgh, UK (September).

MORTENSEN, K., Polymers Studied by Neutron Scattering. Material Research on Risø, Danish Society for Polymer Technology, Risø, Denmark (March).

MORTENSEN, K., Structural Studies of the Aggregation of Block-Copolymers in Aqueous Solution. European Macromolecular Club, Uppsala, Sweden (June).

MORTENSEN, K., Disorder to Crystalline Order Transition in Aqueous Solution of a Triblock Copolymer. EPS Conference on Macromolecular Physics, Crete, Greece (September).

MORTENSEN, K., Block Copolymer in Aqueous Solution: Micelle Formation and Crystallization. Structured Fluids and Microemulsions, Copenhagen (December).

MORTENSEN, K., ALMDAL, K., BATES, F.S., and KOPPI, K., Order and Disorder in Block-Copolymer Melts. Danish Physical Society Spring Meeting , Nyborg, Denmark (May).

PEDERSEN, J. SKOV, Gaussian-Like Resolution Functions and Their Application in Indirect Fourier Transformation and Model Fitting of SANS Data. Workshop on the Analysis of Small Angle Neutron Scattering and Neutron Reflectivity Data, Institute Laue-Langevin, Grenoble, France (March).

PEDERSEN, J. SKOV, Small-Angle Neutron Scattering: Structure Determination at Low Resolution of Biological Substances in Solution. Det 24. Danske Krystallografimøde (The 24'th Danish Crystallography Meeting), Risø, Denmark (June).

PEDRYS, R., WARCZAK, B. and SCHOU, J., Erosion of Heavy Water by Electron Impact. The 6th Conference on Radiation Effects in Insulators, Weimar, Germany (June).

POSSELT, D., PEDERSEN, J. SKOV and MORTENSEN, K., A SANS Investigation on Absolute Scale of a Homologous Series of Base Catalysed Silica Aerogels. 3'rd International Symposium on Aerogels, Würzburg, Germany (September).

POULSEN, H.F., ANDERSEN, N.H., ANDERSEN, J.V., BOHR, H., and MOURITSEN, O.G., Modelling the Relationship between Oxygen Ordering and Superconductivity Transition Temperature in $YBa_2Cu_3O_x$. American Physical Society March Meeting, Cincinnati, USA (March).

POULSEN, H.F., ANDERSEN, N.H., ANDERSEN, J.V., BOHR, H., and MOURITSEN, O.G., Temporal Variation of Superconductivity Transition Temperature and Dynamical Scaling of Oxygen Ordering in $YBa_2Cu_3O_x$. American Physical Society March Meeting, Cincinnati, USA (March).

POULSEN, H.F., ANDERSEN, N.H., ANDERSEN, J.V., BOHR, H., and MOURITSEN, O.G., Oxygen Ordering and High-Temperature Superconductivity. Spring Meeting of the Danish Physical Society, Nyborg, Denmark (May).

POULSEN H.F, ANDERSEN N.H., ANDERSEN J.V., BOHR, H., and MOURITSEN O.G. Oxygen ordering and superconductivity in $YBa_2Cu_3O_{6+x}$. International Conference on Materials Science: High Tc Superconductivity, Paris, France (October).

ROTHARD, H., SCHOU, J., KOSCHAR, P., and GROENEVELD, K.-O., Electron Yields from Solids - a Probe for the Energy Loss of Charged Particles? International Workshop on Stopping of Low- and High-Z Ions, STOP91, Middelfart, Denmark (August).

SCHOU, J . Tracks of Electrons Within Solids. 80. WE-HEREAUS-SEMINAR, Radiation Physics: Electron Tracks in Matter, Bad Honnef, Germany (August).

SCHOU, J., ELLEGAARD, O., PEDRYS, R., and SØRENSEN, H., Sputtering of Solid Neon and Argon by Medium Mass Ions. The 6th Conference on Radiation Effects in Insulators, Weimar, Germany (June).

SCHOU, J., STENUM, B., ELLEGAARD, O., SØRENSEN, H., and PEDRYS, R., Sputtering of Solid Hydrogenic Targets by keV Hydrogen Ions. Spring Meeting of the Danish Physical Society, Nyborg, Denmark (May).

VAKNIN, D., ALS-NIELSEN, J., PIEPENSTOCK, M., and LÖSCHE, M., Recognition Processes at Functionalized Lipid Surfaces. Danish Physical Society, Spring Meeting, Nyborg, Denmark (May).

VAKNIN, D., ALS-NIELSEN, J., PIEPENSTOCK, M., and LÖSCHE, M., Protein Recognition Processes at Functionalized Lipid Surfaces: A Neutron Reflectivity Study. X-ray and Neutron Scattering from Surfaces, Bad Honnef, Germany (June).

VAKNIN, D., KJÆR, K., ALS-NIELSEN, J., LÖSCHE, M., and SKOV PEDERSEN, J., Simultaneous Refinement of Combined X-ray and Neutron Reflectivity Data. Workshop on the Analysis of SANS and NR data, ILL, Grenoble, France (March).

VIVES, E., and LINDGÅRD P.-A., Structure of Adsorbed Liquid on a Substrate Studied by Monte Carlo Simulation. The 5th Nordic Symposium on Computer Simulation of Liquids and Solids, Örenäs Castle, Sweden (September).

VIVES, E., and LINDGÅRD, P. -A., Substrate Influence in Two Dimensional Solids and Liquids: A Monte Carlo Simulation Study. The 5th Nordic Symposium on Computer Simulation, Örenäs Castle (September).

WEI, W., TUN, Z., BUYERS, W.J.L., GAULIN, B.D., MASON, T.E., GARRETT, J.D., and ISAACS, E.D., Long Range Antiferromagnetic Order and Its Coexistence with Superconductivity in the Heavy Electron System URu_2Si_2. International Conference on Magnetism, Edinburgh, UK (September).

WINKELMAN, M., GRAF, H.A., ANDERSEN, N.H., ZEISKE, T., and HOHLWEIN, D., Magnetic and Electronic Properties of $Mg_{1-x/2}Li_xCu_{2-x/2}O_3$. International Conference on Magnetism, Edinburgh, UK (September).

WOLNY, J., FRELTOFT, T., and TOPOLNICKA, A., Small Angle Neutron Scattering on Carbon Fibers. Physics for Industry, Cracow, Poland (September).

WOLNY, J., PYTLIK, L., and LEBECH, B., Quasi-Crystals and Twins - Two-Dimensional Model. Workshop on Quasi-crystals, Bilbao, Spain (April).

WULFF, M. and ALS-NIELSEN, J. , X-Ray Beam Sheet Deflection for Liquid Surface Spectrometry, International Conference on Synchrotron Radiation Instrumentation, Chester, England (July).

3.3 Lectures

ALS-NIELSEN, J., Structure of Langmuir Films Studied by Synchrotron X-Ray and Cold Neutron Diffraction, Symposium des SFB 262 : Struktur und Eigenschaften Unkonventioneller Glaser, Max-Planck Institut fur Polymerforschung, Mainz, Germany (January).

ALS-NIELSEN, J., Synchrotron X-Ray Studies of Liquid Surfaces University of Bern, Switzerland (January).

ALS-NIELSEN, J., Interaction of Radiation with Matter: X-Rays and Neutrons, Three Introductory Lectures at HERCULES 1991, Grenoble, France (January).

ANDERSEN, N.H., Neutron Scattering. Winther School in Modern Experimental Physics, arranged by the Danish Physical Society and Risø National Laboratory, Roskilde, Denmark (January).

ANDERSEN, N.H., Superledning (Superconductivity). Information meeting for public school teachers on: Focus on The Future Energy Research, arranged by the District Council of Roskilde and Risø National Laboratory, Roskilde, Denmark (February).

ANDERSEN, N.H., Oxygen Ordering and Superconductivity in $YBa_2Cu_3O_{6+x}$.

NORDITA, Copenhagen, Denmark (May).

University of Copenhagen, Denmark (May).

University of Cologne, Germany (June).

ANDERSEN, N.H., Superledning ved Høje Temperaturer (Superconductivity at High Temperatures). High School Summer Course on Physics, Sorø, Denmark (June).

BOHR, J.,A Symmetry Principle for Epitaxial Rotation. Theory Seminar, AT&T Bell Laboratories, New Jersey, USA (January).

BOHR, J., X-ray Studies of C_{60} Clusters.

University of Copenhagen, Denmark (March).

European Synchrotron Radiation Facility, Grenoble, France (March).

University of Lausanne, Switzerland (March).

BOHR, J., X-ray Studies of Buckminsterfullerene.

Niels Bohr Institute, Copenhagen, Denmark (April).

Odense University, Denmark (April).

BOHR, J., Buckminsterfullerene - C_{60}. Chalmers Technical University, Göteborg, Sweden (May).

BOHR, J., Buckminsterfullerene. Kieler Woche, Christian-Albrechts-Universität, Kiel, Germany (June).

BOHR, J., Symmetry and Epitaxial Rotations. Kieler Woche, Christian-Albrechts-Universität, Kiel, Germany (June).

CLAUSEN, K.N., Neutron Scattering Facilities at Risø National Laboratory, Gruppo Nazionale de Struttura della Materia - CNR, Rome, Italy (May).

FEIDENHANS'L, R., X-ray Scattering. Danish Physical Society: Winter School in Modern Physics, Risø National Laboratory, Roskilde, Denmark (January).

FEIDENHANS'L, R., Surface X-ray Diffraction at the ESRF. Nordsync Information Meeting on the ESRF, Lund, Sweden (September).

FEIDENHANS'L, R., Udstyr til epitaxial vækst af metal-tyndfilm (Equipment for Epitaxial Growth of Metallic Thin Films). Information Meeting for the Center of Surface Reaktions, Lyngby (November).

LINDGÅRD, P. -A., Magnetic Ordering in Cu in a Magnetic Field in Different Symmetry Directions. Johan Gutenberg Universität, Mainz, Germany (April).

LINDGÅRD, P. -A., Exotic Magnetism at Nanokelvin Temperatures. Inst. of Physics and Nuclear Techniques Academy of Mining and Metallurgy, Krakow, Poland (June).

LINDGÅRD, P. -A., Theory and Modeling of the Martensitic Transformations.

Institute Laue-Langevin, Grenoble, France (September).

Technical University of Denmark, Lyngby, Denmark (October).

MASON, T.E., Neutron and X-ray Scattering Studies of Antiferromagnetism in URu_2Si_2.

University of Toronto, Canada (February).

University of Copenhagen, Denmark (May).

MASON, T.E., The Incommensurate Magnetic Fluctuations in $La_{2-x}Sr_xCuO_4$.

McMaster University, Hamilton, Canada (October).

Queens University, Kingston, Canada (October).

I.B.M., Yorktown Heights, USA (November).

NORDITA, Copenhagen (December).

Université de Sherbrooke, Canada. (December).

POSSELT, D., Low Temperature Properties of Silica Aerogel, Institut für Physik, Johannes Gutenberg-Universität, Mainz, Germany (July).

POULSEN, H.F., Høj temperatur superledere. (High T_c Super Conductors). University Extension, Roskilde, Denmark (March).

POULSEN, H.F. Oxygen Ordering and Superconductivity in $YBa_2Cu_3O_{6+x}$.

AT&T Bell Laboratories, Murray Hill, U.S.A. (March).

Brookhaven National Laboratory, Upton, U.S.A. (April).

Argonne National Laboratory, Chigago, U.S.A. (April).

Hasylab, Hamburg, Germany (July).

ESRF, Grenoble, France (October).

VAKNIN, D., 2D Crystallization of Protein under Functionlized Surfaces. Racah Institute of Physics, Hebrew University, Jerusalem, Israel (September).

VAKNIN, D., Protein Recognition Processes at Functionalized Monolayers: Neutron and X-ray Scattering Studies. Weizmann Institute, Rehovot, Israel (September).

WINTER SCHOOL IN MODERN EXPERIMENTAL PHYSICS

21 and 22 January 1991, Risø National Laboratory.

Organizers

KELL MORTENSEN and PER-ANKER LINDGÅRD
Department of Solid State Physics, Risø National Laboratory, and
The Solid State Section, The Danish Physical Society

The school offered a series of lectures giving an elementary introduction to several related powerful and new experimental techniques used in very active areas of physics. Recently discovered physical phenomena, as for example the quantum Hall effect and the high T_c superconductors, have inspired the creation of new experimental methods. Further, new methods are developed for designing and 'building' materials atom by atom. This has led to recent developments of refinements as well as design of new techniques for investigating the materials on a microscopic level.

Approximately 60 persons participated in the school. A third of these participants were graduate students, whereas another third was Ph.D. students. The meeting was supported by Risø National Laboratory, the Danish Natural Science Research Council, and the Danish Physical Society.

Programme

Kell Mortensen, Risø	Introduction to Modern Exp. Physics
Robert Feidenhans'l, Risø	X-Ray Scattering
Niels H. Andersen Risø	Neutron scattering
Kell Mortensen, Risø	Small Angle Scattering
Ivan Stensgaard, Århus Univ.	Scanning Tunneling Microscope
G. Van Tendeloo, Univ. of Antwerp	Electron Microscopy
Claus B. Sørensen, Ørsted Inst.	Molecular Beam Epitaxy
Poul Erik Lindelof, Ørsted Inst.	Molecular Beam Epitaxy
Ove Poulsen, Århus Univ.	Storage Ring Physics
Lars Ladding, Risø	Dynamic Light Scattering

Visit to the Risø Neutron Scattering Facilities

SPRING MEETING, The Danish Physical Society, Solid State Section

21 and 22 May 1991, Nyborg Strand.

The 1991-spring meeting included 25 oral contributions, of which 17 was invited, and approximately 50 posters. The talks included for example Electron Holography by A. Tonomura, Metal Insulator Transitions by L.M. Falicov, Collective 2D Structures by A.R. Bishop, Structural Aspects of High-T_c Superconductors also by A.R. Bishop, Gamma Spectroscopy by J. Schneider and Point Defects in Semiconductors by H.G. Grimmeiss. The after-dinner talk was given by A.R. Mackintosh, who discussed the ongoing physics-evaluation. Approximately 110 persons participated in the meeting. The meeting was supported by: The Danish Natural Research Council, the Tuborg Foundation, the Otto Mønsted Foundatio, and the Danish Physical Society .

Organization:

The Board of the Solid State Section, the Danish Physical Society:
PER-ANKER LINDGÅRD (chairman), Risø National Laboratory,
KELL MORTENSEN, Risø National Laboratory,
BJERNE S. CLAUSEN, Haldor Topsøe a/s,
MADS P. SØRENSEN, Technical University, Lyngby,
PER HEDEGÅRD, H.C. Ørsted Institute, Copenhagen University,
SVEND TOUGAARD, Odense University,
AXEL SVANE (secretary), Århus University,
ARNE NYLANDSTED LARSEN, Århus University.

24. MEETING OF DANISH CRYSTALLOGRAPHERS

10 and 11 June 1991, Risø National Laboratory.

B. LEBECH and R. FEIDENHANS'l organised the 24. Meeting of Danish Crystallographers at Risø National Laboratory June 10 to 11 1991. Seven invited lecturers presented novel aspects of crystallography in four plenary sessions. Contributed papers were presented in two minutes introductory oral contributions followed by poster sessions. The meeting was supported by Tuborgfondet and Risø National Laboratory.

Invited Lectures

K. Kjær Risø	X-ray and Neutron Scattering from Liquid Monolayers
K. Frydenvang Danish School of Pharmacy	Crystallographic Aspects of Protein Studies
J. Engelbrecht, Technical University of Denmark	Neural Networks–Predictions of Human on RNA from linking of DNA Sequences
G. van Tendeloo, University of Antwerpen	Electron Microscopy and Crystallography
B.S. Clausen, Haldor Topsøe's Research Laboratories	EXAFS – Structure of Small Particles and Amophous Materials
S. Steenstrup, University of Copenhagen	Crystallographic Applications of Maximum Entrophy Methods
R.F. Stewart, Carnegie Mellon University	Electrostatic properties from X-ray Diffraction Data

INTERDISCIPLINARY WORKSHOP ON CARBON-60

6 and 7 December 1991, Roskilde

The workshop brought together nearly 100 researchers in the new field of study of carbon-60 and its related molecules, called *fullerenes*. Fifty-three talks were given over the course of two days, and almost every aspect of present C_{60} work was touched upon.

The structures of the fullerene family are especially rich; theoretical and experimental studies detailed the varieties and classification of the fullerene family. It was suggested that large fullerenes may be more common in nature than originally supposed, and that fullerene "caps" may close the ends of macroscopic carbon tubules which have been observed. Experimental work presented at the Workshop considered structural phase transitions of the C_{60} crystal, X-ray, electron and neutron diffraction measurements, chemistry and manufacture of C_{60}, thermodynamic properties, and many varieties of spectroscopy including X-ray photoemission, electron-energy-loss (EELS), Raman, and quasi-elastic neutron scattering. Theoretical work concerned the nature of the crystal phase transition, the classification of possible fullerene symmetries, effects of atom substitution in the molecule on its electronic states and physical structure, and calculations of the electronic and vibrational states of the pure molecule.

Of particular interest to the participants were the compounds of C_{60}, especially the presence of high-temperature superconductors made of C_{60} and the alkali atoms of potassium or rubidium; the magnetic properties of these was the subject of much lively discussion. Other unusual features of C_{60} are the open question to which extend it is possible to trap and hold atoms inside its cage, its degree of toxicity as indicated by standard tests, and the modes of positron annihilation in the crystal.

Funding was provided by the Swedish Consortium on Clusters and Ultra-Fine Particles, and the Danish Ministry of Science and Education.

Organization

J. BOHR, Risø National Laboratory, Denmark,
D. B. PENGRA, Risø National Laboratory, Denmark,
N. MÅRTENSSON, Uppsala University, Sweden.
P. BRÜHWILER, Uppsala University, Sweden,

COURSE IN SURFACE SCIENCE

R. FEIDENHANS'L together with J.K. NØRSKOV, I. CHORKENDORFF and K.W. JAKOBSEN from the Laboratory of Applied Physics, the Technical University (DtH) of Denmark, gave a course in Surface Physics at the DtH. The course consisted of two lectures of 2×35 minutes duration every week together with exercises. R. Feidenhans'l was lecturing four weeks in total eight lectures about Surface Crystallography, Phase Transitions at Surfaces and Epitaxy and Growth.

3.5 Seminars at Risø, 1991

SVERGUN, D., *Institute of Crystallography, USSR Academy of Sciences.* Small-angle Scattering Data Treatment by Means of the Regularization Technique (February).

LEHMANN, M., *Institute Laue-Langevin, Grenoble, France.* Development of a New 2-dimensional Neutron Detector at ILL (April).

ZEGENHAGEN, J., *Max Planck Institut für Festkörperforschung, Stuttgart, Germany.* Structure of Complex Adsorbates Studied by X-ray Standing Wawes: Pb on Ge (5 × 5) on Si(111) (April).

HATTA, I., *Nagoya University, Japan.* Appearance of Secondary Ripple Structure with Two-fold Wavelength in Phospholipids, Studied by X-ray Small Angle Scattering (May).

PENGRA, D.B., *Unive.sity of Washington, Seattle, USA.* The Search for Edge-Melting: A Thermodynamic Study of Monolayer Neon Films (May).

NOVOTNY, M., *Supercomputer Computations Research Institute, Florida State University, USA.* Numerical Investigation of a Model for Oxygen Ordering in $YBa_2Cu_3O_{6+x}$ (May).

BASSEREAU, D., *Université de Montpellier II, France.* Flexibility and Interactions in Smetic Phases of Fluid Bilayers (July).

MONCTON, D., *Argonne National Laboratory, USA.* Advanced Photon Source (APS) - Status and Perspectives (July).

GRUBEL, G., *ESRF, Grenoble, France.* Phase Transitions on Platinum Surfaces (September).

SANDEY, A., *Massachusetts Institute of Technology, Cambridge, USA.* Phase Behaviour of the (111) Surfaces of Au and Pt (September).

SETNA, I., *Cornell University, USA.* Slow Dynamics and the Glass Transition (September).

ELLEAUME, P., *ESRF, Grenoble, France.* X-ray Beams from Insertion Devices at ESRF (September).

BERG, R.H., *Materials Department, Risø National Laboratory, Denmark.* A New Principle for Recognition of DNA (October).

BRUNAK, S., *The Technical University, Denmark.* DNA Sequence Analysis by Neural Network (October).

SPIRGATIS, A., *University of Humburg, IAP, Germany.* Relaxation of the Irreversible Magnetization in the High Temperature Superconductors (October).

CARRA, P., *ESRF, Grenoble, France.* Core-Level Spectroscopy of Magnetic Systems (November).

BÖRJESSON, L., *Chalmers University of Technology, Sweden.* Raman Scattering Studies of High-T_c Superconductors (November).

Bibliographic Data Sheet **Risø-R-610(EN)**

Title and author(s)

Annual Progress Report of the Department of Solid State Physics

1 January – 31 December 1991

Eds. J. Als-Nielsen, J. Skov Pedersen and B. Lebech

ISBN	ISSN
87-550-1788-6	0106-2840 0907-0249

Dept. or group	Date
Department of Solid State Physics	January 1992

Groups own reg. number(s)	Project/contract no.

Pages	Tables	Illustrations	References
145	2	94	82

Abstract (Max. 2000 characters)

Research in the department covers the field of condensed matter physics. The principal activities of the department are presented in the Progress Report covering the period from 1 January to 31 December 1991.

The condensed matter physics research is predominantly experimental utilising diffraction of neutrons and X-rays. The research topics range from studies of two- and three-dimensional structures, magnetic ordering, heavy femions, high T_c superconductivity, phase transitions in model systems to studies of precipitation phenomena and nano-scale structures in various materials. The major interest of the department is in basic research, but projects of more applied nature are often taken up, prompted by the applicability of the developed technique and expertise.

Descriptors INIS/EDB

MAGNETISM; PROGRESS REPORT; RISOE NATIONAL LABORATORY; SOLID STATE PHYSICS; SUPERCONDUCTIVITY

Available on request from Risø Library, Risø National Laboratory, (Risø Bibliotek, Forskningscenter Risø), P.O.Box 49, DK-4000 Roskilde, Denmark.
Telephone +45 42 37 12 12, ext. 2268/2269
Telex 43 116. Telefax +45 46 75 56 27.

Available on request from:
Risø Library
Risø National Laboratory,
P.O. Box 49, DK-4000 Roskilde, Denmark
Phone +45 42 37 12 12, ext. 2268/2269
Telex 43116, Telefax +45 46 75 56 27

ISBN 87-550-1788-6
ISSN 0106-2840
ISSN 0907-0249